

Gas Phase Chemical Physics Program

DOE Principal Investigators'
Abstracts

May, 2020

Chemical Sciences, Geosciences, and Biosciences Division
Office of Basic Energy Sciences
Office of Science
U.S. Department of Energy

The research grants and contracts described in this document are supported by the U.S. DOE Office of Science, Office of Basic Energy Sciences, Chemical Sciences, Geosciences and Biosciences Division.

Foreword

The Gas Phase Chemical Physics (GPCP) program continues to undergo restructuring by broadening its scope to include other areas of gas phase chemical physics in addition to combustion that align with the DOE energy mission. Strategic planning discussions resulted in identification of several research areas focusing on understanding gas phase chemical physics at the level of molecules, atoms, and electrons, which could benefit from the expertise and experience of the gas phase chemical physics community. These discussions resulted in a workshop hosted by SLAC titled “Applications of Ultrafast X-ray Science to Grand Challenge Questions in Gas Phase Chemical Reactions.” Aspects of several of these topics are reflected in this collection of abstracts and align well with the research objectives of the Department of Energy's Office of Basic Energy Sciences (BES).

We appreciate your understanding and patience and your service as reviewers during this challenging time. Your continued commitment to carrying out scientific research under these circumstances is laudable. We also extend a special thanks to Teresa Crockett, Kerry Hochberger, and Gwen Johnson of BES Operations for working behind-the-scenes to ensure smooth operation of the GPCP program. Although the 40th Gas Phase Chemical Physics PI meeting was cancelled this year, a book of abstracts was prepared to highlight your research accomplishments supported by the GPCP program. We look forward to gathering in 2021 for our 40th annual meeting.

Jeff Krause
Wade Sisk

Table of Contents

Table of Contents

Foreword.....	iii
Table of Contents.....	v
Abstracts	1
<u>Principal Investigators' Abstracts</u>	
Musahid Ahmed, Martin Head-Gordon, and Kevin R. Wilson – Molecular Reactivity in Complex Systems.....	1
Scott L. Anderson – Nanoparticle Surface Kinetics and Dynamics by Single Nanoparticle Mass Spectrometry	5
Josette Bellan – Predictive Large-Eddy Simulation of Supercritical-Pressure Reactive Flows in the Cold Ignition Regime	9
Michael Burke – Chemical Kinetic Data of Benchmark Accuracy through Multi-Scale Informatics Strategies.....	13
Rebecca L. Caravan – Kinetics and Mechanisms of Gas-Phase Reactions towards Gas-Particle Interconversions.....	17
David W. Chandler, Jonathan H. Frank, Nils Hansen, Christopher J. Kliewer, Habib N. Najm., David L. Osborn, Krupa Ramasesha, Leonid Sheps, Craig A. Taatjes, Timothy S. Zwier – Advanced Diagnostics.....	21
David W. Chandler, Jonathan H. Frank, Laura M. McCaslin, David L. Osborn, Leonid Sheps, Judit Zádor and Timothy S. Zwier – Chemical Dynamics Methods and Applications.....	25
David W. Chandler, Nils Hansen, Christopher J. Kliewer, Habib N. Najm., David L. Osborn, Leonid Sheps, and Craig A. Taatjes – Gas Phase Interactions with Other Phases.....	29
Jacqueline H. Chen, Nils Hansen, Habib N. Najm, David L. Osborn, Lenny Sheps, Craig A. Taatjes, and Judit Zádor, – Chemical Kinetics for Complex Systems.....	33
Robert E. Continetti – Dynamics and Energetics of Elementary Combustion Reactions and Transient Species.....	37
H. Floyd Davis – Dynamics of Combustion Reactions.....	41
Michael J. Davis – Exploration of chemical-kinetic mechanisms, chemical reactivity, and thermochemistry using novel numerical analysis.....	45
Richard Dawes – Electronic structure methods and protocols with application to dynamics, kinetics and thermochemistry.....	49
Gary Douberly and Henry F. Schaefer III – Theoretical and Experimental Studies of Elementary Hydrocarbon Species and Their Reactions.....	53
Michael A. Duncan – Coordination and Solvation of Actinide Cations Studied with Selected-Ion Infrared Spectroscopy.....	57
Robert W. Field – Spectroscopic and Dynamical Studies of Highly Energized Small Polyatomic Molecules.....	61

Jonathan H. Frank, Farid El Gabaly, Nils Hansen, Christopher J. Kliewer, David L. Osborn, Coleman Kronawitter and Ambarish Kulkarni – Imaging the Near-Surface Gas Phase: A New Approach to Coupled Gas-Surface Chemistry.....	65
C. Franklin Goldsmith – Gas Phase Chemical Kinetics Under Extreme Conditions.....	69
William H. Green – Computer-Aided Construction of Chemical Kinetic Models.....	73
Martin Head-Gordon, Eric Neuscammann, and David Prendergast – Theory of Electronic Structure and Chemical Dynamics.....	77
Ahren W. Jasper – Semiclassical Methods for Pressure Dependent Kinetics and Electronically Nonadiabatic Chemistry	81
Ralf I. Kaiser – Probing the Reaction Dynamics of Hydrogen-Deficient Hydrocarbon Molecules and Radical Intermediates via Crossed Molecular Beams.....	85
Christopher J. Kliewer, David W. Chandler, Krupa Ramasesha, and Jonathan H. Frank – Ultrafast Physics: Nonlinear Optical Spectroscopy and Diagnostics.....	89
Ahren W. Jasper, Stephen J. Klippenstein (PI), Raghu Sivaramakrishnan, Robert S. Tranter, Leonid Sheps, Nils Hansen, and Craig A. Taatjes (PI) – Argonne-Sandia Consortium on High-Pressure Combustion Chemistry.....	93
Stephen J. Klippenstein - Theoretical Chemical Kinetics.....	97
Coleman Kronawitter and Ambarish Kulkarni- Developing New Mechanistic Insights into Oxidative Coupling of Methane through Combined Gas-Phase and Surface-Sensitive Spectroscopies with Site-Isolated Catalysts.....	101
Nicole J. Labbe, G. Barney Ellison, and John W. Daily - A Coupled Theoretical and Experimental Approach to Elucidating the Mechanisms of Methyl Esters.....	105
Marsha I. Lester – Spectroscopy and Dynamics of Reaction Intermediates in Combustion Chemistry.....	109
Robert P. Lucht – Advanced Nonlinear Optical Methods for Quantitative Measurements in Flames.....	113
Laura R. McCunn – Thermal Decomposition of Cyclic, Oxygenated Hydrocarbons.....	117
Habib Najm, Judit Zádor, Michael Eldred, Hope Michelsen – Machine Learning for Understanding Heavy Hydrocarbon Clustering.....	121
David J. Nesbitt - Spectroscopy, Kinetics and Dynamics of Combustion Radicals.....	125
Stephen R. Leone and Daniel M. Neumark– Fundamental Molecular Spectroscopy and Chemical Dynamics.....	129
Kang-Kuen Ni – State-to-State Reactions in the Ultracold Regime.....	133
William J. Pitz and Charles K. Westbrook – Chemical Kinetic Modeling of Combustion Chemistry.....	137
Stephen B. Pope and Perrine Pepiot - Investigation of Non-Premixed Turbulent Combustion.....	141
Stephen T. Pratt - Optical Probes of Atomic and Molecular Decay Processes.....	145
Kirill Prozument – Reaction Mechanisms Studied with Chirped-Pulse Rotational Spectroscopy.....	149
Krupa Ramasesha, Laura M. McCaslin, Leonid Sheps, Christopher J. Kliewer, Nils Hansen, Habib Najm – Ultrafast Chemistry: Spectroscopic Probes of Non-Adiabatic Dynamics.....	153
Hanna Reisler - Photoinitiated Reactions of Radicals and Diradicals in Molecular Beams.....	157

Melanie Reber – Ultrafast Transient Absorption Spectroscopy of Hydrocarbon Radicals.....	161
Branko Ruscic – Active Thermochemical Tables.....	163
Trevor J. Sears – Spectroscopic Investigations of Molecular Symmetry Breakdown.....	167
Ron Shepard – Theoretical Studies of Potential Energy Surfaces and Computational Methods.....	171
Raghu Sivaramakrishnan – Mechanisms and Models for Simulating Gas Phase Chemical Reactivity.....	175
John F. Stanton – Quantum Chemistry of Radicals and Reactive Intermediates.....	179
Arthur G. Suits – Universal and State-Resolved Imaging Studies of Chemical Dynamics.....	183
Jeffrey A. Sutton – Multiscale Interaction of Turbulence, Temperature, and Soot Formation: Measurements for Critical Assessments of Chemical Kinetics and Mechanisms.....	187
Robert S. Tranter – Elementary Reactions of PAH Formation.....	191
Lai-Sheng Wang – Probing Nonvalence Excited States of Anions Using Photodetachment and Photoelectron Spectroscopy.....	195
Margaret S. Wooldridge, Andrew B. Mansfield, and Robert S. Tranter – Fundamental Chemical Kinetics of Siloxane and Silicon Compounds.....	199
Hua Guo, Donald G. Truhlar, and David R. Yarkony – Nonadiabatic Photochemistry.....	203

Molecular Reactivity in Complex Systems

Musahid Ahmed, Martin Head-Gordon and Kevin R. Wilson

Lawrence Berkeley National Laboratory, 1 Cyclotron Road, Berkeley, CA-94720.

mahmed@lbl.gov, mhead-gordon@lbl.gov, krwilson@lbl.gov.

Program Scope: We seek to understand complex multistep and multiphase chemical transformations that extend beyond elementary unimolecular and excited state reactions. The approach builds complexity from isolated elementary bimolecular reactions to gas surface reaction dynamics to coupled networks of elementary unimolecular and bimolecular pathways embedded at a gas/solid or liquid interface. In each of these areas, the gas phase is central for controlling reactivity. Activities in this subtask drive new theory and simulation to enrich the molecular level interpretation of experiments. Cross-cutting themes of *Chemistry at Complex Interfaces* and *Reaction Pathways in Diverse Environments* are explored, providing valuable basic insights into microscopic processes relevant to energy generation, storage and combustion.

Recent Progress:

Molecular Reactivity in clusters and high temperature environments: The goal of this research is to use synchrotron based photoionization mass spectrometry coupled with electronic structure calculations to study chemical reactivity and molecular growth.¹ Ahmed and Head-Gordon have formulated an understanding as to how non-covalent interactions can drive chemical reactivity in small acetylene clusters upon photoionization. A dramatic dependence of product distribution on the photoionization conditions is observed and interpreted by theory.² Within a polycyclic aromatic hydrocarbon (PAH) system interacting with water, there is an increase in the scope for interesting structural rearrangements to stabilize the positive charge upon ionization, as well as increased potential for reactive chemical events to occur upon ionization.³

The multistep reaction network of PAHs with free radicals is being examined in collaboration with Ralf Kaiser (Hawaii) and Alex Mebel (Florida International). This is achieved by simulating combustion relevant conditions (pressure, temperature, reactant molecules) in a high temperature ‘chemical reactor’.⁴ Four distinct pathways have been identified: Hydrogen Abstraction – acetylene Addition type mechanisms (HACA),⁵ the barrierless Hydrogen Abstraction – Vinylacetylene Addition mechanism (HAVA),⁶⁻⁸ the Phenyl Addition – dehydroCyclization pathway (PAC), and Radical-Radical Recombination (RRR). These complementary mechanisms lead to the formation of fundamental building blocks of two and three dimensional carbon nanostructures. A unified low-temperature reaction mechanism on the formation of acenes, phenacenes, and helicenes is revealed.⁹ This mechanism is mediated through a barrierless, vinylacetylene mediated gas-phase chemistry utilizing tetracene, [4]-phenacene, and [4]-helicene (C₁₈H₁₂). Along with the synthesis of triphenylene (C₁₈H₁₂),¹⁰ the HAVA mechanism opens up an isomer-selective route to aromatic structures involving submerged reaction barriers, resonantly stabilized free-radical intermediates, and systematic ring annulation. The PAC pathway was verified computationally and experimentally leading to four-ring PAHs like triphenylene and fluoranthene.¹¹ PAC operates efficiently at high temperatures leading through rapid molecular mass growth processes to complex aromatic structures, which are difficult to synthesize by traditional pathways such as HACA. We revealed that facile, isomer selective route to naphthalene is possible via rapid radical-radical reactions of 1-indenyl with methyl.¹² This versatile route converts five- to six-membered rings and provides a detailed view of high temperature mass growth processes that can eventually lead to graphene-type PAHs and two-dimensional nanostructures. Elements from these four mechanisms were used to explain how five-membered rings (benzindenes) could be formed in naphthyl radical reactions.¹² and the formation of pentacene in the reaction of the 2-tetracenyl radical with vinylacetylene.¹³ The methodology has been extended to study the unimolecular decomposition pathways of jet fuel,^{14, 15} and biomass constituents.¹⁶

Multiphase Reaction Networks: Ongoing efforts¹⁷⁻¹⁹ focus on understanding how gas phase reaction mechanisms of peroxy radicals (RO₂) and Criegee intermediates (CI) are modified by the presence of an interface. Recently, we reported²⁰ a new heterogeneous reaction mechanism for the autoxidation of alkenes. We observed evidence that certain β-hydroxy-peroxy radicals formed by heterogeneous OH radical addition

(in the presence of O₂) leads to the facile production of CI. Analogous pathways in the gas phase, to our knowledge have not been reported. Concurrently, we measured lengthy free radical chain reactions (i.e. effective reaction probabilities > 50). These observations appear to be quite general even for unsaturated hydrocarbons containing multiple allylic and bi-allylic sites as well as unsaturated fatty acids. The results point to an alternative autoxidation mechanism, which is initiated by OH radicals to produce CI, followed by decomposition to reform OH. This new autoxidation mechanism contrasts with the established one, that involves cycling between peroxy radicals and hydroperoxides via H atom transfer reactions. These results suggest that reaction pathways involving CI are more widespread and may even play a role in degradation of lipids in biological systems.

Reaction-Diffusion in Multiphase Reactions: We continue to explore²¹ the formation and evolution of chemical gradients at interfaces undergoing oxidation. The heterogeneous reaction of hydroxyl radicals (OH) on ~200-nm particles of pure squalane (a branched, liquid hydrocarbon) and octacosane (a linear, solid hydrocarbon), and binary mixtures of the two are used to understand how diffusion limitations and phase separation impact gas/surface reactivity. Aerosol mass spectrometry is used to measure the reaction kinetics in bulk and whereas aerosol X-ray photoemission²² is used to examine the reactions at the interface. When diffusion is fast relative to reaction frequency, as is the case for squalane and low viscosity squalane-octacosane mixtures, the reaction is efficient and only limited by the collision frequency of OH. For the alternative case where the diffusion rates are slower than reaction rates, carbon and oxygen K edge X-ray absorption measurements show that the solid octacosane interface is oxidized much more rapidly than that of liquids. The differences in surface oxidation rates are analyzed using a previously published reaction diffusion model,^{23, 24} revealing that a 1-2 nm highly oxidized crust forms on the solid particles, whereas for the liquid case the reaction products are homogeneously mixed within the particle.

Future Plans:

Bimolecular gas phase chemistry - Ahmed in collaboration with Ralf Kaiser and Alex Mebel plan to understand how larger ring (4 and higher) formation leads to the mass-growth processes from simple PAHs to soot particles utilizing the heated reactor coupled to synchrotron based mass spectrometry. The elucidation of the formation routes of key PAHs has the potential to revolutionize the understanding of the underlying mass growth processes from simple precursors via complex PAHs. These theoretical and experimental details will be necessary to design and interpret the reaction mechanisms that will no doubt arise as we move towards understanding the 2D and 3 D structures of these carbon growth processes. A new direction is to probe gas phase hydrocarbon reactions in confined spaces such as in zeolites and MOF's by introducing these species into the heated reactor. We anticipate that our scaled down reactor with chemistry being arrested after microsecond reaction times (typical residence times in our reactor are 20-50 microseconds) will allow for reactive intermediates to be captured in the supersonic expansion of a molecular beam. A key here is that the gas phase chemistry will have been directly probed using the same reactor, to allow a comparison with heterogeneity in the dynamics with an introduction of a surface.

Non-covalent Interactions: Reactions Dynamics in Clusters. We will continue our program on the application of VUV photoionization and theoretical calculations to decipher kinetics, dynamics and photo-induced reactivity in molecular clusters, especially hydrogen-bonded and van der Waals clusters.¹ We will examine glycerol/water as a model for hydrophilic interactions to compare and contrast ongoing work with PAH/water as a model for hydrophobic interactions. Glycerol contains three hydroxyl groups and is miscible with water; we believe that such rich dynamics based upon hydrogen bonding between water and glycerol can become accessible with a judicious combination of experiments and theory. A novel microfluidic device,²⁵ has recently been coupled to mass spectrometry and will be used to probe gas-solid interactions.

Multiphase Reaction Mechanisms: Future work will continue to focus on elucidating the connectivity in heterogeneous reactions between free radical and CI reaction pathways. We will examine the production of OH during heterogeneous ozonolysis. In the gas phase, the formation of OH from the decomposition of CI is well known with numerous measurements quantifying this unimolecular rate. However, for O₃ surface reactions there remains considerable uncertainty as to the OH yield, due in large part to the ambiguity

revealed in recent experiments, from the Beauchamp Group (Caltech) β -hydroxy-peroxy radicals undergo facile decomposition to produce Cl. Experimental measurements are nearly completed for a model hydrocarbon system consisting of a single double bond. Evidence for OH is production observed and we will complete a comprehensive multiphase kinetic model to quantify the OH yield from this reaction, which would further elucidate the coupling of O₃ and OH mechanism. We will continue our collaboration with Martin Head-Gordon's group who is examining mechanisms for the interconversion of hydroxyl peroxy radicals and Cl in an effort to build a predictive multiphase kinetic model of OH addition reaction at organic interfaces. We have also begun heterogeneous measurements of Cl₂ and Cl atom reactions with alkenes. Preliminary results are shown evidence for substantial chain reactions and the potential for some anomalously fast reactions of Cl₂ with alcohol moieties with the aerosol.

We also plan to continue our collaboration^{26,27} with Hope Michelsen (U. of Colorado) to test, using model aerosol systems, some of the key features of her proposed soot inception mechanism (i.e. clustering of hydrocarbons by radical-chain reactions, CHRCR).

Work supported by the BES-GPCP program (2017-present)

1. Ahmed, M.; Kostko, O., From atoms to aerosols: probing clusters and nanoparticles with synchrotron based mass spectrometry and X-ray spectroscopy. *Physical Chemistry Chemical Physics* **2020**, *22*, (5), 2713-2737.
2. Stein, T.; Bandyopadhyay, B.; Troy, T. P.; Fang, Y.; Kostko, O.; Ahmed, M.; Head-Gordon, M., *Ab initio* Dynamics and Photoionization Mass Spectrometry Reveal Ion–Molecule Pathways from Ionized Acetylene Clusters to Benzene Cation. *Proc. Natl. Acad. Sci. U.S.A.* **2017**, *114*, (21), E4125-E4133.
3. Xu, B.; Stein, T.; Ablikim, U.; Jiang, L.; Hendrix, J.; Head-Gordon, M.; Ahmed, M., Probing solvation and reactivity in ionized polycyclic aromatic hydrocarbon-water clusters with photoionization mass spectrometry and electronic structure calculations. *Faraday Discussions* **2019**.
4. Zagidullin, M. V.; Kaiser, R. I.; Porfiriev, D. P.; Zavershinskiy, I. P.; Ahmed, M.; Azyazov, V. N.; Mebel, A. M., Functional Relationships between Kinetic, Flow, and Geometrical Parameters in a High-Temperature Chemical Microreactor. *J Phys Chem A* **2018**, *122*, (45), 8819-8827.
5. Zhao, L.; Kaiser, R. I.; Xu, B.; Ablikim, U.; Ahmed, M.; Evseev, M. M.; Bashkirov, E. K.; Azyazov, V. N.; Mebel, A. M., Low-temperature formation of polycyclic aromatic hydrocarbons in Titan's atmosphere. *Nat Astron* **2018**, *2*, (12), 973-979.
6. Zhao, L.; Kaiser, R. I.; Xu, B.; Ablikim, U.; Ahmed, M.; Joshi, D.; Veber, G.; Fischer, F. R.; Mebel, A. M., Pyrene synthesis in circumstellar envelopes and its role in the formation of 2D nanostructures. *Nat Astron* **2018**, *2*, (5), 413-419.
7. Zhao, L.; Kaiser, R. I.; Xu, B.; Ablikim, U.; Ahmed, M.; Zagidullin, M. V.; Azyazov, V. N.; Howlader, A. H.; Wnuk, S. F.; Mebel, A. M., VUV Photoionization Study of the Formation of the Simplest Polycyclic Aromatic Hydrocarbon: Naphthalene (C₁₀H₈). *J Phys Chem Lett* **2018**, *9*, (10), 2620-2626.
8. Zhao, L.; Kaiser, R. I.; Lu, W.; Xu, B.; Ahmed, M.; Morozov, A. N.; Mebel, A. M.; Howlader, A. H.; Wnuk, S. F., Molecular mass growth through ring expansion in polycyclic aromatic hydrocarbons via radical–radical reactions. *Nature Communications* **2019**, *10*, (1), 3689.
9. Zhao, L.; Kaiser, R. I.; Xu, B.; Ablikim, U.; Ahmed, M.; Evseev, M. M.; Bashkirov, E. K.; Azyazov, V. N.; Mebel, A. M., A Unified Mechanism on the Formation of Acenes, Helicenes, and Phenacenes in the Gas Phase. *Angewandte Chemie International Edition* **2020**, *59*, (10), 4051-4058.
10. Zhao, L.; Xu, B.; Ablikim, U.; Lu, W.; Ahmed, M.; Evseev, M. M.; Bashkirov, E. K.; Azyazov, V. N.; Howlader, A. H.; Wnuk, S. F.; Mebel, A. M.; Kaiser, R. I., Gas-Phase Synthesis of Triphenylene (C₁₈H₁₂). *ChemPhysChem* **2019**, *20*, 791.
11. Zhao, L.; Prendergast, M. B.; Kaiser, R. I.; Xu, B.; Ablikim, U.; Ahmed, M.; Sun, B. J.; Chen, Y. L.; Chang, A. H. H.; Mohamed, R. K.; Fischer, F. R., Synthesis of Polycyclic Aromatic Hydrocarbons by Phenyl Addition–Dehydrocyclization: The Third Way. *Angewandte Chemie International Edition* **2019**, *58*, (48), 17442-17450.

12. Zhao, L.; Prendergast, M.; Kaiser, R. I.; Xu, B.; Ablikim, U.; Lu, W.; Ahmed, M.; Oleinikov, A. D.; Azyazov, V. N.; Howlader, A. H.; Wnuk, S. F.; Mebel, A. M., How to add a five-membered ring to polycyclic aromatic hydrocarbons (PAHs) – molecular mass growth of the 2-naphthyl radical (C₁₀H₇) to benzindenes (C₁₃H₁₀) as a case study. *Physical Chemistry Chemical Physics* **2019**, *21*, (30), 16737-16750.
13. Mebel, A.; Zhao, L.; Kaiser, R. I.; Lu, W.; Ahmed, M.; Evseev, M. M.; Bashkurov, E. K.; Azyazov, V. N.; Tönshoff, C.; Reicherter, F.; Bettinger, H. F., A Free Radical Prompted Barrierless Gas Phase Synthesis of Pentacene. *Angewandte Chemie International Edition* **2020**, *Accepted*, (doi:10.1002/anie.202003402).
14. Zhao, L.; Yang, T.; Kaiser, R. I.; Troy, T. P.; Ahmed, M.; Belisario-Lara, D.; Ribeiro, J. M.; Mebel, A. M., Combined Experimental and Computational Study on the Unimolecular Decomposition of JP-8 Jet Fuel Surrogates. I. n-Decane (n-C₁₀H₂₂). *J. Phys. Chem. A* **2017**, *121*, (6), 1261-1280.
15. Zhao, L.; Yang, T.; Kaiser, R. I.; Troy, T. P.; Xu, B.; Ahmed, M.; Alarcon, J.; Belisario-Lara, D.; Mebel, A. M.; Zhang, Y.; Cao, C. C.; Zoue, J. B., A Vacuum Ultraviolet Photoionization Study on High-Temperature Decomposition of JP-10 (exo-tetrahydrodicyclopentadiene). *Phys Chem Chem Phys* **2017**, *19*, (24), 15780-15807.
16. Ormond, T. K.; Baraban, J. H.; Porterfield, J. P.; Scheer, A. M.; Hemberger, P.; Troy, T. P.; Ahmed, M.; Nimlos, M. R.; Robichaud, D. J.; Daily, J. W.; Ellison, G. B., Thermal Decompositions of the Lignin Model Compounds: Salicylaldehyde and Catechol. *J Phys Chem A* **2018**, *122*, (28), 5911-5924.
17. Arata, C.; Heine, N.; Wang, N.; Misztal, P. K.; Wargocki, P.; Bekö, G.; Williams, J.; Nazaroff, W. W.; Wilson, K. R.; Goldstein, A. H., Heterogeneous Ozonolysis of Squalene: Gas-Phase Products Depend on Water Vapor Concentration. *Environmental Science & Technology* **2019**, *53*, (24), 14441-14448.
18. Heine, N.; Arata, C.; Goldstein, A. H.; Houle, F. A.; Wilson, K. R., Multiphase Mechanism for the Production of Sulfuric Acid from SO₂ by Criegee Intermediates Formed During the Heterogeneous Reaction of Ozone with Squalene. *The Journal of Physical Chemistry Letters* **2018**, *9*, (12), 3504-3510.
19. Heine, N.; Houle, F. A.; Wilson, K. R., Connecting the Elementary Reaction Pathways of Criegee Intermediates to the Chemical Erosion of Squalene Interfaces during Ozonolysis. *Environ. Sci. Technol.* **2017**, *51*, (23), 13740-13748.
20. Zeng, M.; Heine, N.; Wilson, K. R., Evidence that Criegee intermediates drive autoxidation in unsaturated lipids. *Proceedings of the National Academy of Sciences* **2020**, *117*, (9), 4486-4490.
21. Jacobs, M. I.; Xu, B.; Kostko, O.; Wiegel, A. A.; Houle, F. A.; Ahmed, M.; Wilson, K. R., Using Nanoparticle X-ray Spectroscopy to Probe the Formation of Reactive Chemical Gradients in Diffusion-Limited Aerosols. *The Journal of Physical Chemistry A* **2019**, *123*, (28), 6034-6044.
22. Jacobs, M. I.; Kostko, O.; Ahmed, M.; Wilson, K. R., Low energy electron attenuation lengths in core-shell nanoparticles. *Physical Chemistry Chemical Physics* **2017**, *19*, (20), 13372-13378.
23. Houle, F. A.; Wiegel, A. A.; Wilson, K. R., Predicting Aerosol Reactivity Across Scales: from the Laboratory to the Atmosphere. *Environmental Science & Technology* **2018**, *52*, (23), 13774-13781.
24. Wiegel, A.; Liu, M.; Hinsberg, W. D.; Wilson, K. R.; Houle, F. A., Diffusive Confinement of Free Radical Intermediates in the OH Radical Oxidation of Semisolid Aerosol. *Phys Chem Chem Phys* **2017**.
25. Komorek, R.; Xu, B.; Yao, J.; Ablikim, U.; Troy, T. P.; Kostko, O.; Ahmed, M.; Yu, X. Y., Enabling liquid vapor analysis using synchrotron VUV single photon ionization mass spectrometry with a microfluidic interface. *Rev Sci Instrum* **2018**, *89*, (11).
26. Johansson, K. O.; Dillstrom, T.; Elvati, P.; Campbell, M. F.; Schrader, P. E.; Popolan-Vaida, D. M.; Richards-Henderson, N. K.; Wilson, K. R.; Violi, A.; Michelsen, H. A., Radical-radical reactions, pyrene nucleation, and incipient soot formation in combustion. *Proceedings of the Combustion Institute* **2017**, *36*, (1), 799-806.
27. Johansson, K. O.; Head-Gordon, M. P.; Schrader, P. E.; Wilson, K. R.; Michelsen, H. A., Resonance-stabilized hydrocarbon-radical chain reactions may explain soot inception and growth. *Science* **2018**, *361*, (6406), 997-1000.

Nanoparticle Surface Kinetics and Dynamics by Single Nanoparticle Mass Spectrometry

Scott L. Anderson,
Chemistry Department, University of Utah
315 S. 1400 E.
Salt Lake City, UT 84112
anderson@chem.utah.edu

Program Scope

This project is focused on developing and using single nanoparticle mass spectrometry (NPMS) – a new method – to measure reaction kinetics and emission spectroscopy for individual carbon nanoparticles (NPs) at high temperatures. The focus is on sublimation and oxidation of carbon NPs, but NPMS is broadly applicable to nano-structured refractory materials. In addition to providing temperature-dependent reaction kinetics of interest for modeling purposes, we are interested in probing the effects of two different kinds of heterogeneity on NP kinetics and spectroscopy: 1. NPs are inherently heterogeneous, with significant NP-to-NP variation in size, shape, and structure, all of which can affect reaction kinetics and spectroscopy. 2. *Individual NPs* also have distributions of surface sites that react differently, and the site distributions and resulting reaction kinetics can change as individual NPs *evolve* under the influence processes such as annealing, sublimation, and etching of surface atoms. In addition to fundamental interest in understanding heterogeneity effects, this kind of information is essential to understanding and modeling carbon NP chemistry on a molecular level.

Methodology

The instrument¹ used in the experiments, and the optical system needed to record emission spectra for NP temperature (T_{NP}) determination²⁻³ have been described previously. In essence, NPs of the material of interest are gotten into the gas phase by electrospray from a suspension in ammonium acetate, then guided to a split ring-electrode quadrupole trap (SRET),⁴ that is operated with rf voltage of amplitude (V_0) and frequency (F_0). A laser is focused loosely through the trap, while using an avalanche photodiode (APD) to look for optical emission from the trap center. Trapping of a particle is observed as a step in APD signal due to thermal emission from the laser-heated NP, and the trapping process is immediately terminated. Motion of trapped NPs can be described as slow “secular” motion, with superimposed micro-motion at frequency F_0 .⁵ The secular motion is harmonic, with frequencies f_z and f_r , for axial and radial motion, proportional to Q/M . For example, $f_z = \frac{|Q|}{M} \left(\frac{V_0 \sqrt{2}}{F_0 z_0^2 4\pi^2} \right)$, where z_0 is a trap geometric parameter (2.97 mm). To measure f_z , the frequency of a weak AC potential applied to an electrode outside the trap is scanned, and when this drive frequency is resonant with f_z , a dip in APD signal is observed because the NP motional amplitude increases, reducing the fraction of time it spends in the $\sim 50 \mu\text{m}$ APD detection volume. The presence of more than one NP is observed as multiple f_z resonances, in which case the trap is emptied, and NP injection is repeated to trap a single NP. From the measured value of f_z , we know Q/M , and Q can be determined exactly by observing the steps in f_z that occur as a VUV lamp is used to induce single electron changes in Q . (Note: we have shown that there are no significant effects of NP charge on either reactivity or emission spectra).^{3,6} Once the charge stepping process is complete, reaction kinetics can be measured by tracking f_z , hence M , vs. time as the NP is heated and exposed to gaseous reactants. T_{NP} is determined by measuring the emission spectrum, and fitting to a thermal emission model function. This approach allows kinetics to be measured for individual NPs, thus probing NP-to-NP heterogeneity effects, and also allows changes in NP kinetics due to thermal/reaction-driven evolution of NP structure to be followed. To allow kinetics to be associated with NP structure, we are developing a site titration process, described below.

Automation and COVID19

The single NP approach avoids ensemble averaging, thus providing unique insights into heterogeneity and structure-reactivity relationships, but it is a slow method. To enable study of statistically meaningful numbers of NPs we have devoted considerable effort to automating the experiment. We are not yet at the point of 24/7 unattended operation, however, the experiment and data

analysis are sufficiently automated to allow experiments to be run remotely. This has allowed us to continue experiments throughout the COVID19 shutdown, and some remotely obtained results are shown here.

Results in the past year

We started with a detailed study of emission spectra, and how they change after heating, for graphite, graphene, carbon black, nanodiamond, and carbon dot NPs.⁶ Our first kinetics study was of sublimation of graphite and graphene NPs, and a paper on this is under review at JACS.³ One key result from that study is presented below. At the time of the COVID19 shutdown, we were just finishing an initial study of O₂ oxidation kinetics for graphite and graphene NPs, but had to quickly stop and finish automation for remote control so that work could continue during the shutdown. The data acquisition for the O₂ oxidation study was completed using the remote capabilities, and that paper is nearly ready for submission. Meanwhile, experimental work has continued on a study of graphite and graphene NP growth kinetics in reactions with C₂H₂ and C₂H₄. This chemistry is related to the HACA mechanism proposed for soot growth, and one of our goals has been to identify conditions under which growth reactions can be used to titrate NPs, to count the number of low coordination reactions sites. An example is presented below.

Oxidation

To illustrate the method, Fig. 1 shows a simple experiment in which a single graphite NP of initial M = ~26.5 MDa (~33.4 nm, if spherical) was held at T_{NP} = 1700 K while monitoring sublimation and oxidation kinetics. Prior to the start of the data record shown, the NP was charge stepped while being held at T_{NP} ≈ 1200 K to minimize thermal changes. After setting T_{NP} to 1700 K, the M vs. time record was fit (solid blue line) to determine the sublimation rate, which was found to be constant, and equal to loss of 14.3 C atoms/second. To allow rates to be compared for different NPs and to approximately correct for loss of surface area during reactions, we put the rates on a *per* nm² basis, resulting in an area-normalized rate of 4.08 x 10⁻³ C atoms/second/nm². Because the NP shape is unknown, we use the area of a spherical NP of the same mass, which gives a lower limit on the area, and therefore an upper limit on the rate.

After the initial period characterizing the sublimation rate, 2.5 x 10⁻⁵ Torr of O₂ was added to the Ar buffer gas (shaded region), resulting in a sharp increase in mass loss rate, averaging ~3.27 x 10⁻¹ C atoms/second/nm². This rate includes contributions from both oxidation and sublimation, but clearly at this low T_{NP}, sublimation makes only a minor contribution. Experiments by Minton and others have shown that CO loss dominates the oxidation branching, except at low temperatures where significant CO₂ is also observed.⁷ At the end of the experiment, the O₂ flow was stopped to allow the sublimation rate to be re-measured, and the result was 1.23 x 10⁻³ C/sec/nm² ~ 1/3rd of the initial sublimation rate. This change indicates that there was some evolution of the NP structure (distribution of surface sites) during the oxidation period.

In this example, apart from a fluctuation induced by an O₂ pressure glitch near the end of the oxidation period, the oxidative mass loss rate was nearly constant. The total mass lost was ~6 MDa, corresponding to ~5 monolayers if the NP were spherical. Given that oxidation occurs primarily at under-coordinated edge/defect sites, which are far more reactive than graphitic basal planes, this implies that the distribution of such sites was roughly constant as the NP lost mass. As shown below, such steady

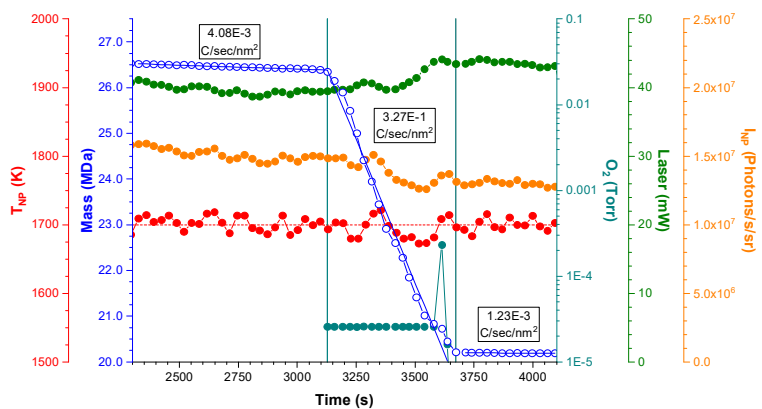


Fig. 1. M, T_{NP}, O₂ pressure, laser power, and integrated emission intensity vs. time for a graphite NP in inert and oxidizing atmospheres.

behavior is often not the case. Note also that during the experiment, the integrated emission intensity (I_{NP}) decreased slightly, even though T_{NP} was constant, as expected from the decrease in emitting surface area as the NP shrank. On the other hand, the 532 nm laser power required to heat the NP initially decreased then increased when O_2 was added, suggesting that the 532 nm absorption cross section dropped when oxidation started. As shown below, for many NPs, the variations in both reaction rates and optical properties are more dramatic, and sometimes quite complex.

Fig. 2 shows an example experimental protocol for measuring oxidation rates as a function of T_{NP} applied to a graphitic NP of initial mass ~ 55.5 MDa. Because sublimation and oxidation both contribute to mass loss, the NP was alternately exposed to inert (unshaded background) and oxidizing (shaded) conditions as T_{NP} was ramped between 1400 and 2300 K. Frame A shows the 1st heat ramp, B and C show details at low and high T_{NP} , and D shows the sublimation and oxidation rates extracted from the data in two sequential heat ramps. Several points are obvious:

1. At low T_{NP} (frame B), the mass loss rate was much faster when O_2 was present, i.e., oxidation was much faster than sublimation.
2. Conversely, at high T_{NP} (frame C) the sublimation rates were fast, and mass loss rate hardly changed when O_2 was added, i.e., oxidation was slow compared to sublimation.
3. Particularly at high T_{NP} (frame C), the mass loss rates are not steady, slowing over time at each T_{NP} . This signals evolution of the NP toward more stable surface site distributions, seen in many examples.
4. Both the sublimation and oxidation rates (D) extracted from the data changed significantly between the 1st heat ramp and a 2nd ramp carried out immediately after the 1st. Again, this shows evolution of the NP as it loses mass, due to a combination of preferential reaction/sublimation at low coordination sites, and annealing.

In addition, a number of other oxidation protocols have been used, such as pressure-dependent rate measurements at constant T_{NP} , and long term oxidation studies in which NPs were oxidized at constant T_{NP} and P_{O_2} , observing sometimes dramatic, non-monotonic changes in oxidation rate as the NP evolved.

Sublimation Kinetics

We completed a quite detailed study of sublimation as a function of T_{NP} , for a large number of graphite and graphene NPs, {Long, 2020 #845} probing NP-to-NP heterogeneity and evolution as a function of time. Fig. 3 summarizes one set of data, showing the

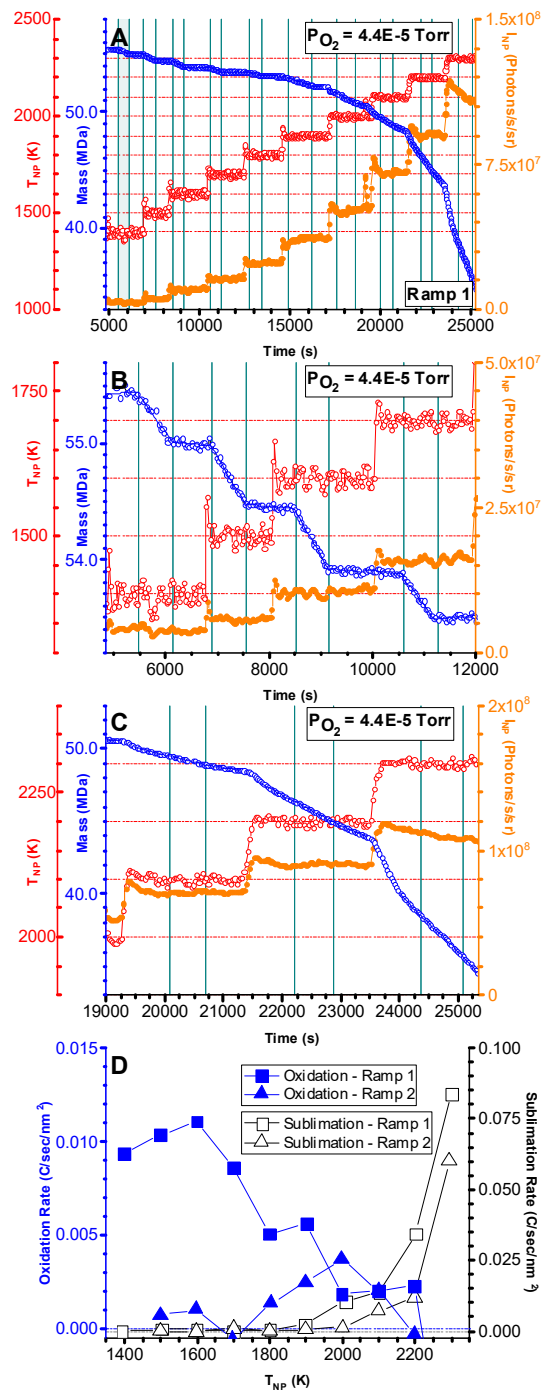


Fig. 2. An example T_{NP} -dependent oxidation experiment.

area-normalized sublimation rates for ~10 individual graphitic NPs as a function of T_{NP} , compared to the rate for bulk graphite. From the slopes, we derived activation energies, which vary substantially from NP to NP, and averaged significantly lower than that for bulk graphite, reflecting the larger fraction of edge and defect sites in NPs, compared to the ~100 μm grains in bulk graphite. The rates and activation energies also evolved with time at temperature, due to the effects of sublimation and annealing on the surface site distributions.

Carbon NP reactions with C_2H_2 and C_2H_4 : Growth and Titration

The reaction kinetics of graphitic NPs with C_2H_2 and C_2H_4 are being studied as a function of temperature and pre-treatment of the NPs. One goal is to find conditions where self-limiting growth allows ‘titration’ of the NP surface, based on the observation that these molecules react preferentially with low-coordination sites. Fig. 4 shows an example where a graphite NP with initial mass = 15.52 MDa, was held at 1600 K, briefly oxidized, and then exposed to ~1.7 mTorr of C_2H_2 . Reaction with C_2H_2 resulted in a relatively fast mass gain of 520 kDa (3.3%), which then stopped spontaneously, indicating that all sites capable of reacting with C_2H_2 had been passivated, presumably by CH termination. Assuming that the reaction was with under-coordinated edge and defect sites, 520 KDa corresponds to there having been ~40,000 such sites on the NP surface at the time of titration. We plan to use this approach to associate oxidation and sublimation rates with numbers of low coordination sites, to achieve NP-by-NP structure-reactivity relationships.

References

- Howder, C. R.; Bell, D. M.; Anderson, S. L., Optically Detected, Single Nanoparticle Mass Spectrometer With Pre-Filtered Electrospray Nanoparticle Source. *Rev. Sci. Instrum.* **2014**, *85*, 014104 - 014110.
- Long, B. A.; Rodriguez, D. J.; Lau, C. Y.; Anderson, S. L., Thermal emission spectroscopy for single nanoparticle temperature measurement: optical system design and calibration. *Appl. Opt.* **2019**, *58* (3), 642-649.
- Long, B. A.; Lau, C. Y.; Rodriguez, D. J.; Tang, S. A.; Anderson, S. L., Sublimation Kinetics for Individual Graphite and Graphene Nano-particles (NPs): NP-to-NP Variations and Evolving Structure-Kinetics and Structure-Emissivity Relationships. *J. Am. Chem. Soc.* **2020**, (submitted), *arXiv:2002.07835*.
- Gerlich, D.; Decker, S., Trapping Ions at High Temperatures: Thermal Decay of C_{60}^+ . *Appl. Phys. B: Lasers Opt.* **2014**, *114*, 257-266.
- Schlemmer, S.; Illemann, J.; Wellert, S.; Gerlich, D., Nondestructive High-Resolution And Absolute Mass Determination Of Single Charged Particles In A Three-Dimensional Quadrupole Trap. *J. Appl. Phys.* **2001**, *90* (10), 5410-5418.
- Long, B. A.; Rodriguez, D. J.; Lau, C. Y.; Schultz, M.; Anderson, S. L., Thermal Emission Spectroscopy of Single, Isolated Carbon Nanoparticles: Effects of Particle Size, Material, Charge, Excitation Wavelength, and Thermal History. *J. Phys. Chem. C* **2020**, *124*, 1704-1716.
- Murray, V. J.; Smoll, E. J.; Minton, T. K., Dynamics of Graphite Oxidation at High Temperature. *J. Phys. Chem. C* **2018**, *122* (12), 6602-6617.

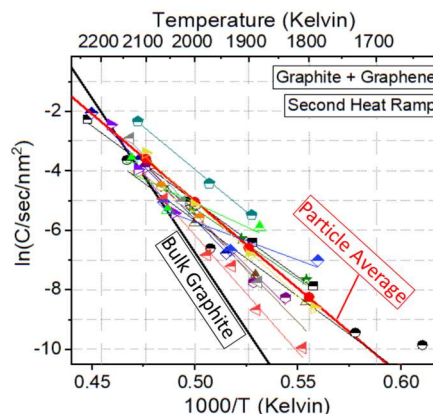


Fig. 3. Aggregated sublimation rate data for graphitic particles, compared to bulk graphite.

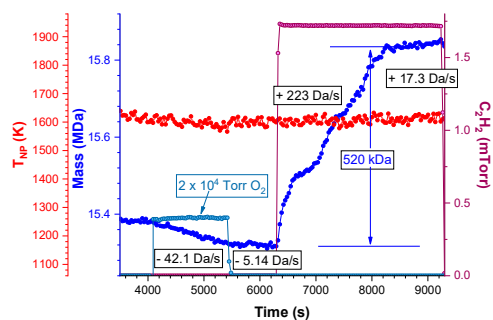


Fig. 4. A C_2H_2 growth experiment

Predictive Large-Eddy Simulation of Supercritical-Pressure Reactive Flows in the Cold Ignition Regime

Josette Bellan

Mechanical and Civil Engineering Department, California Institute of Technology
Pasadena, CA 91125

Josette.Bellan@jpl.nasa.gov

DOE Award Number: **02_GR-ER16107-14-00**

STRIPES award number: **SC0002679/0009**

I. Program Scope

This study addresses issues highlighted in the Basic Energy Needs for Clean and Efficient Combustion of 21st Century Transportation Fuels (DOE BES, 2006) under the topic of Combustion under Extreme Pressure. It is there noted that “the most basic concepts of thermal autoignition” are “based on experience and theory at near atmospheric pressures” and that “as pressure increases significantly..., many of these conceptual pictures begin to change or disappear”. It is also stated “A better description of the coupling and interaction of high pressure flow and molecular transport processes with chemistry is also necessary”, particularly because “Ignition and flame propagation of alternative and renewable fuels, as well as of the changing feed stocks of conventional fossil-based fuels, are very likely to be much different at very high pressures than under the more familiar, lower pressure conditions of current engines.” Recognizing that “Under such (*increasing pressure*) conditions distinctions between gas and liquid phases become moot, new equations of state must be used...”, it is immediately apparent that there must be “a re-examination of the basic assumptions that govern the physics and chemistry related to combustion; and the need for this type of re-examination increases as the combustion pressure increases.” This recognition is also stated under the topic of Multiscale Modeling since due to the new equations of state “The combination of unexplored thermodynamic environments and new physical and chemical fuel properties results in complex interactions among multiphase (*according to the above, the multiphase distinction becomes moot with increasing pressure*) fluid dynamics, thermodynamic properties, heat transfer, and chemical kinetics that are not understood even at a fundamental level.” From the theoretical viewpoint for “systems at high pressure, fluid dynamic time scales can be comparable to chemical time scales.” and therefore “completely diffusion-controlled reactions ... can become important”.

Thus, the objective of this study is the investigation of the coupling among thermodynamics, transport properties, intrinsic kinetics and turbulence under the high-pressure and the relatively (with respect to combustion) low-temperature conditions typical of the auto-ignition regime, with particular emphasis on the manifestation of this coupling on the effective kinetic rate.

II. Recent Progress

This report contains results obtained during the previous year of funding. Having tested during the previous year the concept of the Double-Conditioned Source-term Estimation (DCSE) formalism for obtaining an accurate model of the turbulent reaction rate under high-pressure (high-p) conditions using formalism-needed elements extracted from our Direct Numerical Simulations (DNS) [i], and having found the DCSE model promising [ii], this year we examined potential models for these elements that had previously been extracted from DNS as this information would not be available to a user conducting Large Eddy Simulation

(LES). There are several such elements: (1) the evaluation of the smallest number of ensembles in which the conditional-filtered values of the reactive scalars can be assumed to have modest gradients in space, (2) options for the computation of the conditional-filtered reaction rate, (3) options for the computation of the conditional-filtered temperature, density and mass fractions, and (4) options for computing the joint probability density function (JPDF). To understand the challenge of the computations, the spatial distribution of the

reaction rate in one plane is displayed in Fig. 1 for the filtered-and-coarsened DNS (FCDNS) at the time station of the spatial-domain-integrated peak pressure (t_{pp}^*). Clearly, $\dot{\omega}$ is large in the lean regime and in this region there is a structure resembling a triple flame. It is also clear that there is still ignition propagating towards the oxidizer region. Small structure vortices are evident in the reaction zone, thus invalidating any attempt to consider the reaction zone to be laminar. Finally, it is obvious that the reaction rate will not be well-resolved on the FCDNS mesh, no matter how appropriate the turbulence-chemistry interaction model in terms of assumptions. To further understand the effect of filtering the DNS, in Fig. 2 is illustrated the probability density function (PDF) of the DNS reaction rate, the filtered DNS reaction rate (FDNS) and of the FCDNS. The filtering dramatically reduces the maximum reaction rate, as with the box filter used here the filtered reaction rates are averaged over LES volumes; the

corollary is that the values of the FDNS PDF exceed those of the DNS PDF in the small value regime, and scrutiny of the PDF even shows a peak (not visible on the plot), unlike the $\dot{\omega}$ PDF which is a monotonic function. Coarsening the FDNS field to obtain the FCDNS field incurs another penalty since during coarsening, the uniform sampling over the domain favors the more prevalent small $\dot{\omega}$ values and a portion of the largest FDNS values is lost. There is clearly a philosophical conundrum in modelling the FCDNS $\dot{\omega}$, but it clear that in order to preserve the paltry remnants of the DNS reaction rate, one should focus on success in the large reaction rate regime. The two conditioning variables for DCSE are the mixture fraction and a species progress variable. The findings of the study is that the reduction in the number of spatial ensembles from the optimal that would be each FCDNS volume only matters when the reduction is drastic, but after a drastic reduction, further reductions to a single ensemble representing the entire domain does not deteriorate the model when all other model elements are computed from the DNS. Computing the conditional-filtered scalars using an inversion equation does introduce some error, and this error is of same general magnitude as that found by reducing the number of ensembles in which the conditional-filtered values of the reactive

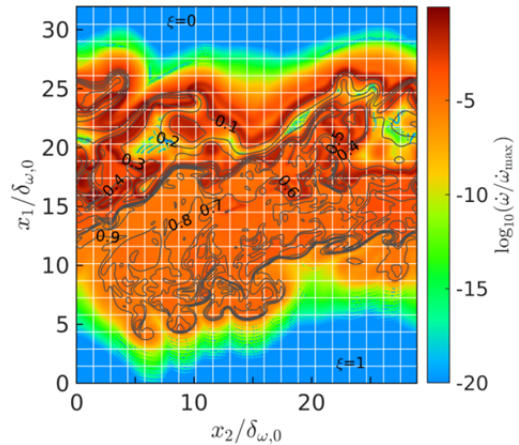


Figure 1. Superposition of $\log_{10}(\dot{\omega}/\dot{\omega}_{\max})$ and nine ξ isopleths shown at even 0.1 intervals in the plane $x_3/L_3=0.42$. The grid shows the edges of the filter volumes for the FCDNS at t_{pp}^* .

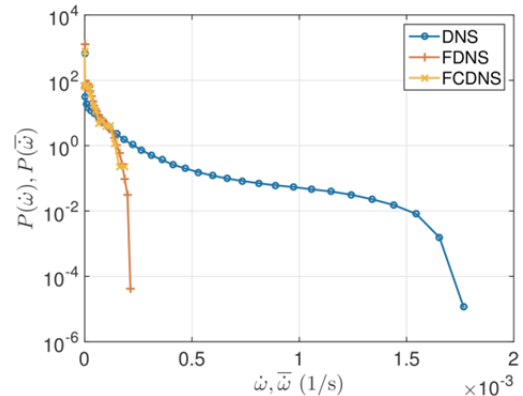


Figure 2. PDF of the reaction rate, showing the unfiltered (DNS), filtered (FDNS) with a filter width such that $\Delta/\Delta_{\text{DNS}}=24$, and filtered-and-coarsened (FCDNS) PDFs where $\Delta_{\text{LES}}=\Delta$.

scalars can be assumed to have modest gradients. However, by far the largest source of error is due to the poor representation of the JPDF of the conditioning scalars by the product of the marginal PDFs, where each PDF is represented by the β PDF. The issues are illustrated in Fig. 3. Two examples are shown, each corresponding to the situation at one FCDNS grid node. In one example, in which the JPDF model of the DNS-extracted PDF is accurate, Figs. 3a and 3b, the means of the two conditioning variables are similar in magnitude, their variances are small, but the assumption of statistical independence is not well satisfied. In the other example

in which the JPDF is not accurate, Figs. 3c and 3d, one of the means has \sim twice the value of the other, the variances have larger magnitudes but the assumption of statistical independence between the two conditioning variables is better satisfied.

Thus, the key model is the JPDF of the conditioning variables.

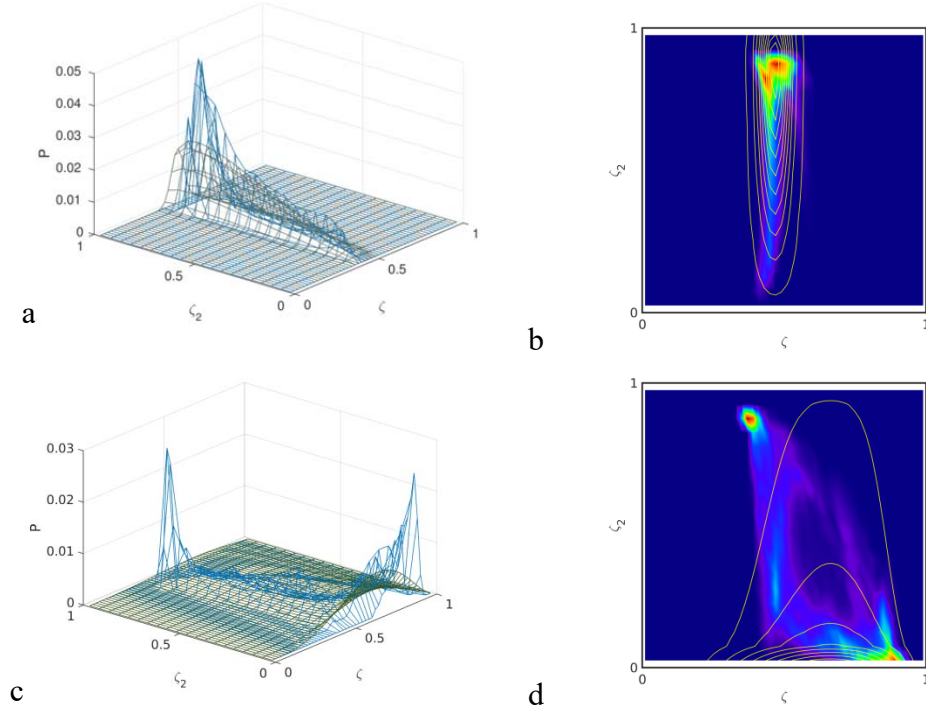


Figure 3. Superposition of the DNS calculated JPDF and the modeled JPDF at two different points: (a, b) for one point, (c,d) for another point of the FCDNS data. (a,c) show superposition of the DNS-extracted PDF (blue) and modeled PDF (green). (b,d) show the projections in the conditional variables plane of the JPDFs (color background represents the DNS, yellow contours represent the modeled JPDF).

III. References

- i. Bellan, J., *Combust. Flame.*, **2017** 176 245
- ii. Devaud, C.B., Bushe, W. K., Bellan, J. *Combust. Flame.*, **2019** 207 205

IV. Publications and presentations supported by this project (only 2015- 2020 are listed)

- [1] Borghesi, G.; Bellan, J., Irreversible entropy production rate in high-pressure turbulent reactive flows, *Proc. of the Comb. Inst.*, 35, 1537-1547, 2015
- [2] Borghesi, G.; Bellan, J., *A priori* and *a posteriori* analysis for developing Large Eddy simulations of multi-species turbulent mixing under high-pressure conditions, *Phys. Fluids.*, 27, 035117 (35 pages), 2015
- [3] Bellan, J., Direct Numerical Simulation of a high-pressure turbulent reacting mixing layer, *Combust. Flame*, 176, 245-262, 2017
- [4] Gnanaskandan, A.; Bellan, J., Numerical Simulation of jet injection and species mixing under high-pressure conditions, *Journal of Physics*, Institute of Physics Conference Series: Materials Science and Engineering, 821, 012020, 2017

- [5] Bellan, J., Evaluation of mixture-fraction-based turbulent-reaction-rate model assumptions for high-pressure reactive flows, *Combust. Flame*, 179, 253-266, 2017
- [6] Gnanaskandan, A.; Bellan, J., Side-jet effects in high-pressure turbulent flows: Direct Numerical Simulation of nitrogen injected into carbon dioxide, *J. Supercritical Fluids*, 140, 165-181, 2018
- [7] Sciacovelli, L.; Bellan, J., The influence of the chemical composition representation according to the number of species during mixing in high-pressure turbulent flows, *Journal of Fluid Mechanics*, 863, 293-340, 2019
- [8] Devaud, C.; Bushe, W.K.; and J. Bellan, J., The modeling of the turbulent reaction rate under high-pressure conditions: *a priori* evaluation of the Conditional Source-term Estimate concept, *Combustion and Flame*, 207, 205–221, 2019
- [9] Gnanaskandan, A.; Bellan, J., Large Eddy Simulations of high pressure jets : Effect of subgrid scale modeling, Chapter 11, 461-481, *AIAA Progress Series* book titled *High Pressure Flows for Propulsion Applications* (Ed. J. Bellan), 2020
- [10] Bushe, W.K.; Devaud, C.; Bellan, J., Turbulent high-pressure reaction-rate modelling using the Double-conditioned Conditional Source-term Estimation method: a priori investigation of modelling elements and numerical aspects, *Combustion and Flame*, 217, 131-151, 2020
- [11] Bellan, J., Modeling and numerical simulations of multi-species high-pressure reactive flows, **Invited Plenary Lecture**, Summer Program of the SFBTRR40, Institute of Aerodynamics and Fluid Mechanics Technische Universität München, Garching, Germany, August 3, 2015
- [12] Bellan, J., Modeling and numerical simulations of multi-species high-pressure reactive flows, **Invited Seminar**, Purdue University, West Lafayette, IN., October 22, 2015
- [13] Bellan, J., Reduced models for the simulation of multi-scale problems in physics and chemistry, **Invited Seminar**, Cornell University, Ithaca, NY., November 17, 2015
- [14] Bellan, J., Modeling and Numerical Simulations of Multi-Species High-Pressure Turbulent Mixing and Combustion, **Invited Seminar**, SpaceX, Hawthorne, CA., 12/14/2016
- [15] Borghesi, G.; Bellan, J., Models for the LES equations to describe multi-species mixing occurring at supercritical pressure, paper 2014-0823 presented at the 52nd Aerospace Sciences Meeting, New Harbor, MD, January 13-17, 2014 Borghesi, G. and Bellan, J., Irreversible entropy production rate in high-pressure turbulent reactive flows, *Proc. of the Comb. Inst.*, 35, 1537-1547, 2015
- [16] Borghesi, G.; Bellan, J., *A priori* and *a posteriori* analyses of multi-species turbulent mixing layers at supercritical-*p* conditions, paper 2015-0162 presented at the 53rd Aerospace Sciences Meeting, Kissimmee, FL., January 5-9, 2015; also presented at the 9th US National Combustion Meeting, Cincinnati, OH., May 17-20, 2015
- [17] Bellan, J., The mixture fraction for high-pressure turbulent reactive flows, paper 2016-1686 presented at the 54th Aerospace Sciences Meeting, San Diego, CA, January 4-8, 2016
- [18] Gnanaskandan, A.; Bellan, J., Large Eddy Simulations of high pressure jets: Effect of subgrid scale modeling, paper 2017-1105 presented at the 55th Aerospace Sciences Meeting, Grapevine, TX, January 9-13, 2017
- [19] Sciacovelli, L.; Bellan, J., Mixing in high pressure flows: the influence of the number of species, paper 2018-1189, presented at the 56th Aerospace Sciences Meeting, Kissimmee, FL., January 8-12, 2018
- [20] Devaud, C.; Bushe, W.K.; Bellan, J., Assessment of Conditional Source-term Estimation for High-Pressure Turbulent Combustion Modeling, presented at SciTech 2019, January 7-11, 2019, San Diego, FL; also presented at the 11th US. National Meeting of the Combustion Institute, March 24-27, 2019, Pasadena, CA.
- [21] Banuti, D.; Bellan, J., Influence of the real-gas equation-of-state binary interaction coefficients on the turbulent mixing of many species at diesel-engine high-pressure conditions, presented at the 11th US. National Meeting of the Combustion Institute, March 24-27, 2019, Pasadena, CA
- [22] Bushe, W.K.; Devaud, C.; Bellan, J., Turbulent high-pressure reaction rate modeling using the Double-conditioned Conditional Source-term Estimation method, paper AIAA-2020-1153 presented at SciTech 2020, January 6-10, Orlando, Fl.
- [23] Banuti, D.; Bellan, J., Inter-species molecular attraction effect in the development of a two-species mixing layer, paper 2020-1155 presented at SciTech 2020, January 6-10, Orlando, Fl.

Chemical Kinetic Data of Benchmark Accuracy through Multi-Scale Informatics Strategies

Michael P. Burke

*Department of Mechanical Engineering, Department of Chemical Engineering, & Data Science Institute
Columbia University, New York, NY 10027
mpburke@columbia.edu*

Program Scope

The reliability of predictive simulations for advanced energy conversion devices depends on the availability of accurate data for thermochemistry, chemical kinetics, and transport. In that regard, accurate data are critically important for both their direct use in predictive simulations and for benchmarking improved theoretical methodologies that can similarly produce accurate data for predictive simulations. The use of informatics-based strategies for the determination of accurate thermochemical data with well-defined uncertainties, i.e. the Active Thermochemical Tables (ATcT),¹ has revolutionized the field of thermochemistry – ATcT provides thermochemical data of unprecedented accuracy for direct use in predictive simulation and has served as a key enabler of *ab initio* electronic structure methodologies of equally impressive accuracy. The goal of this program is to develop an active database for chemical kinetics, akin to that for thermochemistry, to establish high-accuracy kinetic data for predictive simulation and to evaluate emerging *ab initio*-based theoretical kinetics methods, using our multi-scale informatics approach. We are particularly interested in reaction systems where non-thermal kinetic sequences arise and/or where combining theoretical and experimental data is necessary to unravel complex reaction data into chemical information.

Recent Progress

There are several significant challenges in deriving high-accuracy kinetic data of relevance to the complex reactions encountered in combustion, planetary atmospheres, and interstellar environments. First, even the most “direct” experimental rate constant determinations are often influenced by uncertainties in secondary reactions – leading to a complex web of interdependences among kinetic parameters for many reactions (and an opportunity to gain more information than has been attained previously, since uncertainties are seldom at the noise floor of the measurements). Second, there is rarely enough experimental data to constrain the full temperature, pressure, and composition ($T/P/X$) dependence of many rate constants – rendering usual rate-parameter-based uncertainty quantification approaches ineffective. Third, many reactions of interest to various application domains and gas-phase theoretical chemistry involve non-thermal kinetic sequences¹⁻⁷ – posing an additional problem for rate-parameter-based approaches.

During the past several years, we have been developing a multi-scale uncertainty quantification approach, MultiScale Informatics (MSI),^{8-10,i-iii} to address the challenges involved in 1) unraveling the complex web of interdependences among reactions in complex systems data (by reinterpreting the raw data from multi-reaction systems used to determine rate constants experimentally), 2) sufficiently constraining the $T/P/X$ dependence of rate constants (by incorporating theoretical calculations to extrapolate constraints imposed by limited data), and 3) analyzing data from reaction systems involving non-thermal kinetic sequences (by leveraging the physics-based framework to account for such processes). In this program, we are applying and expanding MSI to develop a high-accuracy kinetics database through carefully chosen reaction systems that serve to both anchor the database and grow it in ways leveraging its anchored foundations.

$CH_3 + HO_2 = CH_4 + O_2$, $CH_3 + HO_2 = CH_3O + OH$. We have now completed our analysis^{i,iii} leveraging our earlier MSI model of the H_2O_2 decomposition system^{8,10} to reinterpret data for the $CH_3 + HO_2$ reaction,

for which many experimental rate constant determinations are relatively indirect. In this recent analysis, we incorporated the theoretical treatment of $\text{CH}_3 + \text{HO}_2$ from Jasper and co-workers¹¹ and analyzed raw experimental data^{12,13} originally used to derive rate constants for $\text{CH}_3 + \text{HO}_2$. The general conclusion from this analysis was that, once constraints from theoretical data were imposed, the experiments provided minimal additional information about these rate constants. With minimal changes to the rate constants for $\text{CH}_3 + \text{HO}_2$ reactions, MSI reproduces the raw experimental data^{12,13} as well as the original interpretations.

These results highlight the utility of interpreting the raw data in a manner that leverages information from other sources and quantifies the information content of the data accurately. They similarly also indicate the challenges in constraining rate constants across wide $T/P/X$ ranges and achieving data redundancy necessary to identifying “optimistic” uncertainty assignments – motivating the use of MSI and our planned methodological developments to enable more data types to be used to constrain kinetic parameters.

$\text{HO}_2 + \text{HO}_2 = \text{H}_2\text{O}_2 + \text{O}_2$ and $\text{HO}_2 + \text{HO}_2 = \text{OH} + \text{OH} + \text{O}_2$. For several decades, $\text{OH} + \text{HO}_2 = \text{H}_2\text{O} + \text{O}_2$ (R1) and $\text{HO}_2 + \text{HO}_2 = \text{H}_2\text{O}_2 + \text{O}_2$ (R2) had been topics of significant attention and, frequently, debate. In 1995 and 2002, Troe and co-workers¹⁴⁻¹⁵ provided the first two rate constant determinations at combustion-relevant temperatures by fitting a four-reaction kinetic model to UV-laser-absorption time profiles during shock-heated H_2O_2 decomposition. Debate arose from both rate constants exhibiting unusually deep minima at 1000-1200 K followed by a sharp rise with increasing temperature. The existence, exact value, and exact temperature of these minima were known to have significant modeling implications. In 2006 and 2010, Srinivasan et al.¹⁶ and Hong et al.¹⁷ determined rate constants for R1 at higher temperatures that instead showed little temperature dependence with values close to atmospheric temperature measurements – leading many to suspect that R1 did not exhibit a minimum.

In 2013, our MSI analysis⁸ of previous data and multi-species measurements of shock-heated H_2O_2 decomposition by Hong et al.¹⁸ both yielded rate constants with a local minimum, albeit with much milder temperature dependence, thereby resolving the previous inconsistencies – at least for R1. For R2, the determinations by Hong et al.,¹⁸ whose three time-resolved species measurements appeared likely to fully constrain the four-reaction system, were instead consistent with that of Troe and co-workers.¹⁴⁻¹⁵

Recent theory calculations¹⁹⁻²⁰ reveal consistent values at lower intermediate temperatures but instead show a milder temperature dependence – suggesting that inconsistencies among theoretical and experimental data

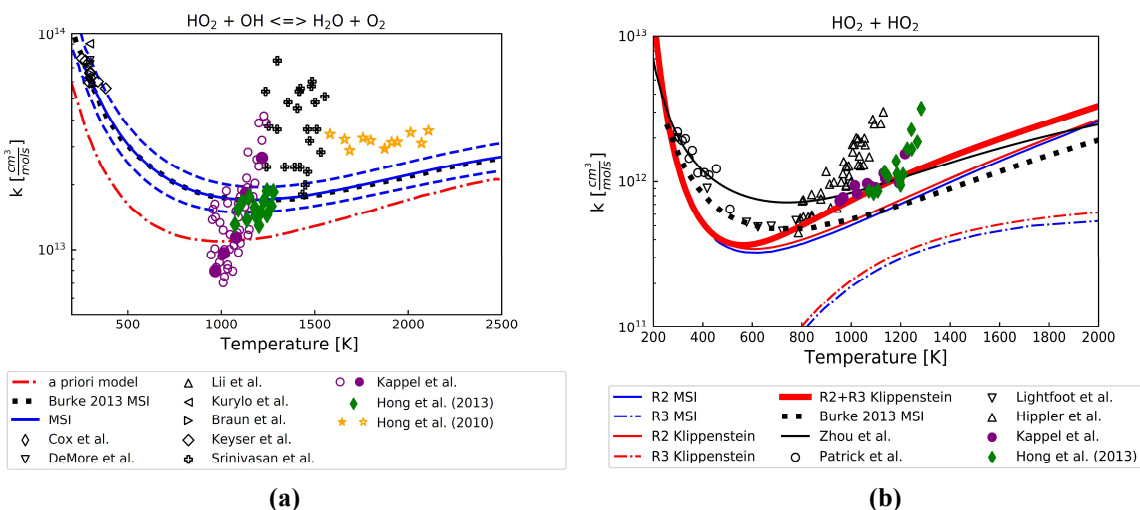


Fig. 1. Rate constants for (a) $\text{OH} + \text{HO}_2 = \text{H}_2\text{O} + \text{O}_2$ (R1) and (b) $\text{HO}_2 + \text{HO}_2$ (R2, R3). Lines represent prior model rate constants (from Klippenstein et al.^{8,20}) and MSI model rate constants. Symbols represent experimental determinations.^{8,14-18} Solid symbols represent experimental determinations^{15,17,18} for which the MSI model reproduces the raw experimental data from^{15,17,18} (e.g. see Fig. 2) with the MSI rate constants shown above.

still remain for R2. Furthermore, calculations of Klippenstein et al.²⁰ indicate a previously unknown channel $\text{HO}_2 + \text{HO}_2 = \text{OH} + \text{OH} + \text{O}_2$ (R3), which may confound all earlier analyses, and likewise reveal additional theory uncertainties of relevance.

We performed an MSI analysisⁱⁱ reinterpreting theoretical and raw experimental data, including data across the full temperature range for the highly constraining multi-species measurements of Hong et al.,¹⁸ with the goal of achieving similar resolution of the remaining apparent inconsistencies for R2 and R3. Our present MSI results (in blue in Figs. 1-2) indicate that the theoretical calculations for R2 and R3 near their nominal values (in red in Fig. 1) exhibit no systematic inconsistencies with the raw experimental data, including at the lowest and highest experimental temperatures of Hong et al.¹⁸

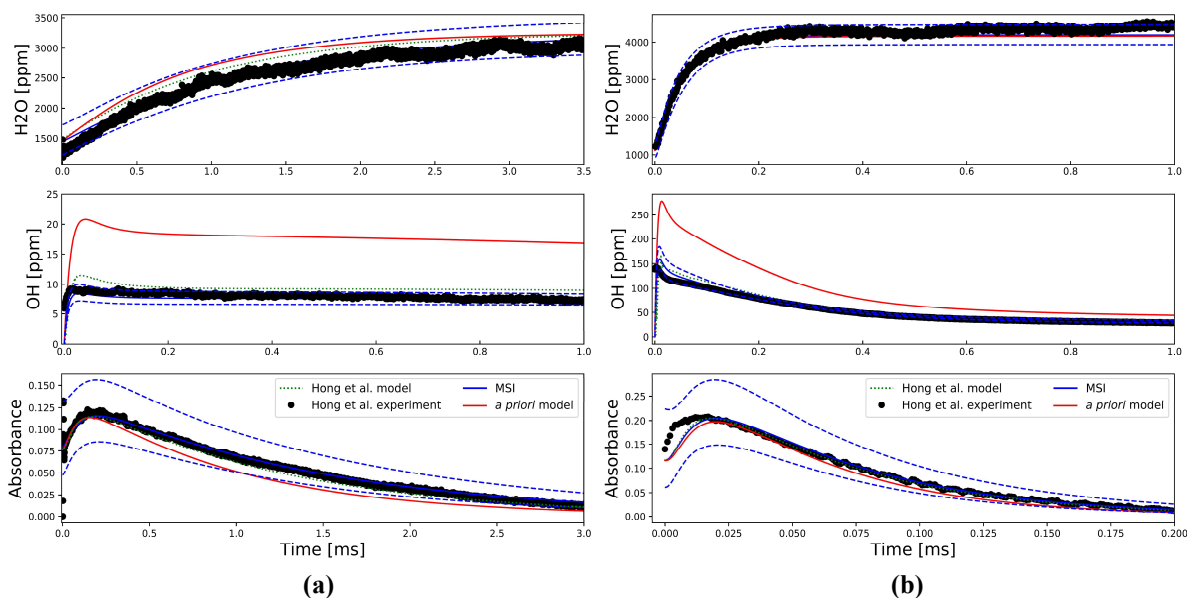


Fig. 2. Time profiles for H_2O , OH , and absorbance at 227 nm in shock-heated $\text{H}_2\text{O}_2/\text{H}_2\text{O}/\text{O}_2/\text{Ar}$ mixtures (a) near 1073 K and 1.786 atm and (b) near 1283 K and 1.635 atm. Symbols denote experimental data from Hong et al.,¹⁸ lines denote the original model interpretations of Hong et al.¹⁸ and predictions of the prior and MSI models.

$\text{H} + \text{O}_2 = \text{OH} + \text{O}$, $\text{OH} + \text{H}_2 = \text{H}_2\text{O} + \text{H}$, $\text{O} + \text{H}_2 = \text{OH} + \text{O}$. We have begun analysis on these three (commonly entangled) chain-branching/carrying reactions important to combustion. We expect that this analysis will benefit from recently added MSI capabilities in simulating raw data (discussed below).

Methodological improvements. We have now completed a rewrite of our MSI code in Python with an emphasis on making the code more modular and, therefore, more amenable to future additions of new data types. To this end, we have now added the functionality to handle measurements of flow reactor time profiles (used for some $\text{CH}_3 + \text{HO}_2$ and $\text{CH}_3 + \text{O}_2$ rate constant determinations) and ignition delay times (used for many $\text{H} + \text{O}_2 (+\text{M}) = \text{HO}_2 (+\text{M})$ rate constant determinations).

We have also begun implementing a procedure (similar in spirit to that of Najm and co-workers²¹) for simulating the raw data from experimental studies, where the raw data were not reported, from information reported in those studies. Our results for analysis of data for $\text{H} + \text{O}_2 = \text{OH} + \text{O}$ yielded posterior probability distribution functions that agree remarkably well with the results from Bayesian inference.²¹ This procedure has recently been part of our standard approach for adding data to the MSI database.

We are also now in the process of creating a general-purpose wrapper for the MESS code²² for automated calculations of non-Boltzmann sequences spanning multiple potential energy surfaces. We hope to make this code available for general use and we plan to incorporate it into MSI for rigorous evaluations of data from reaction systems involving non-Boltzmann kinetic sequences.

Future Plans

In the coming months, we plan to complete our analyses of $\text{HO}_2 + \text{HO}_2$, $\text{H} + \text{O}_2 = \text{OH} + \text{O}$, $\text{OH} + \text{H}_2 = \text{H} + \text{H}_2\text{O}$, and $\text{O} + \text{H}_2 = \text{H} + \text{OH}$ (leveraging new MSI capabilities for simulating raw data) and continue to anchor the database using measurements and theory for $\text{H} + \text{HO}_2 = \text{products}$ and $\text{H} + \text{O}_2 (+\text{M}) = \text{HO}_2 (+\text{M})$ (leveraging new MSI capabilities for including ignition delays among the targets, recent 2D-ME calculations,²³ and mixture rule considerations²⁴).

Afterwards, we plan to continue venturing into less characterized and difficult-to-isolate subsystems, such as those involving CH_3 , CH_2OH , and HCO where the anchored database can be leveraged for the analysis, and then non-equilibrium kinetic sequences. Along the way, we plan to continue methodological improvements to the MSI approach that allow data for collisional energy transfer kernels, product energy distributions, microcanonical rate constants, and photolysis quantum yields, among others, to be included as targets. We anticipate that these data types will allow a greater degree of data redundancy and allow more rigorous evaluations of theoretical methodologies for calculating non-equilibrium kinetic sequences.

References

1. B. Ruscic, R. Pinzon, M. L. Morton, G. Laszevski, S. Bittner, S. G. Nijssure, K. A. Amin, M. Minkoff, A. F. Wagner. *J Phys Chem A* 108 (2004) 9979–9997.
2. M.P. Burke, S.J. Klippenstein. *Nature Chemistry* 9 (2017) 1078–1082.
3. D.R. Glowacki, J. Lockhart, M.A. Blitz, S.J. Klippenstein, M.J. Pilling, S.H. Robertson, P.W. Seakins, *Science* 337 (2012) 1066.
4. M.C. Barbet, K. McCullough, M.P. Burke. *Proc Combust Inst* 37 (2019) 347–354.
5. M.P. Burke, C.F. Goldsmith, Y. Georgievskii, S.J. Klippenstein. *Proc Combust Inst* 35 (2015) 205–213.
6. R.E. Cornell, M.C. Barbet, M.P. Burke. *Proc Combust Inst* (2021) in review.
7. L. Lei, M.P. Burke. *Proc Combust Inst* (2021) in review.
8. M.P. Burke, S.J. Klippenstein, and L.B. Harding. *Proc Combust Inst* 34 (2013) 547–555.
9. M.P. Burke, et al. *J Phys Chem A* 119 (2015) 7095–7115.
10. M.P. Burke. *International Journal of Chemical Kinetics* 48 (2016) 212–235.
11. A.W. Jasper, S.J. Klippenstein, L.B. Harding. *Proc Combust Inst* 32 (2009) 279–286.
12. Z. Hong, D.F. Davidson, K.-Y. Lam, R.K. Hanson. *Combustion and Flame* 159 (2012) 3007–3013.
13. N.K. Srinivasan, J.V. Michael, L.B. Harding, S.J. Klippenstein. *Combust Flame* 149 (2007) 104–111.
14. H. Hippler, H. Neunaber, J. Troe. *J Chem Phys* 103 (1995) 3510–3516.
15. C. Kappel, K. Luther, J. Troe. *Phys Chem Chem Phys* 4 (2002) 4392–4398.
16. N.K. Srinivasan, M.C. Su, J.W. Sutherland, J.V. Michael, B. Ruscic. *J Phys Chem A* 110 (2006) 6602–6607.
17. Z. Hong, S.S. Vasu, D.F. Davidson, R.K. Hanson. *J Phys Chem A* 114 (2010) 5520–5525.
18. Z. Hong, K.-Y. Lam, R. Sur, S. Wang, D.F. Davidson, R.K. Hanson. *Proc Combust Inst* 34 (2013) 565–571.
19. D. D. Zhou, K. Han, P. Zhang, L. B. Harding, M. J. Davis, R. T. Skodje. *J Phys Chem A* 116 (2012) 2089–2100.
20. S. J. Klippenstein, et al. 11th U.S. National Combustion Meeting (2019).
21. M. Khalil, H.N. Najm. *Combust Theor Model* 22 (2018) 635–665.
22. Y. Georgievski, J.A. Miller, M.P. Burke, S.J. Klippenstein. *J Phys Chem A* 117 (2013) 12146–12154.
23. M. Verdicchio, A.W. Jasper, et al. manuscript in preparation.
24. L. Lei, M.P. Burke. *Combust. Flame* 213 (2020) 467–474.

BES-supported products (9/2018-present)

- i. C.E. LaGrotta, M.C. Barbet, L. Lei, M.P. Burke. Towards a High-Accuracy Kinetic Database Informed by Theoretical and Experimental Data. 11th U.S. National Combustion Meeting, March 2019, Pasadena, CA.
- ii. C.E. LaGrotta, L. Lei, M.C. Barbet, Z. Hong, D.F. Davidson, R.K. Hanson, M.P. Burke. Towards Resolution of Lingering Discrepancies in the H_2O_2 Decomposition System: $\text{HO}_2 + \text{HO}_2$. 2020 Spring Technical Meeting of the Eastern States Section of the Combustion Institute, Columbia, South Carolina, March 2020.
- iii. C.E. LaGrotta, M.C. Barbet, L. Lei, M.P. Burke, “Towards a High-Accuracy Kinetic Database Informed by Theoretical and Experimental Data: $\text{CH}_3 + \text{HO}_2$ as a Case Study,” accepted for presentation at the 38th International Symposium on Combustion, in review for *Proceedings of the Combustion Institute* (2020).

Kinetics and Mechanisms of Gas-Phase Reactions towards Gas-Particle Interconversion

Rebecca L. Caravan
Chemical Sciences and Engineering Division
Argonne National Laboratory
Lemont, IL 60439
caravarl@anl.gov

Program scope. I am developing a new experimental program to study the kinetics and mechanisms of gas-phase reactions involving reactive intermediate species. Experiments will interrogate the reactivity of zwitterions and radical intermediates to understand the different roles that they play in phenomena such as gas-particle transformations in complex environments. Through synergistic collaborations with theoreticians the influence of, for example, zwitterion vs. radical character and chemical structure on reactivity will be explored for potential molecular-weight growth reactions. This will deduce the chemical physics driving gas-particle interconversion, and ultimately it will aid the development and validation of predictive capabilities. Interdisciplinary collaborations will address the wider implications of our work, answering questions that are both interesting at a fundamental level and that have broader implications.

Understanding the chemical mechanisms driving gas-to-particle conversion underpins one of the four basic science research thrusts of the DOE Gas Phase Chemical Physics research program. In some complex environments, such as Earth's troposphere, sequential oxidation of volatile organic compounds (VOCs) leads to the formation of highly oxygenated, lower volatility molecules that experimental studies have pointed to as key precursors to the formation of particulate matter (PM).¹ With a sufficiently high O:C ratio and low volatility, these species will undergo condensation leading to PM formation and growth. However, the sequential chemical mechanisms leading to their formation remain uncertain.¹

Longer timescale experiments to examine complete oxidation processes under ambient conditions (i.e., using atmospheric simulation chambers) can be utilized to provide insight into the interactions between competing and coupled reactions. They have facilitated the determination of key potential chemical precursors for PM generation, by using scavengers to isolate the role of intermediate-specific chemistry. Specifically, researchers have identified the role of alkyl peroxy (ROO) and Criegee intermediate (CI) initiated chemistry (originating from the OH and O₃ initiated oxidation of VOCs, respectively) in PM formation.¹⁻⁴ However, complex chemical models are often needed to interpret and extract information from such experiments, due to the multiple competing reactions on the long reaction timescales on which these experiments are performed. This leads to limited mechanistic and kinetic insight, inhibiting direct comparisons with theoretical work.

The chemical reactions within sequential pathways leading from VOCs through to highly oxygenated, low volatility molecules need to be individually characterized and assessed, so that predictive theoretical methodologies for gas-to-particle transformations can be developed and validated. This requires comprehensive direct studies of targeted single reaction steps – using photolytic precursors to generate reactive intermediates – to elucidate the chemical mechanisms and obtain crucial reaction parameters, such as rate coefficients and product branching ratios.

The first setup I am constructing to address this research objective is a broadband UV-Visible time-resolved absorption experiment. This will enable kinetics and mechanistic studies using multiplexed species detection over a broad range of temperatures and pressures. This technique has been demonstrated to be a versatile and powerful approach for kinetics studies of reactive intermediates — and my new experimental setup will incorporate elements from the recent successful designs of Sheps⁵ and other groups⁶ worldwide. Direct generation of reaction intermediates from photolytic precursors sets an unambiguous reaction start time, thus enabling time-resolved absorption spectra to be obtained with sub-millisecond time resolution. Through collaborations with experimentalists and theorists in the Argonne Chemical Physics in the Gas Phase group and elsewhere, we will gain fundamental chemical physics insights into what drives and

influences reaction kinetics and mechanisms of intermediates. For example, my experimental work at Argonne is complemented by ongoing collaborative work I am part of at the Advanced Light Source (Lawrence Berkeley National Laboratory) with research teams from across the program (Klippenstein, Lester, Osborn, Sheps & Taatjes), and collaborators in the atmospheric chemistry community.

Recent Progress. In parallel with developing the new capabilities at Argonne, I have been continuing investigations of zwitterion reactivity with Klippenstein, Lester, Osborn, Sheps, Taatjes, and further collaborators outside the program.

Our recent work includes the first direct kinetic measurements of the *syn*-conformer of the isoprene-derived four-carbon resonance-stabilized CI, methyl-vinyl ketone oxide (MVK-oxide), following on from the first direct production and spectroscopic characterization by Lester. Direct kinetic measurements were performed using the broadband UV-Visible time-resolved experiment of Sheps, and complemented by mechanistic and product investigations at the Advanced Light Source MPIMS experiment of Osborn and Taatjes. The experimental work was complemented by high-level theoretical investigations performed by Klippenstein, which together revealed the chemical reactivity of MVK-oxide to be distinct from smaller, H- or alkyl-substituted CIs, due to the conjugation of the unsaturated side-chain with the CI COO functional group. For reactions with submerged barriers (e.g. SO₂ and formic acid), the overall rate coefficients are not significantly altered compared to unconjugated CIs. In contrast, the reaction of MVK-oxide with water — which has a positive barrier to reaction — is found to be at least 3 orders of magnitude slower than for the simplest CI, CH₂OO. This has significant implications for our understanding of the role of CI chemistry in gas-particle interconversion in complex environments. For example, reaction with water and unimolecular decomposition have previously been assumed to be the dominant loss processes of all CIs in the atmosphere, yet MVK-oxide (which we find reacts very slowly with water), has the highest steady-state atmospheric concentration of all CIs.

Our results, together with the prior work of Lester, demonstrate that the *syn* conformer of MVK-oxide will survive high-humidity environments, implying that bimolecular reactions with other chemical species, such as organic acids, are more important than previously thought. Our experimental and theoretical investigations reveal the reaction of MVK-oxide with formic acid leads to the formation of a highly oxygenated and higher molecular weight functionalized hydroperoxide species, via a novel 1,4-insertion mechanism. Functionalized hydroperoxides have been implicated as potentially important precursors in gas-particle conversion.

Future Directions. Immediate future work includes the completion of the renovation of a new laser laboratory at Argonne in collaboration with Tranter, in which we will both set up new experimental capabilities for chemical kinetics and mechanistic studies. The design of the new broadband absorption experiment will be finalized, and its construction will begin in the new laboratory space. In parallel, ongoing collaborations at the Advanced Light Source will continue to support the goals of this new research direction.

DOE Supported Publications 2020

1. R. L. Caravan, M. F. Vansco, K. Au, M. A. H. Khan, Y.-L. Li, F. A. F. Winiberg, K. Zuraski, Y.-H. Lin, W. Chao, N. Trongsirawat, P. J. Walsh, D. L. Osborn, C. J. Percival, J. Jr-Min Lin, D. E. Shallcross, L. Sheps, S. J. Klippenstein, C. A. Taatjes & M. I. Lester, Direct kinetic measurements and theoretical predictions of an isoprene-derived Criegee intermediate, *Proceedings of the National Academy of Sciences*, 2020 (DOI: 10.1073/pnas.1916711117).
2. M. F. Vansco, R. L. Caravan, K. Zuraski, F. A. F. Winiberg, K. Au, N. Trongsirawat, P. J. Walsh, D. L. Osborn, C. J. Percival, M. A. H. Khan, D. E. Shallcross, C. A. Taatjes & M. I. Lester, Experimental evidence of dioxole unimolecular decay pathway for isoprene-derived Criegee intermediates, *Journal of Physical Chemistry A*, 2020 (DOI: 10.1021/acs.jpca.0c02138).

References

1. M. Ehn, T. Berndt, J. Wildt & T. Mentel, Highly oxygenated molecules from atmospheric autoxidation of hydrocarbons: a prominent challenge for chemical kinetics studies, *International Journal of Chemical Kinetics*, **49(11)**, 821-831 (2017).
2. Y. Sakamoto, S. Inomata & J. Hirokawa, *Journal of Physical Chemistry A*, **117(48)**, 12912-12921 (2013).
3. Y. Zhao, L. M. Wingen, V. Perraud, J. Greaves & B. J. Finlayson-Pitts, *Physical Chemistry Chemical Physics*, **17**, 12500-12514 (2015).
4. M. Ehn *et al.*, *Nature*, **506**, 476 (2014).
3. M. Zeng, N. Heine & K. R. Wilson, *Proceedings of the National Academy of Sciences*, **117(9)**, 4486-4490, 2020.
5. L. Sheps & D. W. Chandler, Time-resolved broadband cavity-enhanced absorption spectroscopy for chemical kinetics, SAND2013-2663, *Sandia National Laboratories*, 2013.
6. T. Lewis, D. E. Heard & M. A. Blitz, A novel multiplex absorption spectrometer for time-resolved studies, *Review of Scientific Instruments*, **89**, 024101 (2018).

ADVANCED DIAGNOSTICS

David W. Chandler, Jonathan H. Frank, Nils Hansen, Christopher J. Kliewer, Habib N. Najm, David L. Osborn, Krupa Ramasesha, Leonid Sheps, Craig A. Taatjes, Timothy S. Zwier
Combustion Research Facility, Sandia National Laboratories, MS 9055, Livermore, CA 94551-0969
chand@sandia.gov, jhfrank@sandia.gov, nhansen@sandia.gov, cjkliew@sandia.gov,
hnnajm@sandia.gov, dlosbor@sandia.gov, kramase@sandia.gov, lsheps@sandia.gov,
cataatj@sandia.gov, tszwier@sandia.gov

PROGRAM SCOPE

A unifying theme throughout the experimental work in this task is the need for incisive advanced diagnostics that illuminate the hidden world of molecules. Over the years, our program has made many innovations that support chemical physics research in areas such as non-linear spectroscopy, ion imaging, 3-dimensional laser-induced fluorescence, multiplexed photonization / photoelectron spectroscopy, and x-ray absorption and scattering. These approaches include *in situ* laser and light source-based techniques that directly probe reacting environments, and *ex situ* techniques that extract species from reactive environments before implementing diagnostics that would be impossible under the native conditions of the chemical reaction. We leverage these experimental innovations with theoretical advances that predict dynamics and kinetics to compare with experiment, and to inform the improvement of diagnostics. Our recent work in optimal experimental design adds a new dimension to the coupling between experiment and theory, providing a feedback loop to optimize an experiment, thereby maximizing extracted information and quantifying uncertainty. Our proposed research includes new developments in areas where we are well established, and additional ideas that broaden our work on both ends of the electromagnetic spectrum. Ultrafast non-linear spectroscopy in the soft and hard x-ray region is a new area of emphasis, as well as combining broadband microwave spectroscopy with specialized molecular sources to enable new spectroscopy of reactive intermediates. As these advanced diagnostics mature, they provide the new tools that enable deeper exploration in Gas Phase Chemical Physics

RECENT PROGRESS

Bayesian Optimal Experimental Design, Application to Time-of-Flight Mass Spectrometry We worked on development of a Bayesian optimal experimental design method targeting high-pressure photolysis reaction measurement using time of flight mass spectrometry (TOFMS). We have modeled the system, including both the reactor and the TOFMS instrument, accounting for uncertainty in initial conditions and system parameters. Relying on Bayesian inference with Gaussian process modeling of discrepancies between data and model predictions, we completed the representation of the pre-photolysis data. We have also begun the study of Hamiltonian Monte Carlo methods for handling of high-dimensional integrals, a necessity for the ultimate experimental design work.

Building a Time-Resolved Photoelectron Photoion Coincidence Spectrometer Our earlier work building and testing a prototype PEPICO spectrometer at the Swiss Light Source evaluated all the design aspects before finalizing plans for a new time-resolved PEPICO spectrometer. This year we have designed and built, but not yet commissioned, this new instrument. We designed the apparatus to enable experiments both at Sandia and at the Chemical Dynamics Beamline of the Advanced Light Source Synchrotron of Lawrence Berkeley National Laboratory, where tunable vacuum ultraviolet photons maximize the power of the instrument. We have made many design improvements based upon the experience we obtained during the prototype phase. First, the new apparatus has 80 mm diameter time- and position-sensitive detectors for velocity map imaging of both cations and electrons, compared to 40 mm detectors on the prototype. Our simulations predict that the larger diameter will enable collection of fixed-frequency excitation photoelectron spectra directly from velocity-mapped electron images for photoelectrons with 0 – 4 eV kinetic energy obtaining energy resolution of $\Delta E/E \sim 1\%$. Obtaining photoelectron fingerprint

spectra without the need for synchrotron-produced tunable VUV photons will provide significantly improved productivity, enabling experiments at Sandia using fixed-frequency VUV photon sources.

PROPOSED WORK

Bayesian Optimal Experimental Design, Application to Time-of-Flight Mass Spectrometry We will proceed with the application of Bayesian optimal experimental design to high-pressure photolysis reaction measurements using time of flight mass spectrometry. We will work on Bayesian modeling of the post-photolysis data, and will establish the validity of the construction using targeted measurements. These results will bring us to the actual experimental design activity, which will require development of efficient statistical estimation of marginal likelihoods, thereby facilitating computation of expected information gain for any proposed design. In this regard, we will continue our current work with efficient adaptive Hamiltonian Monte Carlo sampling, and will explore the use of polynomial chaos surrogates for efficient representation of the marginal likelihood.

Characterizing the new Photoelectron Photoion Coincidence Spectrometer In the next year we will fully characterize the new instrument PEPICO instrument, both at Sandia and at the Chemical Dynamics Beamline of the Advanced Light Source (ALS). Our dual goals of high mass resolution for cations concurrent with high kinetic energy resolution for electrons necessitates the use of many ion / electron optic plates surrounding the point of ionization. Our final design has 48 total plates so that the electric field gradients provide Wiley-McLaren space focusing (for good mass resolution), whereas curved lines of equipotential form electrostatic lenses later in the flight path for dual (and independent) velocity map imaging of electrons and cations. Our first goal, therefore, is to test this operation on simple systems. At the ALS, where we can utilize tunable, monochromatized VUV radiation, ionization of the rare gases Ar, Kr, and Xe from a supersonic expansion source will allow us to optimize both mass resolution and velocity mapping of cations and electrons.

Ultrafast soft X-ray core-level transient absorption spectroscopy of chemical dynamics Core-to-valence transient absorption spectroscopy combines the element-specificity of core orbitals with the sensitivity of valence orbitals to bonding environment, making this technique a powerful, site-specific probe of non-adiabatic dynamics. We will build a source for ultrafast soft X-ray pulses spanning ~150-350 eV for use in core-to-valence transient absorption spectroscopy at the sulfur L- and the carbon K-edges of gas phase molecules. A grant from Sandia's Laboratory-Directed Research and Development program is funding the construction of an apparatus for high harmonic generation (HHG) of extreme ultraviolet pulses (XUV, ~30-110 eV) and transient absorption spectroscopy. Pushing the photon energies into the soft X-ray regime requires driving HHG using near-infrared pulses, because the high harmonic cut-off photon energy is proportional to the square of the wavelength of the HHG driver pulses. However, the efficiency of HHG drops precipitously with increasing wavelength of the HHG driver pulses, to the inverse sixth power of the wavelength of HHG driver pulses. This fact necessitates the use of a high-power source of near-infrared pulses to produce sufficient soft X-ray flux for use in pump-probe experiments. Upgrading our XUV apparatus to generate soft X-ray pulses therefore requires a high-power ultrafast laser system coupled to a high-power optical parametric amplifier (OPA). The BES GPCP program has funded the purchase of a carrier-envelope-phase stabilized 13 W laser system, which will soon be installed. This laser will pump an existing high-energy commercial OPA (HE-TOPAS-Prime Plus, Light Conversion), which generates near-infrared pulses ranging in wavelength from 1100 nm to 2600 nm. The near-infrared pulses will be used for driving HHG in helium gas maintained at near-atmosphere pressure in a semi-infinite gas cell. The rest of the apparatus will be largely unchanged from XUV operation, except for small changes to the X-ray spectrometer alignment to allow for high photon energy detection.

Broadband Microwave Spectroscopy for Isomer-specific Detection of Transient Intermediates With the aim of developing complementary techniques to photoionization/photoelectron spectroscopies, we propose a research program built on the newly developed chirped-pulse Fourier transform microwave (CP-FTMW)

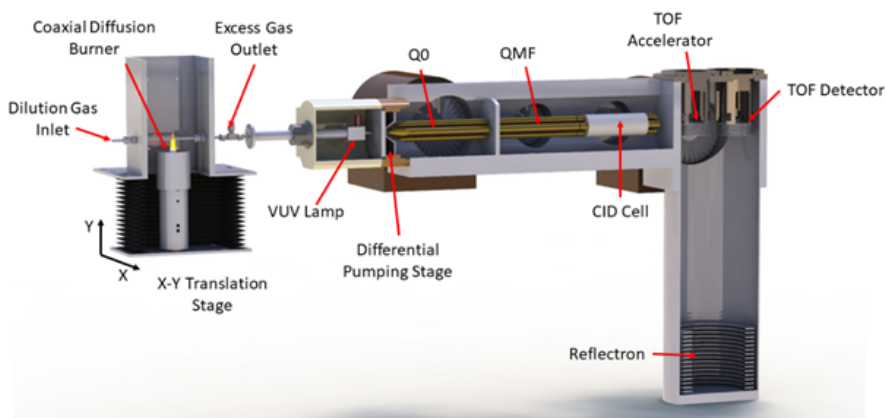
technique. As a basis for this program, an existing CP-FTMW spectrometer has been transferred from Purdue University that covers a frequency range from 2-18 GHz. A unique feature of this instrument is its combination with VUV photoionization (118 nm) time-of-flight mass spectrometry, enabling the detection of mass-correlated broadband microwave spectra. The VUV TOF mass spectrum is a means of identifying and optimizing new microwave transitions that have the same dependence on source conditions as a particular mass in the TOF mass spectrum. There are significant opportunities for application of CP-FTMW spectroscopy to reacting mixtures that contain free radicals or other highly reactive intermediates. In exploratory work, we combined an atmospheric pressure jet-stirred reactor (JSR) with the broadband chirped-pulse microwave spectrometer to identify key reactive intermediates in low-temperature and ozone-assisted oxidation processes. For additional source flexibility, we propose to couple CP-FTMW detection with two chemical reactors in addition to the JSR: a flash pyrolysis nozzle and a fast-flow reactor (in each case, developing appropriate interfaces for optimized detection of intermediates). In parallel, we propose to build a cryo-cooled buffer gas cell outfitted for microwave interrogation, as a complementary scheme to supersonic expansion for cooling reactive intermediates.

The injection of the effluent from any of these sources into a cryo-cooled buffer gas cell offers improvements in sensitivity that we will explore. Compared to a pulsed supersonic expansion, injection into the buffer gas cell cools the molecules and holds them in the cell for much longer interrogation times (>10 ms) before removal on the cold walls. This makes it possible to interrogate at 50 kHz repetition rate (for a 20 μ s free induction decay), with the same molecules contributing to the signal throughout their residence time in the cell. With careful attention to noise reduction in the electronics and to maximizing residence times, the recent characterization of Porterfield *et al.* indicates that the combination of a buffer gas cell with broadband techniques offers sensitivity comparable to high-Q cavity microwave spectrometers. We propose to target initially, in a ZrO₂ flash pyrolysis source, a series of reactions of the resonance-stabilized radicals (RSRs) propargyl (C₃H₃), cyclopentadienyl (C₅H₅), and benzyl (C₇H₇) with O₂. Secondly, we propose to study the microwave spectra of select organic peroxy radicals, RO₂. When R=cyclohexyl radical, we anticipate the presence of up to six different conformeric structures of the peroxy radical involving boat, chair, and twist ring conformations, with the O₂ attached at either the axial or equatorial sites, putting the microwave detection scheme to a challenging test.

Finally, we will apply the broadband microwave detection scheme to the analysis of oxidation reactions in their full complexity using a recently-developed, small-volume (~1 cm³) high-pressure laminar flow reactor (HPFR), capable of operating at up to 100 bar and 1000 K. The HPFR was built by Sheps using LDRD funding in 2019. To demonstrate the feasibility of this idea, we will quantify the formation of several crucial early intermediates in diethyl ether oxidation.

APPI-Tandem Mass Spectrometry for Molecular-Weight Growth Reactions To address fundamental issues in more complex molecular systems, i.e. molecular-weight growth reaction networks, our current experimental techniques might not be feasible to provide the necessary level of detail with the desired accuracy. Therefore, to complement and extend photoionization spectroscopy, PEPICO, and rotational spectroscopy, we propose to add tandem mass spectrometry to our array of diagnostic techniques. The experimental apparatus, built with funds from Sandia's LDRD program, is shown schematically below. The mass spectrometer consists of an atmospheric pressure photoionization (APPI) source, a quadrupole mass filter, a collision cell filled with Ar for the collision-induced dissociation (CID) process, and a reflectron time-of-flight spectrometer to mass analyze the ions. In the APPI source, flame-sampled species are ionized using 10.0 eV photons from a continuous vacuum-ultraviolet (VUV) Kr discharge lamp. This energy is sufficient to ionize targeted aromatic and highly oxygenated species. After the quadrupole mass filter ($\Delta m \sim 1$), the ions of the respective flame-sampled components are accelerated into the argon-filled CID cell, where they undergo fragmentation into a neutral and an ion fragment. The velocity of the ions, which controls the collision energy, can be scanned automatically to allow for an assessment of the respective strength of the breaking bond. The fragment ion is then extracted into a high-resolution reflectron time-of-

flight mass spectrometer ($m/\Delta m \sim 8000$) and these fragment mass spectra can be used to extract structural information on the sampled components, as successfully shown with the identification of aliphatically bridged and aliphatically substituted PAHs.



We propose to modify the interface to the APPI source to allow for sampling from flash pyrolysis sources for the investigation of radical-radical and radical-molecule reactions in high-temperature hydrocarbon rich environments. The emphasis of this work will be on the detection

of aliphatically bridged multi-core PAHs, and on the identification of cross-linked PAHs, which are the centerpieces in the proposed radical-radical chain reaction sequence for soot formation.

Furthermore, we propose to follow low-temperature oxidation chemistry and the various O_2 addition sequences by interfacing a jet-stirred reactor with the tandem mass spectrometer. This approach is motivated by the fact that the 3rd O_2 addition reaction products have only been observed in such zero-dimensional reactors and by the opportunities tandem mass spectrometry offers for unraveling the molecular structures of the complex intermediates. The first targets include the oxidation of neo-pentane and cyclohexane.

BES-sponsored publications, 2018 – present

1. S. M. Fritz, P. Mishra, J. Wullenkord, P. G. Fugazzi, K. Kohse-Höinghaus, T. S. Zwier, N. Hansen, Detecting Combustion Intermediates Via Broadband Chirped-Pulse Microwave Spectroscopy, *Proceedings of the Combustion Institute*, submitted.
2. B. Zhou, T. Li, J. H. Frank, A. Dreizler, B. Bohm, Simultaneous 10 kHz three-dimensional CH₂O and tomographic PIV measurements in a lifted partially-premixed jet flame, *Proceedings of the Combustion Institute*, submitted.
3. T. Li, B. Zhou, J. H. Frank, A. Dreizler, B. Böhm, High-speed volumetric imaging of formaldehyde in a lifted turbulent jet flame using an acousto-optic deflector, *Exp. Fluids* **2020**, 61 (4), 112.
4. N. Hansen, R. S. Tranter, J. B. Randazzo, J. P. A. Lockhart, and A. L. Kastengren, Investigation of sampling-probe distorted temperature fields with X-ray fluorescence spectroscopy, *Proc. Combust. Inst.*, **2019**, 37, 1401-1408.
5. B. Zhou, A. J. Ruggles, E. Huang, J. H. Frank, Wavelet-based algorithm for correction of beam-steering artefacts in turbulent flow imaging at elevated pressures. *Exp. Fluids* **2019**, 60 (8), 136.
6. T. C. W. Lau, J. H. Frank, G. J. Nathan, Resolving the three-dimensional structure of particles that are aerodynamically clustered by a turbulent flow. *Phys. Fluids* **2019**, 31 (7), 071702.
7. K. Voronova, K. M. Ervin, K. G. Torma, P. Hemberger, A. Bodi, T. Gerber, D. L. Osborn and B. Sztáray, Radical thermometers, thermochemistry, and photoelectron spectra: A photoelectron photoion coincidence spectroscopy study of the methyl peroxy radical, *J. Phys. Chem. Lett.*, **2018**, 9, 535.
8. L. G. Dodson, J. D. Savee, S. Gozem, L. Shen, A. I. Krylov, C. A. Taatjes, D. L. Osborn, and M. Okumura, Vacuum ultraviolet photoionization cross section of the hydroxyl radical, *J. Chem. Phys.* **2018**, 148, 184302.

CHEMICAL DYNAMICS METHODS AND APPLICATIONS

David W. Chandler, Jonathan H. Frank, Laura M. McCaslin, David L. Osborn, Leonid Sheps, Judit Zádor,
Timothy S. Zwier

Sandia National Laboratories, MS 9051, Livermore, CA 94551-0969

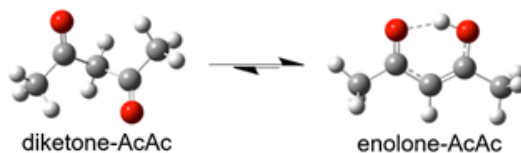
chand@sandia.gov, jhfrank@sandia.gov, lmccas@sandia.gov, dlosbor@sandia.gov,
lsheps@sandia.gov, jzador@sandia.gov, tszwier@sandia.gov

PROGRAM SCOPE

This program focuses on the chemical dynamics of gas phase molecular species, the detailed study of the motion of molecules and atoms on inter- or intra-molecular potential energy surfaces to learn about the details of the surface as well as the dynamics of their interactions. This task studies processes, typically at a single-collision or quantum state-resolved level, that underlie the complex reactions and processes studied in the “Chemical Kinetics for Complex Systems” task. Advanced optical techniques reveal the detailed motion of matter and energy within and between molecules, enabling direct comparison with theoretical predictions. The studies here are on time scales slower than atomic motions and generally reflect study of initial reagent preparation and final product detection. Atomic motion time scale studies are reported in the Ultrafast Physics (energy flow) and Ultrafast Chemistry (atomic motion) tasks. Our program includes detailed investigations into energy transfer processes in photodissociation, inelastic and reactive molecular scattering, electron scattering and dissociative electron attachment, ionization, and molecular alignment by light-matter interactions. We use a suite of multiplexed spectroscopy and mass spectrometry techniques in combination with molecular dynamics simulations to provide fundamental insights into reaction dynamics, often relying on methods developed in the Advanced Diagnostics task. Velocity mapped imaging (VMI) of ions and electrons is used in single and crossed molecular beam configurations to provide time-resolved velocity measurements of products. Time-resolved multiplexed photoionization mass spectrometry (MPIMS) provides a universal method to sensitively and selectively probe chemical reactions and reaction intermediates. Advances in photoelectron photoion coincidence spectroscopy (PEPICO) provide a powerful tool for time-resolved probing of gas phase chemical reactions with superior performance in many areas compared to MPIMS. A multi-stage mass spectrometer outfitted with a cryo-cooled ion trap is used for laser spectroscopy and dynamics of large ions and ion complexes.

RECENT PROGRESS

Acetylacetonone: Rich Photochemistry in a Bifunctional Molecule Acetylacetonone (AcAc, pentane-2,4-dione) is the smallest β -diketone, but in the gas phase at 300 K, it exists predominantly in its enolone form, as shown below, which is stabilized by both conjugation and an internal hydrogen bond.



We became interested in the photochemistry of this molecule because it contains structural elements of carbonyls (the C=O bond), alkenes (C=C bond), conjugated polyenes (O=C-C=C π molecular orbitals), and enols (C=C-OH group). The photochemistry of these first three groups are well studied, and we wished to learn which aspects of AcAc’s electronic and molecular structure determine its photochemistry. Most of the previous literature describing dynamics following excitation of the strong, structureless $\pi\pi^*$ ($S_2 \leftarrow S_0$) transition, concluded that OH loss by simple bond cleavage from the enolone isomer is the only product channel. These previous investigations determined the C-OH bond strength experimentally and theoretically to be ~ 90 kcal \cdot mol $^{-1}$. We utilized three complementary time-resolved methods to study this system following 266 and 248 nm excitation: 1) multiplexed vacuum ultraviolet (VUV) photoionization mass spectrometry, 2) VUV photoelectron photoion coincidence (PEPICO) spectroscopy, and 3) infrared (IR) absorption spectroscopy of OH X($^2\Pi$). Our results reveal a much richer photochemistry than

previously appreciated. We observed 15 unique products representing 6 one-photon product channels. In addition, we observed several two-photon product channels that were previously assumed by others to result from absorption of a single photon. PEPICO spectroscopy provides the best spectral fingerprints to make isomer-specific assignments of these product channels. Finally, our use of photoionization spectroscopy shows that distinct daughter ions arise from each of the two neutral AcAc tautomers via dissociative ionization. From the temperature dependence of these daughter ion signals, we measured the equilibrium constant of this keto-enol tautomerization on S_0 from 320 to 600 K and extract $\Delta H = 4.1 \pm 0.3 \text{ kcal}\cdot\text{mol}^{-1}$, and $\Delta S = 6.8 \pm 0.5 \text{ cal}\cdot\text{mol}^{-1}\cdot\text{K}^{-1}$ using a van't Hoff analysis.

Alignment of the Hydrogen molecule in the electronically excited E, F state Stereochemistry has been the subject of chemist investigation for years. With the advent of lasers that could produce strong electromagnetic fields there was opportunity to create alignment of a molecule. Alignment and orientation of molecules has been achieved in collisions, by static electric fields and by optical fields. In particular, intense off-resonant laser fields can align molecules due to the difference in the polarizability of the molecule along a bond versus perpendicular to that bond. We report this sort of strong field alignment on the hydrogen molecule by non-resonant 1064-nm radiation after first being excited to the (E,F) electronic state. This work builds upon an earlier one-color experiment where alignment was studied with 532-nm light. Our findings support previous theoretical predictions that the (E,F) state is easily mixed with nearby B and C states and that this mixed state is extremely polarizable, therefore making H_2 easy to align when initially promoted to this state having a 200 ns lifetime. The angular distributions were described by a two-state model involving the Stark mixing of the initially-prepared $J = 0$ with the $J = 2$ rotational state. This model is able to reproduce all of the observed H^+ angular distributions, and permits us to extract from the fit the polarizability anisotropy of H_2 (E,F) electronic state that is mixed with the nearby B and C states to be $(3.7 \pm 1.2) \times 10^3 \text{ A.U.}$ Because this value is extremely large in comparison to what one would expect from the pure H_2 (E,F) electronic state, we hypothesize that this enhancement comes from the 1064-nm radiation mixing nearby electronic states with the (E,F) state, generating a mixed state (E,F**) with an extremely large polarizable anisotropy. H_2 excited to the (E,F) state is easier to align, by an order of magnitude, than any molecule in its ground electronic state. We submitted a manuscript to Molecular Physics in collaboration with the group of Dr. Peter Rakitzis of the University of Crete.

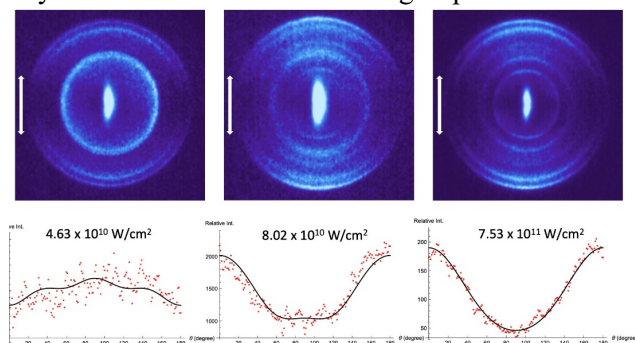


Figure Caption: Population distribution as a function of 1064-nm field value. White arrows indicate the laser polarization (vertical). Only the ring of H^+ that is brightest on the left most panel is analyzed. At lower intensities (left) the population has a major distribution orthogonal to the laser field and peaks on the horizontal axis. At intermediate energies (middle), it peaks vertically but isn't yet saturated. At the highest energies, the horizontal population is depleted and all of the prepared (E,F) H_2 is aligned.

QOOH Thermochemistry and Evidence for Roaming Dynamics QOOH radicals are central to low-temperature autooxidation. QOOH radicals typically decompose rapidly to form $\text{OH} + \text{radical}$ or $\text{HO}_2 + \text{closed-shell bimolecular pairs}$. Perhaps not surprisingly, accurate experimental thermodynamic parameters are absent in the literature for QOOH radicals. In collaboration with Bálint Sztáray (University of the Pacific) we studied the dissociative photoionization processes of methyl hydroperoxide, the smallest organic hydroperoxide, because its first dissociative ionization channel leads to CH_2OOH^+ , the smallest QOOH radical's cation. We used a combination of theory and experiment to arrive at an accurate mixed

resolution. Corresponding electronic structure calculations will be performed to investigate these pathways. *Ab initio* molecular dynamics (AIMD) simulations will be performed to investigate timescales and mechanisms of processes of vibrationally quasi-stable and electronically stable anions.

Related studies will utilize complexes of Kr or Xe with small to moderate sized molecules in which the Kr/Xe will be electronically excited to an electronic state where there is competition between exciting a charge transfer state of the complex and Penning ionization (a two-electron process) of the molecule. Monitoring this competition will provide information on non-Born Oppenheimer effects in chemistry. All of these studies will be accompanied by high-level excited state calculations to investigate energetics and locate regions of the PES where conical intersections and avoided crossings occur, requiring treatment of non-adiabatic effects, as described in the Ultrafast Chemistry task.

In a new set of experiments designed to measure the pair-correlation function in molecule-molecule scattering, and to observe resonances in collisional processes, we will utilize ultra-high-resolution infrared quantum cascade lasers that counter-propagate against the molecular beam to vibrationally excite molecules. This geometry allows the laser beam to Doppler select molecules in the molecular beam with milliKelvin velocity distributions. These molecules (initially NO) will then collide with a speed-chirped molecular beam of molecules at a small crossing angle in order to obtain very high scattering velocity resolution. This resolution will mean that we should be able to resolve the quantum states of the scattering partner in the quantum state of the detected molecule. Such observations have only previously been achieved for molecules (excluding H₂) with the use of a complicated Stark decelerator. The capability will allow us to study potential energy surfaces of molecule-molecule interactions where all previous measurements were with atom-molecule systems.

New experiments involving electronic energy transfer between chromophores attached to a stiff scaffold will be initiated to study the mechanism for energy transfer when nearly identical chromophores span a range of separations. Unlike previous FRET experiments using two fluorescing molecules, we will study energy transfer between chromophores of a cryo-cooled ion, in which energy transfer breaks a bond adjacent to the acceptor molecule. Since we operate under cryo-cooled conditions, we can selectively excite single vibronic levels of the chromophores, and do not need donors and acceptors to absorb at very different wavelengths in order to assign fluorescence to the donor or acceptor. As a result, we can explore circumstances in which subtle energy differences between the chromophores makes vibronic coupling important. For instance, we can deuterate one ring and not deuterate another in order to study electronic energy transfer between them after selective excitation of *either* chromophore. We plan to build up arrays of nearly identical chromophores, much as exist in photosynthetic reaction centers, but selectively excite one and watch where the energy transfers by the distribution of side chain breakage at each chromophore. These experiments are made possible by the combination of a new cryo-cooled ion spectrometer and access to tethered helices synthesized to place UV chromophores at specific locations.

BES-sponsored publications, 2018 – present

- 1) To Boldly Look Where No One Has Looked Before: Identifying the Primary Photoproducts of Acetylacetone, I. Antonov, K. Voronova, M. W. Chen, B. Sztaray, P. Hemberger, A. Bodi, D. L. Osborn, and L. Sheps, *J. Phys. Chem. A* **123**, 5472 (2019).
- 2) Non-intuitive rotational reorientation in collisions of NO(A²Σ⁺) with Ne from direct measurement of a four-vector correlation, T. R. Sharples, J. G. Leng, T. F. Luxford, K. G. McKendrick, P. G. Jambrina, F. J. Aoiz, D. W. Chandler, M. L. Costen, *Nat. Chem.*, **10**, 1148-1153 (2018).
- 3) Photo-tautomerization of acetaldehyde as a photochemical source of formic acid in the troposphere, M. F. Shaw, B. Sztaray, L. K. Whalley, D. E. Heard, D. B. Millet, M. J. T. Jordan, D. L. Osborn, and S. H. Kable, *Nat. Comm.* **9**, 2584 (2018).
- 4) Photoionization of methyl hydroperoxide: Thermochemistry of the smallest QOOH radical and the detection of a roaming fragmentation channel, K. Covert, K. Voronova, K. G. Torma, A. Bodi, J. Zádor, B. Sztáray, *Phys. Chem. Chem. Phys.*, **20**, 21085-21094 (2018).

GAS PHASE INTERACTIONS WITH OTHER PHASES

David W. Chandler, Nils Hansen, Christopher J. Kliewer, Habib N. Najm, David L. Osborn, Leonid Sheps and Craig A. Taatjes
Combustion Research Facility, Sandia National Labs, Livermore, CA 94550

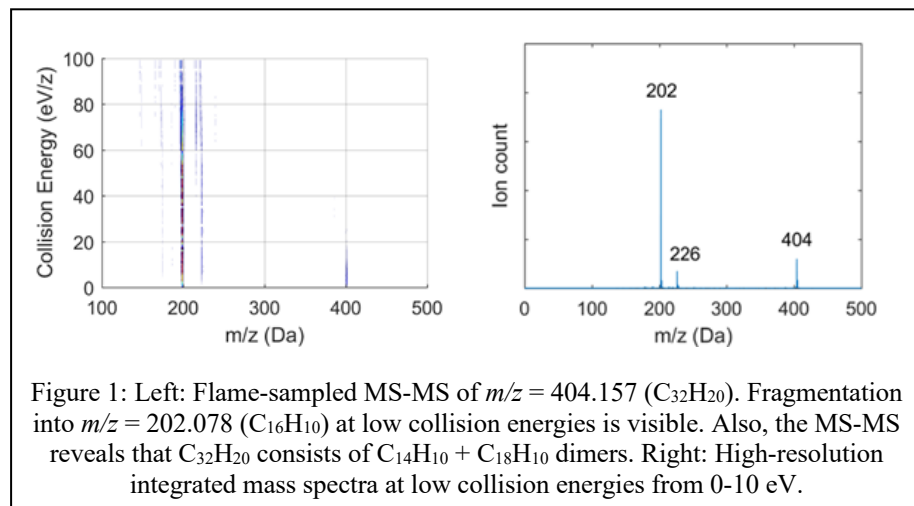
chand@sandia.gov, nhansen@sandia.gov, cjkliew@sandia.gov, hnnajm@sandia.gov,
dlosbor@sandia.gov, lsheps@sandia.gov, cataatj@sandia.gov

Program Scope

This research program encompasses experimental and computational investigations of a wide range of multiphase phenomena, investigating the formation of particulates in gas-phase reaction systems, measuring and modeling the gas-phase processes at reactive interfaces and probing the physical and chemical interactions between phases. Understanding reactions that lead to particle formation and calculating surface reactions draw on work in the Sandia “Chemical Kinetics for Complex Systems” task, and experiments employ innovations from the “Ultrafast Physics: Nonlinear Optical Spectroscopy and Diagnostics” and “Advanced Mass Spectrometry and X-Ray Diagnostics” tasks. Recent emphasis is on chemically controlled gas-to-particle conversion; proposed new directions will extend work into understanding the interactions of gas-phase molecules with liquid and solid surfaces. These initiatives complement the catalytic surface investigations in Sandia’s “Imaging the Near-Surface Gas Phase” program.

Recent Progress

Assessment of the role of PAH dimers for particle inception Although dimerization of moderately sized polycyclic aromatic hydrocarbons (PAH) is thermodynamically unfeasible at high temperatures,¹ dimerization of PAHs like pyrene continues to be proposed as a key step to particle inception. We recently employed flame-sampling tandem mass spectrometry to critically assess the role of PAH dimers in flames.

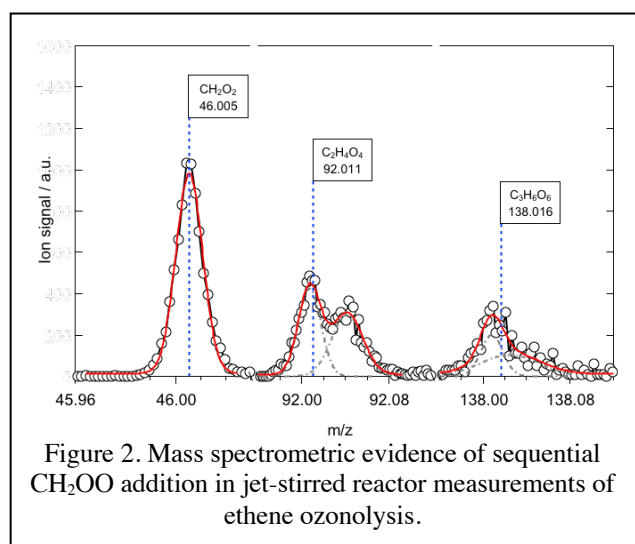


This work both showed how tandem mass spectrometry can be used to detect and identify PAH dimers, and yielded experimental evidence (matching theory predictions¹⁻⁶) that pyrene dimers do not exist in flames. A three-dimensional plot of the flame-sampled MS-MS spectra of $m/z = 404.157$ ($C_{32}H_{20}$) is shown in Fig. 1 (left). In this plot, the ion intensity is shown as

function of the mass-to-charge ratio (x-axis) and the collision energy (on the y-axis). The plot clearly reveals signal at $m/z = 404.157$ that is stable at low collision energies but fragments at relatively low collision energy into $m/z = 202.078$ ($C_{16}H_{10}$) fragments, identifying the detected $C_{32}H_{20}$ component as $C_{16}H_{10}$ dimer. The very low collision energy needed to break the $m/z = 404.157$ complex indicates that $C_{32}H_{20}$ is a weakly bound complex. After demonstrating that the dimers could be detected and characterized, careful dilution studies proved that the dimer signals arose entirely from condensation in the sampling process. The

measurements confirmed that pyrene dimer concentrations in the flame are below detectability; pyrene dimers cannot be a key intermediate in particle inception at elevated flame temperatures.

Oligomerization Sequences of Carbonyl Oxides In the Sandia “Chemical Kinetics for Complex Systems” task we have shown that ozone-initiated oxidation leads to sequential addition of carbonyl oxide Criegee intermediates to form highly oxygenated molecules.⁷ As increasing oxygenation correlates with decreasing volatility, these sequences have been proposed to lead to aerosol formation, and controlled ozonolysis experiments indeed form particles in laboratory investigations.⁸ Our atmospheric chemistry collaborators Tom Bannan at the University of Manchester and Carl Percival at the Jet Propulsion Laboratory have observed such sequences in field experiments in the Amazon rainforest, where high isoprene emissions are expected to result in substantial Criegee intermediate concentrations. We have recently combined measurements of individual reactions of carbonyl oxides and ozone-initiated oxidation experiments in a jet-stirred reactor with computational kinetics studies by Stephen Klippenstein (Argonne), aiming to develop a rigorous model for possible sequences of reactions that could lead to particle formation.



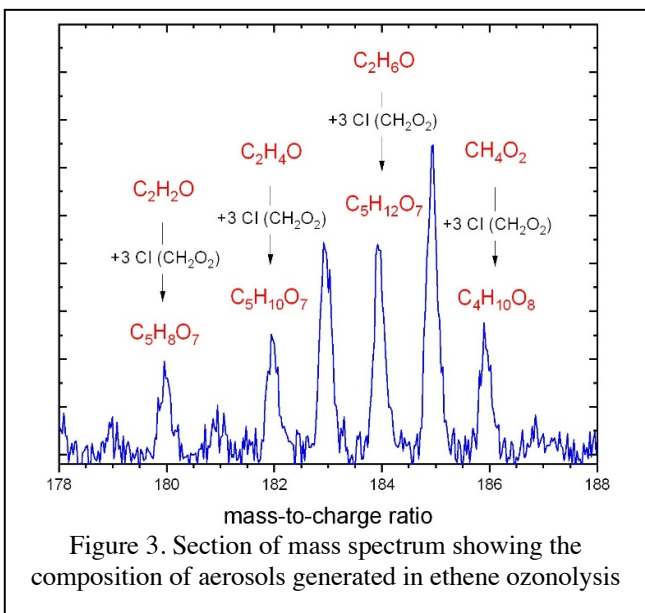
Measurements of ozone-initiated oxidation of ethylene characterized sequential addition of the Criegee intermediate CH₂OO (formaldehyde oxide) to multiple precursor molecules, always beginning with insertion of the CH₂OO into an O—H bond to form a hydroperoxide, for example the sequence shown in Figure 2, built on initial reaction of CH₂OO to formic acid to form hydroperoxymethyl formate. Subsequent reactions are thought to proceed mainly by insertion of the CH₂OO into the hydroperoxide O—H bond, each time forming another hydroperoxide product. The individual reactions in these sequences can also be initiated by photolytic formation of CH₂OO and measured directly. We have compared photoionization spectra of insertion reaction products from JSR ozonolysis measurements and

photolytically initiated kinetics measurements to confirm that both experiments are probing the same processes. Both ozonolysis and the photolysis measurements of CH₂OO + H₂O₂ yield a reaction product at the exact mass of CH₄O₄, with the similar PIE spectra confirming their identical isomeric structure. This supports the role of CI + ROOH reactions in ozonolysis studies – including the chamber work of Sakamoto *et al.* where SOA formation was attributed to CI + ROOH reactions.⁸ Direct kinetics measurements of insertion reactions with prototype hydroperoxides HOOH and (CH₃)₃COOH with CH₂OO have been compared to theory from Stephen Klippenstein, and the comparison confirms that high-level theory predicts such reactions accurately. The combination of theory and experimental kinetics now can constrain the chemistry that governs modeling of secondary organic aerosol formation.

Proposed work

The program will continue to use experiments, theory, and data science methods to investigate gas-phase molecular weight growth reactions and the nature of the interactions that lead to particulate formation, e.g., the radical-product channels of recombination reactions of resonance-stabilized radicals that drive the radical chain-reaction mechanism for soot inception. We will experimentally investigate the response of liquid interfaces under high gas pressures to laser-induced temperature gradients. We plan investigations of reactive interactions of the gas-phase with solid carbonaceous and liquid organic surfaces (complementing catalytic surface investigations in “Imaging the Near-Surface Gas Phase”) and eventually extend such studies to the gas phase near electrochemical three-phase boundaries.

Particles from Carbonyl Oxide Oligomerization To test the hypothesis that oligomeric hydroperoxides built from carbonyl oxide can nucleate, and to develop a framework to follow the chemistry and physics of this nucleation step, we propose to follow the kinetics of particle inception and mass growth. As a first step, we propose a comprehensive and systematic study of the chemical composition of particles generated in controlled laboratory environments. To the end, we will collaborate with Kevin Wilson from the Lawrence Berkeley National Laboratory who has developed an aerosol mass spectrometer to probe atmospheric aerosols. Following the successful measurement of gas-phase photoionization measurements of carbonyl

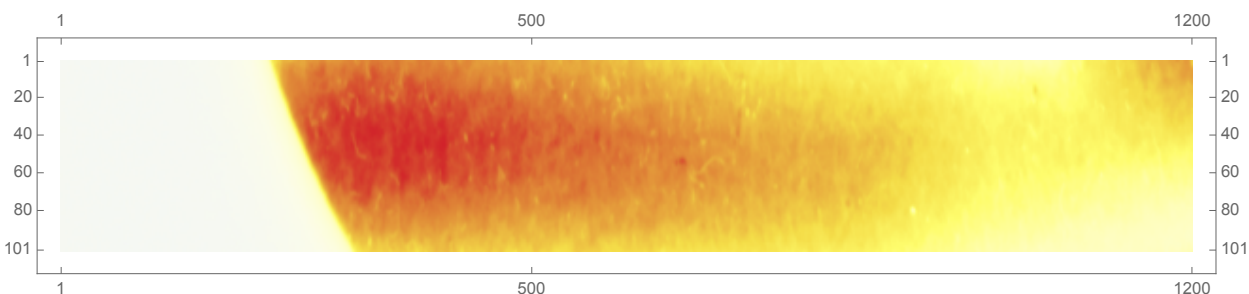


oxide oligomerization reactions in an atmospheric pressure jet-stirred reactor, we have performed some proof-of-principle experiments, connecting the jet-stirred reactor chamber to Wilson's aerosol mass spectrometer via a transfer line, in which the sampled particles are immediately diluted to reduce further coagulation.

An example is provided in Fig. 3 in which mass peaks are indicated that potentially originate from sequential addition of CI to ketene (C_2H_2O), acetaldehyde (C_2H_4O), ethanol (C_2H_6O), and methylhydroperoxide (CH_4O_2) following the ozonolysis of ethylene at room temperature. As can be seen, highly oxygenated species, containing 7-8 oxygen atoms, are formed. We plan to begin systematic investigations with the well-understood ethene ozonolysis reaction network, which, because of

its simplicity, provides a perfect test case. We anticipate that similar sequences will be observed in the gas-phase and aerosol mass spectrometer; controlling the oxidation conditions and identifying differences between the phases will enable oligomerization reaction mechanisms to be tested.

Detection of spatially resolved reaction products near a surface using REMPI and ion imaging Improved instrumentation for monitoring the location and kinetics of chemically or catalytically active domains on an arbitrary surface is an attractive and potentially transformative goal. However, any efforts to monitor the concentration of a target gas very near a surface that is producing the target gas is very dependent on the size of the reactive domains and the spatial resolution associated with sampling the target gas. To investigate and advance our technology in this area, we propose to use Resonant Enhanced Multiphoton Ionization (REMPI) imaging with velocity filtering to spatially image specific gaseous species near a



reactive surface. In a proof of principle experiment, we replaced the repeller plate of our traditional three lens velocity mapped ionization apparatus with an electrode patterned with catalytically active and inactive domains. Molecular beams of H_2 and D_2 were simultaneously directed at the patterned surface and the HD

product was detected by 2+1 REMPI through the E,F state. The resulting HD⁺ was accelerated toward and imaged on a position sensitive detector to yield a spatial map of HD production over the catalytically active domains of the electrode surface. This preliminary experiment demonstrated that REMPI has sufficient sensitivity to detect the HD product and that our apparatus can successfully image a projection of the REMPI laser beam waist. However, with the present set up, the image is blurred by the HD velocity distribution and the amount of magnification is insufficient to resolve micron-sized structures.

In order to eliminate spatial blurring from the HD velocity distribution, we will place a pin hole at the focus plane. At this focus, the image is velocity mapped so a pinhole will only pass a small fraction (perhaps 10%) of the entire velocity distribution which will sharpen the image. With our existing apparatus we believe we can easily obtain a factor of 14 in magnification thereby obtaining spatial resolution of 2.3 μm . By increasing the flight length of our apparatus, we should be able to increase the magnification factor to 23 providing an approximately 1-micron resolution near the surface.

Kinetic Monte Carlo for surface kinetics We will pursue studies of catalytic surface kinetics using the advances in kinetic Monte Carlo (KMC) methods carried out under the Sandia “Chemical Kinetics for Complex Systems” task. We will use lattice-KMC constructions, coupled with fast time integration relying on computational singular perturbation methods, to facilitate computations over time-horizons necessary for exploration of steady-state limit estimates for CO oxidation on RuO₂.

References

1. Sabbah, H.; Biennier, L.; Klippenstein, S. J.; Sims, I. R.; Rowe, B. R., Exploring the role of PAHs in the formation of soot: pyrene dimerization. *J. Phys. Chem. Lett.* **2010**, *1*, (19), 2962-2967.
2. Totton, T. S.; Misquitta, A. J.; Kraft, M., A transferable electrostatic model for intermolecular interactions between polycyclic aromatic hydrocarbons. *Chem. Phys. Lett.* **2011**, *510*, (1-3), 154-160.
3. Totton, T. S.; Misquitta, A. J.; Kraft, M., A quantitative study of the clustering of polycyclic aromatic hydrocarbons at high temperatures. *Phys. Chem. Chem. Phys.* **2012**, *14*, (12), 4081-4094.
4. Wong, D.; Whitesides, R.; Schuertz, C.; Frenklach, M., Molecular dynamics simulations of PAH dimerization. In *Combustion Generated Fine Carbonaceous Particles*, Bockhorn, H.; D'Anna, A.; Sarofim, A. F.; Wang, H., Eds. KIT Publishing: Karlsruhe, 2009; pp 247-257.
5. Zhang, H.-B.; You, X.; Wang, H.; Law, C. K., Dimerization of polycyclic aromatic hydrocarbons in soot nucleation. *J. Phys. Chem. A* **2014**, *118*, (8), 1287-1292.
6. Mao, Q.; van Duin, A. C.; Luo, K., Formation of incipient soot particles from polycyclic aromatic hydrocarbons: A ReaxFF molecular dynamics study. *Carbon* **2017**, *121*, 380-388.
7. Rouso, A. C.; Hansen, N.; Jasper, A. W.; Ju, Y. G., Identification of the Criegee intermediate reaction network in ethylene ozonolysis: impact on energy conversion strategies and atmospheric chemistry. *Phys. Chem. Chem. Phys.* **2019**, *21*, (14), 7341-7357.
8. Sakamoto, Y.; Inomata, S.; Hirokawa, J., Oligomerization Reaction of the Criegee Intermediate Leads to Secondary Organic Aerosol Formation in Ethylene Ozonolysis. *J. Phys. Chem. A* **2013**, *117*, (48), 12912-12921.

IV. Published journal articles supported by this project 2018-2020

1. N. Hansen, B. D. Adamson, S. A. Skeen, M. Ahmed, “Nucleation of Soot: Experimental Assessment of the Role of Polycyclic Aromatic Hydrocarbon (PAH) Dimers,” *Z. Physik. Chem.* in press (2020).
2. Q. Wang, P. Elvati, D. Kim, K. O. Johansson, P. E. Schrader, H. A. Michelsen, and A. Violi, "Spatial dependence of polycyclic aromatic compound growth in counterflow flames", *Carbon* **149**, 328-335. (2019).
3. K. O. Johansson, M. P. Head-Gordon, P. E. Schrader, K. R. Wilson, and H. A. Michelsen, "Resonance-stabilized hydrocarbon-radical chain reactions may explain soot inception and growth", *Science* **361**, 997-1000 (2018).

Chemical Kinetics for Complex Systems

Jacqueline H. Chen, Nils Hansen, Habib N. Najm, David L. Osborn, Lenny Sheps,
Craig A. Taatjes, and Judit Zádor

Sandia National Laboratories, MS 9055, Livermore, CA 94551-0969

jhchen@sandia.gov, nhansen@sandia.gov, hnnajm@sandia.gov, dlosbor@sandia.gov,
lsheps@sandia.gov, cataatj@sandia.gov, jzador@sandia.gov

Program Scope

This program employs a unique set of experimental and theoretical studies with the goal of elucidating mechanisms of elementary chemical reactions, which impacts the research theme of Reaction Pathways in Diverse Environments. This task is linked with many other parts of the Sandia program; it extends the high-resolution view of the “Chemical Dynamics Methods and Applications” task to encompass complex interactions in collisional environments, and it provides a basis for the interface studies in the “Gas Phase Interactions with Other Phases” task. Methods developed under the “Advanced Diagnostics” task and analytical tools that use tunable vacuum ultraviolet light from the Advanced Light Source synchrotron at Lawrence Berkeley National Laboratory enable sensitive and sometimes even isomer-specific ionization of reactant and product molecules sampled from chemical reactions. These individual reaction studies are linked to controlled measurements of more complex reaction systems as found in well-defined laboratory-scale zero- and one-dimensional reactors. Alongside, we use master equation (ME) frameworks to characterize the kinetics on complex potential energy surfaces (PESs), and approaches to study stochastic and nonthermal effects at the mesoscale.

Recent Progress

Isomer-Resolved Detection of Keto-hydroperoxides We have developed routines to provide partially isomer-resolved detection and quantification of keto-hydroperoxides (KHPs) that form during the low-temperature oxidation. We used the oxidation of tetrahydrofuran (THF, *cycl.*-O-CH₂CH₂CH₂CH₂-) to describe how these short-lived KHPs were detected, isomer-specifically identified, and quantified using integrated experimental and theoretical approaches.

Ozone-Initiated Oxidation Chemistry of Ethylene and Criegee Intermediate Insertion Reactions We used our expertise in the detection, identification, and quantification of keto-hydroperoxides in complex reaction networks to experimentally prove the existence of a keto-hydroperoxide (hydroperoxyl-acetaldehyde, HOOCH₂CHO) in the ozonolysis of ethylene, that so far had only been predicted theoretically. As part of this work, a network of CI reactions was identified, which can be described best by the sequential addition of CI with ethylene, water, formic acid, and other molecules containing hydroxy, aldehyde, and hydroperoxy functional groups. Species resulting from as many as four sequential CI addition reactions were observed, and these highly oxygenated oligomers that are known components of secondary organic aerosols in the atmosphere, as described in the Sandia “Gas Phase Interactions with Other Phases” task.

Comparison of Cyclohexane and Tetrahydropyran Oxidation Chemistry We employed the laser-photolysis / multiplexed photoionization mass spectrometry method to investigate the Cl-atom-initiated oxidation of cyclohexane and tetrahydropyran. Earlier infrared absorption measurements of OH and HO₂ formation in these systems showed the importance of ring-opening in tetrahydropyran. In these MPIMS experiments, a collaboration with Brandon Rotavera (U. Georgia), ketohydroperoxide formation from the second O₂ addition was measured for both reactions, but the ketohydroperoxide contribution was relatively diminished in tetrahydropyran, especially at higher temperatures, because ring-opening in R and QOOH species reduces the possibility of second O₂ addition.

Automated Kinetics Our KinBot code automatically locates and characterizes chemically significant stationary points on multiwell PES and generates input to master equation calculations. We have made the code open source (<https://github.com/zadorlab/KinBot>) and demonstrated its abilities on a range of systems.

Chemistry of Ring-Enlargement Reactions Ring-enlargement reactions have been hypothesized to provide a fast route towards the formation of six-membered single-ring or polycyclic aromatic hydrocarbons (PAHs). We investigated the participation of the cyclopentadienyl (C₅H₅) radical in ring-enlargement

reactions in high-temperature environments. Results showed that, while the addition of methane enhances the production of methylcyclopentadiene and benzene, the concentration of larger polycyclic hydrocarbons was reduced. The observed increase of benzene is certainly attributable to the ring-enlargement reaction between the methyl and the cyclopentadienyl radicals. The impact of cyclopentadienyl ring-enlargement chemistry on the formation pathways of toluene, ethylbenzene, naphthalene was investigated and found to be not of importance.

Nonthermal Processes in Heterogeneous Environments We have begun to assess the impact of nonthermal effects in a turbulent flame through a phenomenological model in collaboration with Sivaramakrishnan and Klippenstein of ANL. Nonthermal chemistry has a ~16% impact on the turbulent fuel consumption rate in H₂/CH₄/air premixed turbulent flame at 10 atm. We have also confirmed the validity of Direct Simulation Monte Carlo (DSMC) in the continuum regime for treating fast transport processes including a normal shock and a turbulent shear layer.

Stochastic Chemical Systems We continued our work on using computational singular perturbation theory for enabling stable large time-step explicit time integration of stiff stochastic mesoscale models of chemical systems, employing the chemical Langevin equation (CLE) model. We focused on the handling of the CLE stiff diffusion term where special handling of fast diffusional processes is necessary for accuracy purposes in large time step updating. We developed a method relying on analytical integration of locally-linearized approximate diffusion terms over time-scales smaller than the integration time step. We are in the process of studying error convergence and accuracy of this construction.

Proposed Work

Further Developments in Automated Kinetics We propose numerous developments to our KinBot software to expand its features to enable the exploration of a wider chemical space, to enable the calculation of more accurate rate coefficients, and to improve its performance. The chemical space will be extended to new chemical elements, to bimolecular reactions and weakly bound states, to molecules with several rings and to cations. We will also implement calculations supporting VTST and certain anharmonic effects, and approaches to incorporate calculations for barrierless reactions. We will enable automated sensitivity analysis of master equation calculations. Finally, we will also improve KinBot's search algorithms by combining KinBot's combinatorial search with collective variables representing a reaction pathway.

Theoretical Investigation of ROO + HO₂ Reactions ROO and HO₂ radicals can react both on the singlet and triplet surface, most likely producing alkyl hydroperoxides (ROOH) + O₂ via a barrierless entrance and a submerged barrier. We propose to characterize the ROO + HO₂ reactions in more detail using multi-reference electronic structure methods necessitated by the substantial multi-reference character of the critical barrier, an effective two-transition state for the accurate determination of the capture rate coefficients, and using nonadiabatic TST for calculating the branching between the singlet and the triplet surfaces.

Product Branching in Radical-Radical Reactions Reactions of ROO with other radicals proceed on singlet and triplet surfaces, and product branching can show the influence of intersystem crossing. For example, in ROO self-reaction XMC-QDPT2 calculations by Kurtén and co-workers (*J. Phys. Chem. A* **2019**, *123*, 6596-6604) highlighted that intersystem crossing is required for formation of the ROOR product, and that this ISC must compete with both fragmentation to RO· + R'O and the intermolecular RO H-transfer to form R-H=O + ROH. Flow cell experiments from Berndt *et al.* (*Angew. Chem. Int. Ed.* **2018**, *57*, 3820-3824) recently showed substantial ROOR production from complex ROO radical reactions. Formation of ROOR from self-reaction of small ROO species has not been clearly demonstrated, although Kurtén and co-workers predict very rapid intersystem crossing (10^{13} s^{-1}) is predicted for the R = CH₃ system. From photoionization mass spectrometry experiments we have clear indication for formation of CH₃OOCH₃ from the self-reaction of CH₃OO, and we will pursue ways to quantify its yield as a function of pressure. We will also extend investigations to other ROO self (and cross) reactions; preliminary measurements of CH₃CH₂OO self-reaction observed product formation at $m/z = 90$ (C₂H₅OOC₂H₅).

Ozone-Initiated Oxidation Chemistry Following up on our earlier studies, work on the ozone-initiated chemistry and the chemistry of the Criegee Intermediate reaction network will continue. In particular, we are interested in effect of ozone reactions on low-temperature oxidation reaction networks.

Molecular-Weight Growth in Hydrocarbon Rich Environments In order to investigate kinetics of resonance-stabilized radicals at high temperatures, we will develop a new resistively heated plug-flow reactor for kinetics, and couple it to our existing suite of mass-spectrometric analysis tools. We will work to interface such reactors with our uniquely powerful measurement tools of PEPICO and MS-MS (see the abstract on Advanced Diagnostics) Coupling the reactor to the PEPICO experiment will enable finer resolution of isomeric species than simple photoionization spectrometry affords, which can be crucial for larger molecules, where the number of feasible isomers is high, and the ionization energies may be similar. Targets are the propargyl + propargyl reactions and ring-enlargement reactions involving cyclopentadienyl radicals with allyl and propargyl.

Non-thermal Processes in Heterogeneous Environments We plan to use DSMC to study selected combustion systems behind a normal shock and turbulent shear layer triggered by a Kelvin–Helmholtz instability between streams of H₂/O₂/N₂ at 300 K and air at 1000 K. We propose a data driven approach where detailed molecular scale quantities of interest, e.g. molecular energy distribution functions or their summaries in the form of moments, computed using DSMC at representative conditions are mapped to ensemble averaged local species mass fractions and temporal and spatial gradient information over a length scale corresponding to the resolution of the continuum simulations.

Stochastic Chemical Systems: We plan further developments with the use of computational singular perturbation (CSP) time integration for the chemical Langevin equation system. We will finalize the small time-step diffusion handling, and explore computational improvements relying on linearizing the dependence of the eigendecomposition of the Jacobian around the mean state. We will also explore utility of other iterative refinement means of evolving CSP basis vectors that eschew too-frequent re-computation of the Jacobian eigen-structure. We will also start formulation and development of CSP for dealing with the time integration of mesoscale chemical systems with the discrete kinetic Monte Carlo method.

List of Publications (2018-2020):

1. Baroncelli, M.; Felsmann, D.; Hansen, N.; Pitsch, H. Investigating the Effect of Oxy-Fuel Combustion and Light Coal Volatiles Interaction: A Mass Spectrometric Study. *Combustion and Flame* **2019**, *204*, 320-330.
2. Baroncelli, M.; Mao, Q.; Galle, S.; Hansen, N.; Pitsch, H. Role of Ring-Enlargement Reactions in the Formation of Aromatic Hydrocarbons. *Physical Chemistry Chemical Physics* **2020**, *22*, 4699-4714.
3. Bierkandt, T.; Höner, M.; Gaiser, N.; Hansen, N.; Köhler, M.; Kasper, T. Experimental Flat Flame Study of Monoterpenes: Insights into the Combustion Kinetics of α -Pinene, B-Pinene, and Myrcene. *Proceedings of the Combustion Institute* **2020**, accepted for oral presentation.
4. Bourgalais, J.; Caster, K. L.; Durif, O.; Osborn, D. L.; Le Picard, S. D.; Goulay, F. Product Detection of the CH Radical Reactions with Ammonia and Methyl-Substituted Amines. *Journal of Physical Chemistry A* **2019**, *123*, 2178-2193.
5. Braun-Unkoff, M.; Hansen, N.; Dietrich, M.; Methling, T.; Moshhammer, K.; Yang, B. Entanglement of N-Heptane and Iso-Butanol Chemistries in Flames Fueled by Their Mixtures. *Proceedings of the Combustion Institute* **2020**, accepted for oral presentation.
6. Caravan, R. L.; Khan, M. A. H.; Zador, J.; Sheps, L.; Antonov, I. O.; Rotavera, B.; Ramasesha, K.; Au, K.; Chen, M. W.; Rosch, D., et al. The Reaction of Hydroxyl and Methylperoxy Radicals Is Not a Major Source of Atmospheric Methanol. *Nature Communications* **2018**, *9*.
7. Caravan, R. L.; Vansco, M. F.; Au, K.; Khan, M. A. H.; Li, Y.-L.; Winiberg, F. A. F.; Zuraski, K.; Lin, Y.-H.; Chao, W.; Trongsirawat, N., et al. Direct Kinetic Measurements and Theoretical Predictions of an Isoprene-Derived Criegee Intermediate. *Proceedings of the National Academy of Sciences* **2020**, 201916711.
8. Chen, B.; Wang, H.; Wang, Z.; Han, J.; Alqaity, A. B. S.; Wang, H.; Hansen, N.; Sarathy, S. M. Ion Chemistry in Premixed Rich Methane Flames. *Combustion and Flame* **2019**, *202*, 208-218.
9. Chen, M. W.; Rotavera, B.; Chao, W.; Zador, J.; Taatjes, C. A. Direct Measurement of OH and HO₂ Formation in R + O₂ Reactions of Cyclohexane and Tetrahydropyran. *Physical Chemistry Chemical Physics* **2018**, *20*, 10815-10825.
10. Chhantyal-Pun, R.; Rotavera, B.; McGillen, M. R.; Khan, M. A. H.; Eskola, A. J.; Caravan, R. L.; Blacker, L.; Tew, D. P.; Osborn, D. L.; Percival, C. J., et al. Criegee Intermediate Reactions with Carboxylic Acids: A Potential Source of Secondary Organic Aerosol in the Atmosphere. *ACS Earth and Space Chemistry* **2018**, *2*, 833-842.
11. Chhantyal-Pun, R.; Shannon, R. J.; Tew, D. P.; Caravan, R. L.; Duchi, M.; Wong, C.; Ingham, A.; Feldman, C.; McGillen, M. R.; Khan, M. A. H., et al. Experimental and Computational Studies of Criegee Intermediate Reactions with NH₃ and CH₃NH₂. *Physical Chemistry Chemical Physics* **2019**, *21*, 14042-14052.
12. Czekner, J.; Taatjes, C. A.; Osborn, D. L.; Meloni, G. Study of Low Temperature Chlorine Atom Initiated Oxidation of Methyl and Ethyl Butyrate Using Synchrotron Photoionization ToF-Mass Spectrometry. *Physical Chemistry Chemical Physics* **2018**, *20*, 5785-5794.
13. Davis, J. C.; Koritzke, A. L.; Caravan, R. L.; Antonov, I. O.; Christianson, M. G.; Doner, A. C.; Osborn, D. L.; Sheps, L.; Taatjes, C. A.; Rotavera, B. Influence of the Ether Functional Group on Ketohydroperoxide Formation in Cyclic Hydrocarbons: Tetrahydropyran and Cyclohexane. *Journal of Physical Chemistry A* **2019**, *123*, 3634-3646.
14. Dodson, L. G.; Savee, J. D.; Gozem, S.; Shen, L. H.; Krylov, A. I.; Taatjes, C. A.; Osborn, D. L.; Okumura, M. Vacuum Ultraviolet Photoionization Cross Section of the Hydroxyl Radical. *Journal of Chemical Physics* **2018**, *148*.
15. Eskola, A. J.; Dontgen, M.; Rotavera, B.; Caravan, R. L.; Welz, O.; Savee, J. D.; Osborn, D. L.; Shallcross, D. E.; Percival, C. J.; Taatjes, C. A. Direct Kinetic Study of CH₂O + Methyl Vinyl Ketone and CH₂O + Methacrolein Reactions and an Upper Limit Determination for CH₂O + CO Reaction. *Physical Chemistry Chemical Physics* **2018**, *20*, 19373-19381.
16. Fritz, S. M.; Mishra, P.; Wullenkord, J.; Fugazzi, P. G.; Kohse-Höinghaus, K.; Zwier, T. S.; Hansen, N. Detecting Combustion Intermediates Via Broadband Chirped-Pulse Microwave Spectroscopy. *Proceedings of the Combustion Institute* **2020**, accepted for oral presentation.
17. Grambow, C. A.; Jamal, A.; Li, Y.-P.; Green, W. H.; Zádor, J.; Suleimanov, Y. V. Unimolecular Reaction Pathways of a Γ -Ketohydroperoxide from Combined Application of Automated Reaction Discovery Methods. *Journal of the American Chemical Society* **2018**, *140*, 1035-1048.

18. Han, X.; Najm, H. N. Effective Construction of Eigenvectors for a Class of Singular Sparse Matrices. *Applied Mathematics Letters* **2019**, *97*, 121-126.
19. Han, X.; Valorani, M.; Najm, H. N. Explicit Time Integration of the Stiff Chemical Langevin Equations Using Computational Singular Perturbation. *The Journal of Chemical Physics* **2019**, *150*, 194101.
20. Hansen, N.; He, X.; Griggs, R.; Moshhammer, K. Knowledge Generation through Data Research: New Validation Targets for the Refinement of Kinetic Mechanisms. *Proceedings of the Combustion Institute* **2019**, *37*, 743-750.
21. Hansen, N.; Kasper, T.; Yang, B. Synchrotron-Based VUV Photoionization Mass Spectrometry in Combustion Chemistry Research. In *Synchrotron Radiation Applications*, World Scientific, 2018; pp 37-65.
22. Hansen, N.; Kukkadapu, G.; Chen, B.; Dong, S.; Curran, H. J.; Taatjes, C. A.; Eskola, A. J.; Osborn, D. L.; Sheps, L.; Pitz, W. J., et al. The Impact of the Third O₂ Addition Reaction Network on Ignition Delay Times of Neo-Pentane. *Proceedings of the Combustion Institute* **2020**, accepted for oral presentation.
23. Hansen, N.; Moshhammer, K.; Jasper, A. W. Isomer-Selective Detection of Keto-Hydroperoxides in the Low-Temperature Oxidation of Tetrahydrofuran. *The Journal of Physical Chemistry A* **2019**, *123*, 8274-8284.
24. Holland, R.; Khan, M. A. H.; Chhantyal-Pun, R.; Orr-Ewing, A. J.; Percival, C. J.; Taatjes, C. A.; Shallcross, D. E. Investigating the Atmospheric Sources and Sinks of Perfluorooctanoic Acid Using a Global Chemistry Transport Model. *Atmosphere* **2020**, *11*, 407.
25. Huang, C.; Li, S.; Tao, T.; Zhang, F.; Hansen, N.; Law, C. K.; Qi, F.; Yang, B. From Inherent Correlation to Constrained Measurement: Model-Assisted Calibration in Mbms Experiments. *Proceedings of the Combustion Institute* **2020**, accepted for oral presentation.
26. Khan, M. A. H.; Lyons, K.; Chhantyal-Pun, R.; McGillen, M. R.; Caravan, R. L.; Taatjes, C. A.; Orr-Ewing, A. J.; Percival, C. J.; Shallcross, D. E. Investigating the Tropospheric Chemistry of Acetic Acid Using the Global 3-D Chemistry Transport Model, Stochem-Cri. *Journal of Geophysical Research-Atmospheres* **2018**, *123*, 6267-6281.
27. Khan, M. A. H.; Percival, C. J.; Caravan, R. L.; Taatjes, C. A.; Shallcross, D. E. Criegee Intermediates and Their Impacts on the Troposphere. *Environmental Science-Processes & Impacts* **2018**, *20*, 437-453.
28. Koritzke, A. L.; Davis, J. C.; Caravan, R. L.; Christianson, M. G.; Osborn, D. L.; Taatjes, C. A.; Rotavera, B. Qooh-Mediated Reactions in Cyclohexene Oxidation. *Proceedings of the Combustion Institute* **2018**.
29. Koritzke, A. L.; Davis, J. C.; Caravan, R. L.; Christianson, M. G.; Osborn, D. L.; Tootjes, C. A.; Rotavera, B. (Q) over Dotooh-Mediated Reactions in Cyclohexene Oxidation. *Proceedings of the Combustion Institute* **2019**, *37*, 323-335.
30. Kukkadapu, G.; Wagnon, S. W.; Pitz, W. J.; Hansen, N. Identification of the Molecular-Weight Growth Reaction Network in Counterflow Flames of the C₃H₄ Isomers Allene and Propyne. *Proceedings of the Combustion Institute* **2020**, accepted for oral presentation.
31. Leon, L.; Ruwe, L.; Moshhammer, K.; Seidel, L.; Shrestha, K.; Wang, X.; Mauss, F.; Kohse-Höinghaus, K.; Hansen, N. Chemical Insights into the Larger Sooting Tendency of 2-Methyl-2-Butene Compared to N-Pentane. *Combustion and Flame* **2019**, *208*, 182-197.
32. Lia, H.; Shiqing, K.; Hansen, N.; Zhang, F.; Yang, B. Influence of Ozone Addition on the Low-Temperature Oxidation of Dimethyl Ether in a Jet-Stirred Reactor. *Combustion and Flame* **2020**, *214*, 277-286.
33. Liao, H.; Tao, T.; Sun, W.; Hansen, N.; Law, C. K.; Yang, B. Investigation of the Low-Temperature Oxidation of N-Butanal in a Jet-Stirred Reactor. *Proceedings of the Combustion Institute* **2019**, *37*, 453-460.
34. Liao, H.; Tao, T.; Sun, W.; Hansen, N.; Yang, B. Isomer-Specific Speciation Behaviors Probed from Premixed Flames Fueled by Acetone and Propanal. *Proceedings of the Combustion Institute* **2020**, accepted for oral presentation.
35. Pieper, J.; Hemken, C.; Büttgen, R.; Graf, I.; Hansen, N.; Heufer, K. A.; Kohse-Höinghaus, K. A High-Temperature Study of 2-Pentanone Oxidation: Experiment and Kinetic Modeling. *Proceedings of the Combustion Institute* **2019**, *37*, 1683-1690.
36. Prendergast, M. B.; Kirk, B. B.; Savee, J. D.; Osborn, D. L.; Taatjes, C. A.; Hemberger, P.; Blanksby, S. J.; da Silva, G.; Trevitt, A. J. Product Detection Study of the Gas-Phase Oxidation of Methylphenyl Radicals Using Synchrotron Photoionisation Mass Spectrometry. *Physical Chemistry Chemical Physics* **2019**, *21*, 17939-17949.
37. Rouso, A.; Hansen, N.; Jasper, A.; Ju, Y. J. P. C. C. P. Identification of the Criegee Intermediate Reaction Network in Ethylene Ozonolysis: Impact on Energy Conversion Strategies and Atmospheric Chemistry. *Physical Chemistry Chemical Physics* **2019**, *21*, 7341-7357.
38. Rouso, A. C.; Hansen, N.; Jasper, A. W.; Ju, Y. Low-Temperature Oxidation of Ethylene by Ozone in a Jet-Stirred Reactor. *The Journal of Physical Chemistry A* **2018**, *122*, 8674-86.
39. Ruwe, L.; Cai, L.; Moshhammer, K.; Hansen, N.; Pitsch, H.; Kohse-Höinghaus, K. The C₅ Chemistry Preceding the Formation of Polycyclic Aromatic Hydrocarbons in a Premixed 1-Pentene Flame. *Physical Chemistry Chemical Physics* **2019**, *206*, 411-423.
40. Ruwe, L.; Cai, L.; Wullenkord, J.; Schmitt, S. C.; Felsmann, D.; Baroncelli, M.; Chen, B.; Moshhammer, K.; Hansen, N.; Pitsch, H., et al. N-Heptane Combustion Chemistry in Less Studied Configurations: Aromatics Formation and Oxidation Chemistry in Counterflow Flame and Flow Reactor. *Proceedings of the Combustion Institute* **2020**, accepted for oral presentation.
41. Ruwe, L.; Moshhammer, K.; Hansen, N.; Kohse-Höinghaus, K. Influences of the Molecular Fuel Structure on Combustion Reactions Towards Soot Precursors in Selected Alkane and Alkene Flames. *Physical Chemistry Chemical Physics* **2018**, *20*, 10780-10795.
42. Schmitt, S.; Wick, M.; Wouters, C.; Ruwe, L.; Graf, I.; Andert, J.; Hansen, N.; Pischinger, S.; Kohse-Höinghaus, K. Effects of Water Addition on the Combustion of Iso-Octane Investigated in Laminar Flames, Low-Temperature Reactors, and an Hcci Engine. *Combustion and Flame* **2020**, *212*, 433-447.
43. Sun, W.; Lailliau, M.; Serinyel, Z.; Dayma, G.; Moshhammer, K.; Hansen, N.; Yang, B.; Dagaut, P. Insights into the Oxidation Kinetics of a Cetane Improver-1, 2-Dimethoxyethane (1, 2-Dme) with Experimental and Modeling Methods. *Proceedings of the Combustion Institute* **2019**, *37*, 555-564.
44. Sun, W.; Tao, T.; Lailliau, M.; Hansen, N.; Yang, B.; Dagaut, P. Exploration of the Oxidation Chemistry of Dimethoxymethane: Jet-Stirred Reactor Experiments and Kinetic Modeling. *Combustion and Flame* **2018**, *193*, 491-501.
45. Sun, W.; Tao, T.; Liao, H.; Hansen, N.; Yang, B. Probing Fuel-Specific Reaction Intermediates from Laminar Premixed Flames Fueled by Two C₅ Ketones and Model Interpretations. *Proceedings of the Combustion Institute* **2019**, *37*, 1699-1707.
46. Sun, W.; Wang, J.; Huang, C.; Hansen, N.; Yang, B. Providing Effective Constraints for Developing Ketene Combustion Mechanisms: A Detailed Kinetic Investigation of Diacetyl Flames. *Combustion and Flame* **2019**, *205*, 11-21.
47. Taatjes, C. A.; Khan, M. A. H.; Eskola, A. J.; Percival, C. J.; Osborn, D. L.; Wallington, T. J.; Shallcross, D. E. Reaction of Perfluorooctanoic Acid with Criegee Intermediates and Implications for the Atmospheric Fate of Perfluorocarboxylic Acids. *Environmental Science & Technology* **2019**, *53*, 1245-1251.
48. Tao, T.; Kang, S.; Sun, W.; Wang, J.; Liao, H.; Moshhammer, K.; Hansen, N.; Law, C. K.; Yang, B. A Further Experimental and Modeling Study of Acetaldehyde Combustion Kinetics. *Combustion and Flame* **2018**, *196*, 337-350.
49. Tao, T.; Sun, W.; Hansen, N.; Jasper, A. W.; Moshhammer, K.; Chen, B.; Wang, Z.; Huang, C.; Dagaut, P.; Yang, B. Exploring the Negative Temperature Coefficient Behavior of Acetaldehyde Based on Detailed Intermediate Measurements in a Jet-Stirred Reactor. *Combustion and Flame* **2018**, *192*, 120-129.
50. Van de Vijver, R.; Van Geem, K. M.; Marin, G. B.; Zádor, J. Decomposition and Isomerization of 1-Pentanol Radicals and the Pyrolysis of 1-Pentanol. *Combustion and Flame* **2018**, *196*, 500-514.
51. Van de Vijver, R.; Zádor, J. Kinbot: Automated Stationary Point Search on Potential Energy Surfaces. *Computer Physics Communications* **2020**, *248*, 106947.
52. Vansco, M. F.; Caravan, R. L.; Zuraski, K.; Wimberg, F. A. F.; Au, K.; Trongsiwat, N.; Walsh, P. J.; Osborn, D. L.; Percival, C. J.; Khan, M. A. H., et al. Experimental Evidence of Dioxole Unimolecular Decay Pathway for Isoprene-Derived Criegee Intermediates. *The Journal of Physical Chemistry A* **2020**.
53. Wang, Z.; Chen, B.; Moshhammer, K.; Popolan-Vaida, D. M.; Sioud, S.; Shankar, V. S. B.; Vuilleumier, D.; Tao, T.; Ruwe, L.; Bräuer, E. N-Heptane Cool Flame Chemistry: Unraveling Intermediate Species Measured in a Stirred Reactor and Motored Engine. *Combustion and Flame* **2018**, *187*, 199-216.
54. Wang, Z.; Hansen, N.; Jasper, A. W.; Chen, B.; Popolan-Vaida, D. M.; Yalamanchi, K. K.; Najjar, A.; Dagaut, P.; Sarathy, S. M. Cool Flame Chemistry of Diesel Surrogate Compounds: N-Decane, 2-Methylnonane, 2,7-Dimethyloctane, and N-Butylcyclohexane. *Combustion and Flame* **2020**.
55. Wang, Z.; Herbinet, O.; Hansen, N.; Battin-Leclerc, F. Exploring Hydroperoxides in Combustion: History, Recent Advances and Perspectives. *Progress in Energy and Combustion Science* **2019**, *73*, 132-181.
56. Zádor, J.; Miller, J. A. Comment on "Influence of Multiple Conformations and Paths on Rate Constants and Product Branching Ratios. Thermal Decomposition of 1-Propanol Radicals". *The Journal of Physical Chemistry A* **2019**, *123*, 1129-1130.

Dynamics and Energetics of Elementary Combustion Reactions and Transient Species

Grant DE-FG03-98ER14879

Robert E. Continetti (rcontinetti@ucsd.edu)

Department of Chemistry and Biochemistry, University of California San Diego
9500 Gilman Drive, La Jolla, CA 92093-0340

I. Program Scope

This research program obtains experimental results that benchmark fundamental advances in the theoretical understanding of chemical reactions, including the development of accurate potential energy surfaces (PESs) and computational studies of the dynamics of chemical reactions. The primary focus has been on the bimolecular reactions of the hydroxyl radical and oxygenated carbon radicals, with an initial foray during this project period into pump-probe studies of dissociative photodetachment (DPD) processes. These recent studies have implications for understanding the photochemistry of negative ions, transient anion resonances, and using these resonances to promote unique chemical pathways. This experimental program has been characterized by the development and application of advanced experimental techniques using photodetachment and DPD of anionic precursors to prepare energized radicals and collision complexes. Laser photodetachment, coupled with the detection of photoelectrons, stable photoneutrals, and photofragments in coincidence has allowed us to establish the technique of photoelectron-photofragment coincidence (PPC) spectroscopy, providing kinematically complete measurements of energy partitioning in reaction dynamics. During the last year, we published on the dissociation dynamics of the OH-CH₄ complex in collaboration with Jun Li and Hua Guo examining the dynamics of OH/OD + CH₄/CD₄ → H₂O + CH₃/CD₃ initiated by photodetachment of the OH⁻-hydrocarbon complexes.¹ Interpretation of the experimental results were aided by quasi-classical trajectory (QCT) calculations that showed general agreement between experiment and theory (DOE pub. 7). We extended our hydroxyl radical reaction studies to include OH-C₂H₄ and OH-CH₃OH systems expected to have similar dynamics to the OH-CH₄ complex. We also investigated the DPD of OCH₃⁻(CH₃OH) and OH⁻(CH₃OH) complexes, extending on previous studies of the F⁻(CH₃OH) complex.² Ongoing efforts also include characterization of the photodissociation of nitrogen oxide species such as N₂O₂⁻ providing the first state-resolved data on the autodetachment of the highly vibrationally and rotationally excited NO anion products in the near-UV. In addition, the dissociation dynamics of three low-lying electronic states of the oxyallyl diradical, C₃H₄O, were studied via PPC and initial pump-probe studies of the multiphoton DPD and photodissociation of the C₃H₄O⁻ anion were carried out. In the following sections, recent progress will be discussed in more detail, followed by a brief review of future work, as well as returning to the IR excitation experiments^{3, 4} (DOE pub. 2) to study the excitation and isomerization of the HOCO system.

II. Recent Progress

A. Hydroxyl Radical Reactions: OH + CH₄/C₂H₄ → H₂O + CH₃/C₂H₃

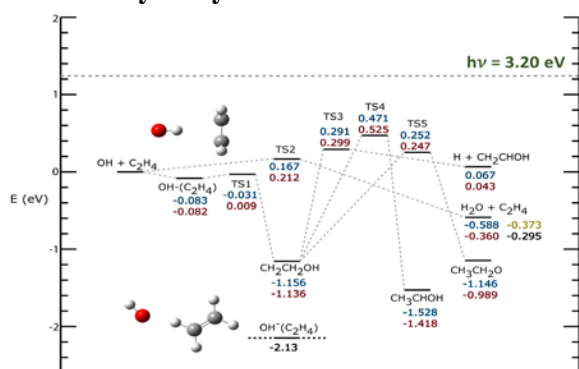


Figure 1. Energetics diagram for the OH-C₂H₄ system showing anion and neutral geometries. Energetic values in blue,⁵ yellow,⁶ and red⁷ correspond to literature values at various levels of theory. Preliminary energetic values in black are at the CCSD(T)/aug-cc-pVTZ level.

The hydroxyl radical plays a critical role in reactions involving volatile organic compounds in atmospheric and combustion processes. The reactions between OH and simple alkanes, alkenes, and alcohols have been particularly of interest in this program. A recent PPC spectroscopy study revealed key aspects of the dissociation dynamics of the OH-CH₄ system (DOE pub.7).¹ Photodetachment of OH⁻(CH₄) at 3.20 eV photon energy resulted in a stable van der Waals complex, OH-CH₄, and the reactant channel, OH + CH₄. The dominant channel was DPD to OH + CH₄ + e⁻, with a small fraction yielding excitation in the C-H symmetric and asymmetric stretches of CH₄. These experimental observations were qualitatively reproduced by QCT calculations that not only validated the accuracy of the potential energy surfaces used but aided in the interpretation of the experimental observations. Extending these studies to the OH-C₂H₄

system revealed similarities to the dissociation dynamics of OH-CH₄. PPC measurements carried out on OH⁻(C₂H₄) at a photon energy of 3.20 eV yielded stable, OH-C₂H₄ + e⁻, and dissociative, OH + C₂H₄ + e⁻, channels. The main channel formed was dissociation to the reactant channel as well as a minor channel with excitation in the C-H symmetric or asymmetric modes of C₂H₄. Similar to DPD of OH-CH₄, the weak repulsion between OH-C₂H₄ resulted in a low kinetic energy release (KER) of the dissociating fragments. A relevant energetics diagram for this system is shown in Figure 1, with the relevant energetics derived from the literature as noted in the caption. Using experimental results and preliminary calculations at the CCSD(T)/aug-cc-pVTZ level, we calculate D₀(OH⁻-C₂H₄) = 0.30 eV compared to D₀(OH⁻-CH₄) = 0.24 eV. This is consistent with an expectation that the binding energy between OH⁻ and C₂H₄ would be stronger than that of OH⁻-CH₄ due to the polarizability of the carbon-carbon double bond in C₂H₄. To correctly model the DPD process, an accurate full-dimensional potential energy surface of the anion is required. Lacking that, an impulsive model to account for rotational energy partitioning of the resulting photofragments has been shown to have good agreement with experimental results.^{8,9} Extension of an impulsive model to account for the high dimensionality of the OH-C₂H₄ system is currently in progress.

B. Dissociative Photodetachment of OH⁻(CH₃OH) / OCH₃⁻(CH₃OH)

PPC studies were extended to include hydroxyl radical reactions with methanol by studying the DPD of the OH(CH₃OH) system. The neutral OH-CH₃OH system lies in the entrance channel for an exothermic reaction, analogous to F-CH₃OH which was previously studied² and shown to yield both reactant, F + CH₃OH, product, HF + CH₃O, and metastable channels. The dominant channel in the fluorine reaction yielded product OCH₃ fragments in their ground vibrational state and that is also expected to be a spectator in the OH + CH₃OH → H₂O + CH₃O reaction. However, photodetachment of the precursor OH⁻(CH₃OH) anion at 3.20 eV is expected to have the best Franck-Condon overlap with the entrance channel and is therefore expected to exhibit similar dynamics to the OH-CH₄ and OH-C₂H₄ systems rather than F-CH₃OH. Both OH + CH₃OH and H₂O + CH₃O channels are accessible at 3.20 eV photon energy. Regrettably, the product mass resolution prevents unambiguous identification of the H₂O + CH₃O channel, and the data suggests it is not an important pathway. Preliminary calculations at the CCSD/aug-cc-pVDZ level suggest that the main dissociative channel formed is OH + CH₃OH (ν₆, ν=1) + e⁻. The proposed anion geometry has a bent configuration about the shared hydrogen between the oxygen in the OH moiety and the oxygen in the OCH₃ moiety. Since OH is expected to be a spectator, the mode that is excited upon DPD is the OH bending mode of CH₃OH, ν₆. Further analysis of this system is currently in progress and will be compared to the DPD of OCH₃⁻(CH₃OH).

These studies have been extended to a larger system—the reaction involving OCH₃ and CH₃OH. Similar dynamics may be expected with CH₃O⁻(HOCH₃). However, this is a symmetric thermoneutral reaction, where the anion complex most likely has Franck-Condon overlap with a pre-reactive CH₃O(HOCH₃) complex. If accessing the product channel via proton transfer from H-OCH₃ unto OCH₃, the newly formed HOCH₃ fragment would likely have significant vibrational excitation along the H-O coordinate. Preliminary calculations at the CCSD/aug-cc-pVDZ level show that the PPC spectrum is consistent with the OCH₃ + HOCH₃ products being produced with 1 quanta of vibrational excitation in the OH bending, ν₆, and stretching, ν₁, modes of CH₃OH, as shown in Figure 2. This assignment, however, assumes no rotational excitation, which is an assumption that is being investigated now in the impulse approximation. The dissociation dynamics for these systems with

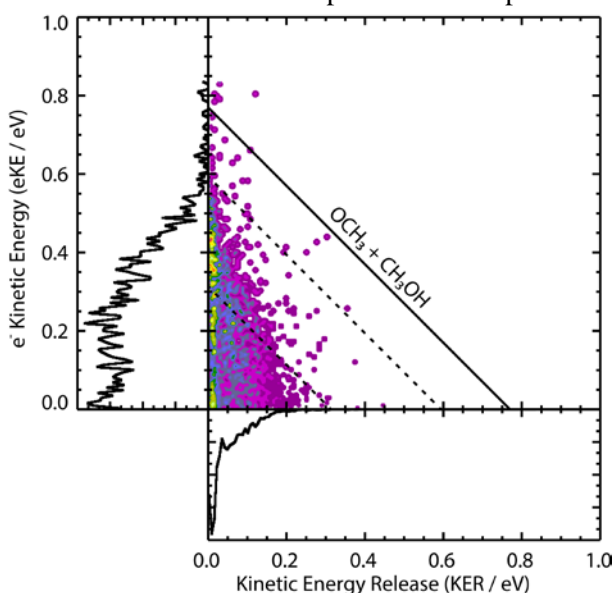


Figure 2. Photoelectron-Photofragment Coincidence spectrum of OCH₃-CH₃OH at 3.20 eV photon energy. The solid line at 0.77 eV corresponds to the kinetic energy maximum (KE_{max}) of the OCH₃ + CH₃OH channel. The dashed diagonal lines at 0.59 and 0.31 eV correspond to ν=1 in CH₃OH ν₆ and ν₁ modes, respectively.

more degrees of freedom represent a significant challenge for theory, providing further future benchmarks for studying increasingly complex reactions.

C. Photodissociation and Autodetachment of N_2O_2^-

The N_2O_2 system is an important intermediate in atmospheric processes and has been shown to have several dissociation pathways.^{10, 11} The use of the cryogenic octopole accumulation trap (COAT)¹² allowed for production of precursor N_2O_2^- anions in their ground vibrational states. Three ionic photodissociation channels were observed at 3.20 eV, revealing information about both vibrational excitation in NO^- and the dissociation dynamics for this system. Two of these channels involve photodissociation of N_2O_2^- to $\text{NO} + \text{NO}^-$ followed by either photodetachment of $\text{NO}^-(v=0)$ via a second photon or autodetachment of excited $\text{NO}^-(v>0)$. These two pathways are shown as follows: $\text{N}_2\text{O}_2^- + h\nu \rightarrow \text{NO} + \text{NO}^-(v=0) + h\nu \rightarrow \text{NO} + \text{NO} + e^-$, and $\text{N}_2\text{O}_2^- + h\nu \rightarrow \text{NO} + \text{NO}^-(v>0) \rightarrow \text{NO} + \text{NO} + e^-$, with $\text{NO}^-(v>0)$ undergoing autodetachment due to the low electron affinity of NO. The third channel observed resulted in $\text{N}_2\text{O} + \text{O}$, via a two-photon process: $\text{N}_2\text{O}_2^- + h\nu \rightarrow \text{N}_2\text{O} + \text{O}^- + h\nu \rightarrow \text{N}_2\text{O} + \text{O} + e^-$. These coincidence measurements provide state-resolved data on the autodetachment of the highly vibrationally and rotationally excited NO^- . This data is encoded in the PPC spectrum with higher vibrational excitation in NO^- appearing at higher electron kinetic energy—the opposite of a direct DPD process. This is a result of the maximum Δv vibrational autodetachment transitions that dominate in NO^- . The observed photodissociation processes are found to be consistent with photoexcitation of only the ground state *trans*-ONNO⁻ anion.

D. Dissociative Photodetachment of the Oxyallyl Anion at 388nm

Studies of the dissociation dynamics of the oxyallyl diradical, $\text{C}_3\text{H}_4\text{O}$, have been carried out by DPD of the oxyallyl anion, $\text{C}_3\text{H}_4\text{O}^-$, at 3.20 eV. The oxyallyl diradical has two nearly degenerate $^3\text{B}_2$ and $^3\text{B}_1$ electronic states as well a $^1\text{A}_1$ low-lying excited state, as previously shown by anion photoelectron spectroscopy¹³ and other experimental and theoretical techniques.¹⁴ The singlet $^1\text{A}_1$ is predicted to undergo ring closure to the more energetically stable cyclopropenone.¹⁴ Earlier work showed that a true minimum singlet C_{2v} structure could not be identified, and it was determined that the Franck-Condon region of this system is a transition state in this cyclization.¹³ Our continued work on this system follows our earlier measurement of the photoelectron spectrum in coincidence with a single stable product that resulted in the reassignment of the photoelectron spectrum of ethylenedione (OCCO)¹⁵ to the oxyallyl diradical ($\text{C}_3\text{H}_4\text{O}$),¹⁶ as reported in DOE pub. [4].

PPC spectroscopy allows resolution of the contributions of the three low-lying electronic states of the oxyallyl diradical system by the distinct kinetic energy release distributions. Photodissociation of each state results in the formation of molecular products $\text{CO} + \text{C}_2\text{H}_4$. Photodissociation occurs from the $^3\text{B}_2$ and higher-lying $^3\text{B}_1$ states via intersystem crossing to the singlet surface above the barrier to $\text{CO} + \text{C}_2\text{H}_4$. Direct photoexcitation of the $^1\text{A}_1$ state, on the other hand, creates an oxyallyl radical that is significantly different from the cyclopropenone global minimum. Photodissociation of the two triplet states, as well as the $^1\text{A}_1$ state following direct photoexcitation, results in characteristically different internal excitation in the molecular products, allowing these channels that overlap in the photoelectron spectrum to be resolved in the PPC spectrum.

Preliminary pump-probe PPC studies were performed at a photon energy of 1.6 eV in order to provide further insights into the two-photon dissociation process in the oxyallyl system reported in DOE pub. 5. Those measurements revealed a delayed ionization pathway made possible by excitation to a dipole-bound state (DBS) before autodetachment or dissociative photodetachment, the latter being a two-photon process. The timescale of this process was by definition below the laser pulsewidth of 1.2 ps. The ps Ti:Sapphire regenerative amplifier was converted into a femtosecond laser with some grating changes, producing a measured pulsewidth of 276 fs. This facilitated the design and implementation of pump-probe experiments using 775 nm light in order to quantify the two-photon process leading to dissociation of the oxyallyl diradical DBS into neutral products $\text{CO} + \text{C}_2\text{H}_4$. These efforts are still ongoing and preliminary results are currently being analyzed.

E. Future Work

In the coming months, we will finish analysis of the DPD of hydroxide and methoxide clusters mentioned above as well as the pump-probe studies on the oxyallyl system. In addition, time permitting, we will contribute to our previous studies of relevant hydroxyl radical clusters by conducting PPC

measurements on $\text{OH}^-(\text{C}_2\text{H}_2)$ and $\text{OH}^-(\text{NO})$. The important priority for later in 2020, however, is to resume studies of the IR excitation of precursor anions, with the goal of controlling product branching ratios. We will use this capability first to vibrationally induce the *cis*- $\text{HOCO}^-/\text{trans}$ - HOCO^- and $\text{HCO}_2^-/\text{HOCO}^-$ isomerizations (DOE pub. 2), and then study the mode-specific dissociation dynamics of HOCO using dissociative photodetachment. These will be the first IR excitation studies conducted on the PPC spectrometer since the implementation of COAT, allowing for greater control of precursor anion starting conditions. This work will create a blueprint for future studies of transient species with controlled internal excitation, providing benchmark data for understanding important chemical phenomena relevant to the atmosphere and combustion processes.

F. DOE-supported publications by this project 2017-2020

1. B. Shen, Y. Benitez, K. G. Lunny, R. E. Continetti, *Internal energy dependence of the photodissociation dynamics of O_3^- using cryogenic photoelectron-photofragment coincidence spectroscopy*, *J. Chem. Phys.* **147**, 094307 (2017).
2. A. W. Ray, J. Ma, R. Otto, J. Li, H. Guo, R. E. Continetti, *Effects of vibrational excitation on the $\text{F} + \text{H}_2\text{O} \rightarrow \text{HF} + \text{OH}$ reaction: dissociative photodetachment of overtone-excited $[\text{F-H-OH}]^-$* , *Chem. Sci.* **8**, 7821-7833 (2017).
3. R.E. Continetti and H. Guo, *Dynamics of transient species via anion photodetachment*, *Chem. Soc. Rev.* **46**, 7650-7667 (2017).
4. K. G. Lunny, Y. Benitez, Y. Albeck, D. Strasser, J. F. Stanton, R. E. Continetti, *Spectroscopy of Ethylenedione and Ethynediolide: A Reinvestigation*, *Angew. Chemie. Int. Ed.* **57**, 5394-5397 (2018). <https://doi.org/10.1002/anie.201801848>
5. Y. Albeck, K. G. Lunny, Y. Benitez, A. J. Shin, D. Strasser and R. E. Continetti, *Resonance-Mediated Below-Threshold Delayed Photoemission and Non-Franck-Condon Photodissociation of Cold Oxyallyl Anions* *Angew. Chem. Int. Ed.* **58**, 5312-5315 (2019). <https://doi.org/10.1002/anie.201900386>
6. B. Shen, K. G. Lunny, Y. Benitez, R. E. Continetti, *Photoelectron-Photofragment Coincidence Spectroscopy with Ions Prepared in a Cryogenic Octopole Accumulation Trap: Collisional Excitation and Buffer Gas Cooling*, *Front. Chem.* **7**, 295 (2019).
7. Y. Benitez, D. Lu, K. G. Lunny, J. Li, H. Guo, R. E. Continetti, *Photoelectron-Photofragment Coincidence Studies on the Dissociation Dynamics of the OH-CH_4 Complex*, *J. Phys. Chem. A.* **123**, 4825-4833 (2019).

III. References

1. Y. Benitez, D. Lu, K. G. Lunny, J. Li, H. Guo and R. E. Continetti, *J. Phys. Chem. A* **123**, 4825-4833 (2019).
2. A. W. Ray, J. Agarwal, B. B. Shen, H. F. Schaefer and R. E. Continetti, *Phys. Chem. Chem. Phys.* **18**, 30612-30621 (2016).
3. R. Otto, A. W. Ray, J. S. Daluz and R. E. Continetti, *EPJ Techniques and Instrumentation* **1**, 3 (2014).
4. A. W. Ray, J. Ma, R. Otto, J. Li, H. Guo and R. E. Continetti, *Chem. Sci.* **8**, 7821-7833 (2017).
5. E. Kamarchik, L. Koziol, H. Reisler, J. M. Bowman and A. I. Krylov, *J. Phys. Chem. Lett.* **1**, 3058-3065 (2010).
6. B. Ruscic and D. H. Bross, (ATcT.anl.gov, 2019).
7. J. P. Senosiain, S. J. Klippenstein and J. A. Miller, *J. Phys. Chem. A* **110**, 6960-6970 (2006).
8. C. C. Womack, W.-H. Fang, D. B. Straus and L. J. Butler, *J. Phys. Chem. A* **114**, 13005-13010 (2010).
9. B. J. Ratliff, C. C. Womack, X. N. Tang, W. M. Landau, L. J. Butler and D. E. Szpunar, *J. Phys. Chem. A* **114**, 4934-4945 (2010).
10. J. Ryden, *Nature* **292**, 235-237 (1981).
11. R. Li and R. E. Continetti, *J. Phys. Chem. A* **106**, 1183-1189 (2002).
12. B. B. Shen, Y. Benitez, K. G. Lunny and R. E. Continetti, *J. Chem. Phys.* **147**, 094307 (2017).
13. T. Ichino, S. M. Villano, A. J. Gianola, D. J. Goebbert, L. Velarde, A. Sanov, S. J. Blanksby, X. Zhou, D. A. Hrovat and W. T. Borden, *J. Phys. Chem. A* **115**, 1634-1649 (2011).
14. V. Mozhayskiy, D. J. Goebbert, L. Velarde, A. Sanov and A. I. Krylov, *J. Phys. Chem. A* **114**, 6935-6943 (2010).
15. A. R. Dixon, T. Xue and A. Sanov, *J. Chem. Phys.* **144**, 234305 (2016).
16. K. G. Lunny, Y. Benitez, Y. Albeck, D. Strasser, J. F. Stanton and R. E. Continetti, *Angew. Chem. Int. Ed.* **57**, 5394-5397 (2018).

Dynamics of Combustion Reactions

H. Floyd Davis
Department of Chemistry and Chemical Biology
Cornell University, Ithaca, NY 14853-1301
hfd1@cornell.edu

I. Program Scope:

Polyatomic free radicals undergo unimolecular and bimolecular reactions via multiple reaction intermediates and transition states, leading to competing product channels. Over the past year we have focused most of our attention on experimental studies of unimolecular reactions involving radicals. Experiments involve measuring product branching ratios as well as the product kinetic energy and angular distributions. The goal of these experimental studies is to gain insight into the topography of the relevant ground and excited electronic state reactive potential energy surfaces.

II. Recent Progress:

Our DOE-supported research employs Endstation 1 (ES1), a rotatable source crossed molecular beams apparatus originally utilizing synchrotron radiation for product photoionization detection. This apparatus has been combined with a VUV beamline in the 8.8-11.9 eV range at Cornell employing tabletop pulsed lasers.¹

a) Subpicosecond HI Elimination from Branched Alkyl Iodides²

We observed HI elimination in the 266 nm photodissociation of 2-iodopropane (~6%) and t-butyl iodide (~13%), but not for 1-iodopropane (<0.12%). The HI product angular distribution and kinetic energy release were nearly identical to those observed for the $I(^2P_{3/2})$ atomic channel. Thus HI elimination occurs on timescales shorter than 1 picosecond, *i.e.*, comparable to the timescale for direct C-I bond fission on repulsive potential energy surfaces. As described in a full paper in PCCP, we conclude that the motion of the heavy I atom in HI is largely derived from the repulsive nature of the potential energy surface correlating to R + I, with the light H atom picked up by the departing I atom late in the exit channel. This strongly contrasts HX elimination in most halogen substituted hydrocarbons, which typically follows internal conversion to the ground state surface.

b) Primary Carbene Formation from C-C Bond Fission in Alkyl Radical Photodissociation³

We have observed both C-H and C-C bond fission from 248 nm photolysis of 1- and 2-propyl radicals, and in the 266 and 320 nm photolysis of t-butyl radicals. For most experiments, flash pyrolysis of azo compounds provides intense beams of alkyl radicals. An interesting observation is that C-C bond fission appears to lead exclusively to formation of carbenes, instead of their more stable alkene isomers. For example, 2-propyl (CH_3CHCH_3) dissociates to produce CH_3 + ethylidene (CHCH_3). Somewhat surprisingly, we also observed this in the photodissociation of 1-propyl ($\text{CH}_3\text{CH}_2\text{CH}_2$). Since C-C bond fission can produce ethylene directly, this *could* be taken as evidence that isomerization of the 1-propyl radical to the 2-propyl form occurs prior to C-C bond fission. However, an alternative possibility is that isomerization of the 1-propyl radical to the more stable 2-propyl form occurs *in our pyrolysis source*, prior to supersonic expansion of radicals from the nozzle. To clarify this issue, we are carrying out parallel studies of 1- and 2-propyl radical photodissociation using *photolytic* sources of radicals, which are much less likely to undergo isomerization. For t-butyl radical photodissociation at 266 nm and 320 nm, C-C bond fission leads to exclusive production of CH_3 + dimethylcarbene (CH_3CCH_3). Our measured translational energy release distribution is in good agreement with that from the Neumark group, who studied the photodissociation at 248 nm using conventional electron impact ionization detection of products.⁴

However, the signal to noise ratios obtainable using tabletop pulsed VUV light sources in our laboratory are significantly better than possible using conventional electron impact ionization.

c) Direct Observation of Ethylidene (CH_3CH)- the Elusive High-Energy Isomer of Ethylene⁵

Since the earliest development of the concept of bonding, chemists have been fascinated by molecules exhibiting high reactivity and unusual bonding characteristics. One of the most elusive is ethylidene, CH_3CH , with a calculated enthalpy of formation about 70 kcal/mol (~ 3 eV) above its alkene isomer, ethylene ($\text{CH}_2=\text{CH}_2$). Ethylidene is thought to be a transient reaction intermediate in reactions of oxygen atoms with alkenes. It is also a ligand in transition metal chemistry. Despite extensive searches by chemists over more than sixty years, there exists no direct laboratory observation of free CH_3CH , in the gas, liquid or solid phases.

The origin of ethylidene's elusive character, first established by early theoretical electronic structure calculations, derives from the occurrence of a fast 1,2- hydrogen atom shift yielding highly vibrationally excited ethylene.⁶ On the singlet potential energy surface correlating to the ground electronic state of ethylene, there is widespread agreement that the barrier is less than a few kcal/mol, with some estimates as low as 0 kcal/mol, *i.e.*, that ethylidene is unbound relative to ethylene. Previous attempts towards the preparation of free ethylidene have primarily involved UV photolysis of stable molecules such as diazoethane (CH_3CHN_2), or its cyclic isomer, methyldiazirine. Owing to their relatively high enthalpies of formation, and because their first allowed electronic absorptions lie in the UV, nascent ethylidene is invariably produced from these precursors with very high levels of internal energy. Since spin conservation favors formation of the singlet excited state, in all previous experiments only vibrationally excited ethylene was detected.

Although no experimental values exist for ethylidene's enthalpy of formation, theory predicts that the methyl group preferentially stabilizes the singlet, lowering the singlet-triplet energy gap from 9.0 kcal/mol in methylene (CH_2) to only ~ 3.0 kcal/mol in ethylidene, with the triplet being the ground state.⁷ The height of the potential energy barrier for 1,2-H atom migration in triplet ethylidene is expected to be significant.⁸ However, the close proximity to the excited singlet surface could make intersystem crossing followed by isomerization to ethylene an important deactivation pathway even for triplet ethylidene.

In an effort to characterize ethylidene, CH_3CH , we investigated the UV photodissociation of methylketene (CH_3CHCO). Using this approach, we observed formation of both singlet and triplet ethylidene. Remarkably, at 355 nm, electronic excitation of acrolein ($\text{CH}_2=\text{CHCHO}$), a structural isomer of methylketene with nearly identical enthalpy of formation, leads exclusively to 1,3- H atom migration producing methylketene, which dissociates to form identical products. Our measurements lead to the first direct experimental determinations of the enthalpy of formation of ethylidene and the ethylidene singlet-triplet splitting.

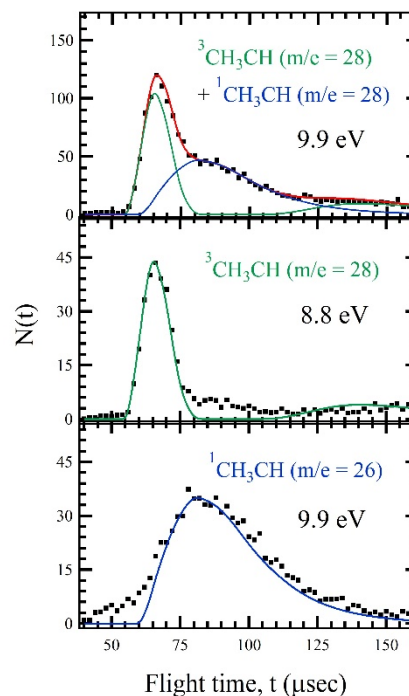


Fig. 1: Time-of-flight spectra for products from 355 nm photodissociation of acrolein at 10° : black dots are experimental data; green lines are calculated best fits for ${}^3\text{CH}_3\text{CH} + \text{CO}$ channel; blue lines are calculated best fits for the ${}^1\text{CH}_3\text{CH} + \text{CO}$; red line is overall fit. The relevant $P(E)$ s are depicted in Fig. 2.

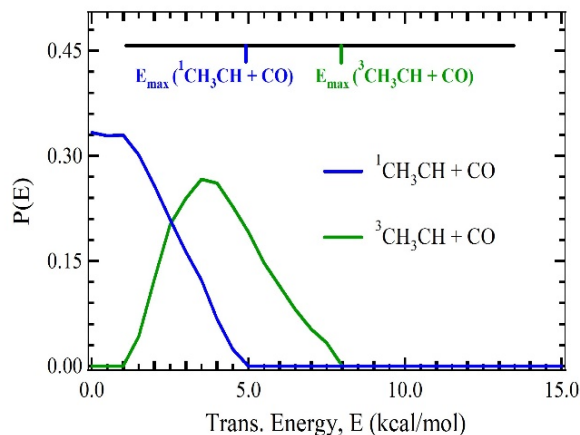


Fig. 2: Translational energy distributions for $^3\text{CH}_3\text{CH} + \text{CO}$, and $^1\text{CH}_3\text{CH} + \text{CO}$ from 355 nm photodissociation of acrolein and methyl ketene.

triplet ethylidene remains bound during transit to our detector on ~ 60 microsecond timescales, and is photoionized at 9.9 or 8.8 eV producing the parent ion, consistent with the calculated ionization energy. We believe that the slower component, observed at $m/e = 28$ and at $m/e = 26$ using 9.9 eV photoionization, corresponds to the singlet ethylidene channel. After the CO departs, the singlet ethylidene products undergo a 1,2-H shift to form highly vibrationally excited (~ 3 eV) ethylene. Although the ionization energy of cold ethylene is ~ 10.5 eV, due to the internal excitation, ionization can proceed at 9.9 eV, but much less efficiently at 8.8 eV.

Clearly, the use of methylketene or acrolein is the key to the laboratory production of ethylidene. The thermodynamic stability of these precursors, and their weak ($\sigma \sim 4 \times 10^{-20} \text{ cm}^2$ at 355 nm) relatively low-energy UV absorptions, make it possible to produce ground state ethylidene at extremely low levels of internal energy, thereby facilitating its direct observation. We recently extended our measurements to 367 nm, an energy 2.6 kcal/mol lower than at 355 nm, and observed a decreased translational energy release, as expected.

d) Photochemistry of 3-H Diazirine ($c\text{-CH}_2\text{N}_2$)⁹

First discovered in the 1960s, diazirines are the cyclic isomers of diazoalkanes. Consisting of a three-member ring, the simplest example is 3-H diazirine, $c\text{-CH}_2\text{N}_2$. Like diazoalkanes, diazirines can be explosive under certain conditions. However, they are chemically much less reactive than diazoalkanes, despite having considerably higher enthalpies of formation. Diazirines are favored carbene precursors using thermal or photochemical methods. Although many theoretical studies have been carried out on the photochemistry of simple diazirines, to date there has been relatively little work aimed at elucidating their primary photochemistry.

In Fig. 1, the TOF spectra for the $m/e = 28$ (CH_3CH) and $m/e = 26$ daughter ions from photodissociation of acrolein at 355 nm are shown. The corresponding translational energy distributions are shown in Fig. 2. Following isomerization to methylketene, dissociation occurs via the triplet and singlet surfaces, yielding ground state CO plus triplet and singlet CH_3CH . The translational energy distribution for the dominant ground state triplet ethylidene peaks well away from zero, suggesting the presence of a potential energy barrier for this channel. At 355 nm, methylketene is excited about 8 kcal/mol above the dissociation threshold for formation of ground state $^3\text{CH}_3\text{CH} + \text{CO}$. Due to the large fraction of available energy appearing as translation, the triplet ethylidene is formed with internal energies insufficient to allow intersystem crossing to the excited singlet ethylidene. Therefore,

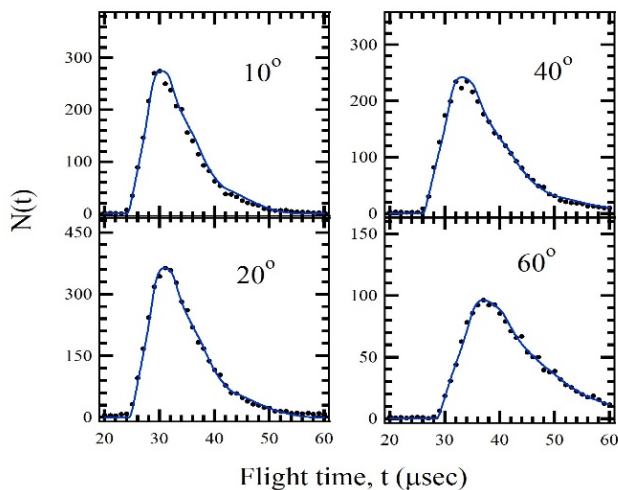


Fig. 3: Time-of-flight spectra for CH_2 ($m/e=14$) from 314.77 nm photolysis of diazirine ($c\text{-CH}_2\text{N}_2$) at indicated lab angles: The $P(E)$ is depicted in Fig. 4.

As a proof of principle towards the use of diazirines as carbene precursors, we synthesized 3-H diazirine and studied its primary photochemistry at two wavelengths. In agreement with expectations, the photodissociation products are $^1\text{CH}_2 + \text{N}_2$. Figure 3 shows the TOF spectra for CH_2 products detected using 9.9 eV photoionization. At 9.9 eV, only singlet electronically excited CH_2 is ionized. However, using electron impact ionization, we see no evidence for any significant yield of faster CH_2 products, indicating that triplet methylene is not produced to any significant extent. The translational energy distribution, shown in Fig. 4, reveals that a significant fraction of available energy is deposited into internal excitation of the products. The product angular distribution is characterized by a highly negative anisotropy (β) parameter, as expected for the perpendicular nature of the electronic transition.

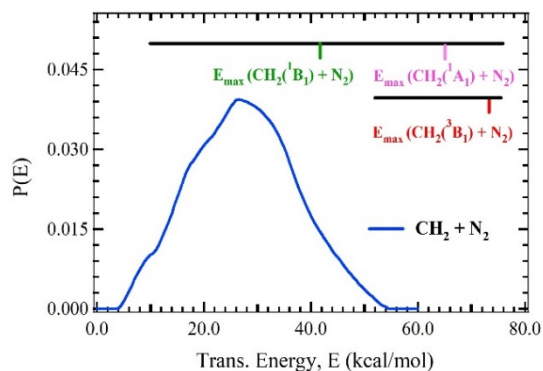


Fig. 4: Translational energy distribution for $\text{CH}_2 + \text{N}_2$ from 314.77 nm photolysis of diazirine.

III. Future Plans:

As noted above, ketenes and diazirines can be used for direct production of alkylcarbenes. We plan to continue work on these systems, initially focusing on unimolecular reactions. Our immediate primary focus will be on ethylidene (CHCH_3) and dimethylcarbene (CH_3CCH_3). For dimethylcarbene the second methyl substituent leads to additional stabilization of the singlet state. Consequently, the ground state is of singlet multiplicity, with the excited triplet thought to lie several kcal/mol higher in energy.

We have carried out some preliminary studies of reactions of hydroxyl radicals (OH) with alkenes, with our primary focus on the channels forming enols. Our recent development of an intense 8.8 eV light source for pulsed photoionization detection allows selective photoionization detection of enols without interference by their aldehyde and ketone isomers, which have higher ionization energies. We have also made some progress recently in studies of bimolecular reactions involving organic radicals such as 1- and 2- C_3H_7 and $t\text{-C}_4\text{H}_9$ with small molecules such as O_2 and C_2H_4 . These studies are ongoing.

IV. References (* denotes recent publications supported by this DOE grant):

1. D.R. Albert and H.F. Davis "Experimental Studies of Bimolecular Reaction Dynamics Using Pulsed Tabletop VUV Photoionization Detection", *Phys. Chem. Chem. Phys.* **15**, 14566-14580 (2013).
- 2*. M. A. Todt, S. Datta, A. Rose, K. Leung, and H. F. Davis, "Subpicosecond HI Elimination in the 266nm Photodissociation of Branched Iodoalkanes", *Phys. Chem. Chem. Phys.*, in press.
- 3*. S. Datta, M.A. Todt, and H. F. Davis, "C-C bond fission in alkyl radical photodissociation", manuscript in preparation.
4. B. Negru, G.M.P. Just, D. Park, and D.M. Neumark, "Photodissociation dynamics of the t-butyl radical via photofragment translational energy spectroscopy at 248 nm.", *Phys. Chem. Chem. Phys.*, **13**, 8180 (2011).
- 5*. S. Datta and H.F. Davis, "Direct observation of ethylidene, the elusive high-energy isomer of ethylene", manuscript in preparation.
6. H.F. Schaefer, "The 1,2-H Shift: A Common Vehicle for the Disappearance of Evanescent Molecular Species", *Acc. Chem. Res.* **12**, 289 (1979).
7. M.T. Nguyen, M.H. Matus, W.A. Lester, and D.A. Dixon, "Heats of formation of triplet ethylene, ethylidene, and acetylene", *J. Phys. Chem. A.* **112**, 2082 (2007).
8. L. B. Harding, "Ab Initio Studies of 1,2-H Migration in Open Shell Hydrocarbons", *J. Am. Chem. Soc.*, **103**, 7469 (1981).
- 9*. S. Datta and H.F. Davis, "Photodissociation Dynamics of 3-H Diazirine", manuscript in preparation.

Exploration of chemical-kinetic mechanisms, chemical reactivity, and molecular spectroscopy using novel numerical analysis

Michael J. Davis

Chemical Sciences and Engineering Division
Argonne National Laboratory
Lemont, IL 60439

Email: davis@tcg.anl.gov

The work explores chemically reactive systems using novel numerical analyses. One focus of the work is exploration and theoretical validation of chemical-kinetic mechanisms, using global sensitivity analysis. An effort on reaction pathway analysis has been underway. The expertise developed in the earlier work has led to the implementation of these techniques for studying problems in chemical reactivity, including isolated chemical kinetics and dynamics. There is a major effort underway for using such techniques for fitting potential energy surfaces. Another major effort underway is the application of computational optimal transport to molecular spectroscopy and dynamics. This effort includes studies of the mixing of probability densities using optimal transport and related methods. The mixing includes geodesics along positive semidefinite matrices and density matrices, which may have quantum-information applications.

Recent Progress

There was a focus on two new sets of projects. Both of these sets of projects relied on studying the geometry of probability distributions. The first of these used computational optimal transport to study molecular spectra and is a collaboration with Siefert and Prozument in our group. This work was motivated by earlier work of Zalesky and Prozument. That work depended on matching line positions and the present work compares two spectra using line positions and intensities employing computation optimal transport. A second set of projects uses optimal transport and related geometric methods to study geodesics for probability distributions and positive semidefinite matrices. The goal of that work is to design novel ways of mixing functions different than linear combinations and designing quantum systems with specific properties.

The distance between two spectra is defined by the optimal transport equation:

$$d(1,2) = \min_{t_{ij}} (\sum_{ij} c_{ij} t_{ij}), \quad c_{ij} = |\omega_i - \omega_j|^n. \quad (1)$$

The c 's are the cost of moving intensity from lines in one spectrum to the other and the t 's describe the transport of intensity. We typically use $n = 1$, which is called the Earth movers distance or the Wasserstein-1 distance, which becomes the Wasserstein-2 distance when $n = 2$. An alternative formulation to the discrete algorithm for $n=1$ calculates the distance from the cumulative distribution functions (cdf) of a spectrum:

$$d(1,2) = \int_0^{\omega_{max}} |F_1(\omega) - F_2(\omega)| d\omega. \quad (2a)$$

This formulation can be used for the comparison of two discrete spectra, two continuous spectra, or a discrete spectrum and a continuous spectrum. A cumulative distribution function is defined as:

$$F(\omega) = \int_{-\infty}^{\omega} P(\omega) d\omega. \quad (2b)$$

For a discrete spectrum this is written as a sum:

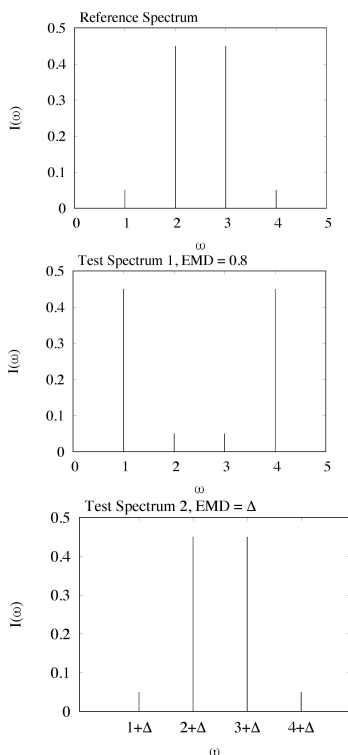


Fig. 1. A reference spectrum on top, followed by two test spectra below.

$$F(\omega_k \leq \omega < \omega_{k+1}) = \sum_{m=1}^{m=k} I_m. \quad (2c)$$

A toy problem explains how optimal transport is implemented. The following are cost matrices and optimal transport matrices for the comparison of the spectra in Fig. 1.

$$C(r,1) = \begin{pmatrix} 0 & 1 & 2 & 3 \\ 1 & 0 & 1 & 2 \\ 2 & 1 & 0 & 1 \\ 3 & 2 & 1 & 0 \end{pmatrix}, C(r,2) = \begin{pmatrix} \Delta & 1+\Delta & 2+\Delta & 3+\Delta \\ 1+\Delta & \Delta & 1+\Delta & 2+\Delta \\ 2+\Delta & 1+\Delta & \Delta & 1+\Delta \\ 3+\Delta & 2+\Delta & 1+\Delta & \Delta \end{pmatrix} \quad (3a)$$

$$T(r,1) = \begin{pmatrix} 0.05 & 0.40 & 0 & 0 \\ 0 & 0.05 & 0 & 0 \\ 0 & 0 & 0.05 & 0 \\ 0 & 0 & 0.40 & 0.05 \end{pmatrix}, T(r,2) = \begin{pmatrix} 0.05 & 0 & 0 & 0 \\ 0 & 0.45 & 0 & 0 \\ 0 & 0 & 0.45 & 0 \\ 0 & 0 & 0 & 0.05 \end{pmatrix} \quad (3b)$$

The label “r” refers to the spectrum on top and “1” and “2” the ones below it. The transport matrices, the T’s, are optimal. The Earth mover’s distance is calculated from these matrices:

$$d(r,1) = c_{12}t_{12} + c_{43}t_{43} = 0.4 + 0.4 = 0.8 \quad (4a)$$

$$d(r,2) = c_{11}t_{11} + c_{22}t_{22} + c_{33}t_{33} + c_{44}t_{44} = 0.05\Delta + 0.45\Delta + 0.45\Delta + 0.05\Delta = \Delta \quad (4b)$$

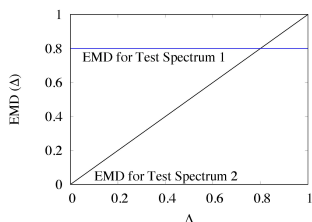


Fig. 2. Comparison of the transport distance for the two test spectra in Fig. 1.

The transport distances are plotted in Fig. 2. Test spectrum 1 has the same line positions as the reference spectrum but has different intensities. Test spectrum 2 has the same intensities as the reference but is displaced. Figure 2 and Eqs (4a) and (4b) demonstrate that this displacement must be significant, 0.8, before the distance between spectrum 2 and the reference is greater than the distance between spectrum 1 and the reference.

This happens because the intensity differences are large between spectrum 1 and the reference, indicating that the transport distance takes into account both the line displacements and the differences in intensity.

We have done a number of tests of transport distances. Consider the spectrum on the top of Fig. 3 which consists of a progression of 7 lines with structure inside each progression. The top spectrum and the ones below it are studied to demonstrate the difference between least squares fits and optimal transport. A least squares fit is based on Euclidean geometry and may not be useful for probability distributions such as the spectra illustrated in Fig. 3. The bottom two spectra in Fig. 3 have the same line positions as the spectrum at the top, but the line intensities have been randomly varied. The headings of the middle and bottom plots show the ordinary Euclidean distance as “d” and the transport distance as “t_d”. These cannot be compared directly because the units differ, but the comparisons between the spectra in the bottom two plots are what is relevant. The Euclidean distance changes somewhat between the two spectra, but the transport distance

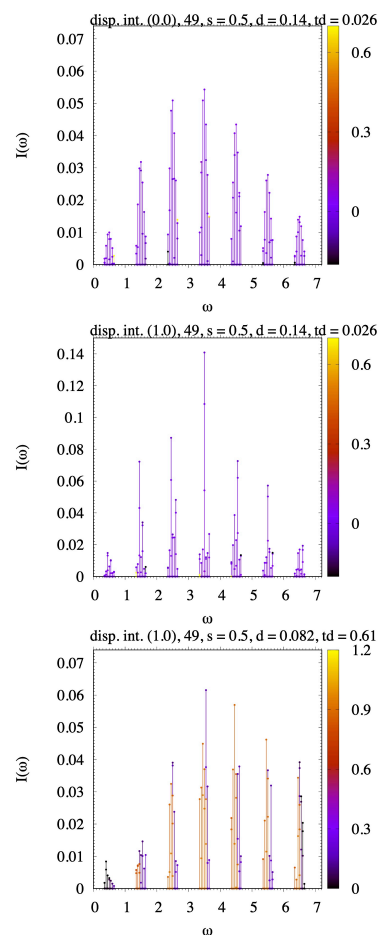


Fig. 3. Comparison of the bottom two spectra to the top.

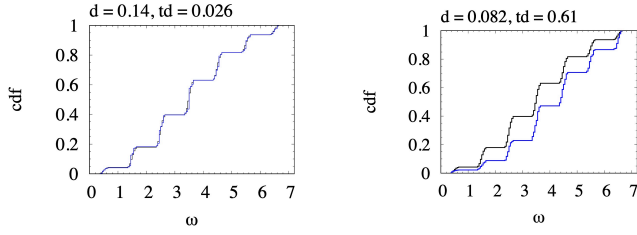


Fig. 4.

changes significantly. This is indicated by the color coding of the lines on the right, which indicates the distance in frequency space (Eq. 1) that lines move to match the spectrum at the top. The difference in t_d

occurs because the fluctuations in the spectrum of the middle panel to generate the spectrum at the top are mostly local, as the sum of the intensities in each clump is about the same for the top and middle panel. This local structure has little effect on the least squares case.

Figure 4 is a more direct view of the differences in the spectra. The black curves show the cdf for the reference spectrum and the blue curve in the left panel shows the cdf for the middle spectrum of Fig. 3 and the blue curve in the right panel shows the cdf for the spectrum in the lower panel of Fig. 3. The overtone structure of the spectra is obvious in the stairsteps. The heights of the step structures are quite different for the blue curves, leading to very different t_d 's.

The distances for spectra can be extended to continuous probability distributions. The square of the Wasserstein-2 distance between two multivariate Gaussian distributions is:

$$d^2(1,2) = \|\mathbf{m}_1 - \mathbf{m}_2\|^2 + \text{Tr}\rho_1 + \text{Tr}\rho_2 - 2\text{Tr}\left(\rho_1^{1/2}\rho_2\rho_1^{1/2}\right)^{1/2}. \quad (5)$$

The \mathbf{m} 's are the centers of the Gaussians and the ρ 's their respective covariance matrices. The probability distributions are continuous and geodesics can be calculated that connect the two distributions. The centers change along a geodesic:

$$\mathbf{m}_\tau = (1 - \tau)\mathbf{m}_1 + \tau\mathbf{m}_2, 0 \leq \tau \leq 1 \quad (6)$$

and the covariance matrix also changes along the geodesic:

$$\rho_\tau = \alpha^2\rho_1 + \alpha\beta(\sqrt{\rho_1\rho_2} + \sqrt{\rho_2\rho_1}) + \beta^2\rho_2. \quad (7a)$$

This geodesic can be used for symmetric/Hermitian positive definite matrices (all eigenvalues greater than zero), positive semidefinite matrices (some eigenvalues are zero), or quantum mechanical density matrices, positive semidefinite with their traces = 1. For positive semidefinite and definite matrices:

$$\alpha = (1 - \tau), \beta = \tau, 0 \leq \tau \leq 1 \quad (7b)$$

and for density matrices:

$$\alpha = \cos\tau - \sin\tau\cot\theta, \beta = \frac{\sin\tau}{\sin\theta}, \cos\theta = \text{Tr}\sqrt{\rho_1^{1/2}\rho_2\rho_1^{1/2}} \quad (7c)$$

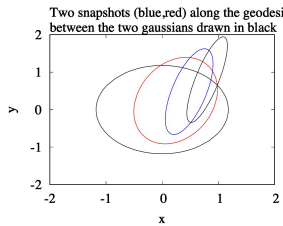


Fig. 5. Snapshots along a geodesic.

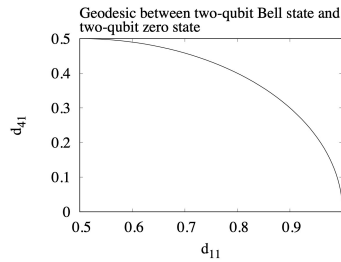


Fig. 6. Geodesic between two density matrices

To see the utility of a geodesic, first consider the case of a geodesic between Gaussians and a two-dimensional example is shown in Fig. 5. The curves are full width at half maximum for four Gaussians along the geodesic. The black curves are the initial and final Gaussians and the red and blue Gaussians along the geodesic.

The set of Gaussians generated along the geodesic are fundamentally different than a linear combination of functions and thus it provides an alternative way for designing quantum processes and basis functions from different types of favorable functions.

Because many quantum mechanical problems in chemistry are described by positive semidefinite matrices, there are many possible applications, including quantum information ones.

A collaboration with Cortes and Gray (CNM) has been initiated to study quantum information aspects of the geodesics and other paths in the space of density matrices. The following equation shows two density matrices along the geodesic between two two-qubit states, an unentangled “zero state” on the left and a fully entangled Bell state on the right:

$$\begin{pmatrix} 1.0 & 0 & 0 & 0 \\ 0 & 0 & 0 & 0 \\ 0 & 0 & 0 & 0 \\ 0 & 0 & 0 & 0 \end{pmatrix} \rightarrow \begin{pmatrix} 0.94 & 0 & 0 & 0.24 \\ 0 & 0 & 0 & 0 \\ 0 & 0 & 0 & 0 \\ 0.24 & 0 & 0 & 0.06 \end{pmatrix} \rightarrow \begin{pmatrix} 0.75 & 0 & 0 & 0.43 \\ 0 & 0 & 0 & 0 \\ 0 & 0 & 0 & 0 \\ 0.43 & 0 & 0 & 0.25 \end{pmatrix} \rightarrow \begin{pmatrix} 0.5 & 0 & 0 & 0.5 \\ 0 & 0 & 0 & 0 \\ 0 & 0 & 0 & 0 \\ 0.5 & 0 & 0 & 0.5 \end{pmatrix} \quad (8)$$

A visualization of this geodesic is in Fig. 6, which shows nonlinearity as expected from Eq. (7a). It is interesting that this particular geodesic path is so simple, involving changes in just a few matrix elements. This contrasts to successive density matrices that result from typical unitary gates applied to achieve the same final state and may be relevant to optimal control of qubits

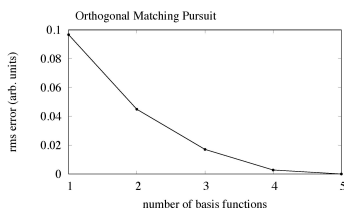


Fig. 7. Behavior of omp.

The project for fitting potential energy surfaces, a collaboration with Jasper, has continued. The sampling procedures developed in previous years have been extended to larger molecular systems. The final part of the project is to develop systematic basis selection procedures to limit the size of the basis sets used to fit the surfaces. We have implemented an “orthogonal matching pursuit” (omp) algorithm. A set of potential basis functions are chosen and omp selects functions from this set one at a time based on their overlap with the

current residual error. After choosing a new function a subsequent fit is made and a new residual vector is calculated. The procedure is repeated until the least squares error reaches a predefined minimum value. Figure 7 shows an example. The omp algorithm chose 5 basis functions out of a set of 200 test functions to accurately reproduce the model.

Future Plans

The work on molecular spectra will continue with the study of more realistic molecular spectra, both theoretical and experimental. Included in this work is the molecular inversion problem: extracting molecular specific information from spectra. Although there are some important projects underway elsewhere, the optimal transport may provide a useful and more direct approach and its utility will be investigated. The extended sampling procedures will be applied to several of the five potentials studied in the cited paper. Orthogonal matching pursuit will be tested on those potential energy surfaces. The study of the geometry of matrices will be continued, including density matrices. In particular we want to compare the behavior along geodesics with the action of quantum gates. We also want to use the geodesics as part of a quantum design process, that is the mixing of states based on the geometry of wavefunctions and density matrices.

Publications

1. M. J. Davis, W. Liu, and R. Sivaramakrishnan, “Global Sensitivity Analysis with Small Sample Sizes: Ordinary Least Squares Approach”, *J. Phys. Chem. A* **121**, 553-570 (2017).
2. G. M. Magnotti, Z. Wang, W. Liu, R. Sivaramakrishnan, S. Som, and M. J. Davis, “Sparsity Facilitates Chemical Reaction Selection for Engine Simulations”, *J. Phys. Chem. A* **122**, 7227-7237 (2018).
3. S. Bai, R. Sivaramakrishnan, M. J. Davis, and R. T. Skodje, “A Chemical Pathway Perspective on the Kinetics of Low-Temperature Ignition of Propane”, *Combustion and Flame* **202**, 154-178 (2019).
4. A. W. Jasper and M. J. Davis, “Parameterization Strategies for Intermolecular Potentials for Trajectory-Based Collision Parameters”, *J. Phys. Chem. A* **123**, 3464-3480 (2019).
5. A. Mannodi-Kanakkithodi, M. Y. Toriyama, F. G. Sen, M. J. Davis, R. F. Klie, and M. K. Y. Chan, “Machine-Learned Impurity Level Prediction for Semiconductors: The Example of Cd-Based Chalcogenides”, *NPJ Comput. Mater.* **6**, Article 39 (2020).

Electronic structure methods and protocols with application to dynamics, kinetics and thermochemistry

Richard Dawes, dawesr@mst.edu
Missouri University of Science and Technology
400 W. 11th street, Rolla, MO 65409

I. Program Scope:

(NOTE – this project is supported jointly through the CTC and GPCP programs and this report will be submitted to both programs)

Hydrocarbon combustion involves the reaction dynamics of a tremendous number of species beginning with many-component fuel mixtures and proceeding via a complex system of intermediates to form primary and secondary products. Combustion conditions corresponding to new advanced engines and/or alternative fuels rely increasingly on autoignition and low-temperature-combustion chemistry. In these regimes various transient radical species such as HO₂, ROO·, ·QOOH, HCO, NO₂, HOCO, and Criegee intermediates play important roles in determining the detailed as well as more general dynamics. A clear understanding and accurate representation of these processes is needed for effective modeling. Given the difficulties associated with making reliable experimental measurements of these systems, computation can play an important role in developing these energy technologies.

Accurate calculations have their own challenges since even within the simplest dynamical approximations such as transition state theory, the rates depend exponentially on critical barrier heights and these may be sensitive to the level of quantum chemistry. Moreover, it is well-known that in many cases it is necessary to go beyond statistical theories and consider the dynamics. Quantum tunneling, resonances, radiative transitions, and non-adiabatic effects governed by spin-orbit or derivative coupling can be determining factors in those dynamics.

Building upon progress made during a period of prior support through the *DOE Early Career Program*, this project combines developments in the areas of potential energy surface (PES) fitting and multistate multireference quantum chemistry to allow spectroscopically and dynamically/kinetically accurate investigations of key molecular systems (such as those mentioned above), many of which are radicals with strong multireference character and have the possibility of multiple electronic states contributing to the observed dynamics.

An ongoing area of investigation is to develop general strategies for robustly convergent electronic structure theory for global multichannel reactive surfaces including diabatization of energy and other relevant surfaces such as dipole-transition. Combining advances in *ab initio* methods with automated interpolative PES fitting allows the construction of high-quality PESs (incorporating thousands of high level data) to be done rapidly through parallel processing on high-performance computing (HPC) clusters.

In addition, new methods and approaches to electronic structure theory will be developed and tested through applications. This project will explore limitations in traditional multireference calculations (*e.g.*, MRCI) such as those imposed by internal contraction, lack of high-order correlation treatment and poor scaling. Methods such as DMRG-based extended active-space CASSCF and various Quantum Monte Carlo (QMC) methods will be applied (including VMC/DMC and FCIQMC). Insight into the relative significance of different orbital spaces and the robustness of application of these approaches on leadership class computing architectures will be gained.

A computational thermochemistry project recently conducted through support by the DOE SCGSR student fellowship program and collaboration with Branko Ruscic (Argonne National Labs) will be extended. A workflow framework that allows community driven expansion of the ATcT thermochemical database will be further developed. Synergy with other components of this research program such as

automated PES fitting and multireference quantum chemistry will be used to address challenges encountered by the standard approaches to computational thermochemistry (those being single-reference quantum chemistry and perturbative treatments of the anharmonic vibrational energy, which break down for some cases of electronic structure or floppy strongly coupled vibrational modes).

Recent Progress: This section describes recent progress achieved along various directions of the project occurring over the past 13 months since the project began in March 2019 (start date of this project was 03-01-2019).

Seven new articles citing DOE support have been published (or are under review) since early 2019.¹⁻⁷ A book chapter came out at the end of 2018,⁸ citing prior DOE support since the start of this project was slightly delayed. Some critical mass seems to have been reached as two invited articles are now pending. A *JPCA* feature article and a review for *Ann. Rev. of Phys. Chem.* are both due in June 2020.

The thermochemistry project spearheaded by graduate student Bradley Welch and in collaboration with Branko Ruscic and David Bross (both from ANL) has resulted in a family of user-friendly scripts implementing the thermochemistry protocol on parallel HPC clusters. This was initially reported in a publication focused on a family of methylperoxy species,⁶ and has since been extended to general benchmarks on over 200 small molecules.⁹ These scripts have already been extended to other projects by myself and by undergraduate students. Graduate student Bradley Welch defended his thesis and graduated with his PhD. He has recently moved to pursue a postdoc position under the guidance of Angela Wilson at Michigan State University.

A main thrust mentioned above has been on robust calculation and fitting of energy and property surfaces for strongly coupled and intersecting excited electronic states. We have made some excellent progress in this area and recently completed fitting 20 different states and property surfaces in the notoriously tricky NO₂ system. Rovibrational calculations solving an exact Hamiltonian were used to compare the bound states on the ground electronic state with experiment. The RMSE for the 76 levels up to 7000 cm⁻¹ above ZPE are 14.1 and 82.2 cm⁻¹ for MRCI(Q) and MRCI based PESs respectively. This confirmed the anticipated necessity of using the Davidson correction, which can introduce some technical issues when applied to high-lying intersecting states. The Davidson corrected ground state PES is the most accurate produced to date and the accuracy does not degrade for the higher energy levels. This will enable predictive quality calculations to be performed for a number of states and processes.

Success was achieved with a much greater challenge in NO₂, that of diabaticization and fitting of a number of strongly coupled and intersecting excited state energy and property surfaces. Some examples are shown in Figures 1-3 and use of these to study the complex photophysics of this system are underway.

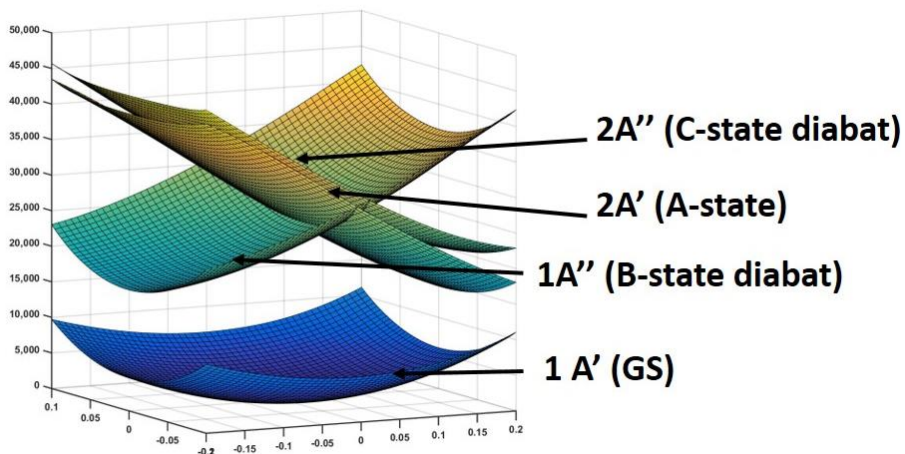


Figure 1: The two A'' states ($B + C$) are plotted in the diabatic representation for modes (v_1, v_3) , and the A -state of A' symmetry is added to the plot. The A -state is seen to closely shadow the dark C -state.

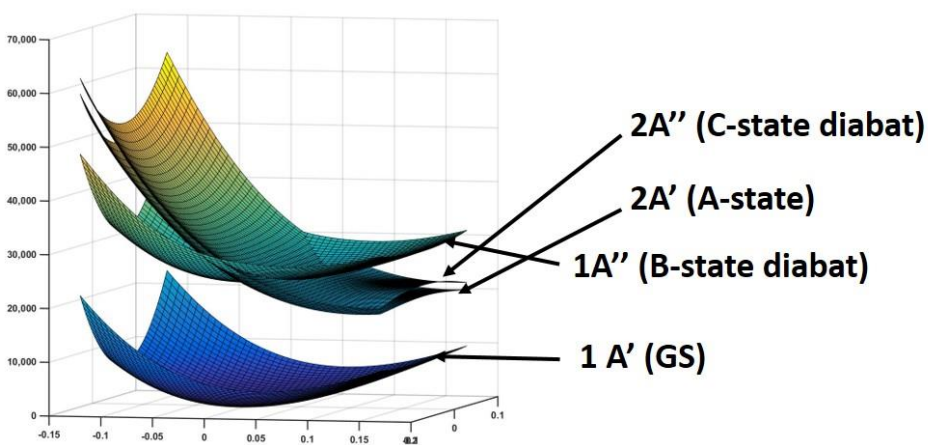


Figure 2: Same as Figure 1, but as a function of coordinates (v_2, v_3)

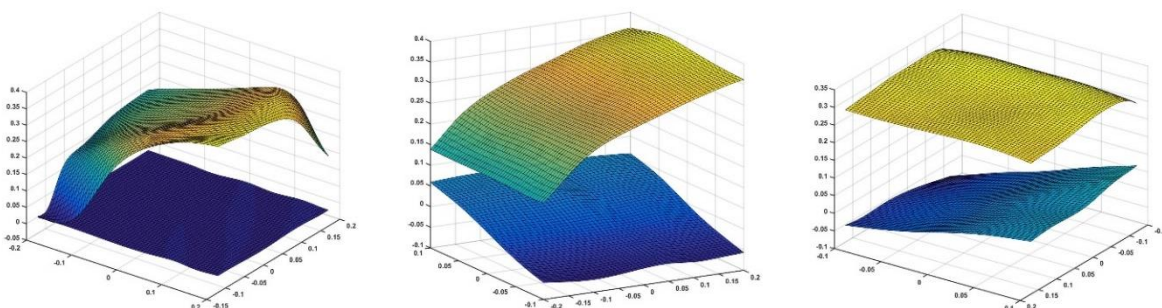


Figure 3: (left) $\langle 1.1 | \mu_x | 1.2 \rangle$ and $\langle 1.1 | \mu_x | 2.2 \rangle$ are plotted in atomic units for modes (v_1, v_2) . $\langle 1.1 | \mu_x | 2.2 \rangle$ is zero for C_{2v} geometries (when mode 3 is not displaced). (middle) $\langle 1.1 | \mu_x | 1.2 \rangle$ and $\langle 1.1 | \mu_x | 2.2 \rangle$ are plotted in atomic units for modes (v_1, v_3) . (right) $\langle 1.1 | \mu_x | 1.2 \rangle$ and $\langle 1.1 | \mu_x | 2.2 \rangle$ are plotted in atomic units for modes (v_2, v_3) .

Further progress was also made with time dependent quantum scattering with two papers by postdoc Ndengue being published.^{4,5} Ndengue continues to collaborate with our group, but has accepted a permanent position at the newly established ICTP-East African Institute for Fundamental Research, University of Rwanda. Ndengue (originally from Cameroon) is very pleased with this successful outcome.

Grant Numbers and Grant Titles

Grant No. DE-SC0019740; Electronic structure methods and protocols with application to dynamics, kinetics and thermochemistry

Grant No. DE-SC0010616; Multiple coupled potential energy surfaces with application to combustion

Postdoc(s): Steve A. Ndengué; Ernesto Quintas Sánchez

Student(s): Bradley K. Welch; Sangeeta Sur

Up to Ten Publications Acknowledging these Grants in the last 18 months

¹ Yang, Dongzheng, Junxiang Zuo, Jing Huang, Xixi Hu, Richard Dawes, Daiqian Xie, and Hua Guo. "A Global Full-Dimensional Potential Energy Surface for the K₂Rb₂ Complex and Its Lifetime." *The Journal of Physical Chemistry Letters* 11, no. 7 (2020): 2605-2610.

² Shanyu Han, Carolyn E. Gunthardt, Richard Dawes, Daiqian Xie, Simon W. North, and Hua Guo, "Origin of the 'Odd' Behavior in the Ultraviolet Photochemistry of Ozone: Solving a 30 Year Old Mystery" PNAS MS# 2020-06070

³ E. Q. Sanchez, R. Dawes. K. Lee, M.C. McCarthy, "Automated construction of potential energy surfaces suitable to describe vdW complexes with highly-excited nascent molecules: the rotational spectra of Ar--CS(v) and Ar--SiS(v)" JPC A (jp-2020-02685g).

⁴ Ndengué, Steve A., Yohann Scribano, David M. Benoit, Fabien Gatti, and Richard Dawes. "Intermolecular rovibrational bound states of H₂OH₂ dimer from a MultiConfiguration Time Dependent Hartree approach." *Chemical Physics Letters* 715 (2019): 347-353.

⁵ Han, Shanyu, Xianfeng Zheng, Steve Ndengué, Yu Song, Richard Dawes, Daiqian Xie, Jingsong Zhang, and Hua Guo. "Dynamical interference in the vibronic bond breaking reaction of HCO." *Science advances* 5, no. 1 (2019): eaau0582.

⁶ Welch, Bradley K., Richard Dawes, David H. Bross, and Branko Ruscic. "An Automated Thermochemistry Protocol Based on Explicitly-Correlated Coupled-Cluster Theory: The Methyl- and Ethylperoxy Families." *The Journal of Physical Chemistry A* 123, 5673 (2019).

⁸ Dawes, Richard, and Ernesto Quintas-Sanchez. "The Construction of ab initio-based potential energy surfaces." *Rev. Comput. Chem* 31 (2018): 199-264.

⁹ Welch, Bradley K., Richard Dawes, David H. Bross, and Branko Ruscic. (in prep).

Theoretical and Experimental Studies of Elementary Hydrocarbon Species and Their Reactions (DE-SC0018412)

Gary E. Douberly and Henry F. Schaefer III

University of Georgia, Center for Computational Quantum Chemistry and Department of Chemistry, 1004 Cedar St., Athens, GA 30602-1546

douberly@uga.edu

Program Scope

New theoretical and experimental methods in chemical physics being developed by the PIs provide great opportunities for the study of molecular species and chemical reactions of fundamental importance in combustion processes. In this research, high level quantum mechanical formalisms are a significant source of critical predictions concerning molecular systems that may be challenging for experiments. Moreover, our helium droplet experiments have opened whole new vistas for the spectroscopic study of molecular species relevant to combustion environments. Theoretical developments proposed herein include a focus on obtaining highly accurate energetics for species pertinent to combustion reactions. Experimental developments focus on strategies to characterize transient combustion intermediates associated with low-temperature hydrocarbon oxidation processes, which have been difficult to probe with other methodologies. The combination of theory and experiment to solve problems inaccessible to either alone is a hallmark of this research.

Nearly all of the proposed non-methodological experimental research will benefit from state-of-the-art molecular electronic structure theory. In some cases, the experimental group needs theoretical predictions prior to beginning a new set of experiments. In other cases, experimental findings are puzzling and need theory for interpretation. We have an abundance of experiences with both sets of problems, and the PIs have already collaborated in several such situations. Some situations where theory-experiment interaction will be particularly important include: (i) the $C_nH_m + O(^3P)$ reactions, where predictions of structures, energetics, and spectroscopic properties of complexes and adducts on both singlet and triplet potential energy surfaces will be required; (ii) the spectroscopic studies of $(NH_2)_2$, $NH-(NH_2)$, and other pre-reactive radical-radical complexes, where an interpretation will require computations of structures, energetics, and intersystem crossing rates; (iii) the near-IR and mid-IR studies of HOO-alkene complexes and related QOOH species, where computations of the excited state potential energy surface in the vicinity of the exit-channel complex will be essential; and (iv) the mid-IR studies of $\cdot C_nH_{2n+1}$ radicals, where the spectra are complicated by anharmonic and Coriolis resonances to an extent that the interpretation of these spectra will only be achievable through comparisons to effective Hamiltonian computations that employ highly accurate quartic force fields and Coriolis parameters.

Recent Projects

Infrared Spectroscopy of Alkyl and Alkyl Peroxy Radicals in Solid *para*-Hydrogen

We have initiated a collaboration with Yuan-Pern Lee's group at the National Chiao Tung University in Taiwan. One of the Douberly group's graduate students, Gregory T. Pullen, visited Professor Lee's group, and he measured spectra of alkyl radicals and alkyl peroxy radicals isolated in solid *para*-H₂. We are now analyzing the spectra, and we have recently published a paper in the *Journal of Molecular Spectroscopy* that reports the comprehensive assignment of the mid-IR spectra of *n*- and *i*-propyl radicals. Papers on propyl peroxy and butyl radicals are forthcoming. In these studies, we are employing both normal mode

and local mode effective Hamiltonian models to help assign spectra. We are studying the transferability of local mode Hamiltonian coupling parameters over a range of alkyl radical systems. We have recently recorded spectra of all four butyl radicals in helium droplets. These spectra are compared directly to those recorded for the solid-para hydrogen matrix environment. We are finding that the local mode anharmonic vibrational model is working for the more complicated butyl radical systems. Papers describing the butyl radical spectra are in preparation.

Selection of Theory Projects (no experimental contribution to the work).

A. E. Wiens, A. V. Copan, and H. F. Schaefer, “Multi-Fidelity Gaussian Process Modeling for Potential Energy Surfaces,” *Chem. Phys. Lett.: X* **3**, 100022 (2019). DOI: 10.1016/j.cpletx.2019.100022.

In our published work titled “Multi-Fidelity Gaussian Process Modeling for Potential Energy Surfaces,” we sought to draw attention to the multi-fidelity Gaussian process (GP) technique known as autoregressive Gaussian process (ARGP) modeling. This model uses transfer learning to achieve further improvements over ordinary GP regression. The ARGP technique has not been applied to the modeling of high-accuracy chemical energy surfaces before. It is particularly well-suited to electronic structure theory, where energy points can be expensive, but a large variety of approximations are available. We demonstrated the applicability of the ARGP method by presenting results for the N₂ dissociation curve and the near-equilibrium potential energy surface of H₂O. Our preliminary benchmarks suggest that it can yield substantial gains in learning efficiency.

G. J. R. Aroeira, A. S. Abbott, S. N. Elliott, J. M. Turney, and H. F. Schaefer, “The Addition of Methanol to Criegee Intermediates,” *Phys. Chem. Chem. Phys.* **19** 17760-17771 (2019). DOI: 10.1039/C9CP03480C.

Another paper that we would like to highlight is the published work titled “The Addition of Methanol to Criegee Intermediates.” Carbonyl oxides, commonly known as Criegee intermediates (CI), first gained attention as intermediates in the ozonolysis of alkenes. The important role of CIs play in tropospheric chemistry has motivated its reactions with a number of different species including alcohols. In our work, we investigated using high-level theoretical methods the potential energy surface of the reaction formaldehyde and acetone oxide with methanol through which proceeds through CIs. Experimentally it has been shown that there is a dual temperature dependence for the rate constant of the reaction of acetone oxide with methanol. We found that solely the height of the transition state barrier commands this behavior and not multiple reactions paths has had been previously suggested.

Ongoing Experimental Work and Future Plans

Sequential Capture of O(³P) and Alkenes by Helium Nanodroplets: Infrared Spectroscopy and Ab Initio Computations of the Triplet Biradical Intermediates

According to Smith *et al.* [Smith, I. W. M.; Sage, A. M.; Donahue, N. M.; Herbst, E.; Quan, D. *Faraday Discuss.* **2006**, 133, 137.], for molecule + radical reactions, the energetic difference between the molecule’s ionization energy (IE) and the radical’s electron affinity (EA) can provide insight into the nature of the reaction barrier, either *above* or *below* the reactant asymptote. They propose that a difference (IE – EA) greater than 8.75 eV indicates a real barrier above the asymptotic limit, whereas a value below 8.75 eV indicates a submerged barrier. Indeed, this difference for the O(³P) + HCN system is 12.2 eV. Accordingly, the barrier to oxygen insertion into the CN π system is \sim 10 kcal/mol above the reactant asymptote, and a van der Waals complex is observed when these species are brought together in a 0.4 K helium nanodroplet. However, O(³P) reactions with *alkenes* are predicted to cross the postulated 8.75 eV threshold as the alkene substitution pattern evolves from ethene (no substitution) to propene (methyl group substitution) to butene

(dimethyl substitution, of which there are four different isomers), and this trend was tested by Sabbah *et al.* [Sabbah, H.; Biennier, L.; Sims, I.R.; Georgievskii, Y.; Klippenstein, S.J.; Smith, I. W. *Science* **2007**, 317, 102.]. Their findings corroborated the behavior predicted by Smith *et al.* The HCN + O(³P) results presented here demonstrate the feasibility for analogous alkene + O(³P) spectroscopic studies, in which O(³P) and alkenes of varying substitution are combined in helium droplets *via* the sequential capture scheme. As the *real* reaction barrier (*i.e.* for the ethene and propene reactions) evolves to being *submerged* below the asymptotic limit (*i.e.* for the butene reactions), one might expect that strongly bound reaction intermediates, such as triplet biradicals, will be observed in helium droplets, rather than van der Waals complexes. Given the fact that a 10,000 atom helium droplet can dissipate 140 kcal/mol, it should be possible to quench the internal energy of these reaction intermediates and probe them for the first time spectroscopically.

Selected Publications acknowledging DOE support (2014-2020):

1. Christopher M. Leavitt, Christopher P. Moradi, John F. Stanton and Gary E. Douberly "Communication: Helium Nanodroplet Isolation and Rovibrational Spectroscopy of Hydroxymethylene" *Journal of Chemical Physics* **140**, 171102 (2014). Published: May 5, 2014.
2. Bernadette M. Broderick, Laura McCaslin, Christopher P. Moradi, John F. Stanton and Gary E. Douberly "Reactive Intermediates in ⁴He Nanodroplets: Infrared Laser Stark Spectroscopy of Dihydroxycarbene" *Journal of Chemical Physics* **142**, 144309 (2015). Published: April 14, 2015.
3. Christopher P. Moradi and Gary E. Douberly "On the Stark Effect in Open Shell Complexes Exhibiting Partially Quenched Electronic Angular Momentum: Infrared Laser Stark Spectroscopy of OH-C₂H₂, OH-C₂H₄, and OH-H₂O" *Journal of Molecular Spectroscopy* **314**, 54-62 (2015). Published: June 22, 2015.
4. Bernadette M. Broderick, Christopher P. Moradi and Gary E. Douberly "Infrared Laser Stark Spectroscopy of Hydroxymethoxycarbene in ⁴He Nanodroplets" *Chemical Physics Letters* **639**, 99-104 (2015). Published: September 7, 2015.
5. Christopher P. Moradi, Changjian Xie, Martin Kaufmann, Hua Guo and Gary E. Douberly "Two-center Three-electron Bonding in ClNH₃ Revealed via Helium Droplet Infrared Laser Stark Spectroscopy: Entrance Channel Complex along the Cl + NH₃ → ClNH₂ + H Reaction" *Journal of Chemical Physics*, **144**, 164301 (2016). Published: April 2016.
6. Martin Kaufmann, Daniel Leicht, Martina Havenith, Bernadette M. Broderick, Gary E. Douberly "Infrared Spectroscopy of the Tropylium Radical in Helium Droplets" *Journal of Physical Chemistry A*, **120**, 6768-6773 (2016). Published: August 16, 2016.
7. Joseph T. Brice, Tao Liang, Paul L. Raston, Anne B. McCoy, Gary E. Douberly "Infrared Stark and Zeeman spectroscopy of OH-CO: The Entrance Channel Complex along the OH + CO → *trans*-HOCO Reaction Pathway" *Journal of Chemical Physics*, **145**, 124310 (2016). Published: September 2016.
8. Peter R. Franke, Daniel Tabor, Christopher P. Moradi, Gary E. Douberly, Jay Agarwal, Henry F. Schaefer, Edwin L. Sibert "Infrared Laser Spectroscopy of the *n*-propyl and *i*-propyl Radicals: Stretch-Bend Fermi Coupling in the Alkyl CH Stretch Region" *Journal of Chemical Physics*, **145**, 224304 (2016). Published: December 2016.
9. Paul L. Raston, Emmanuel I. Obi, Gary E. Douberly "Infrared Spectroscopy of the Entrance Channel Complex Formed Between the Hydroxyl Radical and Methane in Helium Nanodroplets" *Journal of Physical Chemistry A*, **121**, 7597-7602 (2017). Published: September 2017.

10. Alaina R. Brown, Peter R. Franke, Gary E. Douberly "Helium Nanodroplet Isolation of the Cyclobutyl, 1-Methylallyl and Allylcarbinyl Radicals: Infrared Spectroscopy and Ab Initio Computations" *Journal of Physical Chemistry A*, **121**, 7576-7587 (2017). Published: September 2017.
11. Joseph T. Brice, Peter R. Franke, Gary E. Douberly "Sequential Capture of O(³P) and HCN by Helium Nanodroplets: Infrared Spectroscopy and Ab Initio Computations of the ³Σ O-HCN Complex" *Journal of Physical Chemistry A*, **121**, 9466-9473 (2017). Published: November 2017.
12. Peter R. Franke, Joseph T. Brice, Christopher P. Moradi, Henry F. Schaefer, Gary E. Douberly, "Ethyl + O₂ in Helium Nanodroplets: Infrared Spectroscopy of the Ethylperoxy Radical" *Journal of Physical Chemistry A*, **123**, 3558-3568 (2019). DOI: 10.1039/c9cp01476d. Published: April 2019.
13. Alaina R. Brown, Joseph T. Brice, Peter R. Franke, Gary E. Douberly, "Infrared Spectrum of Fulvenallene and Fulvenallenyl in Helium Droplets" *Journal of Physical Chemistry A*, **123**, 3782-3792 (2019). DOI: 10.1021/acs.jpca.9b01661. Published: April 2019.
14. Peter R. Franke, Kevin B. Moore, Henry F. Schaefer, Gary E. Douberly, "*tert*-Butyl Peroxy Radical: Ground and First Excited State Energetics and Fundamental Frequencies" *Physical Chemistry Chemical Physics*, **21**, 9747-9758 (2019). DOI: 10.1039/C9CP01476D. Published: April 2019.
15. Michael C. Bowman, Gary E. Douberly, Henry F. Schaefer, "Convergent Energies and Anharmonic Vibrational Spectra of Ca₂H₂ and Ca₂H₄ Constitutional Isomers" *Physical Chemistry Chemical Physics*, **21**, 10914-10922 (2019). DOI: 10.1039/c9cp01643k. Published: May 2019.
16. Gustavo J. R. Aroeira, Adam S. Abbott, Sarah N. Elliott, Justin M. Turney, and Henry F. Schaefer, "The Addition of Methanol to Criegee Intermediates," *Physical Chemistry Chemical Physics*, **19** 17760-17771 (2019). DOI: 10.1039/C9CP03480C. Published: July 2019.
17. Avery E. Wiens, Andreas V. Copan, and Henry F. Schaefer, "Multi-Fidelity Gaussian Process Modeling for Potential Energy Surfaces," *Chemical Physics Letters*, **X 3**, 100022 (2019). DOI: 10.1016/j.cpletx.2019.100022. Published: July 2019.
18. Gregory T. Pullen, Peter R. Franke, Karolina A. Haupa, Yuan-Pern Lee, Gary E. Douberly, "Infrared Spectroscopy of *n*-Propyl and *i*-Propyl Radicals in Solid *para*-Hydrogen" *Journal of Molecular Spectroscopy*, **363**, 111170 (2019). DOI: 10.1016/j.jms.2019.07.001. Published September 2019.
19. Mathew M. Davis, Jared D. Weidman, Adam S. Abbott, Gary E. Douberly, Justin M. Turney, Henry F. Schaefer, "Characterization of the 2-Methylvinoxy Radical + O₂ Reaction: A Focal Point Analysis and Composite Multireference Study" *Journal of Chemical Physics*, (2019), 151, 124302. 10.1063/1.5113800. Published: September 2019.
20. Jonathon P. Misiewicz, Kevin B. Moore, Peter R. Franke, W. James Morgan, Justin M. Turney, Gary E. Douberly, and Henry F. Schaefer, "Sulfurous and Sulfonic Acids: Predicting the Infrared Spectrum and Setting the Surface Straight" *Journal of Chemical Physics*, **152**, 024302 (2020). DOI: 10.1063/1.5133954. Published January 2020.

Coordination and Solvation of Actinide Cations Studied with Selected-Ion Infrared Spectroscopy
DOE Award No. DE-SC0018835

Michael A. Duncan
Department of Chemistry, University of Georgia, Athens, Georgia 30602

maduncan@uga.edu

Program Scope

Actinide metal and metal oxide cation-molecular complexes are studied in the gas phase to investigate their bonding, ligand coordination and solvation. Cation-molecular complexes of the form $M^{n+}(L)_y$, where $M = U$ or Th in singly- or doubly-charged states, and $L =$ small molecules such as H_2O , CO , N_2 , CO_2 , O_2 , or CH_3CN , are produced in a molecular beam by pulsed laser vaporization of solid metal targets. Similar methods are used to produce metal oxide complexes. Complexes containing a metal or oxide core ion with a specific number of ligand or solvent molecules are cooled by a supersonic expansion, size-selected in a time-of-flight mass spectrometer, and studied with infrared laser photodissociation spectroscopy. The resulting vibrational spectra reveal the shifts that occur for ligand/solvent vibrations upon binding to these metals and how these vary with the charge state, the number of ligands or solvent molecules present, the geometric and electronic structures of complexes, and the possible occurrence of ligand reactions mediated by the metal center. Additional experiments employ photofragment imaging technology to further investigate cation-molecular bond energies, and photodissociation experiments on larger metal oxide clusters. The experimental work is complemented by computational chemistry, with careful attention to relativistic and spin-orbit effects. The goal of these studies is an increased understanding of the fundamental interactions and electronic structure involved in actinide bonding, coordination and solvation.

Recent Progress

In a study of uranium oxide clusters, laser ablation with a few percent of oxygen added to a helium expansion was employed to produce cluster ions of the form $U_nO_m^+$. Figure 1 shows the mass spectrum obtained, which exhibits non-statistical formation of certain oxide stoichiometries. The abundant masses produced are likely determined by both the stability of oxide clusters and the kinetics of oxidation reactions. To separate these effects, we use multiphoton dissociation of size-selected clusters, with the understanding that stable clusters will appear repeatedly from many dissociation events, either as abundant cations produced or as inferred neutrals eliminated. The neutral UO_3 molecule was eliminated from many cluster sizes, and the cations $U_2O_5^+$, $U_3O_8^+$, $U_4O_{11}^+$ and $U_5O_{14}^+$ were produced repeatedly from the decomposition of larger clusters, suggesting that these species have enhanced stability. In a computational collaboration with Prof. David Dixon (University of Alabama), we investigated the structures of these species. Each has U-O-U frameworks with terminal U=O groups.

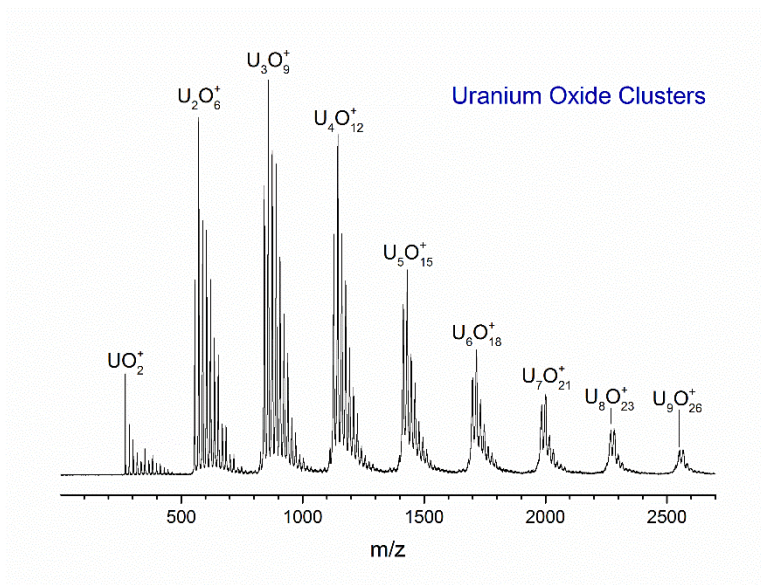


Figure 1. Mass spectrum of uranium oxide cluster cations produced by laser ablation.

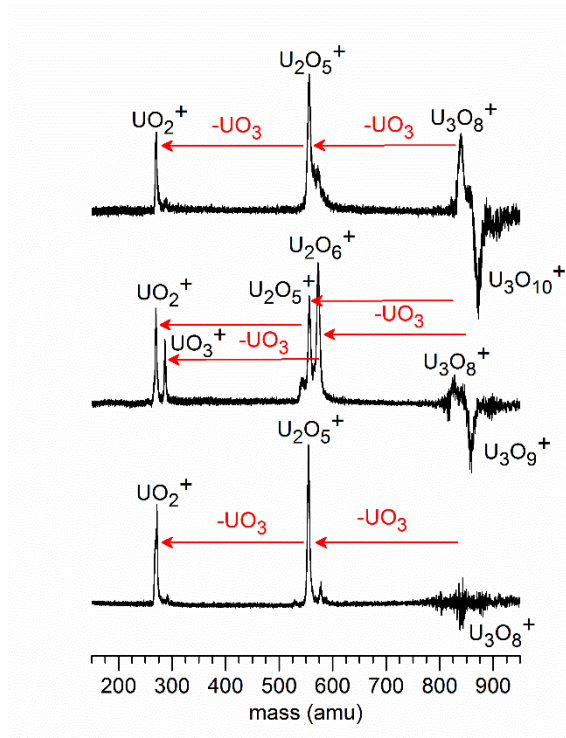


Figure 2. Multiphoton dissociation of the $U_3O_8^+$, $U_3O_9^+$ and $U_3O_{10}^+$ cluster ions at 355 nm. The negative signal represent the amount of parent ion dissociation and the positive signal represents the photofragment cations produced. As shown, the elimination of neutral UO_3 is prominent, and there is preferential formation of $U_2O_5^+$.

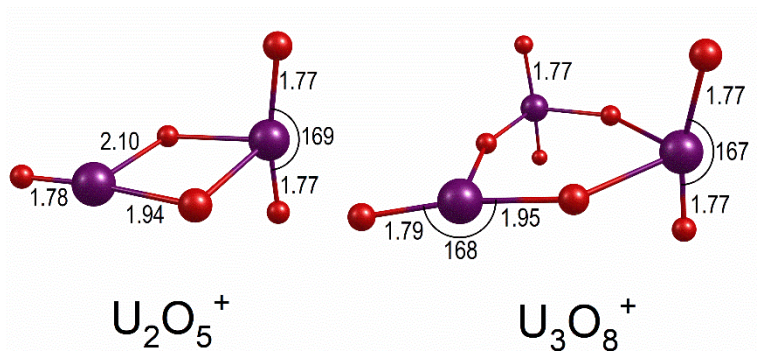


Figure 3. The lowest energy structures predicted by theory for U_2O_5^+ and U_3O_8^+ , both of which are rings with uranyl groups.

We have continued our studies on the infrared spectroscopy of $\text{U}^+(\text{L})_x$ and $\text{UO}_n(\text{L})_x^+$ complexes. In the past, we examined the carbonyl complexes of uranium and uranium oxide cations. In more recent work, we have extended these studies to complexes with $\text{L} = \text{CO}_2, \text{N}_2$, and water. The $\text{U}^+(\text{H}_2\text{O})$ cation has three vibrational bands in the O-H stretching region, consistent with the formation of both a weakly bond cation-water complex and an H-U-OH^+ metal-hydroxy complex. The N-N stretches of the nitrogen complexes were shifted to lower frequencies compared to the free- N_2 stretch, and the mass spectrum indicated a strong preference for an eight-coordinate complex. The spectrum of the $\text{U}^+(\text{N}_2)_8$ complex had a single vibrational band, indicating a high-symmetry structure. Uranium- CO_2 complexes had complex vibrational structure, indicating the possibility of both metal- CO_2 electrostatic complexes and the formation of $\text{O-U}^+-\text{CO}$ reaction products. We were able to obtain infrared spectra for both singly and doubly charged complexes. Computational studies to explain these infrared spectra are ongoing.

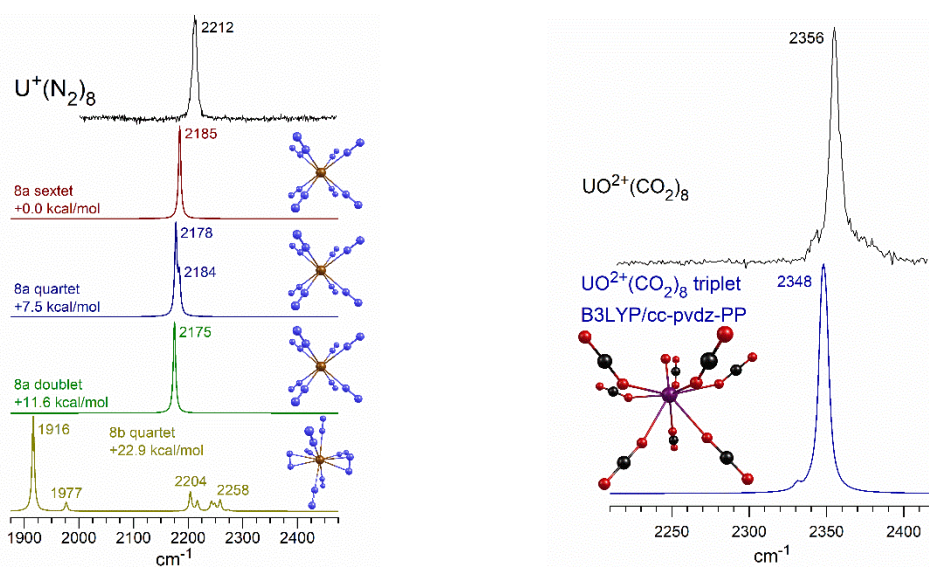


Figure 4. Infrared spectra versus the predictions of theory for the $\text{U}^+(\text{N}_2)_8$ and $\text{UO}_2^+(\text{CO}_2)_8$ complexes. Both have high symmetry structures.

We have also continued work begun under a previous DOE grant on transition metal chemistry, and have studied the complexes of several transition metal cations with acetylene. In the case of vanadium cations, single atom catalysis was observed leading to the cyclotrimerization of acetylene to form benzene. In the case of zinc cations, acetylene complexes formed a pre-reactive structure containing three acetylenes, and then the fourth acetylene was activated to form a metal-vinyl structure with a remote radical site on the distal carbon. Addition of a fifth acetylene led to a vinyl dimerization reaction.

Future Plans

In plans for future research, we will investigate the small oxide clusters of thorium using photodissociation experiments like those shown in Figure 2. We will also initiate computational studies on the species indicated to be stable. We will continue the infrared spectroscopy experiments by examining uranium-acetylene and uranium-benzene complexes. Uranium cations have been suggested previously to catalyze the cyclo-trimerization reaction to form benzene, but there is no spectroscopic evidence to confirm this.

BES Supported Publications (2017 – present; *from previous funding in the CPIMS Program)

1. *T. B. Ward, E. Miliordos, P. D. Carnegie, S. S. Xantheas, M. A. Duncan, "Ortho-Para Interconversion in Cation-Water Complexes: The Case of $V^+(H_2O)$ and $Nb^+(H_2O)$ Clusters," *J. Chem. Phys.* **146**, 224305 (2017). DOI: 10.1063/1.4984826.
2. M. A. Duncan, "Metal Cation Coordination and Solvation Studied with Infrared Spectroscopy in the Gas Phase," in *Physical Chemistry of Cold Gas Phase Functional Molecules and Clusters*, T. Ebata and M. Fujii, eds., Springer, Berlin, 2019, p. 157.
3. J. H. Marks, T. B. Ward, A. D. Brathwaite, S. Ferguson, M. A. Duncan, "Cyclotrimerization of Acetylene in Gas Phase $V^+(C_2H_2)_n$ Complexes: Detection of Intermediates and Products with Infrared Spectroscopy," *J. Phys. Chem. A* **123**, 6733–6743 (2019). DOI: 10.1021/acs.jpca.9b04962.
4. P. D. Carnegie, J. H. Marks, A. D. Brathwaite, T. B. Ward, M. A. Duncan, "Microsolvation in $V^+(H_2O)_n$ Clusters Studied with Selected-Ion Infrared Spectroscopy," *J. Phys. Chem. A* **124**, 1093–1103 (2020). DOI: 10.1021/acs.jpca.9b11275.
5. J. H. Marks, P. Kahn, M. Vasiliu, D. A. Dixon, M. A. Duncan, "Photodissociation and Theory to Investigate Uranium Oxide Cluster Cations," *J. Phys. Chem. A* **124**, 1940–1953 (2020). DOI: 10.1021/acs.jpca.0c00453.

Spectroscopic and Dynamical Studies of Highly Energized Small Polyatomic Molecules

Robert W. Field
Massachusetts Institute of Technology
Cambridge, MA 02139
rwfield@mit.edu

I. Introduction

The aim of this research program is to develop models for qualitative and quantitative understanding of complex processes in small molecules, such as vibronic coupling, predissociation, photodissociation, and isomerization. Simple models capture physical insights and lead to intuitive ideas that can enlighten a broad array of problems. Numerical fits can provide predictive power, but rarely impart insights into the underlying mechanisms responsible for the observed phenomena. This program prioritizes a quantum mechanical understanding over a perfect numerical fit of spectra. Finding few-parameter models, when those parameters have physical meaning, allows the insights gained from one problem to be easily applied to other systems. The systems currently under investigation include atmospherically relevant sulfur-containing compounds, various unimolecular processes of electronically excited acetylene, and rovibrational dynamics of formaldehyde and SO₂.

II. Recent Progress

A. PFAS Detected Hot- and Cold-Band Spectroscopy of Acetylene

We have developed a method for studying the first excited singlet state of acetylene. In this method, the UV excitation laser is focused on a molecular beam. Resonance-enhanced (at the one-photon level) multi-photon excitation occurs, which results in electronically excited photofragment species. Fluorescence from these excited species is collected as the frequency of the UV laser is scanned. This method, Photofragment Fluorescence Action Spectroscopy (PFAS), offers advantages over other detection methods. First, PFAS detection requires only one tunable laser. PFAS should apply to several other molecules, including formaldehyde, sulfur dioxide, and isocyanic acid. This one-color scheme guides and simplifies extensions to double resonance experiments. Second, the multi-photon dissociation rate can be made to compete with the decay rate of predissociated S₁ vibrational states. Third, the detected fluorescence photons are distant in frequency from that of the excitation laser, permitting efficient blocking of scattered laser light.

We have used PFAS in pursuit of two goals: (i) detailed characterization of the mechanism of *cis-trans* isomerization in S₁ acetylene and (ii) characterization of the predissociation mechanisms at energies higher than the energy of the *cis-trans* isomerization barrier.

The vibrational spectrum of S₁ acetylene above the isomerization barrier is very complicated. The usual polyad-based energy level patterns are destroyed. Assignments require systematic observation of four classes of vibration-rotation levels: even- and odd- K_a levels of both *gerade* and *ungerade* vibrational symmetry. The HCCH $\tilde{A}^1A_u-\tilde{X}^1\Sigma_g$ bands are bent \leftrightarrow linear transitions that follow $u\leftrightarrow g$ vibronic and $|K_a'-\ell''|=1$ rotational selection rules. Transitions from the zero-point vibrational level of the electronic ground state terminate in the $K_a'=1$ rotational levels of *gerade* vibrational levels. The *trans*-bending mode, ν_4 , of the \tilde{X} state is of π_g symmetry and "hot-band" transitions out of $\nu_4''=1$ ($\ell''=1$) terminate in $K_a'=0$ and 2 rotational levels of *gerade* vibrational levels of the \tilde{A} state. Doubly- hot-band transitions out of $\nu_4''=2$ ($\ell''=0$ and 2) vibrational levels terminate in $K_a'=1$ and 3 rotational levels of *gerade* vibrational levels of the \tilde{A} state. To excite into *ungerade* vibrational levels of the \tilde{A} state, one needs to exploit either IR-UV double resonance excitation or excitation via $\nu_5''(\pi_u)$ hot bands.

The first type of experiment that we have performed is cold-band spectroscopy of S_1 acetylene. In order to achieve a more complete description of the unimolecular dynamics in the S_1 state, vibrational levels that lie far above the predissociation barrier must be systematically observed and assigned. The minimum of the *cis* geometry well of the S_1 surface lies $\sim 4000\text{ cm}^{-1}$ above the minimum of the *trans* well, the predissociation onset lies about 1000 cm^{-1} above this, and the barrier to isomerization lies $\sim 1000\text{ cm}^{-1}$ higher still. Unfortunately, states with energies near and above the isomerization barrier have sufficiently short lifetimes that disentangling their Laser Induced Fluorescence (LIF) signal from scattered excitation laser light is difficult. PFAS, however, offers the tools required to observe such states. Experiments in this energy region have been performed, and the detection and assignment of additional transitions has improved our characterization of the *cis-trans* isomerization transition state on the S_1 potential energy surface.

The second type of experiment is hot-band spectroscopy of S_1 acetylene. Both linear and *trans*-bent electronic states of acetylene possess *g/u* symmetry. Vibrational states of both *gerade* and *ungerade* symmetries must be observed in order to complete the characterization of the *cis-trans* isomerization transition state on the S_1 electronic surface. In order to access states with *ungerade* vibrational symmetry, either two-photon (IR-UV double resonance) excitation or an *ungerade* lower state vibrational level must be used. Hot-band spectroscopy has been performed by expanding the acetylene gas from a specially designed heated tube. Collisions in the supersonic expansion are very efficient at cooling rotation, but much less so at cooling vibration. The interrogated molecules, then, have enhanced hot-band signal without sacrificing the ease of making of rotational assignments. Figure 1 illustrates how the relative intensities of hot ($\Delta \leftarrow \Pi 2^1 3^3$, $K_a'=2$) and cold ($\Pi \leftarrow \Sigma 1^1 3^1$, $K_a'=1$) bands are affected by the electric power applied to the heated tube.

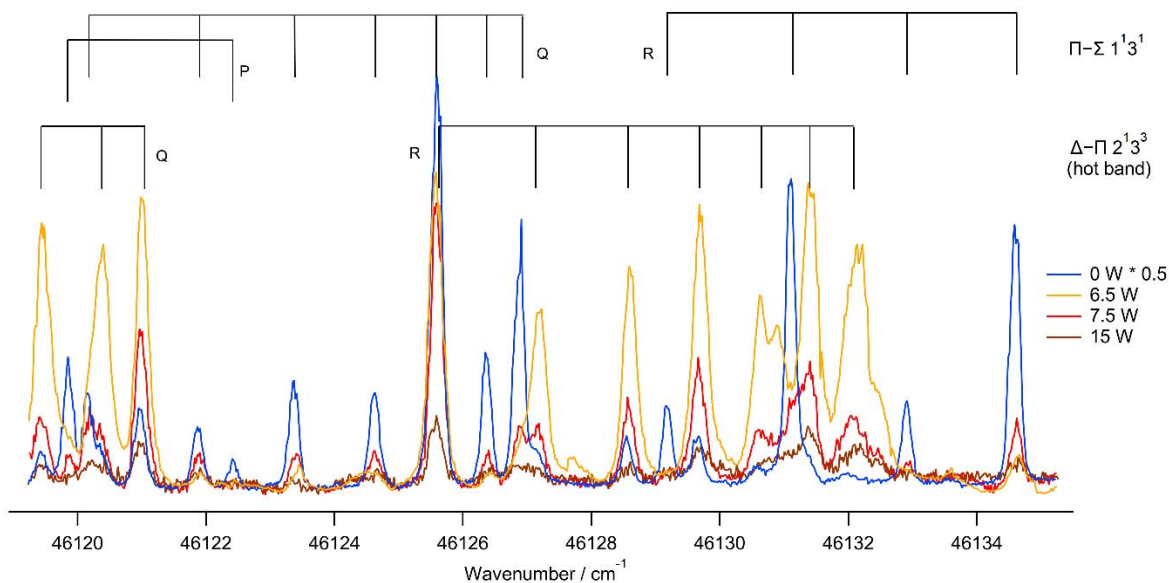


Figure 1: Changes in a portion of the spectrum of acetylene due to a change in temperature of the heated nozzle (expressed as power dissipated). The intensities of hot-band lines increase while the intensities of the cold band lines decrease when the heater is turned on. The total intensity decreases as the temperature of the heated-nozzle increases, but the large intensity increase in the hot bands offsets this decrease.

The PFAS experiments provide symmetry-allowed access to two of the four classes of vibration-rotation states required to characterize the S_1 surface. The ν_4 and ν_6 vibrational modes of the *trans*-bent isomer are strongly mixed by Darling-Dennison and Coriolis interactions. The vibrational states form polyads, with conserved quantum number, $B=\nu_4+\nu_6$. The Darling-Dennison

matrix element is independent of K_a and the Coriolis matrix element is linear in K_a . Thus, in order to understand the three factors that affect the energies of the bending modes (the unperturbed energies and the Coriolis and the Darling-Dennison interaction matrix elements), information from $K_a'=0, 1, 2$ rotational levels must be obtained. which can be obtained from S_0 vibrational levels that belong to at least one even (0 or 2) and one odd (1) value of ℓ'' . Access to both *gerade* and *ungerade* vibrational levels is also required. While it might seem unfortunate that the same energy region of the S_1 state must be examined four times for completeness, it provides an opportunity to take advantage of Franck-Condon factors to guide the choice of optimal S_0 state vibrational levels. It also means that the spectrum is roughly 1/4 as cluttered as it would be if all levels needed were visible at once, significantly simplifying analysis of the spectra.

II. Future work

Figure 2 illustrates unexpected effects observed in the acetylene PFAS spectrum that merit further investigation. In the heated-nozzle PFAS spectrum, each feature in the spectrum exhibits multi-exponential fluorescence-decay. The fast and slow decay rates are associated with formation of electronically excited C_2 and C_2H photofragments, respectively. The fast:slow ratio exhibits strong and unexplained line-to-line variations. We have observed similar decay rate variations in other S_1 acetylene spectra. However, previous observations of level-specific decay patterns have utilized excitation via different S_1 vibrational states or alternate filter-schemes were designed to optimize detection of a specific fluorescent photofragment. In the example displayed in **Figure 2**, different lines within the same energy region, and even within the same vibrational band, exhibit distinctly different decay characteristics. Whether this is a statistical anomaly or indicative of the competing photofragmentation mechanisms warrants further investigation.

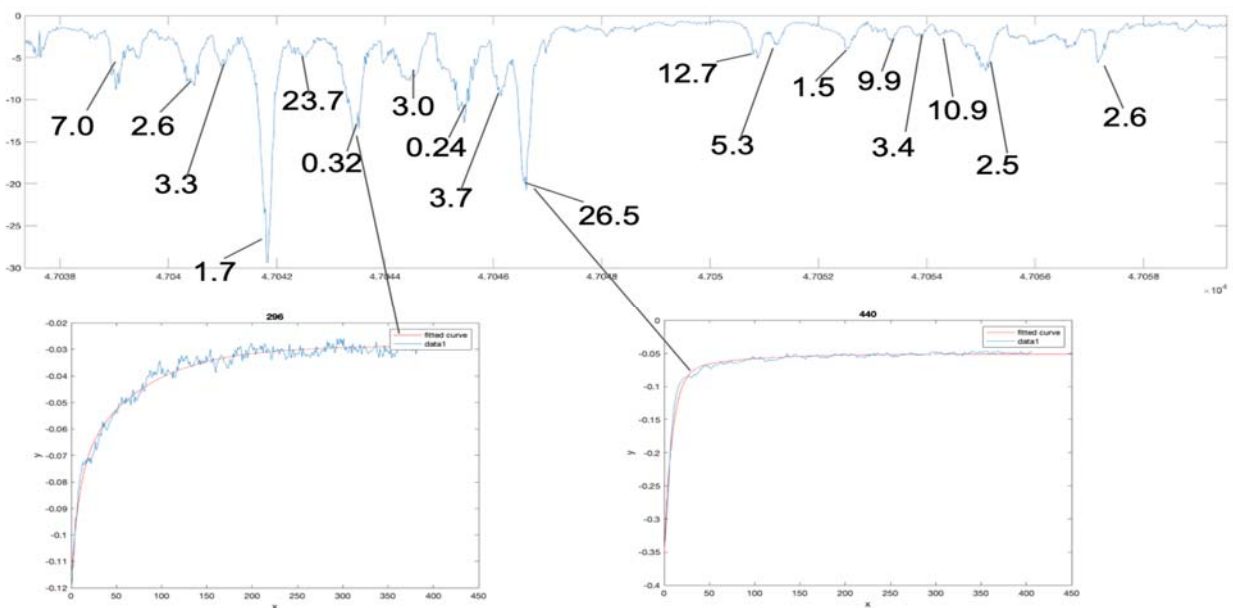


Figure 2: Photofragment Branching Ratios in the Acetylene PFAS Spectrum. Each of the features in the heated nozzle PFAS spectrum exhibit multi-exponential decays: a fast component due to formation of electronically excited C_2 and a slow component due to formation of electronically excited C_2H . The fast:slow amplitude ratios for each feature in the PFAS spectrum are displayed in the upper panel and two decay curves (with ratios 0.32 and 26.5) are shown, each connected by a tie line, in the lower panels. Interesting photodissociation dynamics may be uncovered with further investigation.

We are interested in investigating two problems using Discrete Variable Representation eigenstate analysis. The first problem involves the \tilde{C} state of SO_2 . The \tilde{C} state of SO_2 is subjected to

a two-step diagonalization process, in which a partial diagonalization was performed prior a full diagonalization. The partial diagonalization transforms the normal mode matrix into a Kellman mode matrix, which treats the most important anharmonic and Coriolis resonances. In the original analysis, several interactions between normal modes were ignored in the partial diagonalization. We believe it may be worth investigation to set some couplings of internal coordinates, such as the coupling between θ , the central angle of the molecule, and the bond lengths, r_1 and r_2 , to zero instead, and observing how that alters the Kellman modes, and the Kellman representation of the eigenvectors. We also believe that DVR offers a fruitful avenue of investigation for S_1 acetylene. DVR allows for quick classification of states (as long as the dimensionality of the problem investigated is not too high), as the basis functions are simple and a relatively small number of them is sufficient to describe most systems. We suspect that a participation-number based analysis, where participation number is roughly equivalent to the number of basis states significantly involved in representing an eigenstate, will yield relevant information about the transitions from normal mode coordinates to local mode coordinates in the region of an isomerization barrier

III. Publications supported by this project 2016-2020

1. K. Prozument, J. H. Baraban, P. B. Changala, G. B. Park, R. G. Shaver, J. S. Muentner, S. J. Klippenstein, V. Y. Chernyak, and R. W. Field, "Photodissociation Transition States Characterized by Chirped Pulse Millimeter Wave Spectroscopy," *Proc. Natl. Acad. Sci.* **117**, 146-151 (2020).
2. J. Jiang, A. Muthike, T. Erickson, and R. W. Field, "One-color (212-220nm) Resonantly-Enhanced (S_1 - S_0) Multi-photon Dissociation of Acetylene," *J. Mol. Spectrosc.* **36**, 24-33(2019).
3. J. Jiang, C. Saladrigas, T. Erickson, C. Keenan and R. W. Field, "Probing the Predissociated Levels of the S_1 State of Acetylene via H-atom Fluorescence and Photofragment Fluorescence Action Spectroscopy" *J. Chem. Phys.* **149** 174309 (2018).
4. J. Jiang, Z. Du, and R. W. Field, "Determination of the Sign of the Population Difference in a Two-Level System by Frequency-Modulation Spectroscopy," *Mol. Phys.* (2020).
5. J. Jiang, Z. Du, J. Liévin, and R. W. Field, "One-Color (~220 nm) Resonance-Enhanced (S_1 - S_0) Multi-Photon Dissociation of Acetylene: Probe of the C_2 A-X Band by Frequency Modulation Spectroscopy," *Mol. Phys.* (2020).
6. W. Transue, A. Velian, M. Nava, M.-A. Martin-Drumel, C. Wommack, J. Jiang, G.-L. Hou, X.-B. Wang, M. McCarthy, R. W. Field, and C. Cummins, "A Molecular Precursor to Phosphoacetylene and its Application in Synthesis of Aromatic 1,2,3,4-Phosphatriazolate Anion" *J.A.C.S.* **138**, 6731 (2016).
7. G. B. Park and R. W. Field, "Perspective: The First Ten Years of Broadband Chirped Pulse Fourier Transform Microwave Spectroscopy" *J. Chem. Phys.* **144**, 200901 (2016).
8. G. B. Park, J. Jiang, and R. W. Field, "The origin of unequal bond lengths in the \tilde{C}^1B_2 State of SO_2 : Signatures of high-lying potential energy surface crossings in the low-lying vibrational structure" *J. Chem. Phys.* **144**, 144313 (2016).
9. J. Jiang, G. B. Park, and R. W. Field, "The Rotation-vibration Structure of the SO_2 \tilde{C}^1B_2 State Explained by a New Internal Coordinate Force Field" *J. Chem. Phys.* **144**, 144312 (2016).
10. G. B. Park, J. Jiang, C. A. Saladrigas, and R. W. Field, "Observation of b_2 Symmetry Vibrational Levels of the SO_2 \tilde{C}^1B_2 State: Vibrational Level Staggering, Coriolis Interactions, and Rotation-vibration Constants" *J. Chem. Phys.* **144**, 144311 (2016).

IMAGING THE NEAR-SURFACE GAS PHASE: A NEW APPROACH TO COUPLED GAS-SURFACE CHEMISTRY

Jonathan H. Frank, Farid El Gabaly, Nils Hansen, Christopher J. Kliewer, David L. Osborn
Sandia National Laboratories, Livermore, CA

jhfrank@sandia.gov, felgaba@sandia.gov, nhansen@sandia.gov, cjkliew@sandia.gov,
dlosbor@sandia.gov

Coleman Kronawitter and Ambarish Kulkarni

Department of Chemical Engineering, University of California, Davis
ckrona@ucdavis.edu, arkulkarni@ucdavis.edu

PROGRAM SCOPE

The chemical reactivity of gases with solid surfaces is ubiquitous in natural and industrial energy transformation. Cooperative effects that couple gas phase chemistry with surface chemistry are critical for foundational understanding but challenging to probe experimentally and theoretically. Heterogeneous catalysis is an ideal field to expose and isolate the fundamental chemical physics of these cooperative effects. We have recently started a program to characterize gas-surface coupling, through chemically specific, temporally and spatially resolved probes of both reacting surfaces and the near-surface gas phase. The program combines optical and mass spectrometry probes of both gas phase and surface species. The long-term goal of the proposed work is to elucidate the fundamental mechanisms of cooperative gas-surface chemistry, influencing DOE mission research in catalysis, synthesis, and energy transformation.

This program comprises two interrelated thrusts that are distinguished by the physical mechanism of gas-surface coupling – transport or reaction – and employ differing degrees of chemical complexity and control over the model catalyst surface. The first thrust explores how molecular transport in the gas phase may mediate coupling between different domains on a surface without gas-phase chemical reactions and employs well-controlled reactions on atomically cleaned crystalline and polycrystalline surfaces prepared under UHV conditions, with reactivity studied under pressures of 10^{-6} to 760 torr. The second thrust adds the complexity of reactive coupling, with bond breaking and formation among intermediates occurring in the gas phase as well as on the surface. Thrust 2 utilizes both single crystal metal oxide and more complex surfaces (e.g., doped metal oxides, and bifunctional supported catalysts), with reactivity studied at elevated temperatures (700 - 1250 K) and pressures of 1 – 1500 torr.

RECENT PROGRESS

Design and Procurement of an Optically Accessible Ambient Pressure Imaging X-Ray Photoelectron Spectrometer

We have designed a truly novel experimental system that simultaneously allows for optical spectroscopy techniques, including 2D coherent anti-Stokes Raman scattering (2D-CARS), femtosecond sum-frequency generation (SFG) and planar laser-induced fluorescence (PLIF), to be performed alongside 2D imaging ambient pressure X-ray photoelectron spectroscopy (AP-XPS). The system also includes a flexible gas handling system and a variety of surface science techniques such as LEED, Auger and sputtering. Imaging AP-XPS delivers the power of x-ray photoelectron spectroscopy to measure and quantify, via core-level transitions, spatially resolved (~10 microns) oxidation states of surface species. AP-XPS is successful even with gas pressures of 1 – 20 torr above a surface. The addition of laser spectroscopy will add simultaneous observation of near-surface gas phase molecules. This combination enables direct and detailed correlation of surface oxidation states with near-surface gas phase composition. Over the first year of the proposal we worked to complete the design and procurement of this large experimental system which includes: a newly developed, fast CMOS electron detector, a state-of-the-art hemispherical analyzer, a monochromatic X-ray gun capable of operating at gas-pressures of up to 20 torr, a 5-axis motorized sample manipulator, a combination of surface science techniques in a preparation

chamber, and optical access to the sample surface during operation. This special-order system is being manufactured and is expected to be installed in early 2021.

Surface Science Chamber for Ultrafast Sum Frequency Generation, 2D-CARS, and PLIF Analysis of Coupled Gas-Surface Interactions The gas-surface chemical mapping reactor chamber described above will enable breakthrough understanding of the feedback between gas-phase reactants and intermediates and detailed surface chemistry, resolving, for example, the feedback mechanism in many oscillatory hydrocarbon oxidation reactions at surfaces that exhibit time-varying kinetics. The local catalytic product flux will be correlated with imaged surface oxidation. While we await installation of this chamber in early 2021, we have constructed a relatively miniaturized combined ultra-high vacuum (UHV) / high pressure reaction chamber for detailed surface (and near-surface) spectroscopy to be carried out over surfaces that have been atomically cleaned prior to gas-surface reactions. The optical chamber design enables UHV conditions ($\sim 10^{-9}$ Torr) to be reached quickly because of the small surface area. Both the manipulator and turbomolecular pump can be shut off from the chamber through pneumatic gate valves, and the chamber can be filled with reactant gasses with pressure range from UHV to 1 atm. The chamber is equipped with an ion sputtering gun and Auger electron spectrometer, and the sample holder can be heated to 800C or cooled with a liquid nitrogen cold finger. This allows for an atomically clean, annealed surface as the starting point for our gas-surface experiments. Several optical access ports around the sample enable ultrafast 2D-CARS, SFG, and PLIF analysis of the reacting surface and near-surface gas phase. We have recently demonstrated initial studies of time-resolved femtosecond sum-frequency generation vibrational spectroscopy for molecules that are physisorbed to a metal surface. With funding under the final year of a DOE Early Career Award, we have investigated the adsorption, vibrational lifetime, and rotational motion of CH_4 and CO adsorbed on a $\text{Au}(111)$ surface, and characterized the nature of the energy transfer and bonding of these weakly adsorbed species. As described below in Future Work, this apparatus will now be used to image the *local* catalytic production of HD in the H_2/D_2 exchange reaction over a patterned Pt surface using 2D-CARS where the gas phase acts as a reporter on local spatially resolved catalytic activity.

Imaging of Gas-Phase Species in Catalytic Oxidation of Methanol over Ag A great deal of catalysis research has focused on investigating surface chemistry in ultra-high vacuum (UHV). However, most catalysts are operated at pressures that are orders of magnitude above UHV conditions. Elevated pressures involve a different operating regime with higher surface coverage of reactants and a greater probability of gas phase chemical reactions. Therefore, *operando* experiments are needed to provide mechanistic understanding at realistic conditions.

During the first 1.5 years of this research program, we developed an initial flow reactor for gas-phase measurements above a catalyst surface and demonstrated in-situ *operando* measurements using 1D Raman

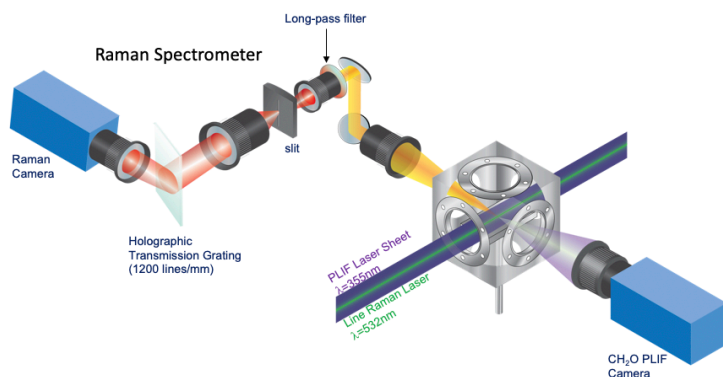


Figure 1: Optically accessible flow reactor

scattering, 2D planar laser-induced fluorescence (PLIF), and molecular beam mass spectrometry of minor species. We demonstrated these diagnostics capabilities through investigations of partial oxidation of methanol over polycrystalline Ag: a system that is widely used for industrial production of formaldehyde. This target catalysis system provides a convenient testbed for developing and implementing a suite of diagnostic techniques relevant to our future work. As the silver surface is heated to temperatures of 350-700C, catalytic production of formaldehyde

progresses via two main pathways of partial oxidation: $2\text{CH}_3\text{OH} + \text{O}_2 \rightarrow 2\text{H}_2\text{CO} + 2\text{H}_2\text{O}$, and dehydrogenation $\text{CH}_3\text{OH} \rightarrow \text{H}_2\text{CO} + \text{H}_2$.

The experimental configuration of our optically accessible flow reactor is shown in Fig. 1. The reactor consists of a 4-inch cube with fused silica windows on opposite sides for collecting LIF and Raman signals. A mixture of reactants enters the cube forming a laminar boundary layer flow across the 150nm thick silver catalyst that is mostly Ag(111) facets. 2D PLIF imaging of formaldehyde and 1D spontaneous Raman scattering from major species are collected on opposite sides as shown.

A representative CH_2O PLIF image and Raman spectrum from this system (the latter taken ~ 50 μm above the catalyst surface) are shown in Fig. 2. In addition to the dominant Raman peaks from the reactant mixture (CH_3OH , O_2 , N_2), we observe peaks from H_2O , CO_2 , O_2 , and CH_2O . Because N_2 is unreactive, its concentration reflects total number density and is used to determine the temperature by the Ideal Gas Law. As a complement to these optical approaches, we have also applied a molecular beam mass spectrometer (MBMS) to provide a global view of the species present in partial oxidation of CH_3OH over Ag (Fig. 3). Unlike conventional downstream analysis of effluent gas by mass spectrometry in previous heterogeneous catalysis experiments, in our approach reaction gases are sampled immediately above the catalysts surface through a quartz nozzle with a 40° cone angle and a ~ 50 μm orifice diameter. The rapid expansion of gas beyond the orifice forms a molecular beam, stopping all

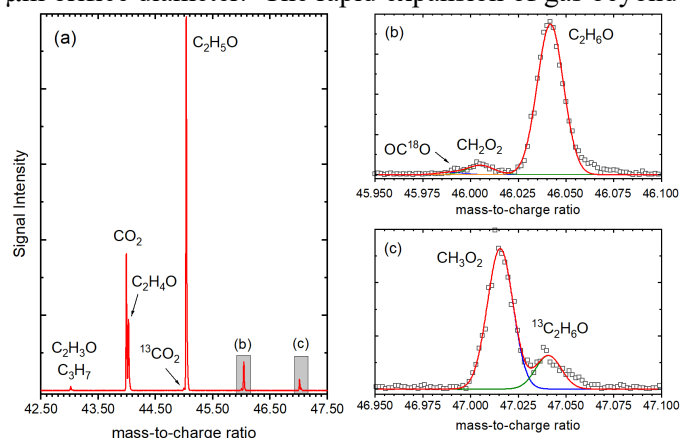


Figure 3: Electron impact ionization molecular beam mass spectra of the $\text{CH}_3\text{OH} / \text{Ag}$ system

and mass spectrometry measurements, which will leverage our long history of developing and applying these diagnostic techniques for studies in combustion science.

FUTURE WORK

Transport-Mediated Gas-Surface Coupling and Domain-Specific Chemistry

Resolving the local reaction kinetics and mechanism during surface catalyzed reactions as they vary from one crystallographic domain to the next, under ambient pressure conditions, is a foundational but elusive measurement for understanding gas-surface catalytic reactions. We aim to accomplish this task by directly monitoring local gas-surface reactive exchange rate across the many crystallographic domains of a typical polycrystalline catalyst. These measurements will show the effects that the local crystallographic termination, structure, and oxidation state, or the local average concentration of steps and defects within a

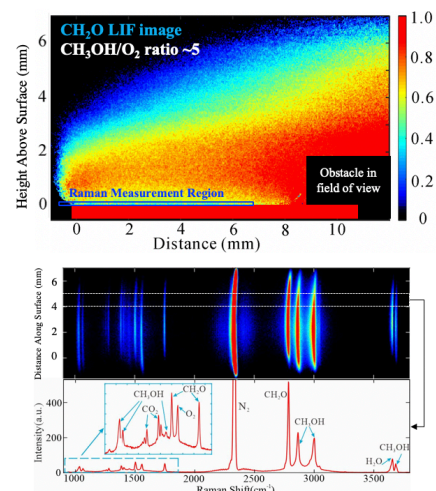


Figure 2: Preliminary optical data of the near-surface gas phase in CH_3OH partial oxidation over Ag

further chemistry, which preserves both closed and open-shell species. These neutral molecules are ionized by either electrons or VUV photons, and analyzed by orthogonal acceleration time-of-flight mass spectrometry. Although the results are preliminary, we detect all the species expected based on the optical measurements, plus many unexpected intermediates such as CH_3 , CH_3O , and other unexpected peaks as shown in Fig. 3. This ability to perform *operando* detection of the spatial distributions of gas-phase species above a catalyst using in-situ measurements is a significant step towards gaining insight into the complex coupling between gas-phase and surface chemistry. Our next steps will involve quantification of both the optical

domain, have on the product formation rate for polycrystalline (nonuniform) catalysts. Gas-phase composition measurements will also determine which key species are transported via the gas-phase to other crystallographic domains.

The full imaging AP-XPS system will be installed early next year as the vendor is now producing the device, and we will prepare for the arrival of this chamber by initiating the optical portion of our first studies in the optical surface science chamber which is currently completed. The first set of experiments in the new instrument will involve joint gas-surface measurements of H₂-D₂ exchange over patterned Pt samples to form HD. We anticipate that the local crystal structure will influence reaction rates, and that this physics could be directly measured by monitoring the gas-surface exchange and product formation rates with 2D-CARS presently, along with surface characterization with ambient pressure XPS to monitor oxidation state when the full system arrives. The resulting dataset will provide a complete picture of the gas-surface chemistry for that catalytic process and will help validate microkinetic models.

Next, we will study the oxidation of H₂ over polycrystalline Rh. It is known that this reaction proceeds with time-varying, even oscillatory reactions kinetics. The unproven mechanism is believed to be a feedback between surface oxidation state, which in turn alters the dissociative adsorption rate of gas phase O₂. As the sub-surface oxide is consumed, the adsorption rate of O₂ increases. Once a high enough surface concentration of O is achieved, sub-surface O begins to form, and the sticking coefficient for O₂ again decreased allowing dissociative adsorption of H₂ to again compete. However, there is little direct proof of this postulate. By combining gas-phase imaging of the reactants and products with surface specific AP-XPS and SFG, we will directly measure if, in fact, this is the true feedback mechanism which creates oscillating kinetics for hydrogen oxidation over Rh.

Mechanistic Studies of Oxidative Coupling of Methane

Concurrent to efforts in technique development, our UC Davis collaborators are designing and fabricating new catalysts to facilitate mechanistic studies of a more complex reaction – the oxidative coupling of methane (OCM) – that involves dynamic exchange of intermediates between the surface and gas phase. Despite nearly four decades of academic and industrial research, OCM has not yet been commercialized. Although much is known about the reaction mechanism, fundamental details about the feedback between gas-phase and surface reactions remain elusive. It is generally accepted that the first C-H activation step is surface-mediated and is related to the activity of the catalyst. The overall OCM reaction on a metal-doped oxide surface involves (1) activation of the C-H bond in methane and desorption of •CH₃, (2) coupling of •CH₃ in the gas phase to form C₂ products, and (3) creation of surface oxygen vacancies by water desorption, which are replenished by O₂ dissociation. Although direct evidence remains lacking, a wide variety of catalysts are believed to follow this mechanism. In collaboration with UC Davis, we aim to directly probe the near-surface reactive species and provide fundamental insights into the reaction mechanism. Specifically, we plan to begin our studies with well-defined thin films of Li-doped MgO(001), owing to the considerable available literature for Li-doped MgO catalysts. Moreover, we hypothesize that this relatively simple catalyst will be more amenable to theoretical simulation than other mixed-oxide materials. Our goal is fundamental mechanistic understanding, derived from 1) experimental probes of gas phase species using PLIF and universal mass spectrometry, and 2) theoretical investigations of how the modified surface (*i.e.* the active site) controls the nature of the interaction with methane and of the subsequent binding/release of radicals. In order to facilitate comparison of our observations with numerical simulations using detailed chemical models (microkinetic modeling), we plan to improve experimental designs to provide simpler flow fields with more well-defined boundary conditions. Further diagnostics will be added to provide measurements of key species relevant to hydrocarbon catalysis chemistry.

BES-sponsored publications, 2018 – present

- 1) The project was funded in September, 2018. A manuscript on partial oxidation of methanol is under preparation.

GAS-PHASE CHEMICAL KINETICS UNDER EXTREME CONDITIONS

C. Franklin Goldsmith, PI

Brown University

Program Scope

One of the grand challenges for the Department of Energy is the ability to simulate the complex interactions between fluid mechanics and chemical kinetics for gases at high pressures (e.g. 100 bar). Under these conditions, the ideal gas equation of state is not valid. Although considerable advances have been made regarding real-gas equations of state for thermodynamic properties, the same cannot be said of chemical kinetics under extreme pressures. The standard approach in computational kinetics assumes that reactions occur under isolated conditions. Real-gas behavior can have a profound effect on the chemical source terms in reactive flow simulations. These many-body interactions can change both the rate constants and the product branching fractions.

In this project, we are investigating different methodologies to quantify many-body effects on transition states and thence high-pressure effects on rate constants. The specific aims are: (i) develop chemically accurate surrogate potential energy surfaces for computational kinetics with explicit solvent molecules, and use this surrogate model within molecular dynamics simulations; (ii) quantify the effects of high pressures on rate constants for different reaction families; (iii) determine the pressure at which solvent cage effects will cause the branching fractions in bond-fission reactions to favor molecular elimination products; and (iv) analyze the results for possible trends that can be applied heuristically.

Recent Progress

The first part of the project has been to investigate how we can build effective, accurate surrogate potential energy surfaces (PES). Our goal is to develop a procedure that is effectively “black box” – *i.e.* it does not require much fine tuning or maintenance from the user. Our initial focus has been on machine learning methods, primarily artificial neural networks (ANN).

One of the key reaction families we wish to investigate is homolysis, or the cleavage of a single bond in a closed-shell species to produce two radicals (the reverse reaction is radical-radical recombination). The current state-of-the-art is variable reaction coordinate transition state theory (VRC-TST) by Dr. Stephen Klippenstein. One of the challenges with VRC-TST is that it is computationally quite demanding. The transition state partition function is multidimensional (typically 5D). The resulting multi-dimensional integrals are solved via Monte Carlo (MC) sampling in which multi-reference calculations (*e.g.* CASPT2) are performed on-the-fly.

Our work has focused on replacing these costly CASPT2 calculations within the MC sampling routine with a surrogate PES. The idea is to first train an ANN to a small subset of CASPT2 calculations. This training data must cover all the relevant regions of phase

space that would be sampled in the VRC-TST algorithm. We experimented with different strategies for generating training data. Ultimately, we settled on using Sobol sequences to create a structured grid in the phase space volume. In order to maximize the accuracy of the surrogate PES while simultaneously minimizing the size of the training data, we generated two sets of training data (see Figure 1). The first set is denser, and it focuses on the region in phase space volume where the forces are largest (*e.g.* $r < 3.5 \text{ \AA}$, where r is the center-of-mass distance between the two radical fragments); we found that $\sim 2,000$ training images in this region is sufficient. The second set focuses on longer-range interactions, where the magnitude of the forces is considerably smaller; this region requires far fewer images, typically ~ 100 . The first dataset prioritizes high-temperature conditions, where the dynamical bottleneck is typically located at small r values, and the second dataset is more appropriate for lower temperatures, where r approaches infinite separation.

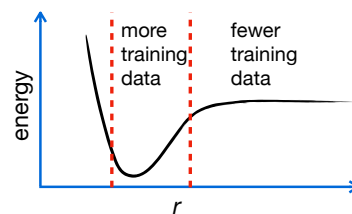


Figure 1: illustration of the two sampling domains.

To test these methods, we considered five different radical-radical recombination reactions: $\text{CH}_3 + \text{CH}_3$, $\text{CH}_2\text{CH} + \text{O}_2$, $\text{CH}_3\text{CCH}_2 + \text{O}_2$, $\text{CH}_3\text{CHCH} + \text{O}_2$, and $\text{CH}_3 + \text{NO}_2$. These reactions were chosen to consider systems with variable number of elements (which is a known challenge for ANN methods) and variable number of atoms. Additionally, we considered two different regression strategies. In the first strategy, the cost function included only the total potential energy. In the second strategy, the cost function also included the forces per atom.

Because training with forces provides so much more data per image, we required far fewer images – typically a factor of ten fewer. The results of these two strategies are presented in Figures 2 and 3, respectively. In both cases, the ANN potential agrees with the CASPT2 results to within 20% over a broad range of temperatures, which was our metric of success.

These results are very encouraging, because a typical MC routine will require tens of thousands of single-point calculations. Moreover, in a typical publication, we will iterate this process over different trial dividing surfaces before settling on a final schema. Thus, the new approach reduces the total number of CASPT2 calculations by at least an order of magnitude, and in most cases closer to two orders of magnitude.

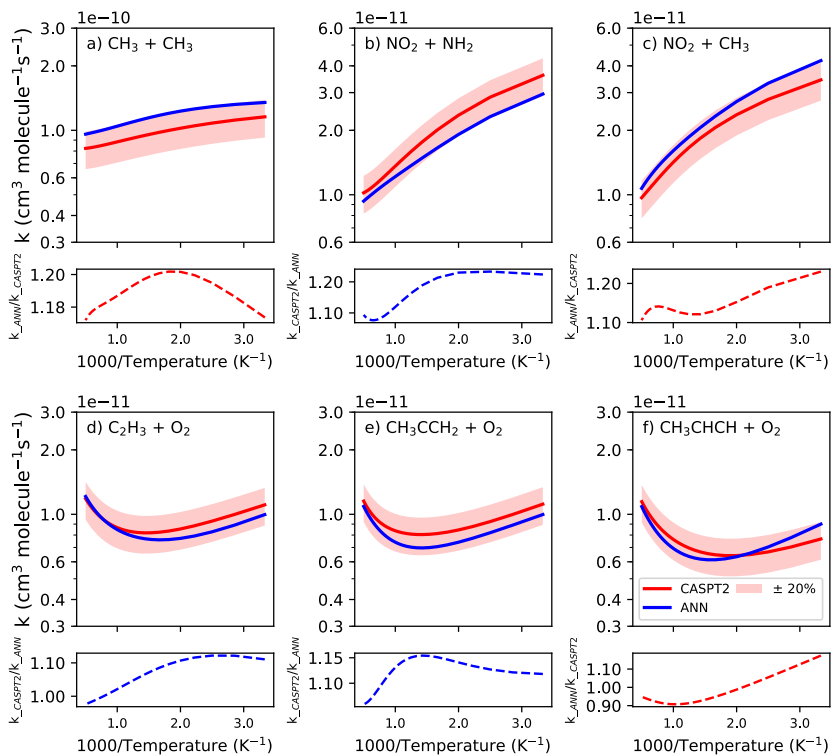


Figure 2: results for training with energy only. The solid red line is the current state-of-the-art, in which the MC sampling routine uses CASPT2. The solid blue line is the result when the ANN potential is used. The pink shaded region is a 20% uncertainty band around the CASPT2 results.

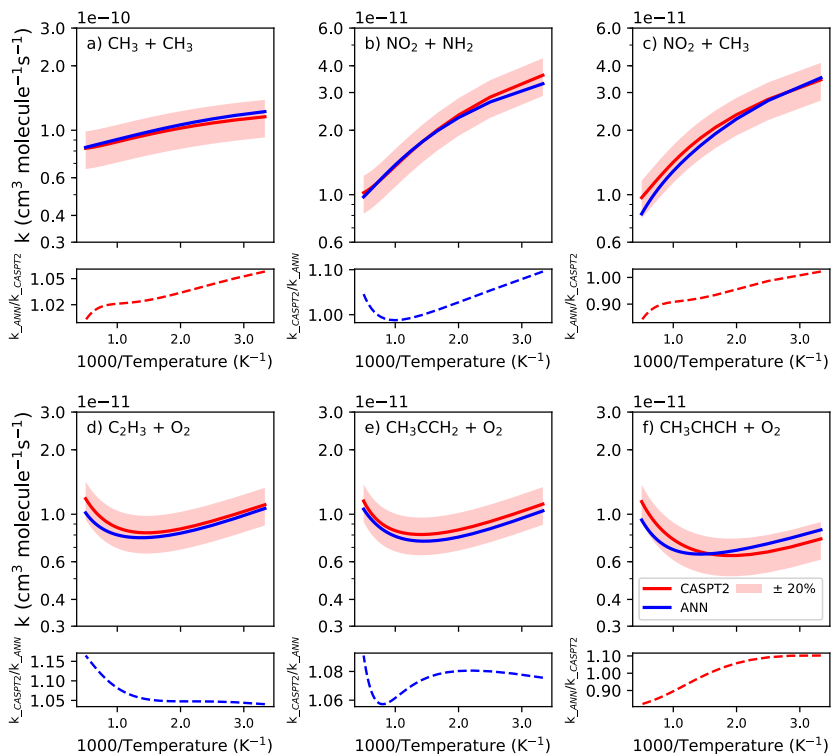


Figure 3: results for training with energy and forces (same symbols as in the previous figure).

The training-with-forces approach yielded better performance with fewer calculations. However, that result doesn't tell the complete picture. MOLPRO provides two different implementations of the CASPT2 method. One implementation is computationally much more efficient, but it lacks analytical gradients, and thus the forces must be computed via finite differences. The other implementation is more efficient at computed forces, but that method (which does not make use of internal contractions) is computationally more demanding for energies. Consequently, even though training with forces requires fewer images, the computational cost ends up being nearly the same.

Additionally, we wanted to investigate how accurate we could make the surrogate model with respect to the baseline case. By increasing the number of training images, we could effectively dial-in the ANN potential to arbitrary accuracy. Figure 4 shows the results when the number of training images increases to ~12,000. At this point, the agreement is within 1%.

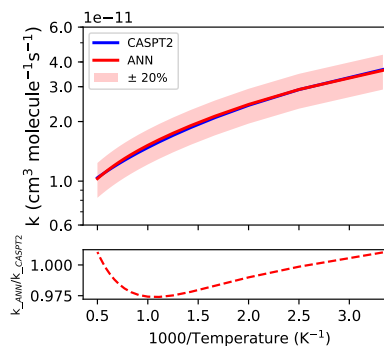


Figure 4: The $\text{CH}_3 + \text{NO}_2$ rate constant, but with more training data.

Future Plans

Presently, we are now working on setting up molecular dynamics simulations involving ANN potentials and forces. Our goal is to compute the change in volume of activation. The current project is to investigate the $\text{CH}_3 + \text{C}_3\text{H}_8 \rightarrow \text{CH}_4 + \text{C}_3\text{H}_7$ reaction in different bath gases, including CH_4 , H_2O , CH_2O , O_2 , and N_2 . We have hired a new post-doc, Dr. Mostafa Abedi, who is developing the methods to perform MD simulations using ANN force fields.

BES Supported Products

- This grant supported Dr. Xi Chen for the final year of her doctoral dissertation. She successfully defended her PhD in Physical Chemistry in September, 2019. As part of her dissertation, she developed a new Python-based implementation of VRC-TST, which is designed to be more user friendly and easier to interface with machine learning methods.
- The results summarized above were published in the *Journal of Physical Chemistry A*, in a special edition devoted to machine learning in physical chemistry. Xi Chen and C. Franklin Goldsmith “Accelerating Variational Transition State Theory via Artificial Neural Networks” *JPCA* 124 (2020) 1038-1046
- The PI was the lead organizer of a symposium “New Techniques in Computational Kinetics” at the 17th International Conference on Numerical Combustion. This symposium brought together researchers from multiple disciplines to discuss cutting-edge methods for automated chemical kinetics.

Computer-Aided Construction of Chemical Kinetic Models

William H. Green
Department of Chemical Engineering
Massachusetts Institute of Technology
Cambridge, MA 02139
whgreen@mit.edu

I. Program Scope

The combustion chemistry of even simple fuels can be extremely complex, involving hundreds or thousands of kinetically significant species. The most reasonable way to deal with this complexity is to use a computer not only to numerically solve the kinetic model, but also to construct the kinetic model in the first place. Because these large models contain so many numerical parameters (e.g. rate coefficients, thermochemistry) one never has sufficient data to uniquely determine them all experimentally. Instead one must work in “predictive” mode, using theoretical values for many of the numbers in the model, and as appropriate refining the most sensitive numbers through experiments. Predictive chemical kinetics is exactly what is needed for computer-aided design of combustion systems based on proposed alternative fuels, particularly for early assessment of the value and viability of proposed new fuels. It is also very helpful in other fuel chemistry problems, and in understanding emissions and environmental chemistry. However, making accurate predictions is very challenging, particularly for the complicated systems where the predictions are most needed.

Our research effort is aimed at making accurate predictive chemical kinetics practical and testing the accuracy of our predictions. This is a challenging goal which requires a range of science advances. Our research spans a wide range from quantum chemical calculations on individual molecules and elementary-step reactions, through the development of improved rate/thermo calculation procedures, the creation of algorithms and software for constructing and solving kinetic simulations, the invention of methods for model-reduction while maintaining error control, and finally comparisons with experiment. Many of the parameters in the models are derived from quantum chemistry, and the models are compared with experimental data measured in our lab or in collaboration with others.

II. Recent Results

A. Aromatic Ring Formation Chemistry

The formation of aromatics, particularly polycyclic aromatics, is a major problem in many systems, leading to particulate air pollution, fouling of equipment and engines, and because some are carcinogenic. While this has been heavily studied, many issues are unresolved and we are still far from having models which are consistent both with experimental observations, rate theory, and the laws of thermodynamics. To try to fill in the gaps in existing knowledge, my group has experimentally measured several different ring-forming reactions [[Smith, JPCA 2020](#); [Chu, PCCP 2019a](#); [Lai, E&F 2020](#)], we have computed many rate and thermochemical parameters using quantum chemistry, and we have made detailed kinetic models for the formation of the first two aromatic rings at a variety of reaction conditions. [[Chu, PCCP 2019b](#); [3](#), [5](#)]

B. Predicting Nitrogen and Sulfur Chemistry

We developed a computer method for rapidly predicting thermal (mostly free-radical) chemistry for nitrogen-containing and sulfur-containing molecules, and distributed it open-source as part of the Reaction Mechanism Generator (RMG) software suite. This was considerably more complicated than C,H,O chemistry because both nitrogen and sulfur have several different valencies, allowing a variety of different resonance forms and quite a rich set of possible functional groups and feasible types of chemical

reactions. Some of these functional groups and reaction types have been well-studied in the literature, but many have not. We filled in the gaps with quantum chemistry calculations. We made the limited experimental data, our computed values, and group-contribution based estimates for rate coefficients and thermochemical parameters based on those values publicly available through the rmg.mit.edu website.

We have applied the new ability to build detailed kinetic models for nitrogen and organonitrogen chemistry to the pyrolysis and oxidation of ethylamine [4] (measured by Ron Hanson's group) and to understand the complicated effects of NO_x addition on the partial oxidation of alkanes measured by Yiguang Ju's group [Zhao, *Energy* (2018)]. We used this new capability to develop a model for hydrazine (N₂H₄) chemistry, starting with its exothermic decomposition, which is important both for satellite thruster design and for safety analysis. We discovered that molecular weight growth chemistry occurs in hydrazine systems simultaneously with the decomposition chemistry, similar to how hydrocarbon pyrolysis leads to a mix of small molecules and large molecules such as polycyclic aromatics. In collaboration with Ahren Jasper we characterized the key reactions involving N₃H_x and N₄H_x molecules [8] formed during hydrazine decomposition.

We also have computed a large number of sulfur-containing molecules and their reaction rates using quantum chemistry, and from them developed methods to estimate rate coefficients and thermochemical parameters for a wide variety of organosulfur compounds, including oxidized sulfur forms. We published a paper demonstrating our ability to predict the pyrolysis chemistry of organic sulfides [Class, *PCCP* (2019)] including the formation of thiophene rings, comparing to our own experimental data, and we compared our automatically-generated detailed kinetic model for the photochemically-driven oxidation of dimethylsulfide at conditions relevant to the troposphere to literature data.[15]

C. Tracking isotopes, correcting symmetry factors in TST calculations

We have added the capability to automatically track isotopic enrichment and specific isotopomers to the RMG software suite. RMG can now very reliably predicted "filiation", e.g. given a certain mixture of ¹³C isotopomers in the initial mixture predict the relative yields of isotopomers in the reaction products, or vice-versa infer the original site-specific isotope enrichment from those measured in the final products.[Goldman, *Chem.Geo.* (2019); Julien, *Chem.Geo.* (2020)] This is very helpful in isotope analysis because it avoids the need to synthesize authentic standards of specific isotopomers.

When predicting isotopomer yields we noticed that the predictions for systems where symmetrical X + X reactions are important were much less accurate than for other systems. Investigation revealed that there was a factor of 2 confusion in the transition state theory formula for X+X reactions presented in an influential 1978 paper, which propagated into many errors in reported k's and TST software over the last 4 decades. In many cases a factor of 2 in a small number of rate coefficients is not significant compared to other errors in a simulation. But a factor of 2 is often much larger than the small differences in reactivity of different isotopomers, so for isotope analysis this is crucial. We have identified and corrected the error and carefully explained the whole issue in recent papers.[12;13]

D. Improvements to the Overall Mechanism Construction Process

We have developed an improved overall workflow, where we iterate between adding additional reactions to the mechanism (e.g. using RMG) and improving the values of uncertain rate and thermo parameters in the existing model (e.g. by automatically spawning quantum chemistry calculations [1;7], and using the results to improve rate and thermo estimates [2;Lai, *JPCA* (2019)]). The first step reduces the mechanism truncation error [10], i.e. it improves the structure of the model, while the second step reduces the error in the model parameters. We are exploring the use of machine learning (ML) to automatically make better estimators for thermochemistry and Ea's [Li, *JPCA* (2019); Grambow, *JPC Lett* (2020)] as additional

information becomes available. We have also assessed methods to quantify the uncertainty in the predictions of ML models for thermochemistry & other molecular properties.[Scalia, [JCIM \(2020\)](#)]. As may have been expected, it is easy to derive good uncertainty estimates for molecules and reactions similar to those already studied, but uncertainty estimates for very different molecules are often way off (and usually too optimistic). We are collaborating with Stephen Klippenstein and Judit Zador on automating the whole process of building a kinetic model including all the needed quantum chemistry calculations. We have made advances in speeding these calculations [[11](#)] and in quantifying the uncertainties in the final kinetic model predictions.[[14](#)] All of the advances reported in this document have been incorporated into the open-source RMG software, new version 3.0. Many of the rate and thermochemistry estimation tools in RMG are also available in human-friendly form at rmg.mit.edu.

III. Future Plans

We are currently working both experimentally and computationally on the reaction sequence that follows when naphthalene radicals are in the presence of acetylene. This rather readily forms acenaphthalene, but at many reaction conditions the rate of formation of anthracene and phenanthrene are rather low, indeed experiments by Kaiser's group could not detect these products. But phenanthrene and anthracene are known to be major products in pyrolytic systems and flames; this suggests there may be other important routes besides the well-known HACA growth mechanism. We are also working on understanding acetylene pyrolysis, trying to model experimental data measured in Deutschmann's lab in Karlsruhe.

A key challenge for this field has been the difficulty of computing reaction rates, largely due to the difficulty of providing a good enough guess at the transition state geometry. We recently succeeded to compute the transition state geometries for more than 10,000 reactions ([Grambow, Sci. Data 2020](#)), and we are now using those geometries to train an ML method for providing good guess TS geometries.

IV. Publications and submitted journal articles supported by DOE BES 2018-2020

1. Colin M. Grambow, Adeel Jamal, Yi-Pei Li, William H. Green, Judit Zador, Yury V. Suleimanov, "Unexpected Unimolecular Reaction Pathways of a γ -Keto hydroperoxide from Combined Application of Automated Reaction Discovery Methods", *Journal of the American Chemical Society* **140**, 1035-1048 (2018). <http://dx.doi.org/10.1021/jacs.7b11009>
2. Kehang Han, Adeel Jamal, Colin M. Grambow, Zachary J. Buras, "An Extended Group Additivity Method for Polycyclic Thermochemistry Estimation", *International Journal of Chemical Kinetics* **50**, 294-303 (2018). <https://doi.org/10.1002/kin.21158>
3. Alan E. Long, Shamel S. Merchant, Aäron G. Vandeputte, Hans-Heinrich Carstensen, Alexander J. Vervust, Guy B. Marin, Kevin M. Van Geem, and William H. Green, "Pressure dependent kinetic analysis of pathways to naphthalene from cyclopentadienyl recombination", *Combustion & Flame* **187**, 247-256 (2018). <https://doi.org/10.1016/j.combustflame.2017.09.008>
4. Alon G. Dana, Beat Buesser, Shamel S. Merchant, and William H. Green, "Automated Reaction Mechanism Generation Including Heteroatoms: Nitrogen", *International Journal of Chemical Kinetics* **50**, 223-258 (2018). <http://dx.doi.org/10.1002/kin.21154>
5. Alexander J. Vervust, Marko R. Djokic, Shamel S. Merchant, Hans-Heinrich Carstensen, Alan E. Long, Guy B. Marin, William H. Green, and Kevin M. Van Geem, "Detailed experimental and

- modeling study of cyclopentadiene pyrolysis in the presence of ethene”, *Energy & Fuels* **32**, 3290-3934 (2018). <https://pubs.acs.org/doi/abs/10.1021/acs.energyfuels.7b03560>
6. Joshua E. Middaugh, Zachary J. Buras, Mickael Matrat, Te-Chun Chu, Young-Seok Kim, Ionut M. Alecu, AnGayle K. Vasiliou, C. Franklin Goldsmith, and William H. Green “A combined photoionization time-of-flight mass spectrometry and laser absorption spectrometry flash photolysis apparatus for simultaneous determination of reaction rates and product branching”, *Review of Scientific Instruments* **89**, 074102 (2018). <https://doi.org/10.1063/1.5024399>
 7. Murat Keceli, Sarah Elliott, Yi-Pei Li, Matthew S. Johnson, Carlo Cavallotti, Yuri Georgievskii, William H. Green, Matteo Pelucchi, Justin M. Wozniak, Ahren W. Jasper, and Stephen J. Klippenstein, “Automated Computational Thermochemistry for Butane Oxidation: A Prelude to Predictive Automated Combustion Kinetics”, *Proc. Combust. Inst.* **37**, 363-371 (2019). <https://doi.org/10.1016/j.proci.2018.07.113>
 8. Alon Grinberg Dana, Kevin B. Moore, Ahren W. Jasper, and William H. Green, “Large Intermediates in Hydrazine Decomposition: A Theoretical Study of the N₃H₅ and N₄H₆ Potential Energy Surfaces”, *Journal of Physical Chemistry A* **123**, 4679-4692 (2019). <https://doi.org/10.1021/acs.jpca.9b02217>
 9. Alon Grinberg Dana, Mengjie Liu, and William H. Green, “Automated Chemical Resonance Generation and Structure Filtration for Kinetic Modeling”, *International Journal of Chemical Kinetics* **51**, 760–776 (2019). <http://dx.doi.org/10.1002/kin.21307>
 10. William H. Green, “Automatic Generation of Reaction Mechanisms” in “Mathematical Modeling of Complex Reaction Systems”, ed. by Tiziano Faravelli, Flavio Manenti, and Eliseo Ranzi, *Computer-Aided Chemical Engineering* **45**, 259-294 (2019). <https://www.sciencedirect.com/bookseries/computer-aided-chemical-engineering/vol/45/suppl/C>
 11. Agnes Jocher, Nick M. Vandewiele, Kehang Han, Mengjie Liu, Connie W. Gao, Ryan J. Gillis, & William H. Green, “Scalability strategies for automated reaction mechanism generation”, *Computers & Chemical Engineering* **131**, 106578 (2019) <https://doi.org/10.1016/j.compchemeng.2019.106578>
 12. Mark J. Goldman, Shuhei Ono, and William H. Green, “Accepted method for computing X+X rates is incorrect, causes large errors in isotope analysis”, *J. Phys. Chem. A* **123**, 2320–2324 (2019). <https://doi.org/10.1021/acs.jpca.8b09024>
 13. Mark J. Goldman, Shuhei Ono, and William H. Green, “Addition to ‘Accepted method for computing X+X rates is incorrect, causes large errors in isotope analysis’”, *Journal of Physical Chemistry A* **124**, 257 (2020). <https://pubs.acs.org/doi/10.1021/acs.jpca.9b11434>
 14. Connie W. Gao, Mengjie Liu, & William H. Green, “Uncertainty Analysis of Correlated Parameters in Automated Reaction Mechanism Generation”, *International Journal of Chemical Kinetics* **52**, 266-282 (2020). <http://dx.doi.org/10.1002/kin.21348>
 15. Ryan J. Gillis & William H. Green, “Thermochemistry Prediction and Automatic Mechanism Generation for Oxygenated Sulfur Systems: A Case Study of Dimethyl Sulfide Oxidation”, *ChemSystemsChem* **2**, e1900051 (2020). <http://dx.doi.org/10.1002/syst.201900051>

Theory of Electronic Structure and Chemical Dynamics

Martin Head-Gordon, Eric Neuscamman, David Prendergast

Chemical Sciences Division, Lawrence Berkeley National Laboratory, Berkeley, California 94720.

mhg@cchem.berkeley.edu, millerwh@berkeley.edu, eneuscamman@berkeley.edu, dgprendergast@lbl.gov

Scope of the Project: To expand knowledge of transient species such as radicals relevant to combustion chemistry, atmospheric photochemistry, and other areas including catalysis, new theoretical methods are needed for reliable computer-based prediction of their properties. In electronic structure theory, focus centers on the development of new density functional theory methods and new wave function theories. Newly developed theoretical methods, as well as existing approaches, are employed to study prototype radical reactions, often in collaboration with experimental efforts in the related subtasks (see separate LBNL abstracts). These studies help to deepen understanding of the role of reactive intermediates in diverse areas of chemistry. They also sometimes reveal frontiers where new theoretical developments are needed in order to permit better calculations in the future.

Recent Progress

Due to length limitations, only a selection of projects can be summarized here.

High Accuracy Excited States and Novel Ansatzes. Neuscamman and co-workers have made substantial progress in both novel ansatz design and excited state methods. For excited states, we have developed a new quantum Monte Carlo methodology for the efficient evaluation and optimization of a rigorous excited state variational principle that allows all aspects of a wave function to be tailored for an individual excited state in much the same way as they have long been for ground states. In addition, the methodology can evaluate a rigorous measure of wave function error for ground and excited states alike and so can take a systematic approach to balancing descriptions of different states. We have also developed a more robust approach for combining linear method and descent techniques for large variable sets. Alongside these optimization improvements, we have been exploring cutting-edge quantum Monte Carlo wave function approximations. These include our own introduction of the variation-after-response ansatz that allows a wave function to fully relax itself within the presence of its own linear response, thus capturing important nonlinear effects that are absent in excited state descriptions such as configuration interaction singles and time-dependent density functional theory. Preliminary investigations have shown this approach to be effective in a number charge-transfer examples, where nonlinear orbital relaxations are especially important, and very recently we have demonstrated the approach to be compatible with diffusion Monte Carlo, which opens a clear path from quantum-chemistry-based initial guesses (e.g. TD-DFT) to exceptionally high accuracy Monte Carlo excited state predictions. Also on the excited state wave function front, we have now brought together recent advances in multi-determinant orbital optimization with our variational excited state methodology to show that it is possible to avoid state averaging in multi-reference treatments of excited states. In particular, we have demonstrated that this approach outperforms multi-reference state averaged perturbation theory in the context of a challenging charge transfer example thanks to its ability to fully relax *all* molecular orbitals and the correlation treatment after the charge transfer excitation changes the system's dipole.

Density functionals. Head-Gordon and co-workers have been interested in seeking the limit of transferable accuracy that can be achieved with current forms for density functionals. This has resulted in the "survival of the most transferable" (SOMT) procedure to design new density functionals. This approach has been used to create very accurate new density functionals, such as the ω B97X-V and ω B97M-V hybrids, and the ω B97M(2) double hybrid. Recently, they have explored how these and other functionals perform for bond-breaking, and have discovered that a class of multiconfigurational open shell singlet states can be accurately treated by DFT using a single determinant of complex molecular orbitals. Their functionals were employed in collaboration with Musa Ahmed to model photoionization-induced reactivity in complexes of naphthalene and water.

Electron correlation methods: Head-Gordon and co-workers are developing wavefunction-based electron correlation methods for problems where DFT suffers from self-interaction and/or strong correlation errors. The simplest such approach is a regularized orbital optimized MP2 method (κ -OOMP2) that removes strong correlation contributions associated with small gaps. κ -OOMP2 can remove artificial spin symmetry-breaking associated with Hartree-Fock, while retaining “essential symmetry-breaking” as a signature of strong correlations because of its single reference character. κ -OOMP2 has been applied to fullerenes to address debate over whether C60 is strongly correlated (we conclude it is not). We have shown that biradicals can be well treated by κ -OOMP2 with the aid of Yamaguchi spin projection, or complex orbitals when such solutions exist. Another recent advance is an efficient implementation of the adaptive sampling CI (ASCI) method, that approximates full CI at dramatically reduced cost by exhibiting soft instead of hard exponential scaling. ASCI has been applied to explore limitations of conventional coupled cluster methods for some small strongly correlated transition metal diatomics (hydrides, halides, oxides, carbides and nitrides).

Excited-state dynamics and transient inner-shell spectroscopy: Prendergast and co-workers are applying both linear response time-dependent DFT and wave-function methods in the context of fewest-switches surface hopping to explore excited-state dynamics of various small molecules. In particular, for photodissociated outcomes, moving beyond single-reference DFT to multireference methods is necessary. Multiconfigurational self-consistent field (MCSCF) using the restricted active space (RAS) SCF method has been effective in reproducing excited state dynamics induced by UV excitation, from equilibrium, through conical intersections and towards fragmentation. To provide interpretation of ultrafast pump-probe inner-shell transient spectroscopy, we have demonstrated how to effectively interpret such spectra from a physical perspective – separating peaks by species and explaining peaks shifts in terms of orbital character and localization, and exciton binding. We have also successfully extended the application of RASSCF to mixed core-valence excited states, as accessed in pump-probe experiments, and further employed RAS state interaction to include spin-orbit interactions for heavier atoms and to calculate transition amplitudes for transient absorption spectra that probe excited states with nontrivial angular momentum ($l=2$ here), with application to methyl iodide.

Future Plans:

(i) *High Accuracy Core Excitations:* Current efforts focus on extending our variational excited state work to core excitations using both stochastic and non-stochastic methods. In these excitations, the ability to capture secondary relaxations beyond the primary excitation are if anything more relevant than in charge transfer excitations. Preliminary data in small-molecule oxygen, carbon, and nitrogen core states show that accuracies of 0.1 to 0.2 eV are possible. In particular, our accuracy balancing approach is especially well-suited for predicting peak positions in core spectra. Work has also begun on treating core states with excited state mean field theory and its partner perturbation theory, which also benefit from full state-specific orbital relaxation. Although these will not have the same accuracy guarantees as Monte Carlo, they are more affordable and can act as a starting point for Monte Carlo optimization where necessary.

(ii) *Density functionals and collaborative chemistry:* Additional tests of density functionals on transition metal systems are underway, and an opposite spin double hybrid functional that can be evaluated at only 4th order computational cost is now finished. Collaborative applications to photoionized clusters of glycerol and water are underway (with Musa Ahmed), and oxidative chemistry in aerosols of long-chain hydrocarbons (with Kevin Wilson), and combustion related reactions of unsaturated radicals (with Hope Michelson).

(iv) *Inner shell excitations and spectra:* Prendergast, Neuscammann and Head-Gordon will explore synergies around computational methods for inner-shell excitations. Prendergast will explore useful active space strategies for inner-shell excitations, and extend such techniques to larger systems, where DFT approaches employing final-state approximations have proven accurate for reproducing

measurable spectra – X-ray absorption in particular. Accurate energy alignment of spectra will be explored using self-consistent field methods, such as the maximum overlap method (MOM).

Recent Publications Citing DOE Support (2017-2020)

- Bertels, L.W.; J. Lee, and M. Head-Gordon, “Third-Order Møller-Plesset Perturbation Theory Made Useful? Choice of Orbitals and Scaling Greatly Improves Accuracy for Thermochemistry, Kinetics and Intermolecular Interactions”, *J. Phys. Chem. Lett.* **10**, 4170–4176 (2019); doi: 10.1021/acs.jpcllett.9b01641
- Blunt, N. S.; Neuscammann, E., Charge-transfer Excited States: Seeking a Balanced and Efficient Wave Function Ansatz in Variational Monte Carlo. *J. Chem. Phys.* **2017**, *147* (19), 194101. DOI: 10.1063/1.4998197.
- Blunt, N. S.; Neuscammann, E., Excited-state diffusion Monte Carlo calculations: a simple and efficient two-determinant ansatz. *J. Chem. Theory Comput.* **2019**, *15*, 178. DOI: 10.1021/acs.jctc.8b00879
- Cotton, S.J., R. Liang, and W. H. Miller, “On the Adiabatic Representation of Meyer-Miller Electronic-Nuclear Dynamics”, *J. Chem. Phys.* **2017**, *147*, 064112; doi: 10.1063/1.4995301
- Fang, J.; D. Hait, M. Head-Gordon, and M.C.Y. Chang, “Chemoenzymatic Platform for Synthesis of Chiral Organofluorines Based on Type II Aldolases”, *Ang. Chem.* **131**, 11967–11971 (2019); doi: 10.1002/ange.201906805
- Goetz, B. V. D.; Neuscammann, E., Suppressing Ionic Terms with Number-Counting Jastrow Factors in Real Space. *J. Chem. Theory Comput.* **2017**, *13*, 2035-2042. DOI: 10.1021/acs.jctc.7b00158
- Hait, D. and M. Head-Gordon, “How accurate is density functional theory at predicting dipole moments? An assessment using a new database of 200 benchmark values.” *J. Chem. Theory Comput.* **14**, 1969–1981 (2018); doi: 10.1021/acs.jctc.7b01252
- Hait, D. and M. Head-Gordon, “xDH double hybrid functionals can be qualitatively incorrect for non-equilibrium geometries: Dipole moment inversion and barriers to radical-radical association using XYG3 and XYGJ-OS”, *J. Chem. Phys.* **148**, 171102 (2018); doi: 10.1063/1.5031027
- Hait, D. and M. Head-Gordon, “Delocalization errors in density functional theory are essentially quadratic in fractional occupation number”, *J. Phys. Chem. Lett.* **9**, 6280–6288 (2018); doi: 10.1021/acs.jpcllett.8b02417
- Hait, D.; A. Rettig, and M. Head-Gordon, “Well-behaved versus ill-behaved density functionals for single bond dissociation: Separating success from disaster functional by functional for stretched H₂”, *J. Chem. Phys.* **150**, 094115 (2019); doi: 10.1063/1.5080122
- Hait, D.; N.M. Tubman, D.S. Levine, K.B. Whaley, and M. Head-Gordon, “What levels of coupled cluster theory are appropriate for transition metal systems? A study using near exact quantum chemical values for 3d transition metal binary compounds” *J. Chem. Theory Comput.* **15**, 5370–5385 (2019); doi: 10.1021/acs.jctc.9b00674
- Johansson, K.O.; M. P. Head-Gordon, P.E. Schrader, K.R. Wilson, and H.A. Michelsen, “Resonance-stabilized hydrocarbon- radical chain reactions may explain soot inception and growth”, *Science* **361**, 997–1000 (2018); doi: 10.1126/science.aat3417
- Lee, J.; D.W. Small, and M. Head-Gordon, “Open-shell coupled-cluster valence-bond theory augmented with an independent amplitude approximation for 3-pair correlations: Application to a model oxygen-evolving complex and single molecular magnet”, *J. Chem. Phys.* **149**, 244121 (2018); doi: 10.1063/1.5052667
- Lee, J.; W. Huggins, M. Head-Gordon, and K.B. Whaley, “Generalized unitary coupled cluster wavefunctions for quantum computation”, *J. Chem. Theory Comput.* **15**, 311-324 (2019); doi: 10.1021/acs.jctc.8b01004
- Lee, J. and M. Head-Gordon, “Distinguishing Artificial and Essential Symmetry Breaking in a Single Determinant: Approach and Application to the C60, C36, and C20 Fullerenes”, *Phys. Chem. Chem. Phys.* **21**, 4763-4778 (2019); doi: 10.1039/c8cp07613h
- Lee, J. and M. Head-Gordon, “Two Single-Reference Approaches to Singlet Biradicaloid Problems: Complex, Restricted Orbitals and Approximate Spin-Projection Combined With Regularized Orbital-Optimized Møller-Plesset Perturbation Theory”, *J. Chem. Phys.* **150**, 244106 (2019); doi: 10.1063/1.5097613
- Lee, J.; L.W. Bertels, D.W. Small, and M. Head-Gordon, “Kohn-Sham density functional theory with complex, spin-restricted orbitals: Accessing a new class of densities without the symmetry dilemma”, *Phys. Rev. Lett.* **123**, 113001 (2019); doi: 10.1103/PhysRevLett.123.113001
- Lehtola, S., J.A. Parkhill and M. Head-Gordon, “Orbital optimization in the perfect pairing hierarchy. Applications to full-valence calculations on linear polyacenes”, *Mol. Phys.* **116**, 547-560 (2018); doi: 10.1080/00268976.2017.1342009

- Lucas, M.; A.M. Thomas, T. Yang, R.I. Kaiser, A.M. Mebel, D. Hait, M. Head-Gordon, “Exotic Chemistry in the Phenyl - Silane System: Exploring the Prototype of a Radical Substitution Mechanism,” *J. Phys. Chem. Lett.* **9**, 5135–5142 (2018); 10.1021/acs.jpcclett.8b02303
- Mardirossian, N.; Pestana, L. R.; Womack, J. C.; Skylaris, C.-K.; Head-Gordon, T.; Head-Gordon, M., Use of the rVV10 Nonlocal Correlation Functional in the B97M-V Density Functional: Defining B97M-rV and Related Functionals. *J. Phys. Chem. Lett.* **2017**, *8*, 35-40; doi: 10.1021/acs.jpcclett.6b02527
- Mardirossian, N. and M. Head-Gordon, “Survival of the most transferable at the top of Jacob’s Ladder: Defining and testing the ω B97M(2) double hybrid density functional”, *J. Chem. Phys.* **148**, 241736 (2018); doi: 10.1063/1.5025226
- Otis, L.; Neuscamman, E., “Complementary First and Second Derivative Methods for Ansatz Optimization in Variational Monte Carlo” *Phys. Chem. Chem. Phys.* **2019**, *21*, 14491; doi: 10.1039/C9CP02269D
- Pestana, L. R.; Mardirossian, N.; Head-Gordon, M.; Head-Gordon, T., “Ab initio molecular dynamics simulations of liquid water using high quality meta-GGA functionals.” *Chem. Sci.* **2017**, *8*, 3554-3565; doi: 10.1039/c6sc04711d
- Pineda Flores, S. D. and E. Neuscamman, Excited State Specific Multi-Slater Jastrow Wave Functions. *J. Phys. Chem. A* **2019**, *123*, 1487. DOI: 10.1021/acs.jpca.8b10671
- Robinson, P. J.; Pineda Flores, S. D.; Neuscamman, E., Excitation Variance Matching with Limited Configuration Interaction Expansions in Variational Monte Carlo. *J. Chem. Phys.* **2017**, *147* (16), 164114. DOI: 10.1063/1.5008743
- Small, D. W.; Head-Gordon, M., Coupled cluster valence bond theory for open-shell systems with application to very long range strong correlation in a polycarbene dimer. *J. Chem. Phys.* **2017**, *147*, 024107; doi: 10.1063/1.4991797
- Small, D. W. and M. Head-Gordon, “Independent amplitude approximations in coupled cluster valence bond theory: Incorporation of 3-electron-pair correlation and application to spin frustration in the low-lying excited states of a ferredoxin-type tetrametallic iron-sulfur cluster”, *J. Chem. Phys.* **149**, 144103 (2018); doi: 10.1063/1.5046318.
- Stein, T., B. Bandyopadhyay, T. Troy, Y. Fang, O. Kostko, M. Ahmed, and M. Head-Gordon, “Ab initio dynamics and photoionization mass spectrometry reveal ion-molecule pathways from ionized acetylene clusters to benzene cation”, *Proc. Nat. Acad. Sci.* **2017**, *114*, E4125-E4133; doi: 10.1073/pnas.1616464114.
- Toulson, B. W.; Borgwardt, M.; Wang, H.; Lackner, F.; Chatterley, A. S.; Pemmaraju, C. D.; Neumark, D. M.; Leone, S. R.; Prendergast, D.; Gessner, O.; Probing ultrafast C–Br bond fission in the UV photochemistry of bromoform with core-to-valence transient absorption spectroscopy, *Structural Dynamics* **2019**, *6*, 054304; doi: 10.1063/1.5113798
- Tubman, N.M., C.D. Freeman, D.S. Levine, D. Hait, M. Head-Gordon, K.B. Whaley, “Modern Approaches to Exact Diagonalization and Selected Configuration Interaction with the Adaptive Sampling CI Method”, *J. Chem. Theory Comput.* **16**, 2139-2159 (2020); doi: 10.1021/acs.jctc.8b00536
- Wang, H.; Odellius, M.; Prendergast, D., A combined multi-reference pump-probe simulation method with application to XUV signatures of ultrafast methyl iodide photodissociation, *J. Chem. Phys.* **2019**, *151*, 124106-; doi: 10.1063/1.5116816
- Witte, J.; Mardirossian, N.; Neaton, J. B.; Head-Gordon, M., Assessing DFT-D3 Damping Functions Across Widely Used Density Functionals: Can We Do Better? *J. Chem. Theory Comput.* **2017**, *13*, 2043-2052; doi: 10.1021/acs.jctc.7b00176
- Witte, J.; Neaton, J. B.; Head-Gordon, M., Effective empirical corrections for basis set superposition error in the def2-SVPD basis: gCP and DFT-C. *J. Chem. Phys.* **2017**, *146*, 234105; doi: 10.1063/1.4986962
- Xu, B.; T. Stein, U. Ablikim, L. Jiang, J. Hendrix, M. Head-Gordon, and M. Ahmed, “Probing solvation and reactivity in ionized polycyclic aromatic hydrocarbon-water clusters with photoionization mass spectrometry and electronic structure calculations”, *Faraday Disc.* **217**, 414-433 (2019); doi: 10.1039/c8fd00229k

Semiclassical Methods for Pressure Dependent Kinetics and Electronically Nonadiabatic Chemistry

Ahren W. Jasper
Chemical Sciences and Engineering Division
Argonne National Laboratory
ajasper@anl.gov

Program Scope

The outcome of a gas phase chemical reaction results from the competition of a variety of underlying microscopic processes, including collisional energy transfer, internal energy redistribution, bonding rearrangements, and inherently quantum mechanical events like electronic transitions. These same phenomena govern reactivity in more complex environments, and a major goal of the project is to develop a comprehensive set of semiclassical approaches for describing the fundamental chemical physics of these phenomena with high accuracy and that are broadly applicable throughout chemistry.

The improvement of first-principles theories via the construction of more and more detailed physical models benefits from the increasing impact of large-scale computing in chemistry, including Argonne's leadership-class resources. Our focus on the development of methods and codes for dynamics and kinetics recognizes that these approaches are now poised to take advantage of the tremendous advances made in electronic structure theory in recent decades. We pursue the development of semiclassical strategies, where the term is used here to describe approaches that incorporate one or more quantum effects into simulations involving classical or nearly classical nuclear motion. Semiclassical methods offer a scalable balance of computational cost and accuracy and are well suited for high performance computing. We focus on the advancement of first principles semiclassical approaches, i.e., methods that are systematically improvable and that may be assigned a priori error bars. We have demonstrated in a variety of contexts that our most detailed semiclassical models have accuracies that match and sometimes even exceed what is possible experimentally and approach the semiclassical accuracy limit of $\sim 20\%$.

The increased accuracy of a priori theory and its use alongside experiment as an independent source of quantitative chemical and physical information may be anticipated to have a transformative effect in chemical modeling. Recent work supported by this project has continued the development of methods and codes for nonadiabatic dynamics and intersystem crossing, collisional energy transfer and transport, potential energy surface fitting, nonequilibrium reactivity, and rovibrational anharmonicity at high energies and temperatures.

Recent Progress

The low-pressure-limit microcanonical rate constants, $\kappa_0(E, J)$, describe the rate of activating bath gas collisions in a unimolecular reaction as a function of the initial internal state (E, J) of the reactant. We showed that κ_0 can be calculated using classical trajectories and quantized thresholds for reaction. The resulting semiclassical rate constants are two-dimensional (in total energy E and total angular momentum J) and are intermediate in complexity between the more-familiar four-dimensional state-to-state collisional energy and angular momentum transfer rate constant, $R(E', J'; E, J)$, and the highly-averaged thermal rate constant, k_0 . We generated results for CH_4 (+M), C_2H_x (+M), $x = 3-6$, and H_2O (+M), and we showed that $\kappa_0(E, J)$ is generally a sensitive function of the bath gas, temperature, and initial state of the unimolecular reactant (Fig. 1). Strong variations in κ_0 with respect to E and J lead to complex trends in relative microcanonical bath gas efficiencies. This underlying complexity may complicate the search for simple explanations for observed trends in relative thermal bath gas efficiencies. A different measure of the microcanonical collision

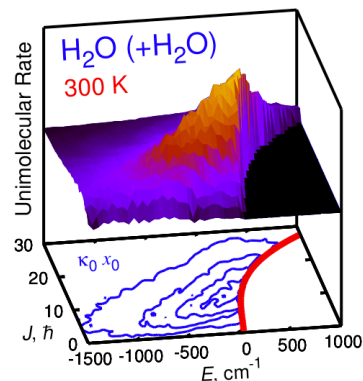


Fig. 1. Contribution to the low-pressure limit rate constant k_0 for H_2O (+ H_2O) shown as a function of the initial state of H_2O .

efficiency that describes the energy range of activating collisions was introduced that supports the empirical decomposition of collisional activation into separable translational-to-vibrational and rotational-to-vibrational activation mechanisms. The two mechanisms depend differently on mass, temperature, and the J -dependence of the threshold energy for reaction, with rotational-to-vibrational activation favored for heavier baths and for reactions with rigid transition states.

Using potential energy surfaces developed by Harding and Georgievskii, Monte Carlo phase space integration (MCPSI) was used to compute full dimensional and fully anharmonic—but classical—rovibrational partition functions for 22 small- and medium-sized molecules and radicals. Several of the species featured multiple minima and low-frequency nonlocal motions, and efficiently sampling these systems was facilitated using curvilinear (stretch, bend, and torsion) coordinates. The curvilinear coordinate MCPSI method was demonstrated to be applicable to the treatment of fluxional species with complex rovibrational structures and as many as 21 fully coupled rovibrational degrees of freedom. Trends in the computed anharmonicity corrections were identified and discussed. In a follow-up study, we implemented our curvilinear coordinate MCPSI code “at scale” on Argonne’s petascale machine, Theta. There, we calculated semiclassical rovibrational state counts and partition functions for systems with two and three coupled torsions and as many as 30 rotational and vibrational modes. These results were used as benchmarks to quantify the accuracy of simpler reduced-dimensional approaches and analyzed for general

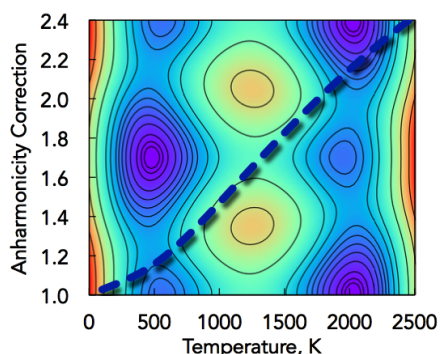


Fig. 2. Correction to the harmonic state count for NH_2OH overlaid over a contour plot of the PES as a function of the $-\text{NH}_2$ inversion and $\text{N}-\text{O}$ torsion coordinates.

physical insights about the nature of fluxional mode coupling at high temperatures and energies. For example, we identified and quantified the effect of low-frequency heavy-atom bends coupling to torsions.

With Davis, several schemes for constructing intermolecular potentials using both class-based pairwise Buckingham representations and system-specific permutationally-invariant polynomials representations were automated and tested. We quantified efficiency and accuracy of improvements related to the choice of sampling strategy and choice of functional form. In our first effort, we considered four sampling strategies: pseudorandom (P), Sobol quasirandom (S), and biased versions of each (bP and bS). Figure 3 shows the convergence in the out of sample (prediction) error as a function of the number of sampled geometries/energies M for each sampling type. For this system, the biased Sobol scheme is 10x more efficient than the unbiased pseudorandom scheme that is most often used. The optimized scheme requires just ~ 3 ab initio data per parameter. These trends persist both for larger alcohols and in the higher-dimensional fits required for larger bath gases.

Future Work

We propose to continue to advance the applicability of MCPSI to include systems where the accuracy of existing anharmonicity approaches has not been well characterized, such as transition states and species involving constrained torsions and rings. In earlier work, we approximated the high-dimensional MCPSI integrals via a hierarchy of expressions based on so-called “ n -mode intrinsic” state densities. The 2-mode (pairwise) intrinsic state density Δ_{ij} , for example, is defined for each pair of coordinates i and j as the state

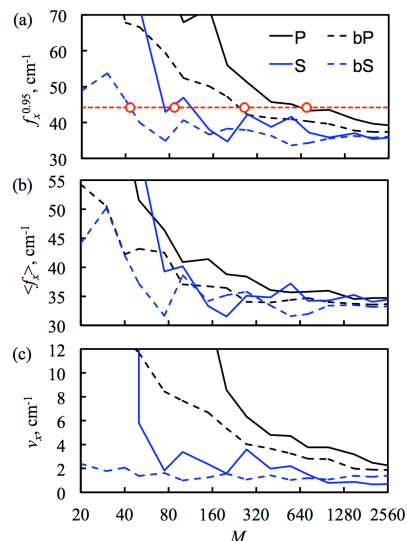


Fig. 3. (a) Convergence of the out of sample error $f_k^{0.95}$ for a separable pairwise $\exp/6$ fit of the $\text{CH}_3\text{OH} + \text{Ar}$ interaction PES as a function of the number of sampled data M . The (b) mean prediction error $\langle f_k \rangle$ and the (c) variance in the fitting error v_k converge at different rates for the four sampling types.

density for those modes not represented by the convolution of the one-dimensional densities ρ_i . The full-dimensional density of states is then approximated through second order via convolutions of Δ_{ij} and ρ_k . Intractable high-dimensional integrals are thus computed from convolutions of readily obtained one- and two-dimensional ones. This 2nd-order result can be systematically improved via 3rd- and higher-order corrections. Despite the significant computational savings of this approach, the number of convolutions required can become cumbersome. We will explore approximations where terms are eliminated based on their order and with respect to the number of intrinsics in the term. Preliminary studies for CH₄ show that retaining terms with just one 2nd-order intrinsic speeds up the calculation by two orders of magnitude with a negligible (2%) loss of accuracy. This strategy provides a route toward practical applications of MCPSI for very large molecular systems.

To support ongoing investigations into nonthermal and nonequilibrium kinetics, we will test the accuracy of studying these processes using transition state theory (TST). The TST expression for the rate constant can be written very generally as $k = \frac{1}{2} \int dx dp f^{\ddagger} v / \int dx dp f_R$, i.e., as $\frac{1}{2}$ the ratio of a phase space integral of the flux through the transition state dividing surfaces and phase space integrals for the reactants. To evaluate this expression, one must *choose* the functions f^{\ddagger} and f_R , which describe the population distributions at the transition state and for the reactants including relative coordinates, respectively. When either microcanonical or thermal equilibration choices are consistently made, the familiar TST expressions result. We will consider alternate choices, including choices appropriate for nonthermal reactions of recent interest like $\text{H}_2\text{O}^* + \text{H} \rightarrow \text{H}_2 + \text{O}_2$, where, in this example, we wish to employ mixed equilibration assumptions with $f_{\text{H}_2\text{O}^*}$ described microcanonically with an internal energy E close to its dissociation threshold while f_{rel} for the relative translational coordinates are described thermally by a local temperature T . The corresponding choice for f^{\ddagger} is not at all obvious (other than it should be some function of E and T), as, of course, unambiguous 1-to-1 relationships between the degrees of freedom at the transition state and those for the reactants do not exist. Quasiclassical trajectories will be used to test and improve the accuracy of competing schemes for choosing f^{\ddagger} . These studies will benefit from recent developments of our MCPSI sampling work, which can be incorporated to explore the effects of anharmonicity as well as the use of generalized (momentum- or energy-dependent) transition state dividing surfaces.

We will continue to develop and apply our general semiclassical dynamics code, DiNT, which includes theories for nonadiabatic dynamics with detailed and validated treatments of (de)coherence and classically forbidden transitions, e.g., as in the Coherent Switching with Decay of Mixing (CSDM) and Fewest-Switches with Time Uncertainty (FSTU) methods. This code has just been deployed on Argonne's petascale machines to facilitate direct dynamics applications. Preliminary results have been obtained for the widely studied ultrafast internal conversion in alkenes, with the goal of testing the impact of several of the many semiclassical treatments of decoherence that have been proposed. These results will also be used to test and improve the performance of tight-binding models for describing coupled potential energy surfaces relevant to alkene nonadiabatic chemistry, with the goal of using these much more efficient representations to study ultrafast photon capture and energy storage via the supramolecular molecules (aromatic hydrocarbons with ~100 atoms) of interest to artificial photosynthesis.

Publications supported by this project since 2018

1. J. B. Randazzo, A. W. Jasper, R. Sivaramakrishnan, T. Sikes, P. T. Lynch, and R. S. Tranter, An experimental and theoretical study of the high temperature reactions of four butyl radical isomers, *Phys. Chem. Chem. Phys.*, submitted (2020).
2. J. A. Miller, R. Sivaramakrishnan, C. F. Goldsmith, M. P. Burke, A. W. Jasper, J. Zádor, N. Hansen, N. J. Labbe, and P. Glarborg, Combustion chemistry in the twenty-first century: Developing theory-informed chemical kinetics models. *Prog. Energy Combust. Sci.*, submitted (2020).
3. Z. Wang, N. Hansen, A. W. Jasper, B. Chen, S. M. Popolan-Vaida, K. K. Yalamanchi, A. Najjar, P. Dagaut, and S. M. Sarathy, Cool flame chemistry of diesel surrogate compounds: n-decane, 2-methylnonane, 2,7-dimethyloctane, and n-butylcyclohexane. *Combust. Flame*, in press (2020).

4. Y. Tao, A. W. Jasper, Y. Georgievskii, S. J. Klippenstein, and R. Sivaramakrishnan, Termolecular chemistry facilitated by radical-radical recombinations and its impact on flame speed predictions. *Proc. Combust. Inst.*, in press (2020).
5. N. Hansen, G. Kukkadapu, B. Chen, S. Dong, H. J. Curran, C. A. Taatjes, A. J. Eskola, D. L. Osborn, L. Sheps, W. J. Pitz, K. Moshhammer, A. W. Jasper, W. Chen, J. Yang, and Z. Wang, The impact of the third O₂ addition reaction network on ignition delay times of neo-pentane. *Proc. Combust. Inst.*, in press (2020).
6. A. W. Jasper, “Third-body” collision parameters for hydrocarbons, alcohols, and peroxides and an effective internal rotor approach for estimating them. *Int. J. Chem. Kinet.* 52, 387–402 (2020).
7. A. W. Jasper, Microcanonical rate constants for unimolecular reactions in the low-pressure limit. *J. Phys. Chem. A* 124, 1205–1226 (2020).
8. N. Hansen, K. Moshhammer, and A. W. Jasper, Isomer-selective detection of keto-hydroperoxides in the low-temperature oxidation of tetrahydrofuran. *J. Phys. Chem. A* 123, 8274–8284 (2019).
9. A. W. Jasper, L. B. Harding, C. Knight, and Y. Georgievskii, Anharmonic rovibrational partition functions at high temperatures: Tests of reduced-dimensional models for systems with up to three fluxional modes. *J. Phys. Chem. A* 123, 6210–6228 (2019).
10. A. G. Dana, K. B. Moore III, A. W. Jasper, and W. H. Green, Large intermediates in hydrazine decomposition: A theoretical study of the N₃H₅ and N₄H₆ potential energy surfaces. *J. Phys. Chem. A* 4679–4692 (2019).
11. A. W. Jasper and M. J. Davis, Parameterization strategies for intermolecular potentials for predicting trajectory-based collision parameters. *J. Phys. Chem. A* 123, 3464–3480 (2019).
12. A. C. Rousso, N. Hansen, A. W. Jasper, and Y. Ju, Identification of the Criegee intermediate reaction network in ethylene ozonolysis: Impact on energy conversion strategies and atmospheric chemistry. *Phys. Chem. Chem. Phys.* 21, 7341–7357 (2019).
13. A. W. Jasper, R. Sivaramakrishnan, and S. J. Klippenstein, Nonthermal rate constants for CH₄* + X = CH₃ + HX, X = H, O, OH, and O₂. *J. Chem. Phys.* 150, 114112 (2019).
14. S. Elliott, Y.-P. Li, M. S. Johnson, C. Cavallotti, Y. Georgievskii, W. H. Green, M. Pelucchi, J. M. Wozniak, A. W. Jasper, and S. J. Klippenstein, Automated computational thermochemistry for butane oxidation: A prelude to predictive automated combustion kinetics. M. Keçeli, *Proc. Combust. Inst.*, 37, 363–371 (2019).
15. D. H. Bross, A. W. Jasper, B. Ruscic, and A. F. Wagner, Toward accurate high temperature anharmonic partition functions. *Proc. Combust. Inst.* 37, 315–322 (2019).
16. A. C. Rousso, N. Hansen, A. W. Jasper, and Y. Ju, Low-temperature oxidation of ethylene by ozone in a jet-stirred reactor. *J. Phys. Chem. A* 122, 8674–8685 (2018).
17. M. Pfeifle, Y.-T. Ma, A. W. Jasper, L. B. Harding, W. L. Hase, and S. J. Klippenstein, Nascent energy distribution of the Criegee intermediate CH₂OO from direct dynamics calculations of primary ozonide dissociation. *J. Chem. Phys.* 148, 174306 (2018).
18. S. J. Klippenstein, M. Pfeifle, A. W. Jasper, and P. Glarborg, Theory and modeling of relevance to prompt-NO formation at high pressure. *Combust. Flame.* 195, 3–17 (2018).
19. A. W. Jasper, Z. B. Gruey, L. B. Harding, Y. Georgievskii, S. J. Klippenstein, and A. F. Wagner, Anharmonic rovibrational partition functions for fluxional species at high temperatures via Monte Carlo phase space integrals. *J. Phys. Chem. A* 122, 1272–1740 (2018).
20. T. Tao, W. Sun, N. Hansen, A. W. Jasper, K. Moshhammer, B. Chen, Z. Wang, C. Huang, P. Dagaut, and B. Yang, Exploring the negative temperature coefficient behavior of acetaldehyde based on detailed intermediate measurements in a jet stirred reactor. *Combust. Flame.* 192, 120–129 (2018).

Probing the Reaction Dynamics of Hydrogen-Deficient Hydrocarbon Molecules and Radical Intermediates via Crossed Molecular Beams

Ralf I. Kaiser

Department of Chemistry, University of Hawai'i at Manoa, Honolulu, HI 96822

ralfk@hawaii.edu

1. Program Scope

The major goals of this project are to explore experimentally by exploiting molecular beams to study the fundamental reaction dynamics and underlying potential energy surfaces (PESs) of hydrocarbon molecules and their corresponding (resonantly free stabilized and aromatic) radical precursors, which are relevant to the formation and molecular growth of polycyclic aromatic hydrocarbons (PAHs). First, reactions are initiated in a crossed molecular beams machine under single collision conditions by crossing two supersonic reactant beams containing radicals and/or closed shell species under a well-defined collision energy and intersection angle. By recording angular-resolved time of flight (TOF) spectra, we obtain information on the reaction products, intermediates involved, branching ratios of competing reaction channels, reaction energetics, and on the underlying reaction mechanisms. Second, in collaboration with Dr. Musahid Ahmed (Chemical Sciences Division, Lawrence Berkeley Laboratory), reactions are carried out in a chemical reactor at well characterized pressure and temperature distributions with reaction products interrogated isomer-selectively by tunable vacuum ultraviolet light (VUV) via photoionization (PI) coupled with a reflectron time of flight mass spectrometer (ReTOFMS). Merged with electronic structure calculations (Prof. Alexander M. Mebel, Florida International University), these data are of fundamental importance to comprehend the underlying formation mechanisms of two key classes of molecules involved in molecular mass-growth processes leading to carbonaceous nanostructures from the bottom up: resonantly stabilized free radicals (RSFRs) and polycyclic aromatic hydrocarbons.

2. Recent Progress

2.1. Reaction Dynamics of the Methylidyne Radical ($\text{CH}(\text{X}^2\text{I})$) with Methylacetylene (CH_3CCH), Allene (H_2CCCH_2), Propylene (C_3H_6), and Benzene (C_6H_6). The chemical dynamics of the elementary reaction of the simplest organic radical – methylidyne - with C3 and C6 hydrocarbons were explored in a crossed molecular beams machine under single collision conditions. In all systems, the reactions commenced with the barrier-less cycloaddition of methylidyne to the π -electron density of the hydrocarbon reactant followed by non-statistical unimolecular decomposition of the doublet collision complexes via atomic hydrogen loss through tight exit transition states yielding the cyclic triafulvene molecule (*c*- C_4H_4) (Figure 1) - the simplest representative of the fulvene family (methylacetylene/allene systems; **P21**) and 1- and 3-methylcyclopropene (C_4H_6) in the propylene system (**P25**). The cyclic fulvenallene (C_7H_6) was synthesized in the reaction of methylidyne with benzene (**P26**). The barrier-less route to fulvenallene involves a Jahn-Teller distorted aromatic tropylium (C_7H_7) radical intermediate and ring opening – ring contraction sequences terminated by atomic hydrogen elimination. This reaction sheds light on the unusual reaction dynamics of Hückel aromatic systems and remarkable (polycyclic) reaction intermediates, which cannot be studied via classical organic, synthetic methods.

2.2. Reaction Dynamics of the 1-Propynyl Radical ($\text{CH}_3\text{CC}(\text{X}^2\text{A}_1)$) – An Isomer of the Resonantly Stabilized Free Propargyl (H_2CCCH) Radical - with Methylacetylene (CH_3CCH), Allene (H_2CCCH_2), Diacetylene (C_4H_2), Ethylene (C_2H_4), and Benzene (C_6H_6). The chemical dynamics of the elementary reaction of the 1-propynyl radical with C2 and C6 hydrocarbons were investigated under single collision conditions in a crossed molecular beams machine. In all systems, the reactions were initiated by the barrierless addition of 1-propynyl with the radical center to the π -electron density of the hydrocarbon reactant. The initial doublet radical collision complexes were found to fragment through tight exit transition states via atomic hydrogen loss yielding the benzene isomers dimethyldiacetylene ($\text{CH}_3\text{CCCCCH}_3$) and 1-propynylallene ($\text{H}_2\text{CCCHCCCH}_3$; C_6H_6 ; **P17**) (methylacetylene reactant), 1-penten-3-yne ($\text{CH}_3\text{CCC}_2\text{H}_3$; C_5H_6 ; **P22**) (ethylene reactant), methyltriacetylene (HCCCCCCH_3 ; C_7H_4 ; **P19**) (diacetylene reactant), and 1-phenyl-1-propyne ($\text{C}_6\text{H}_5\text{CCCH}_3$; C_9H_8 ; **P24**) (benzene reactant) – an

isomer of the thermodynamically more stable indene isomer. Notably, in the allene system, our data exhibit the formation of at least the fulvene ($c\text{-C}_5\text{H}_4\text{CH}_2$; C_6H_6 ; **P17**) isomer via a six step reaction sequence advocating that in the allene - 1-propynyl system, the methyl group of the 1-propynyl reactant is actively engaged in the reaction mechanism and does not act as a spectator (Figure 1).

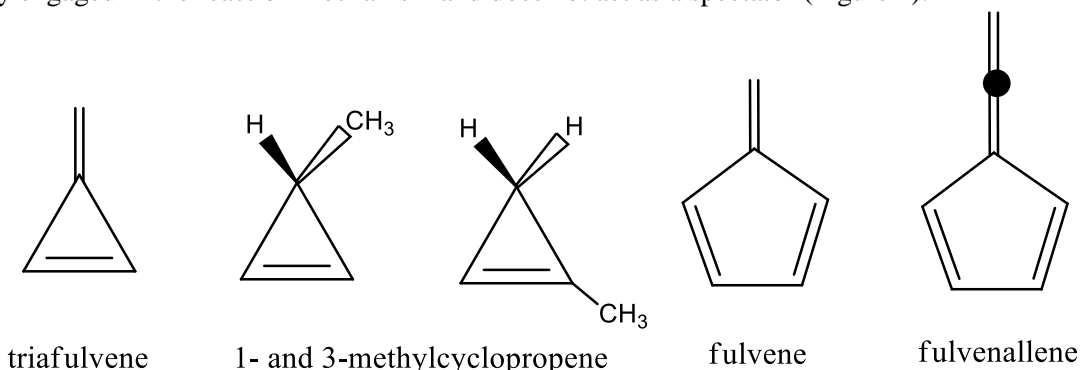


Figure 1: Cyclic reaction products formed in elementary reactions of methylidyne and 1-propynyl with unsaturated C3-C6 hydrocarbons.

2.3. Formation Mechanisms and Reaction Dynamics of Polycyclic Aromatic Hydrocarbons (PAHs)

Carrying up to Four Rings. We elucidated fundamental reaction mechanisms leading to the formation of PAHs carrying up to four rings involving four key reaction mechanisms exploiting a pyrolytic reactor coupled to synchrotron based single photon ionization mass spectrometry: Hydrogen Abstraction – acetylene Addition type mechanism (HACA) (**P18**), the barrierless Hydrogen Abstraction – Vinylacetylene Addition mechanism (HAVA) (**P18**, **P14**, **P27**), the Phenyl Addition – dehydroCyclization pathway (PAC) (**P23**), and Radical-Radical Recombination (RRR) (**P20**). These complementary mechanisms lead to the formation of fundamental building blocks of two and three dimensional carbon nanostructures. *First*, a unified low-temperature reaction mechanism on the formation of acenes, phenacenes, and helicenes – PAHs that are distinct via the linear, zigzag, and ortho-condensed arrangements of fused benzene rings - is revealed. This mechanism is mediated through a barrierless, vinylacetylene mediated gas-phase chemistry utilizing tetracene, [4]-phenacene, and [4]-helicene ($\text{C}_{18}\text{H}_{12}$) as bench- marks contesting established ideas that molecular mass growth processes to PAHs transpire at elevated temperatures (**P27**). Along with the synthesis of triphenylene ($\text{C}_{18}\text{H}_{12}$) (**P13**), the HAVA mechanism opens up an isomer-selective route to aromatic structures involving submerged reaction barriers, resonantly stabilized free-radical intermediates, and systematic ring annulation potentially yielding molecular wires along with racemic mixtures of helicenes. *Second*, the previously proposed PAC pathway could be verified computationally and experimentally leading to four-ring PAHs like triphenylene ($\text{C}_{18}\text{H}_{12}$) and fluoranthene ($\text{C}_{16}\text{H}_{10}$) (**P23**). PAC operates efficiently at high temperatures leading through rapid molecular mass growth processes to complex aromatic structures, which are difficult to synthesize by traditional pathways such as hydrogen-abstraction/acetylene-addition. Finally, we provided testimony on a facile, isomer selective route to naphthalene (C_{10}H_8) via rapid radical-radical reactions of 1-indenyl with methyl (**P20**). This versatile route converts five- to six-membered rings and provides a detailed view of high temperature mass growth processes that can eventually lead to graphene-type PAHs and two-dimensional nanostructures.

3. Future Plans

Having established synthetic pathways to PAHs carrying up to four rings, we will expand our studies to the formation of more complex PAHs carrying five rings (pentacene, [5]-helicene) and six rings (corannulene, [6]-helicene) as fundamental molecular building blocks to two and three dimensional carbon nanostructures. Further, we are expanding our radical – radical reactions to propargyl – propargyl and beyond in an attempt to synthesize aromatic systems with up to three six-membered rings. Finally, we will work toward a better understanding how five-membered rings can be incorporated into aromatic systems. Electronic structure calculations are conducted by Prof. Mebel (Florida International University).

Commercially unavailable precursors are synthesized by Prof. Felix Fischer (UC Berkeley) and Prof. Stan Wnuk (Florida International University). This also helps to define the role and complementary nature of four reaction mechanisms in PAH growth: the Hydrogen Abstraction – acetylene Addition mechanism, the Hydrogen Abstraction – Vinylacetylene Addition mechanism, the Phenyl Addition – dehydrocyclization pathway, and Radical-Radical Recombination.

4. Acknowledgements

This work is supported by US Department of Energy (Basic Energy Sciences; DE-FG02-03-ER15411).

5. Publications Acknowledging DE-FG02-03ER15411 (6/2017 – now)

- 1 D.S.N. Parker, R.I. Kaiser, On the Formation of Nitrogen-Substituted Polycyclic Aromatic Hydrocarbons (NPAHs) in Circumstellar and Interstellar Environments. *Chem. Soc. Rev.* 46, 452-463 (2017).
- 2 A.M. Mebel, A. Landera, R.I. Kaiser, Formation Mechanisms of Naphthalene and Indene: From the Interstellar Medium to Combustion Flames. *J. Phys. Chem. A* 121, 901–926 (2017).
- 3 T. Yang, R.I. Kaiser, T.P. Troy, B. Xu, O. Kostko, M. Ahmed, A.M. Mebel, M.V. Zagidullin, V.N. Azyazov, HACA's Heritage: A Free-Radical Pathway to Phenanthrene in Circumstellar Envelopes of Asymptotic Giant Branch Stars. *Angew. Chem., Int. Ed.* 56, 4515-4519 (2017).
- 4 A.M. Thomas, M. Lucas, T. Yang, R.I. Kaiser, L. Fuentes, D. Belisario-Lara, A.M. Mebel, A Free-Radical Pathway to Hydrogenated Phenanthrene in Molecular Clouds—Low Temperature Growth of Polycyclic Aromatic Hydrocarbons. *ChemPhysChem* 18, 1971-1976 (2017).
- 5 M. Lucas, A.M. Thomas, L. Zhao, R. I. Kaiser, G.-S. Kim, A.M. Mebel, Gas-Phase Synthesis of the Elusive Cyclooctatetraenyl Radical (C_8H_7) via Triplet Aromatic Cyclooctatetraene (C_8H_8) and Non-Aromatic Cyclooctatriene (C_8H_8) Intermediates. *Angew. Chem., Int. Ed.* 56, 13655-13660 (2017).
- 6 M. Lucas, A.M. Thomas, R. I. Kaiser, E.K. Bashkirov, V.N. Azyazov, A.M. Mebel, Combined Experimental and Computational Investigation of the Elementary Reaction of Ground State Atomic Carbon (C ; 3P_j) with Pyridine (C_5H_5N ; X^1A_1) via Ring Expansion and Ring Degradation Pathways. *J. Phys. Chem A*. 122, 3128-3139 (2018).
- 7 A.M. Thomas, M. Lucas, L. Zhao, J. Liddiard, R.I. Kaiser, A.M. Mebel, A Combined Crossed Molecular Beams and Computational Study on the Formation of Distinct Resonantly Stabilized C_5H_3 Radicals via Chemically Activated C_5H_4 and C_6H_6 Intermediates. *Phys. Chem. Chem. Phys.* 20, 10906-10925 (2018).
- 8 L. Zhao, R.I. Kaiser, B. Xu, U. Ablikim, M. Ahmed, D. Joshi, G. Veber, F.R. Fischer, A.M. Mebel, Pyrene Synthesis in Circumstellar Envelopes and its Role in the Formation of 2D Nanostructures. *Nature Astron.* 2, 413-419 (2018).
- 9 L. Zhao, R.I. Kaiser, B. Xu, U. Ablikim, M. Ahmed, M.V. Zagidullin, V.N. Azyazov, A.H. Howlader, S.F. Wnuk, A.M. Mebel, VUV Photoionization Study of the Formation of the Simplest Polycyclic Aromatic Hydrocarbon: Naphthalene ($C_{10}H_8$). *J. Phys. Chem. Lett.* 9, 2620–2626 (2018).
- 10 A.M. Thomas, L. Zhao, C. He, A.M. Mebel, R. Kaiser, A Combined Experimental and Computational Study on the Reaction Dynamics of the 1-Propynyl (CH_3CC)—Acetylene ($HCCH$) System and the Formation of Methylidyne (CH_3CCCCH). *J. Phys. Chem. A* (W.M. Jackson Special Issue) 122, 6663-6672 (2018).
- 11 L. Zhao, R.I. Kaiser, B Xu, U. Ablikim, M. Ahmed, M. Evseev, E.K. Bashkirov, V.N. Azyazov, A.M. Mebel, Low-Temperature Formation of Polycyclic Aromatic Hydrocarbons in Titan's Atmosphere. *Nature Astron.* 2, 973-979 (2018).
- 12 M.V. Zagidullin, R.I. Kaiser, D.P. Porfiriev, I.P. Zavershinskiy, M. Ahmed, V.N. Azyazov, A.M. Mebel, Functional Relationships between Kinetic, Flow, and Geometrical Parameters in a High-Temperature Chemical Microreactor. *J. Phys. Chem. A* 122, 8819–8827 (2018).

- 13** L. Zhao, B. Xu, U. Ablikim, W. Lu, M. Ahmed, M.M. Evseev, E.K. Bashkirov, V.N. Azyazov, A.H. Howlader, S.F. Wnuk, A.M. Mebel, R.I. Kaiser, Gas-Phase Synthesis of Triphenylene (C₁₈H₁₂). *ChemPhysChem*. 20, 791-797 (2019).
- 14** L. Zhao, R.I. Kaiser, B. Xu, U. Ablikim, W. Lu, M. Ahmed, M. Evseev, E. K. Bashkirov, V.N. Azyazov, M.V. Zagidullin, A.N. Morozov, A.H. Howlader, S.F. Wnuk, A.M. Mebel, D. Joshi, G. Veber, F. R. Fischer, *Gas Phase Synthesis of [4]-Helicene*. *Nature Commun.* 10, 1510 (2019).
- 15** A.M. Thomas, C. He, L. Zhao, G.R. Galimova, A.M. Mebel, R.I. Kaiser, Combined Experimental and Computational Study on the Reaction Dynamics of the 1-Propynyl (CH₃CC)—1,3-Butadiene (CH₂CHCHCH₂) System and the Formation of Toluene under Single Collision Conditions. *J. Phys. Chem. A (H. Reisler Special Issue)* 123, 4104-4118 (2019).
- 16** L. Zhao, M.B. Prendergast, R.I. Kaiser, B. Xu, W. Lu, U. Ablikim, M. Ahmed, A.D. Oleinikov, V.N. Azyazov, A.M. Mebel, A.H. Howlader, S.F. Wnuk, Reactivity of the Indenyl Radical (C₉H₇) with Acetylene (C₂H₂) and Vinylacetylene (C₄H₄). *ChemPhysChem* 20, 1437-1447 (2019).
- 17** C. He, L. Zhao, A.M. Thomas, A.N. Morozov, A.M. Mebel, R.I. Kaiser, Elucidating the Chemical Dynamics of the Elementary Reactions of the 1-Propynyl Radical (CH₃CC; X²A₁) with Methylacetylene (H₃CCCH; X¹A₁) and Allene (H₂CCCH₂; X¹A₁). *J. Phys. Chem. A.* 123, 5446-5462 (2019).
- 18** L. Zhao, M. Prendergast, R. I. Kaiser, B. Xu, U. Ablikim, W. Lu, M. Ahmed, A.D. Oleinikov, V.N. Azyazov, A.H. Howlader, S.F. Wnuk, A.M. Mebel, How to Add a Five-Membered Ring to Polycyclic Aromatic Hydrocarbons (PAHs) – Molecular Mass Growth of the 2-Naphthyl Radical (C₁₀H₇) to Benzindenes (C₁₃H₁₀) as a Case Study. *Phys. Chem. Chem. Phys.* 21, 16737-16750 (2019).
- 19** C. He, A. M. Thomas, G. R. Galimova, A.M. Mebel, R.I. Kaiser, Gas Phase Formation of the Interstellar Molecule Methyltriacetylene. *ChemPhysChem*, 20, 1912-1917 (2019).
- 20** L. Zhao, R.I. Kaiser, W. Lu, B. Xu, M. Ahmed, A.N. Morozov, A.M. Mebel, A.H. Howlader, S.F. Wnuk, Molecular Mass Growth through Ring Expansion in Polycyclic Aromatic Hydrocarbons via Radical-Radical Reactions. *Nature Commun.* 10, 3689 (2019).
- 21** A.M. Thomas, C. He, L. Zhao, A.M. Mebel, R.I. Kaiser, Directed Gas Phase Synthesis of Triafulvene under Single Collision Conditions. *Angewandte Chemie – International Edition* 58, 15488 (2019).
- 22** C. He, L. Zhao, A. M. Thomas, A.M. Mebel, R.I. Kaiser, A Combined Experimental and Computational Study on the Reaction Dynamics of the 1-Propynyl Radical (CH₃CC; X²A₁) with Ethylene (H₂CCH₂; X¹A_{1g}) and the Formation of 1-Penten-3-yne (CH₂CHCCCH₃; X¹A⁺). *Physical Chemistry Chemical Physics* 21, 22308 (2019).
- 23** L. Zhao, M. Prendergast, R.I. Kaiser, B. Xu, U. Ablikim, M. Ahmed, B.-J. Sun, A.H.H. Chang, R.K. Mohamed, F.R. Fischer, Phenyl Addition - Dehydrocyclization Triggered Synthesis of Polycyclic Aromatic Hydrocarbons - The Third Way. *Angewandte Chemie – International Edition* 58, 17442 (2019).
- 24** A.M. Thomas, S. Doddipatla, R.I. Kaiser, A.M. Mebel, A Barrierless Pathway Accessing the C₉H₉ and C₉H₈ Potential Energy Surfaces via the Elementary Reaction of Benzene with 1-Propynyl. *Scientific Reports (Special Issue Molecular Reaction Dynamics)* 9, 17595 (2019).
- 25** C. He, A.M. Thomas, G.R. Galimova, A.M. Mebel, R.I. Kaiser, Gas-phase Formation of 1-Methylcyclo-propene and 3-Methylcyclopropene via the Reaction of the Methylidyne Radical (CH; X²Π) with Propylene (CH₃CHCH₂; X¹A⁺). *The Journal of Physical Chemistry A* 123, 10543-10555 (2019).
- 26** C. He, A.M. Thomas, G.R. Galimova, A.M. Mebel, R.I. Kaiser, Gas-Phase Formation of Fulvenallene (C₇H₆) via the Jahn-Teller Distorted Tropylium (C₇H₇) Radical Intermediate under Single-Collision Conditions. *The Journal of the American Chemical Society* 142, 3205-3213 (2020).
- 27** L. Zhao, B. Xu, M. Ahmed, A.M. Mebel, R.I. Kaiser, A Unified Mechanism on the Formation of Acenes, Helicenes, and Phenacenes in the Gas Phase. *Angewandte Chemie – International Edition* 59, 4051-4056 (2020).

ULTRAFAST PHYSICS: NONLINEAR OPTICAL SPECTROSCOPY AND DIAGNOSTICS

Christopher J. Kliewer, David W. Chandler, Krupa Ramasesha, Jonathan H. Frank
Sandia National Laboratories, MS 9051, Livermore, CA 94551-0969
cjkliw@sandia.gov, chand@sandia.gov, kramase@sandia.gov, jhfrank@sandia.gov

Program Scope

This program focuses on the development of innovative laser-based techniques for measuring temperature and concentrations of important gas phase molecular species as well as the investigation of fundamental physical and chemical processes that directly affect quantitative application of these techniques. Our development efforts focus on crossed-beam approaches such as time-resolved nonlinear wave-mixing. A critical aspect of our research includes the study of fundamental spectroscopy, energy transfer, molecular dynamics, and photochemical processes. This aspect of the research is essential to the development of accurate models and quantitative application of techniques to the complex environments encountered in combustion systems. These investigations use custom-built tunable picosecond (ps) and commercial femtosecond lasers, which enable efficient nonlinear excitation, provide high temporal resolution for pump/probe studies of collisional processes, and are amenable to detailed physical models of laser-molecule interactions.

Recent Progress

Tracking Molecules Far from Equilibrium.

Molecular systems far from equilibrium are a grand challenge in chemical physics research, and pose a unique test for our understanding of reaction kinetics and dynamic quantum simulations. Rotation-vibration non-equilibrium and energy transfer is a key area of study for low temperature plasmas that enhances chemical reactivity in applications such as carbon nanotube synthesis[1], plasma catalysis[2], CO₂ dissociation[3], and methane reforming[4]. Furthermore, rotation-vibration non-equilibrium is critical for understanding the aerodynamics and thermal loading of space vehicles re-entering Earth's atmosphere at hypersonic velocities[5]. In both plasmas and hypersonic vehicles, there exist spatial gradients of temperature due to transport across either the cathode sheath layer in low temperature plasmas[6] or through the boundary layer in hypersonic vehicles[5]. Therefore, it is of great interest to be able to conduct spatially resolved measurements of rotation-vibration non-equilibrium in these systems.

Hybrid femtosecond/picosecond coherent anti-Stokes Raman scattering (fs/ps CARS) is a powerful tool to measure species concentration and temperature on the picosecond time scale and tens of microns of spatial resolution, while avoiding non-resonant contributions to the CARS spectrum from four-wave mixing. This is achieved by generating the Raman coherence through efficient ultrafast excitation by a spectrally broad femtosecond laser which provides the pump and Stokes photons. A separate time-delayed spectrally narrow picosecond pulse scatters off this coherence and generates the CARS signal beam. Since the pump/Stokes and the probe beams do not overlap in time, the non-resonant contributions are avoided but many Raman transitions can be probed at once through the broadband excitation by the femtosecond laser.

During this past review period, we developed a 1-D two-beam fs/ps CARS imaging approach capable of measuring the rotational and vibrational state distributions of N₂ in a CH₄/N₂ pin-to-pin nanosecond-pulsed discharge. We found that with a spectrally narrow picosecond probe pulse (~0.3 cm⁻¹ transform-limited spectral FWHM), it is possible to directly measure vibrational contributions to the pure rotational CARS spectrum. As a result, the required number of beams reduces from four, in the case of dual-pump CARS, to two, and one-dimensional imaging of the CARS signal becomes feasible, allowing for the study of transient spatially imaged relaxation rates from nonequilibrium conditions. As a demonstration of this technique, a one-dimensional measurement of rotation-vibration non-equilibrium is presented in Figure 1. There was significant rotation-vibration non-equilibrium and spatial gradients in both temperatures, where the peak rotational and vibrational temperatures along the laser sheet were 380 K

and 5500 K, respectively. The vibrational temperature exhibited a strong rise as distance from the cathode increased and peaked 860 μm from the cathode. After the peak, there was still significant rotation-vibration non-equilibrium, where the vibrational temperature was consistently above 2500 K.

The analysis of the rotational-vibrational nonequilibrium relaxation rates is ongoing, and will be the subject of an imminent publication.

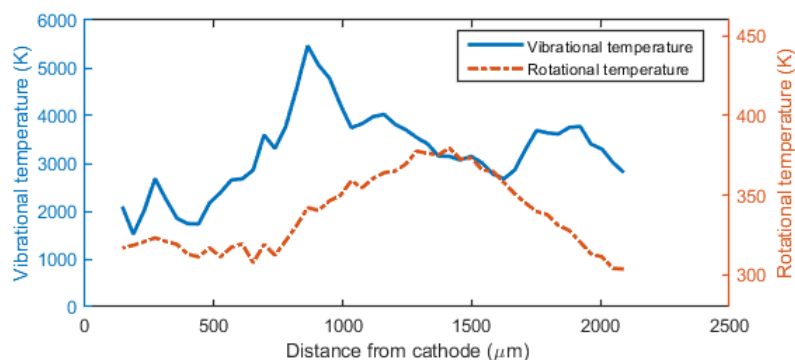


Figure 1. One dimensional spatially-resolved vibrational and rotational temperature 20 μs after the 4kV voltage pulse.

Future Work

Direct visualization of $\text{O}_2(a^1\Delta_g)$ using nonlinear optical methods

The direct time-resolved and spatially-resolved detection and visualization of the concentration $\text{O}_2(a^1\Delta_g)$ has been a difficult goal for many years. A weak absorption cross-section for excitation to the next lowest-lying electronic state thus requires a cavity ring-down or cavity-enhanced type setup for detection. Such methods have very long effective path lengths and are line-of-sight limited and are thus not applicable to many areas of gas phase chemical physics (such as combustion and plasma assisted chemistry) where $\text{O}_2(a^1\Delta_g)$ is known or suspected to play a major kinetic role. We have recently developed a technique to directly visualize $\text{O}_2(a^1\Delta_g)$ with excellent spatial resolution based upon time-domain coherent Raman spectroscopy. In the coming months we will demonstrate this technique by measuring $\text{O}_2(a^1\Delta_g)$, quantifying the detection limits, and then applying the method in measurements of plasma generated $\text{O}_2(a^1\Delta_g)$.

Coherence Lifetime Imaging through Structured Illumination

Coherence dephasing times are often governed by intermolecular interactions. In gas-phase systems, collisional energy transfer is the dominant source of rotational and vibrational coherence dephasing. Thus measuring the coherence decay rate allows for the in-situ mapping of collisional energy transfer rates, which are highly dependent on collision partner, number density, and collision energy. In condensed phase samples, the coherence lifetime gives an indication of the coupling of individual vibrational states to the surrounding environment. In microscopy applications, coherence lifetime would provide a novel imaging contrast mechanism sensitive subtle changes in local chemical environment. In previous work, we demonstrated the ability to measure coherence lifetimes within a single laser shot in the gas phase by separating the probe pulse into four separate weak probe pulses, each with a different phase matching angle [35]. We propose here to develop a 2D coherence lifetime imaging approach which can have impact in both gas-phase chemistry applications as well as in condensed phase fields. Similarly to fluorescence lifetime imaging, the coherence lifetime image will provide information on the chemical coupling and energy transfer to the local environment.

In order to realize single-shot coherence lifetime imaging, we will combine our recently developed 2D-CARS approach, with the structured illumination approach developed by our colleagues at Lund University. More specifically, the probed molecules will be excited with a pump/Stokes femtosecond laser sheet. The probe beam, however, will be separated via beam-splitters into four separate beams. Each of these beams will propagate through a time-of-flight optical delay stage and then be passed through a transmission grating. These gratings will be designed to optimize the +/- 1 orders. The position of the grating will be relay imaged to the experiment. In this way, each of the four probe beams gets imprinted with a fringe pattern at a controllable angle. The CARS beams will then be recombined into a single beam and scattered from the sample. The resulting image will contain four separate probe delays, with independent spatial frequencies, which can be extracted through spatial Fourier transform. In gas phase chemistry applications such as combustion, or coupled gas-surface chemistry, such an approach would enable simultaneous speciation, measurement of energy distributions, as well as provide an assessment of the degree of coupling to other molecules or the surface.

Development of a time-domain impulsive response model for CH₄

Recent work in the Ultrafast Diagnostics laboratory has led to new capabilities in the broadband impulsive excitation of all Raman-active transitions in a molecular ensemble. This was achieved through the development of a ~7 fs impulsive excitation source, coupled to a ps or ns probe pulse. We have demonstrated this approach for the simultaneous detection of CH₄, O₂, CO, CO₂, H₂, and N₂, imaging the gas-phase distribution to within 30 μm of a surface [7]. While this has proven very powerful for speciation, the full spectroscopy of each molecule contains far more information. At some pressures, the full vibrational, rotational, and translational (through the Doppler profile) energy distributions may be measured. However, to glean this information from the spectrum, a highly accurate spectroscopic model must be created and validated. For some simple molecules, such as N₂ and O₂ such detailed models have been published and validated allowing for detailed state populations to be derived from the spectrum. For other important molecules, such as CH₄, such a time-domain model has not been developed, nor validated. The impact of the capability to probe the detailed spectroscopy of CH₄ with ultrafast methods extends to many fields of chemical physics. In gas-surface catalysis, the activation of the C-H bond in CH₄ is the most difficult step in a great many chemical valorization processes, such as during catalytic methane reforming or the partial oxidation of methane. It is currently postulated that gas-phase low temperature plasmas may be used to vibrationally excite CH₄ enhancing catalytic reaction rates at surfaces. This hypothesis remains to be validated. CH₄ is further a combustion-relevant molecule, and the capability to observe gas-surface energy exchange between rotational and vibrational degrees of freedom will provide a new understanding of flame-wall interactions.

We propose to develop a full validated temperature and pressure dependent time-domain coherent Raman spectroscopy code for CH₄, similar to previous work we have published for N₂, O₂, and H₂. Experiments will begin with experiments from 0.1 to 1 bar, and from 300K to 1000K in a heated cell. At each set of conditions, CH₄ will be impulsively excited with a ~7 fs pulse from our hollow-core fiber pulse compressor, and probed with either an ~8 ns pulse (for high resolution experiments), a 65 ps pulse for intermediate spectral resolution, and a 6 ps pulse for which collisional dephasing should be nearly fully suppressed. In this manner, we will test different collisional energy transfer models (such as a simple modified exponential gap model) to assess the agreement under different collisional regimes. The result of this work will be a fully validated time-domain CH₄ spectral model that will enable our unique ultrafast Raman imaging approaches to be applied to a wide-ranging set of physical chemistry problems, such as near-wall combustion, plasma-assisted catalysis, and catalytic methane reforming.

Simultaneous species and temperature measurements of plasma-catalytic CH₄ dry reforming using 2D-CARS (Collaboration with Yiguang Ju and Timothy Chen, Princeton University).

Plasma assisted catalytic fuel reforming is an attractive alternative to large-scale reforming facilities to process methane. The chemical kinetic mechanism and physical understanding of the interaction of the plasma with the sheath layer and catalyst are poorly understood. Our lab has pioneered in recent years the invention of nonlinear optical imaging and broadband detection methods capable of probing in harsh environments, such as those encountered in and following a plasma discharge, on a single-laser shot basis. This is important for tracking transient processes such as that following a dielectric barrier discharge (DBD) plasma breakdown. The vibrational excitation of molecules may enhance dissociation and act as an additional catalyst to the overall reaction. In order to characterize these effects direct measurements of chemical speciation and vibrational/rotational energy distribution in the near surface region following plasma excitation are needed. Timothy Chen from Yiguang Ju's group at Princeton will collaborate at Sandia to make these measurements.

In this study, we will track the spatio-temporal evolution of rotational and vibrational energy distributions as well as chemical speciation in the dry reforming of CH₄ using plasma assisted catalysis, while resolving the transition from the sheath layer to the bulk using 1D and 2D ultrabroadband CARS. We will detect CH₄, CO₂, H₂, CO, CH₂O with this method. It is important to characterize the vibrational and rotational energy distributions of the CH₄ and CO₂ following the plasma discharge. The time-domain CARS code developed over the past several years at Sandia under this BES program currently contains validated models for H₂, N₂, and O₂. For this study, we will add time-domain molecular response models for CH₄, CO, and CO₂. Temperature dependent measurements in a heated cell will provide the baseline for validation of the spectroscopic model.

Journal publications supported by this BES project (2018-2020)

1. T.Y. Chen, B.M. Goldberg, B.D. Patterson, E. Kolemen, Y. Ju, and C.J. Kliewer, "1-D imaging of rotation-vibration non-equilibrium from pure rotational ultrafast coherent anti-Stokes Raman scattering" *Opt. Lett.* *submitted* (2020).

References

- [1] E. Plonjes, P. Palm, G. B. Viswanathan, V. V. Subramaniam, I. V. Adamovich, W. R. Lempert, H. L. Fraser, and J. W. Rich, *Chem. Phys. Lett.* **352**, 342 (2002).
- [2] T. Nozaki and K. Okazaki, *Catal. Today* **211**, 29 (2013).
- [3] T. Kozak and A. Bogaerts, *Plasma Sources Sci. Technol.* **23**, 17, 045004 (2014).
- [4] J. T. Sun and Q. Chen, *J. Energy Chem.* **39**, 188 (2019).
- [5] I. Armenise, M. Capitelli, G. Colonna, and C. Gorse, *J. Thermophys. Heat Transf.* **10**, 397 (1996).
- [6] K. Takashima, Z. Y. Yin, and I. V. Adamovich, *Plasma Sources Sci. Technol.* **22**, 16, 015013 (2013).
- [7] A. Bohlin, C. Jainski, B. D. Patterson, A. Dreizler, and C. J. Kliewer, *Proc. Combust. Inst.* **36**, 4557 (2017).

ARGONNE-SANDIA CONSORTIUM ON HIGH-PRESSURE COMBUSTION CHEMISTRY

Ahren W. Jasper, Stephen J. Klippenstein (PI), Raghu Sivaramakrishnan, Robert S. Tranter
**Chemical Sciences and Engineering Division, Argonne National Laboratory, Argonne, IL, 60439*

Leonid Sheps, Nils Hansen, Craig A. Taatjes (PI)
#*Combustion Research Facility, Mail Stop 9055, Sandia National Laboratories Livermore, CA 94551-0969*
sjk@anl.gov; cataatj@sandia.gov

Program Scope

The goal of this project is to explore the fundamental effects of pressure on chemical kinetics and to employ that knowledge in the development of accurate models for combustion chemistry at the high pressures of current and future combustion devices. We design and implement novel experiments, theory, and modeling to probe high-pressure combustion kinetics from elementary reactions, to submechanisms, and eventual application to flames. We continue to invest in the development of sensitive time-resolved experimental probes of reaction intermediates, which enable direct pressure-dependent studies of chemical systems of interest to high-pressure combustion chemistry and other DOE energy missions. We are applying novel master equation and stochastic simulation methods to accurately predict the kinetics of key processes. The theoretical predictions and experimental observations are employed in non-empirical modeling that provides high fidelity chemical models for combustion processes, and, more importantly, identifies departures from standard chemical kinetics assumptions. Recently, we have been pursuing detailed understandings of non-equilibrium effects and of radical oxidation chemistry. We are currently integrating modeling, experiment, and theory (MET) through feedback loops at all levels of chemical complexity for small alkanes, alcohols, and ethers (including cyclic variants) as key prototype fuels. The consortium expands and enhances collaborations between Argonne's Chemical Dynamics in the Gas Phase Group and the Combustion Chemistry Group in Sandia's Combustion Research Facility.

Recent Progress

HRRST: The HRRST has become a mature device. It reliably produces repeatable reaction conditions with standard deviations in temperature of < 1% over thousands of experiments. This enables the routine use of signal averaging to obtain good signal to noise with molecular beam sampling/photoionization mass spectrometry, the principle analytical method. In the last year, a number of key changes have been made to the driver section that improve longevity and simplify manufacture. PIMS experiments at the ALS have been improved by incorporating a MgF₂ filter, which has reduced dissociative ionization due to high-energy harmonic photons. Consequently, studies of a number of experimental systems, including reactions of alkyl radicals and dissociation of styrene, are now being prepared for publication. These include a study of *i*-butyl radicals (10 bar and 800 K) that complements low pressure laser schlieren experiments. The PIMS results confirm the underlying mechanism developed for recombination, disproportionation, and dissociation of alkyl radicals. They also support theoretical predictions that nonthermal reactions from *i*-butyl + CH₃, which are important at low pressures, are negligible at these conditions.

High-pressure photolysis reactor with mass spectrometric probing: In 2019 we completed the development of a unique high-pressure apparatus consisting of a laser photolysis reactor (HPLPR) and a time-resolved photoionization mass spectrometer (PIMS). This mobile instrument operates at Sandia or at the Advanced Light Source (ALS) with tunable VUV synchrotron radiation. Reactions are initiated by laser photolysis at 1–10 Hz and analyzed with 25 μs time resolution as a function of delay from each photolysis pulse. We measured performance metrics at P up to 50 bar and T up to 700 K, built the associated hardware and software infrastructure, developed operating protocols, and published a comprehensive description of

the instrument. We demonstrated an ~100-fold increase in sensitivity over our previous apparatus and an efficient sampling geometry that allows the detection of reactive radicals – both critical advances for detailed, sensitive, and quantitative probing of complex gas-phase reactions.

Nonthermal Kinetics, Termolecular Chemistry, and their Impact on Flames: Theory and modeling studies have shown that termolecular chemistry can be facilitated through nonthermal reactions of flame radicals (H, O, and OH) or O₂ with highly energized collision complexes (either radical or stable species) formed in exothermic reactions. We developed a global reactive potential energy surface (PES) suitable for studying H₂O* + H reactions. Nonthermal rate constants were computed using quasiclassical trajectories and, as in our previous study of CH₄* + X, were found to be fast ($> 10^{-10}$ cm³ molecule⁻¹ s⁻¹). These data were then used in accompanying modeling studies, which required two modifications: (i) the inclusion of the new nonthermal termolecular reaction rates and (ii) the simultaneous reduction of the competing recombination reaction rates. The former is described with newly derived Arrhenius expressions, and the latter is achieved by perturbing the recombination reaction rate during the simulation. The recombination rate coefficients were seen to be significantly reduced; by up to 15% or 38% for the H₂O and CH₄ systems, respectively. Kinetic modeling indicates that including this nonthermal chemistry for H₂/CH₄-air laminar flames speeds has a noticeable impact on simulated flame speeds.

Collision Parameters for Kinetics and Modeling: The collision parameters required for predicting pressure-dependent kinetics (e.g., the Lennard–Jones parameters σ and ε and the collision efficiency range parameter $\alpha = \langle \Delta E_d \rangle$) are frequently poorly known. We analyzed a large data set of trajectory-based collision parameters computed for more than 300 alkanes, alcohols, and hydroperoxides, including highly-branched species. We showed that σ and ε could be reliably estimated based on the number of heavy atoms, while trends in α were more complex. We developed an approach for estimating α that mapped its expected value for a branched alkane, alcohol, or hydroperoxide onto those for the corresponding linear series via an effective number of heavy atoms N_{eff} , which in turn is obtained by counting internal rotor types. Together, these strategies enable the rapid estimation of collision parameters so long as results for the associated linear series are available.

Future

HRRST: We have identified NO as a potential internal standard for HRRST/PIMS experiments. It is largely inert in pyrolytic systems and photoionization cross-sections are well known over a suitable range of energies. This should allow for signal changes due to pressure changes in the TOFMS to be compensated and allow kinetic as well as mechanistic information to be extracted from the PIMS data. We propose to continue studies related to one a number of systems including roaming reactions in neopentanol and small aromatic systems including the multichannel decomposition of styrene and the role of *o*-benzyne in molecular growth.

Flow Reactors: We will continue to invest in custom experimental tools for high pressure studies by leveraging three recent advances, made under separate funding. First, we plan to use a very rapid laminar flow mixer to reduce the residence (mixing) times of the sample in the HPLPR from 100s to 10s of ms, prior to laser photolysis. This will dramatically lessen unwanted thermal reactions and raise the temperature limit of the HPLPR. Second, we intend to commission a high-pressure fast-flow reactor, in which reactions will be initiated thermally (rather than by photolysis) and analyzed as a function of well-defined residence time. This reactor will be a complement to the HPLPR and will enable simpler modeling of the chemistry by avoiding the need for a photolysis precursor. Third, we will interface both reactors with a new, custom Fluorescence Assay by Gas Expansion (FAGE) apparatus, constructed specifically for time-resolved analysis of effluent from high-pressure sources. This instrument will quantify two key combustion radicals, OH and HO₂, filling a critical gap in our current capabilities.

High-Pressure Jet-Stirred Reactor (HP-JSR): We plan to design and test a high-pressure (up to 40 bar) jet-stirred reactor following the principles outlined by Villermaux, and with guidance from Dagaut (CNRS

Orleans). This HP-JSR will be interfaced with an advanced high-resolution time-of-flight mass spectrometer (MS) that can be used with single-photon VUV ionization (mostly at the Advanced Light Source), electron ionization (EI), and laser-based ionization will provide accurate chemical composition. This HP-JSR will be used to investigate oxidation reactions in the low-T autoignition regime.

Detailed probing of autoignition chemistry: We have recently developed methods for the measurement of absolute photoionization cross-sections (PIXS) of key intermediates in hydrocarbon oxidation: ROO, OOQOOH, and ketohydroperoxides (KHP), as shown in Fig. 1 for the case of diethyl ether (DEE). This is done by careful selection of experimental conditions at which all other species are accounted for, so that ROO, OOQOOH, and KHP can be quantified one at a time from the overall C atom balance. We will perform quantitative measurements of the kinetics of these intermediates for a series of model systems: propane, neo-pentane, dimethyl ether, diethyl ether, cyclopentane, and tetrahydrofuran. These systems span a range of structural motifs and functional groups, enabling fundamental insights into fuel-specific reactivity trends. Theory and modeling studies of these systems will also be performed to gain fundamental understanding of these complex reaction networks.

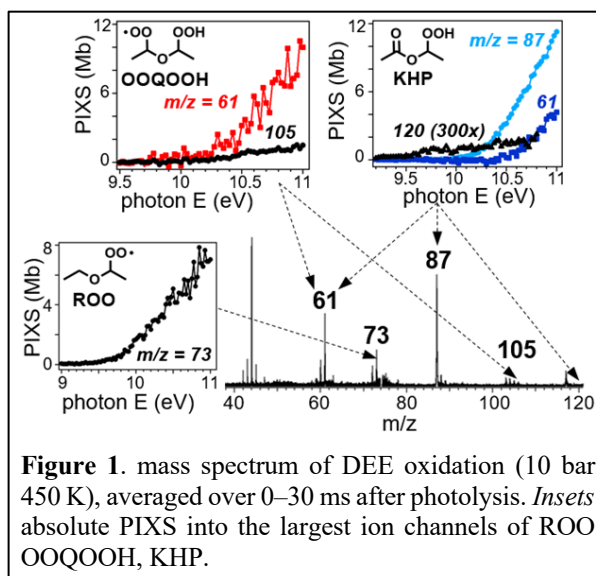


Figure 1. mass spectrum of DEE oxidation (10 bar, 450 K), averaged over 0–30 ms after photolysis. *Insets:* absolute PIXS into the largest ion channels of ROO, OOQOOH, KHP.

Termolecular/Non-Thermal Kinetics: We will continue our dynamical and modeling studies of hydrocarbon radical prompt dissociations and termolecular recombinations. For example, the decomposition reactions of oxygenated radicals are more diverse and yet far less explored than those of hydrocarbon radicals. Thus, we will perform a broad experimental, theoretical, and modeling survey of the T- and P- dependent rates and product branching in the decomposition of several prototypical small oxy-radicals: CH_3OCO , CH_3CHOH , $\text{CH}_2\text{CH}_2\text{OH}$, and CH_3CO , with the goal of understanding the extent of prompt “non-Boltzmann” dissociations. Preliminary simulations with our core mechanism are being used as an aid in the design of PIMS experiments to probe the thermal decompositions of radicals generated with Cl abstractions from ethanol and methyl formate. We also intend to continue our efforts to characterize nonthermal reactions through further studies of the role of branching between stabilization and nonthermal reactivity in two important hydrogen oxidation reactions, $\text{H} + \text{OH} + \text{M} = \text{H}_2\text{O}^* + \text{M}$ and $\text{H} + \text{O}_2 + \text{M} = \text{HO}_2^* + \text{M}$.

Stochastic Dynamics: We propose to combine stochastic sampling of elementary chemical events from a complex reactive mixture with Argonne’s high-performance computing resources so that each sampled event can be treated using high-level dynamics and kinetics theories. Sampled events include both reactive and nonreactive (thermalizing) collisions, with global chemistry emerging naturally via their competition. This approach can be thought of as a stochastic master equation built up from a priori descriptions of the underlying dynamics and kinetics. Preliminary studies show that this approach can resolve ambiguities in analytic collision models that find more practical use in master equation. In more ambitious calculations, the stochastic approach will be used to quantify the accuracy of our 2DME collision kernel using the two-channel $\text{CH}_2\text{O} (+\text{M})$ as a test case and to study the reactivity of transient van der Waals complexes at high pressures. The latter have been implicated via the “chaperone effect” or the radical-complex mechanism to explain the so-called “second high pressure limit” observed experimentally in $\text{CH}_3 + \text{O}_2$. The stochastic approach provides a means of modeling this chemistry *a priori*.

Publications acknowledging support from this program, 2018-Present

1. **Modeling Nitrogen Chemistry in Combustion**, P. Glarborg, B. Ruscic, J. A. Miller, S. J. Klippenstein, *Prog. Energy Combust. Sci.* **67**, 31-68 (2018).
2. **Theory and Modeling of Relevance to Prompt-NO Formation at High Pressure**, S. J. Klippenstein, M. Pfeifle, A. W. Jasper, P. Glarborg, *Combust. Flame* **195**, 3-17 (2018).
3. **Unimolecular Decomposition Kinetics of the Stabilised Criegee intermediates CH₂OO and CD₂OO**, D. Stone, K. Au, S. Sime, D. J. Medeiros, M. Blitz, P. W. Seakins, Z. Decker and L. Sheps, *Phys. Chem. Chem. Phys.* **20**, 24940-24954 (2018).
4. **The Reaction of Hydroxyl and Methylperoxy Radicals is Not a Major Source of Atmospheric Methanol**, R. L. Caravan, M. A. H. Khan, J. Zador, L. Sheps, I. O. Antonov, B. Rotavera, K. Ramasesha, K. Au, M. W. Chen, D. Rosch, D. L. Osborn, C. Fittschen, C. Schoemaeker, M. Duncianu, A. Gira, S. Dusanter, A. Tomas, C. J. Percival, D. E. Shallcross and C. A. Taatjes, *Nature Commun.* **9**, 4343 (2018).
5. **Direct Measurements of Channel Specific Rate Constants in OH + C₃H₈ Illuminates Prompt Dissociations of Propyl Radicals**, R. Sivaramakrishnan, C. F. Goldsmith, S. L. Peukert, J. V. Michael, *Proc. Combust. Inst.* **37**, 231-238 (2019).
6. **Kinetics of 1-Butyl and 2-Butyl Radical Reactions with Molecular Oxygen: Experiment and Theory**, A. J. Eskola, T. T. Pekkanen, S. P. Joshi, R. S. Timonen, S. J. Klippenstein, *Proc. Combust. Inst.* **37**, 291-298 (2019).
7. **High-Pressure Oxidation of Propane**, H. Hashemi, J. M. Christensen, L. B. Harding, S. J. Klippenstein, P. Glarborg, *Proc. Combust. Inst.* **37**, 461-468 (2019).
8. **Reference Natural Gas Flames at Nominally Autoignitive Engine-Relevant Conditions**, A. Krisman, C. Mounaim-Rouselle, R. Sivaramakrishnan, J. A. Miller, J. H. Chen, *Proc. Combust. Inst.* **37**, 1631-1638 (2019).
9. **Comment on “Influence of Multiple Conformations and Paths on Rate Constants and Product Branching Ratios. Thermal Decomposition of 1-Propanol Radicals”**, J. Zador, J. A. Miller, *J. Phys. Chem. A*, **123**, 1129-1130 (2019).
10. **Nonthermal Rate Constants for CH₄* + X → CH₃ + HX, X = H, O, OH, and O₂**. A. W. Jasper, R. Sivaramakrishnan, S. J. Klippenstein, *J. Chem. Phys.* **150**, 114112 (2019).
11. **Influence of Ether Functional Group on Ketohydroperoxide Formation in Cyclic Hydrocarbons: Tetrahydropyran and Cyclohexane**, J. C. Davis, A. L. Koritzke, R. L. Caravan, I. O. Antonov, M. G. Christianson, A. C. Doner, D. L. Osborn, L. Sheps, C. A. Taatjes, B. Rotavera, *J. Phys. Chem. A* **123**, 3634-3646 (2019).
12. **“Third-Body” Collision Parameters for Hydrocarbons, Alcohols, and Peroxides and an Effective Internal Rotor Approach for Estimating Them**, A. W. Jasper, *Int. J. Chem. Kinet.* **52**, 387-402 (2020).
13. **Solenoid Actuated Driver Valve for High Repetition Rate Shock Tubes**, R. S. Tranter, T. Sikes, *Rev. Sci. Instrum.* **91**, in press (2020); DOI: 0.1063/5.0006010
14. **Termolecular Chemistry Facilitated by Radical-Radical Recombinations and Its Impact on Flame Speed Predictions**, Y. Tao, A. W. Jasper, Y. Georgievskii, S. J. Klippenstein, R. Sivaramakrishnan, *Proc. Combust. Inst.* accepted for presentation (2020).
15. **Low Temperature Oxidation of Diethyl Ether: Reactions of Hot Radicals Across Coupled Potential Energy Surfaces**, D. Danilack, S. J. Klippenstein, Y. Georgievskii, C. F. Goldsmith, *Proc. Combust. Inst.* accepted for presentation (2020).
16. **Combustion Chemistry in the Twenty-First Century: Developing Theory-Informed Chemical Kinetics Models**, J. A. Miller, R. Sivaramakrishnan, Y. Tao, C. F. Goldsmith, M. P. Burke, A. W. Jasper, N. Hansen, N. J. Labbe, P. Glarborg, J. Zádor, *Prog. Energy Combust. Sci.* submitted (2020).
17. **An Experimental and Theoretical Study of the High Temperature Reactions of Four Butyl Radical Isomers**, J. B. Randazzo, A. W. Jasper, R. Sivaramakrishnan, T. Sikes, P. T. Lynch, R. S. Tranter, *Phys. Chem. Chem. Phys.* submitted (2020).

THEORETICAL CHEMICAL KINETICS

Stephen J. Klippenstein
Chemical Sciences and Engineering Division
Argonne National Laboratory
Argonne, IL, 60439
sjk@anl.gov

Program Scope

The focus of this program is the development and application of theoretical methods for exploring gas phase chemical kinetics. The research involves a combination of *ab initio* electronic structure calculations, variational transition state theory (TST), classical trajectory simulations, and master equation (ME) calculations. Detailed applications, including careful comparisons with experiment as feasible, are used to (i) develop a deeper understanding of the applicability of various foundational principles of gas phase chemical kinetics, (ii) motivate improvements in theoretical chemical kinetics methodologies, and (iii) enhance our understanding of various aspects of combustion, atmospheric, and interstellar chemistry. The specific reactions studied are generally motivated by global modeling efforts and state-of-the-art experimental observations.

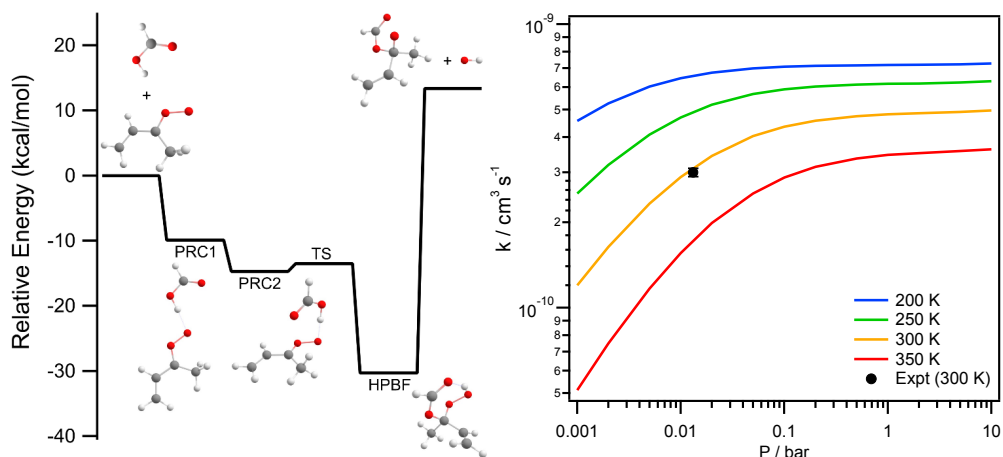
Recent Progress

Automated Kinetics: Large scale implementation of high level computational theoretical chemical kinetics offers the prospect for dramatically improving the fidelity of combustion chemical modeling. To facilitate such efforts, we developed a set of python scripts (AutoMech) that allow for the automatic prediction of the kinetics for a large set of reactions via *ab initio* transition-state-theory based master equation calculations. The primary input is simply the mechanism in standard format (e.g., ChemKin or JSON), a dictionary relating chemically identifiable species descriptors (i.e., SMILES or InChIs) to species labels in the mechanism, and a specification of the electronic structure and transition state theory models to be implemented. We illustrated the utility of such explorations through a study of the initial stages of pyrolysis for 3 sets of fuels: sequences of alkanes, alcohols, and aldehydes. For simplicity, the analysis focused on abstractions from the fuel by H, CH₃, and OH, and the decomposition of the resulting radicals. The code successfully produces meaningful rate estimates for ~95 % of these reactions, including for the pressure dependence of the radical decomposition reactions. A key focus of this continuing effort is on the incorporation of advanced *ab initio* kinetic methodologies.

Kinetics of Criegee Intermediates: Isoprene has the highest emission into Earth's atmosphere of any non-methane hydrocarbon. Atmospheric processing of alkenes, including isoprene, via ozonolysis leads to the formation of zwitterionic reactive intermediates, known as Criegee intermediates (CIs). Direct studies have revealed that reactions involving simple CIs can significantly impact the tropospheric oxidizing capacity, enhance particulate formation and degrade local air quality. Methyl vinyl ketone oxide (MVK-oxide) is a four-carbon, asymmetric, resonance-stabilized CI, produced with 21-23% yield from isoprene ozonolysis, yet its reactivity has not been directly studied. From a chemical physics perspective, it is interesting to probe the effect of this resonance stabilization on its reactivity.

In a multiple group collaboration (with Caravan, Lester, Taatjes, and Osborn, among others) we studied the kinetics of MVK-oxide reacting with water, SO₂, and formic acid both experimentally and theoretically. The *ab initio* transition-state-theory based master equation theoretical analysis yielded predictions for the temperature and pressure dependence of the

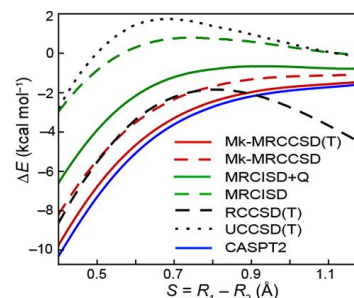
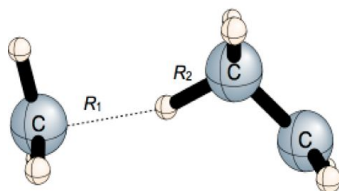
reaction rates and branching ratios. The calculations were based on a combination of density functional theory based rovibrational analyses, coupled cluster-based energy evaluations [including estimates for the CCSDT(Q) corrections], variational transition state theory (including variable reaction coordinate treatments of the pre-reactive complex formation process), and explicitly treated hindered rotational motions. Experiment and theory provide a consistent picture for the kinetics, as illustrated below for the reaction with formic acid. Interestingly, the predictions indicate a significant temperature and pressure dependence to the kinetics at 300 K, even though the rate is close to typical collision rates. The tropospheric implications of these reactions were evaluated through a global chemistry and transport model.



In collaboration with Lester, we also explored experimentally and theoretically the unimolecular dissociation of doubly-substituted methyl-ethyl Criegee intermediate (MECI) as a way to examine the effect of multiple hindered rotors on the kinetics. MECI exhibits four conformers, all of which undergo unimolecular decay *via* a 1,4 H-atom transfer mechanism, followed by rapid release of OH products. Conformers with different orientations of the carbonyl oxide group with respect to the methyl and ethyl substituents (i.e. *anti* and *syn*) decay *via* distinct transition state (TS) barriers (16.1 and 15.4 kcal mol⁻¹, respectively). The experiments used IR action spectroscopy to measure the microcanonical dissociation rates for the strongest features in the IR action spectrum. Corresponding a priori RRKM predictions were obtained for treatments of the underlying hindered rotors at varying levels of sophistication. The experimental rates are in good agreement with the computed RRKM rates for the unimolecular decay of MECI. The theoretical analyses illustrated the variation between single- and multi-structure harmonic, 1- and multi-dimensional hindered rotor treatments, with and without vibrationally adiabatic corrections for the latter method. Comparison with other previously studied Criegee intermediate systems provided insight into substituent effects on unimolecular decay under both energy-dependent and thermal conditions.

Radical-Radical Abstraction: Radical-radical abstractions are generally exothermic with little or no barrier. Although they are of considerable significance in hydrocarbon oxidation chemistry, they have not been well studied either theoretically or experimentally. The primary theoretical challenge is that single reference methods are not really applicable. We evaluated the appropriateness of a variety of multi-reference electronic structure methods through calculations for five prototypical radical-radical hydrogen abstractions: $\text{H} + \text{BeH} \rightarrow \text{H}_2 + \text{Be}$, $\text{H} + \text{NH}_2 \rightarrow \text{H}_2$

+ NH, CH₃ + C₂H₅ → CH₄ + C₂H₄,
 H + C₂H₅ → H₂ + C₂H₄, and H +
 HCO → H₂ + CO. The methods
 evaluated included state-specific
 multireference coupled cluster
 methods Mk-MRCCSD and Mk-
 MRCCSD(T), as well as the
 companion perturbation theory Mk-
 MRPT2, and the established
 MRCISD, MRCISD+Q, and



CASPT2 approaches. Full configuration interaction benchmark computations for the H + BeH, H + NH₂, and H + HCO reactions proved that Mk-MRCCSD(T) provides superior accuracy for the interaction energies in the entrance channel, with mean absolute errors less than 0.3 kcal mol⁻¹ and percentage deviations less than 10% over the fragment separations of relevance to kinetics. CASPT2 also performs quite well in the kinetically relevant regions, with maximum discrepancies of 20 % between Mk-MRCCSD(T) and CASPT2 based kinetic predictions.

Future Directions

We continue to work toward implementing automated high-level theoretical thermochemical kinetics to improve our understanding of classic combustion mechanisms. Currently, those efforts are focused on implementing advanced TST treatments, such as our variable reaction coordinate approach, and at predicting the kinetics for larger alkane species such as n-heptane, iso-octane, and n-dodecane.

Our studies on the kinetics of Creigee intermediates are continuing. Currently, in collaboration with Caravan and Taatjes (and others) we are exploring the oligomerization of CH₂OO through its successive additions to OCHOH. In collaboration with Caravan and Lester we are further examining the kinetics of MVK-Oxide reacting with formic acid.

In collaboration with Jasper, we are exploring the feasibility of developing density functionals that better approximate the saddle point geometries that are so central to kinetics.

DOE Supported Publications, 2018-Present

1. **Anharmonic Rovibrational Partition Functions for Fluxional Species at High Temperatures via Monte Carlo Phase Space Integrals**, A. W. Jasper, Z. B. Gruey, L. B. Harding, S. J. Klippenstein, A. F. Wagner, *J. Phys. Chem. A* **122**, 1727-1740 (2018).
2. **Modeling Nitrogen Chemistry in Combustion**, P. Glarborg, B. Ruscic, J. A. Miller, S. J. Klippenstein, *Prog. Energy Combust. Sci.* **67**, 31-68 (2018).
3. **H-Abstraction Reactions by OH, HO₂, O, O₂, and Benzyl Radical Addition to O₂ and Their Implications for Kinetic Modelling of Toluene Oxidation**, M. Pelucchi, C. Cavallotti, T. Faravelli, S. J. Klippenstein, *Phys. Chem. Chem. Phys.* **20**, 10607-10627 (2018).
4. **Unimolecular Decay of Criegee Intermediates to OH Radical Products: Prompt and Thermal Decay Processes**, M. I. Lester, S. J. Klippenstein, *Acc. Chem. Res.* **51**, 978-985 (2018).
5. **Nascent Energy Distribution of the Criegee Intermediate CH₂OO from Direct Dynamics Calculations of Primary Ozonide Dissociation**, M. Pfeifle, Y.-T. Ma, A. W. Jasper, L. B. Harding, W. L. Hase, S. J. Klippenstein, *J. Chem. Phys.* **148**, 174306 (2018).
6. **Four-Carbon Criegee Intermediate from Isoprene Ozonolysis: Methyl Vinyl Ketone Oxide Synthesis, Infrared Spectrum, and OH Production**, V. P. Barber, S. Pandit, A. M. Green, *J. Am. Chem. Soc.* **140**, 10866-10880 (2018).

7. **Automated Computational Thermochemistry for Butane Oxidation: A Prelude to Predictive Automated Combustion Kinetics**, M. Keceli, S. Elliott, Y.-P. Li, M. S. Johnson, C. Cavallotti, Y. Georgievskii, W. H. Green, M. Pelucchi, J. M. Wozniak, A. W. Jasper, S. J. Klippenstein, *Proc. Combust. Inst.* **37**, 363-371 (2019).
8. **Small Ester Combustion Chemistry: Computational Kinetics and Experimental Study of Methyl Acetate and Ethyl Acetate**, A. Ahmed, W. J. Pitz, C. Cavallotti, M. Mehl, N. Lokachari, E. J. K. Nilsson, J.-Y. Wang, A. A. Konnov, S. W. Wagnon, B. Chen, Z. Wang, H. J. Curran, S. J. Klippenstein, W. J. Roberts, S. M. Sarathy, *Proc. Combust. Inst.* **37**, 419-428 (2019).
9. **Simulating the Density of Organic Species in the Atmosphere of Titan with a Coupled Ion-Neutral Photochemical Model**, V. Vuitton, R. V. Yelle, S. J. Klippenstein, P. Lavvas, S. M. Horst, *Icarus*, **324**, 120-197 (2019).
10. **ESTokTP: Electronic Structure to Temperature- and Pressure-Dependent Rate Constants – A code for Automatically Predicting the Thermal Kinetics of Reactions**, C. Cavallotti, M. Pelucchi, Y. Georgievskii, S. J. Klippenstein, *J. Chem. Theory Comp.* **15**, 1122-1145 (2019).
11. **HO₂ + HO₂: High Level Theory and the Role of Singlet Channels**, S. J. Klippenstein, R. Sivaramakrishnan, U. Burke, K. P. Somers, H. J. Curran, L. Cai, H. Pitsch, M. Pelucchi, T. Faravelli, P. Glarborg, *11th U. S. National Combustion Meeting*, Paper 1A13 (2019).
12. **Ab Initio Kinetics for Pyrolysis and Combustion Systems**, S. J. Klippenstein, C. Cavallotti; in: *Mathematical Modeling of Complex Reaction Systems: Pyrolysis and Combustion*, T. Faravelli, F. Manenti, and E. M. Ranzi, Eds. Computer Aided Chemical Engineering Series, Elsevier: New York, (2019).
13. **Propane Clusters in Titan's Lower Atmosphere: Insights from a Combined Theory/Laboratory Study**, J. Bourgalais, O. Durif, S. D. Le Picard, P. Lavvas, F. Calvo, S. J. Klippenstein, L. Biennier, *Mon. Not. Roy. Ast. Soc.* **488**, 676-684 (2019).
14. **Synthesis, Electronic Spectroscopy, and Photochemistry of Methacrolein Oxide: A Four-Carbon Unsaturated Criegee Intermediate from Isoprene Ozonolysis**, M. F. Vansco, B. Marchetti, N. Tronsiriwat, T. Bhagde, G. Wang, P. J. Walsh, S. J. Klippenstein, M. I. Lester, *J. Am. Chem. Soc.* **141**, 15058-15069 (2019).
15. **Photodissociation Transition States Characterized by Chirped Pulse Millimeter Wave Spectroscopy**, K. Prozument, J. H. Baraban, P. B. Changala, G. B. Park, R. G. Shaver, J. S. Muentner, S. J. Klippenstein, V. Y. Chernyak, R. W. Field, *Proc. Nat. Acad. Sci.* **117**, 146-151(2020).
16. **Reaction Profiles and Kinetics for Radical-Radical Hydrogen Abstraction via Multireference Coupled Cluster Theory**, C.-H. Wu, D. B. Magers, L. B. Harding, S. J. Klippenstein, W. D. Allen, *J. Chem. Theory Comp.* **16**, 1511-1525 (2020).
17. **Experimental and Theoretical Studies of the Doubly-Substituted Methyl-Ethyl Criegee Intermediate: Infrared Action Spectroscopy and Unimolecular Decay to OH Radical Products**, V. P. Barber, A. S. Hansen, S. J. Klippenstein, M. I. Lester, *J. Chem. Phys.* **152**, 094301 (2020).
18. **Direct Kinetic Measurements and Theoretical Predictions of an Isoprene-Derived Criegee Intermediate**, R. L. Caravan, M. F. Vansco, K. Au, M. A. H. Khan, Y.-L. Li, F. A. F. Winiberg, K. Zuraski, Y.-H. Lin, W. Chao, N. Trongsiriwat, P. J. Walsh, D. L. Osborn, C. J. Percival, J. Jr-M. Lin, D. E. Shallcross, L. Sheps, S. J. Klippenstein, C. A. Taatjes, M. I. Lester, *Proc. Nat. Acad. Sci.* in press (2020); DOI: 10.1073/pnas.1916711117
19. **Automated Theoretical Chemical Kinetics: Exploring the Initial Stages of Pyrolysis**, S. N. Elliott, K. B. Moore, A. V. Copan, M. Keceli, C. Cavallotti, Y. Georgievskii, H. F. Schaefer III, S. J. Klippenstein, *Proc. Combust. Inst.* accepted for presentation (2020).

DEVELOPING NEW MECHANISTIC INSIGHTS INTO OXIDATIVE COUPLING OF METHANE THROUGH COMBINED GAS-PHASE AND SURFACE-SENSITIVE SPECTROSCOPIES WITH SITE-ISOLATED CATALYSTS

Coleman Kronawitter and Ambarish Kulkarni
Department of Chemical Engineering, University of California, Davis, CA
ckrona@ucdavis.edu, arkulkarni@ucdavis.edu

PROGRAM SCOPE

Note: This project is co-supported by the Gas Phase Chemical Physics and the Catalysis Science Programs.

The recent increase in supply of natural gas has motivated a wide exploration of strategies for methane valorization in the global catalysis research community. One such strategy, oxidative coupling of methane (OCM), has in this environment witnessed a resurgence of interest in the field of heterogeneous catalysis. A distinguishing characteristic of OCM is the pivotal role played by gas-phase methyl radicals in dictating reaction pathways. Specifically, it is generally accepted that for the most common catalysts and reaction conditions, the dominant mechanism of C₂ product formation involves the near-surface gas-phase coupling of methyl radicals.

The overarching goal of this project is to decouple, understand, and independently optimize the elementary steps that constitute the overall OCM reaction. Our approach is facilitated by recent advances in two until-now unrelated areas of technology development: (1) novel spectroscopic techniques that can probe spatially- and temporally-resolved gas-phase compositions close to a solid surface; and (2) new developments in the synthesis and characterization of uniform, site-isolated catalysts. This project's efforts will directly measure the spatially-resolved concentrations of near-surface reactive intermediates and provide quantitative evidence to develop coupled gas/surface mechanisms. This will be accomplished through close collaboration with Sandia National Laboratories' Combustion Research Facility (SNL CRF), where researchers have developed new techniques in the field of gas phase chemical physics that have only begun to be applied to heterogeneous catalytic systems. Work at SNL CRF on exporting these techniques to applications in catalysis is conducted through an independent grant.

RECENT PROGRESS

Since awarded in September 2019, progress has been made in two key areas: (1) the investigation of near-surface gas-phase species (both closed- and open-shell) associated with heterogeneous catalytic oxidation reactions, and (2) the synthesis and characterization of site-isolated (atomically-dispersed) catalysts.

***Operando* near-surface gas-phase species observed locally during catalytic oxidation of methanol.** To investigate OCM through site-isolated catalysts using the comprehensive suite of surface and near-surface gas-phase characterization techniques mentioned above, we first must demonstrate that the techniques themselves can be leveraged to detect the known intermediates and products associated with OCM. We have determined that methanol oxidation is an ideal reaction to study to perform this critical task because: (1) methanol is a C₁ molecule and its oxidation by O₂ is known to generate a number of C-H-O-containing species that are also generated through OCM; (2) in certain conditions (at specific catalysts and feed compositions) oxidative reactions with methanol yield C-C coupling events, whose identification and characterization is of course critical for OCM; (3) methanol oxidation occurs at lower temperatures than

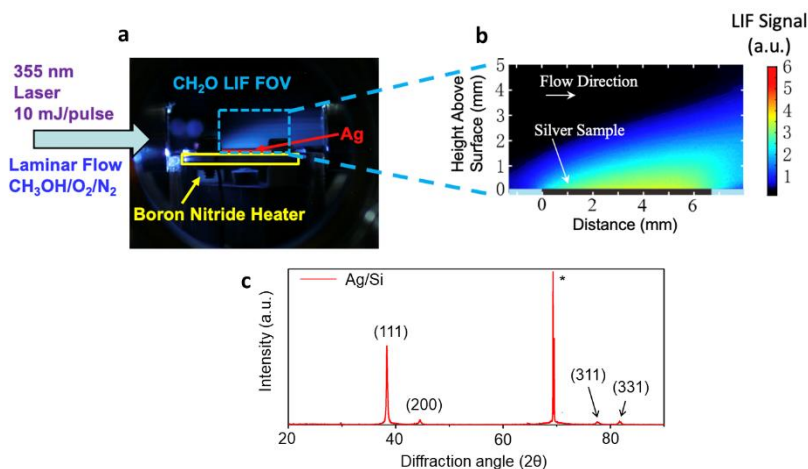


Figure 1. (a) Photograph of experimental setup for *operando* planar laser-induced fluorescence (PLIF) and Raman spectroscopy (from SNL CRF). In this configuration, a film catalyst is utilized. (b) Representative false-color PLIF image, corresponding to field-of-view in photograph in (a), showing spatially-resolved fluorescence signal associated with CH₂O. $P_{\text{total}} = 600$ Torr; $T_{\text{Ag}} = 680$ K; 89 vol% CH₃OH, 2 vol% O₂, balance N₂. Measurements recorded with Hansen, Frank, Osborn (Sandia National Laboratories). (c) X-ray diffractogram of Ag/Si catalyst, showing (111) texture. * indicates Si substrate peak.

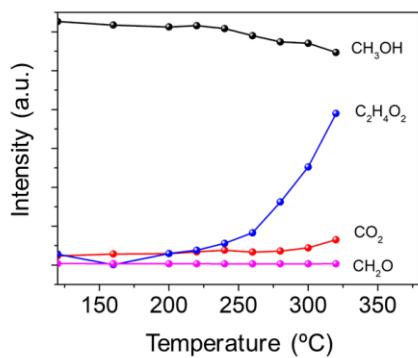


Figure 2. Representative MBMS results associated with methanol oxidation at the surface of AuPd alloy thin film catalysts. 45 vol% CH₃OH, 5 vol% O₂, balance N₂; $P_{\text{total}} = 760$ Torr. Measurements recorded with Hansen, Frank, Osborn (Sandia National Laboratories).

OCM, and so experimental complications associated with high-temperature *operando* spectroscopy can be avoided initially while optimizing methodologies for chemical detection and speciation.

Silver (Ag) was chosen for initial study of methanol oxidation catalysis because of its unique ability to selectively produce formaldehyde (CH₂O), which is an industrially important chemical [G. J. Millar et al. *Ind. Eng. Chem. Res.* **2017**, 56, 9247-9265]. CH₂O is stable and also is a fluorescent molecule, and therefore its spatial distribution can be examined through planar laser-induced fluorescence (PLIF).

Ag thin films were synthesized on single-crystal Si substrates using magnetron sputtering, using a deposition system in the PI's lab. These films were installed in a reactor enabling *operando* PLIF/Raman measurements at SNL CRF. Figure 1a provides a photograph of the first iteration of the experimental setup, wherein reactant mixtures (here, methanol/O₂/inert) are fed at constant flow rate over a temperature-controlled Ag/Si sample. PLIF and Raman spectroscopy measurements are recorded in the field-of-view indicated. Representative PLIF results (Figure 2b) show that the spatial distribution of CH₂O can be directly imaged above the Ag surface. No CH₂O is generated at the bare Si surface, and beginning at the leading edge of the Ag film, the reaction commences and a distinct species-resolved boundary layer is evident. The CH₂O intensity is greatest near the Ag surface, and reduces through the thickness of the boundary layer, as expected for CH₂O generated catalytically directly at the Ag surface. These efforts will be coupled with comprehensive materials characterization using a suite of techniques. For example, an X-ray diffractogram (Figure 1c) of the Ag/Si sample indicates that the Ag films are polycrystalline and oriented (textured) such that Ag(111) facets are dominantly exposed.

The value of the catalytic oxidation of methanol with O₂ to study catalysis and benchmark spectroscopic techniques was discussed above. While exploring the implications of these results, we have determined that

a systematic study across the composition space of metal alloy thin films will provide a unique opportunity to connect catalysis and spectroscopy results with traditional computational catalysis findings based on the binding energies of reactants, intermediates, and products. To this end, we have begun examining methanol oxidation at the surfaces of Au_xPd_y films. For this study, initial work has focused on the use of molecular-beam mass spectrometry (MBMS) because the universality of its speciation in the near-surface gas phase will facilitate direct comparisons of local products among Au_xPd_y catalysts.

Methanol oxidation over AuPd surfaces was investigated under continuous flow conditions with methanol/ O_2 mixture feeds. Figure 2 provides representative preliminary MBMS results identifying local products above the sample surface as a function of increasing reaction temperature. The aerobic oxidation of methanol over AuPd has been reported [R. Wang, et al. *Chem. Commun.*, **2013**, 49, 8250] and methyl formate has been determined to be the primary product. The product temperature profiles in Figure 2 confirm these previous findings by showing a slight decrease in methanol signal and a concurrent rise in the intensity associated with methyl formate. It is also clear that CH_2O , the primary product of methanol oxidation at Ag, is either not produced or produced at very low rates at AuPd. The difference between this data and prior studies is that it is collected locally, several mm above the AuPd surface. This work is ongoing, and data interpretation continues, but these results clearly show the ability of our methodology to probe C-C coupling events, locally (directly above the sample surface), and correlate this information with conventional analysis and quantification of reactor effluent gases.

Synthesis and characterization of atomically-dispersed supported metal catalysts for oxidation reactions. This project hypothesizes that site-isolated catalysts, which consist of well-defined and typically more homogeneous active sites, are likely to present advantages for mechanistic OCM studies. Therefore, the second essential aspect of this project that has been pursued initially is the synthesis and characterization of atomically dispersed Pt on MgO supports, which we have identified as a promising and interesting OCM catalyst system. Figure 3 provides several essential aspects of catalyst characterization required for a complete description of atomically-dispersed Pt/MgO catalysts. This work was conducted in collaboration with Bruce Gates (UC Davis), Simon Bare (Stanford Synchrotron Radiation Lightsource), and Miaofang Chi (Oakridge National Laboratory).

HAADF-STEM images demonstrate the atomic dispersion of Pt (Figure 3a,b) on the MgO support. This is confirmed by EXAFS spectra (not shown), which indicate no evidence of Pt–Pt contributions. Typical catalytic performance data – in this case associated with CO oxidation as a probe reaction – are shown in

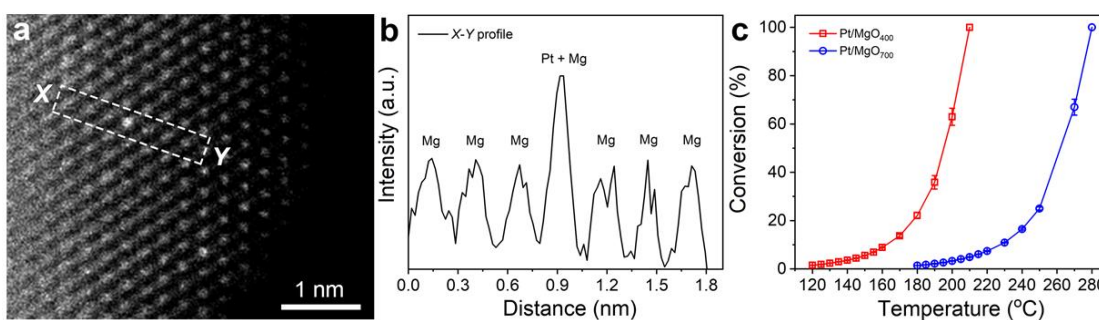


Figure 3. (a) HAADF-STEM image of Pt/MgO700. (b) Intensity profile along the line X-Y in (a). (c) Light-off curves characterizing CO oxidation catalysis on Pt/MgO₄₀₀ and Pt/MgO₇₀₀ (subscripts indicate calcination temperatures). Error bars represent standard deviations determined with data from three independent measurements. Manuscript in preparation (manuscript 2 at end). Work performed in collaboration with Y. Chen (UC Davis), B. Gates (UC Davis), S. Bare (SSRL), and M. Chi (ONL).

Figure 1c. The data collected on this system thus far indicate that low-coordinated isolated Pt on MgO is markedly more active than high-coordinated isolated Pt on MgO. This property can be controlled with synthesis and treatment methodologies that we have developed in this course of this study.

PROPOSED WORK

Given the progress above in studying oxidation reactions and synthesizing site-isolated catalysts, the next steps of this project involve the direct interrogation of OCM and its reaction mechanisms. This will involve using combinations of optical (PLIF and Raman) and mass spectrometry probes, conventional catalytic reactor studies, synchrotron-based X-ray spectroscopies, and a multi-faceted computational approach. We have proven our ability to perform each aspect of this plan, and efforts are underway to extend the work to the high temperature conditions required of OCM. New reactor configurations are under construction. In addition to experiments with the atomically-dispersed catalysts discussed above, we will study OCM using traditional catalysts, such as Li/MgO, which has already been synthesized and characterized in our lab. This will provide a valuable benchmark for literature comparison.

In addition to these experimental efforts, we will perform exhaustive periodic density functional theory (DFT) calculations to evaluate the thermodynamic stability and activity of site-isolated catalysts. We have begun these calculations for the Pt/MgO system studied above. As an illustrative example, Figure 4 shows four possible locations for the Pt atom on the MgO 310 facet. While the structures in (a), (b) and (c) consisting of an exposed Pt atom are predicted to be active for CO oxidation (the probe reaction examined thus far for this catalyst), only the Pt structure in (d) is consistent with EXAFS measurements.

Over the coming months, we plan to simulate the kinetics and selectivity of methane activation using microkinetic modeling through the RMG-Cat software. Preliminary studies will focus on surface reactions, but will be subsequently extended to include the near-surface gas-phase. We highlight that Prof. Richard West (Northeastern University) and Prof. C. Franklin Goldsmith (Brown University) are developers of RMG-Cat and are also collaborators on the Sandia-led project discussed previously. For both methanol oxidation and OCM, we will explicitly calculate the rates of formation of relevant reactive intermediates using DFT-based microkinetic models.

BES-sponsored publications, 2019 – present

The project was funded in September 2019. No peer-reviewed articles have yet been published.

1. A manuscript on partial oxidation of methanol is in preparation. Authors include J. Frank, N. Hansen, E. Huang, A. Kulkarni, C.X. Kronawitter, D. Osborn.
2. A manuscript on supported atomically-dispersed Pt catalysts is in preparation. Authors include Y. Chen, S. Cao, C.-Y. Fang, M. Chi, C.X. Kronawitter, A. Kulkarni, B.C. Gates

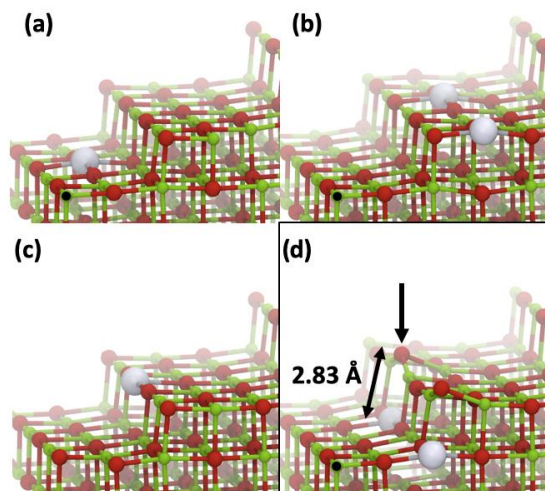


Figure 4. Large-scale DFT calculations are used to examine the stability and activity of various possible isolated Pt-sites on MgO. Diagrams show a subset of possible Pt locations for the MgO 310 step.

A Coupled Theoretical and Experimental Approach to Elucidating the Mechanisms of Methyl Esters

Nicole J. Labbe,¹ G. Barney Ellison,² John W. Daily¹

¹Department of Mechanical Engineering

²Department of Chemistry

University of Colorado Boulder

UCB 427, 1111 Engineering Drive, Boulder, CO 80309

Nicole.Labbe@colorado.edu John.Daily@colorado.edu Barney@jila.colorado.edu

Program Scope

The goal of our program is to probe fundamental kinetics questions regarding the gas phase reactive behavior of oxygenates. In order to succeed, our program involves both an experimental component and a theoretical component. In short, the microreactor experiment at CU Boulder combined with advanced diagnostics allows for resolution of the very short-time thermal decomposition and abstraction chemistry of molecules of interest. The reactors feature a small (1mm ID x ~3cm long) SiC tube that can be heated to 1700 K. The residence time in the reactor is short, 50-200 μ sec, allowing study of the earliest reaction processes. A powerful advantage of our microreactor is the use of two complimentary diagnostic tools to detect products: time-of-flight photoionization mass spectrometry (PIMS) and matrix-isolated infrared spectroscopy (IR). PIMS and IR are universal, multiplexed, and sensitive; all atoms or molecules can be ionized and all polyatomic molecules are IR active, and therefore detectable. The results of our experimental work are compared directly to our theoretical thrust of our program. Electronic structure theory, including QM/DFT, is a powerful tool for calculating energetics of molecules and transition structures at high accuracies. These techniques allow for reliable rate constants and thermochemistry to be calculated, helping to further clarify the mechanistic insights from the experimental work.

In this program, we specifically aim to understand the fundamental chemistry of esters, which are of particular interest due to their use as biofuels and drop in fuel replacements. In the prior year, our work has focused on three primary thrusts, improving our experimental capabilities with the addition of a partially tunable VUV light source for our PIMS experiments, understand the role of acids for the pyrolysis of an ethyl propanoate (an ethyl ester), and to create and test new kinetic models that accurately reflect the chemistry of two model methyl esters, methyl hexanoate ($\text{CH}_3\text{CH}_2\text{CH}_2\text{CH}_2\text{COOCH}_3$), and methyl 5-hexenoate ($\text{CH}_2=\text{CHCH}_2\text{CH}_2\text{COOCH}_3$) to address uncertainties regarding unsaturation in methyl esters.

Recent Progress

Experimental Advances that Probe Fundamental Gas-phase Kinetics: In collaboration with the Kapteyn-Murnane group in JILA at the University of Colorado Boulder, and KM Labs, we have acquired and began testing a new tunable, tabletop, VUV light source for combustion research, specifically for PIMS. An ultrafast fiber laser source in conjunction with highly cascaded four-wave-mixing harmonic generation in a xenon-filled hollow negative-curvature fiber produces a set of spectral lines spaced by 1.2 eV intervals in a laboratory setting. With this new light source, we now have the ability to separate select isomers. As a proof of concept, we used this new VUV source to detect the keto-enol isomerization in four oxygenate combustion intermediates.¹ Specifically, we were able to detect the previously observed tautomerization of acetaldehyde to vinyl alcohol, cyclohexanone to 1-cyclohexenol, and methyl vinyl ketone to 2-

¹ D. E. Couch, Q. L. Nguyen, D. D. Hickstein, H. C. Kapteyn, M. M. Murnane, and N. J. Labbe, Detection of the Keto-Enol Tautomerization in Acetaldehyde, Acetone, Cyclohexanone, and Methyl Vinyl Ketone with a Novel VUV Light Source. Proc. Combust. Inst. 38 (2021), *Under Review*

hydroxybutadiene. In addition to these three tautomerizations, we also were able to experimentally observe the thermal tautomerization of acetone to propen-2-ol for the first time to our knowledge.

The Importance of the Diol in Propionic Acid Pyrolysis: Ethyl propanoate, like other ethyl esters, often decompose to form acids as a major pyrolysis product, though the chemistry of these acids is often unclear. To understand some of the questions regarding these acids, we have studied the pyrolysis of propionic acid,ⁱⁱ the primary decomposition product of ethyl propanoate. Previous published works^{iii,iv} suggested that dehydrogenation of propionic acid to form methylketene is the primary pyrolysis route for propionic acid. And our initial experimental study suggested this was indeed accurate; our PIMS spectra showed methyl ketene as the first visible product in propionic acid pyrolysis using the microreactor. However, our calculated potential energy surface for propionic acid decomposition, in direct contradiction to the experimental observations and prior works, showed that the direct molecular pathway to methyl ketene was not energetically favored. Through our combined theoretical and experimental approach, we determined that the source of methyl ketene observed was actually a well-skipping reaction through a diol intermediate, propene-1,1-diol.

Even with the tunable VUV light source, we have been unable to experimentally determine the presence of propene-1,1-diol. The ionization energy of propionic acid (10.44 eV^v) is such that it can be ionized by the 10.781 eV line of this new VUV source but not the diol. The diol ionization energy was unknown, so we calculated it to be

7.93 eV using the PSI4 computational package with a Dunning's correlation consistent basis set, aug-cc-pVDZ. The equilibrium ground state geometries of the neutral and the corresponding cation species are optimized with the CCSD(T) level of theory. Given the low ionization energy of the diol, we expect the lack of direct observation of the diol is due to the likelihood of the diol to photodissociate to H₂O and the [CH₂CH=C=OH]⁺ ion, m/z 54. Thus, the ion's possible signal would be masked by the methyl ketene signal at m/z 54. Another scan is required using the 8.4 eV spectral line to clarify.

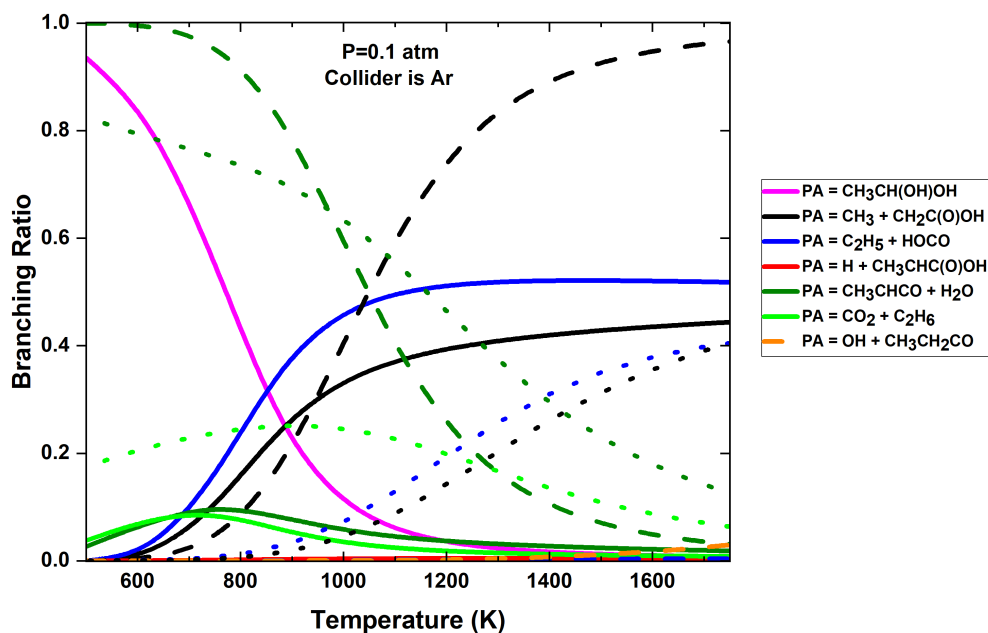


Figure 1: Theoretically calculated branching ratios for propionic acid pyrolysis. Solid lines are branching ratios calculated in this work. The dashed lines are calculated from Metcalfe et al.^{vi} and the dotted lines are from Doolan et al.^{vii}.

ⁱⁱ C. Rogers, K. Lockwood, Q. Nguyen, and N. Labbe, Diol Isomer Revealed as the Source of Methyl Ketene from Propionic Acid *Int. J. Chem. Kin.* (2020), Under Review

ⁱⁱⁱ Metcalfe WK, Dooley S, Curran HJ, Simmie JM, El-Nahas AM, Navarro MV *J Phys Chem A.* 2007;111(19):4001-4014.

^{iv} Doolan KR, Mackie JC, Reid CR. *Int J Chem Kinet.* 1986;18(5):575–596.

^v Thomas RK. *Proc R Soc Lond.* 1972;331(1585):249-261

We also took the energies from the potential energy surface we previously calculated at the CCSD(T)/cc-pV ∞ Z//M062x/cc-pVTZ level of theory and ran the master equation theory code MESS^{vi} to calculate temperature and pressure dependent rate constants for the thermal decomposition of propionic acid. Figure 1ⁱⁱ shows the branching ratios of propionic acid from our submitted work compared to rates from the literature. The route to the diol, in pink, was not contained in either literature mechanism and is in fact the dominant low temperature pathway. Our work showed that $\text{CH}_3\text{CH}_2\text{COOH} = \text{C}_2\text{H}_5 + \text{HOCO}$ is the dominant high temperature decomposition pathway with $\text{CH}_3\text{CH}_2\text{COOH} = \text{CH}_3 + \text{CH}_3\text{COOH}$ also being significant.

First Atmospheric Pressure combustion data of Methyl Hexanoate: We recently collaborated with Prof. Tina Kasper at the University of Duisburg-Essen, Germany, to produce the first quantitative atmospheric pressure combustion data of methyl hexanoate.^{vii} We performed plug flow reactor experiments combined with GC-MS detection for methyl hexanoate in O_2 for varying equivalence ratios. Figure 2^{vii} shows the species profiles for intermediate esters formed during combustion compared to a literature mechanism.^{viii} Notably, methyl acetate is a prominent oxygenate intermediate that was not contained in the mechanism used. Discrepancies between other intermediate ester species profiles and the mechanism show areas of improvement for a future mechanistic study of methyl hexanoate.

The first step of this mechanistic study is to calculate a PES of the thermal decomposition of methyl hexanoate at the level of theory, M062x/cc-pVTZ//CCSD(T)/cc-pV ∞ Z, shown in Figure 3.

The lowest energy transition states are to butene and the enol of methyl acetate at 65.72 kcal/mol, to the enol of methyl hexanoate at 70.14 kcal/mol, and to methanol and butyl ketene at 71.9 kcal/mol. These are also consistent with the PIMS data as peaks at m/z 74 (methyl acetate enol), m/z 56 (butene), and m/z 98 (butyl ketene) are the first to appear at 1200 K. This is likely one missing route to methyl acetate missing in the mechanism used in Figure 2 as the enol of methyl acetate would easily isomerize to methyl acetate. Our previous PIMS spectra were taken at a fixed photon energy (10.487 eV) so we lacked isomer resolution to detect the formation of the enol of methyl hexanoate. A future work is to use the 1.2 eV spaced spectral lines from the new VUV source to look for evidence of the enol of methyl hexanoate in the PIMS experiment. Bond fissions energies were also calculated but are not shown. The lowest energy bond fission reactions are those within the hydrocarbon chain of methyl hexanoate. The C-C bond between second and third carbon is 85.13 kcal/mol and between the third and fourth carbon is 87.28 kcal/mol. These fissions would produce butene, ketene, and formaldehyde and propene, ethylene, CO, and

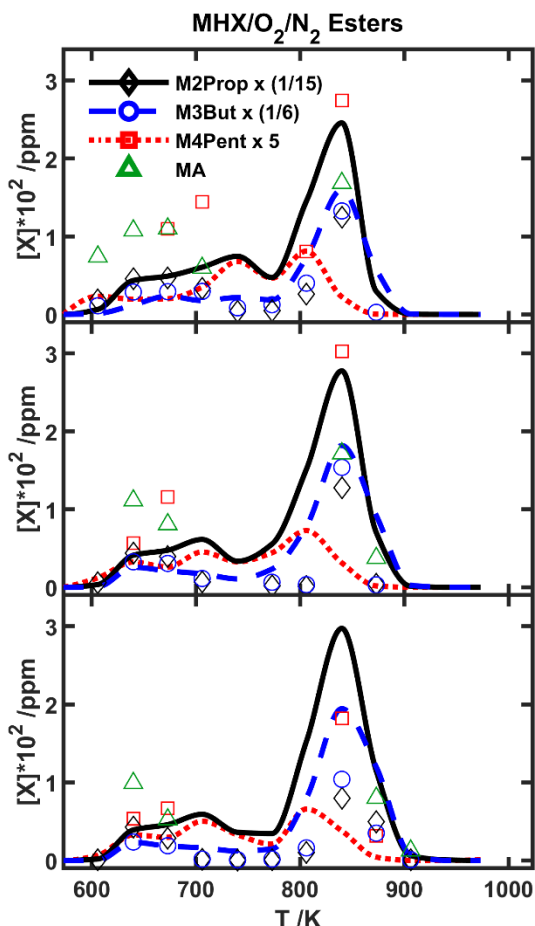


Figure 2: Methyl Hexanoate in O_2 and N_2 in a PFR at 1 atm compared to a literature mechanism by Dayma et al.^{vii} Top $\phi = 1$, Middle $\phi = 1.5$, Bottom $\phi = 2$

^{vi} Georgievskii Y, Miller JA, Burke MP, Klippenstein SJ. *J Phys Chem A*. 2013;117(46):12146-12154..

^{vii} C. O. Rogers, D. Kaczmarek, T. Kasper, and N. J. Labbe, Probing the Low-Temperature Chemistry of Methyl Hexanoate: Insights from Oxygenate Intermediates. *Proc. Combust. Inst.* 38 (2021), *Under Review*

^{viii} G. Dayma, S. Gail, and P. Dagaut, *Energy Fuels* 22 (2008) 1469–1479.

formaldehyde, respectively, from β -scission. This is consistent with PIMS spectra we have taken previously from the pyrolysis of methyl hexanoate in a microreactor. Masses 56 (butene), 42 (ketene or propene), and 28 (ethylene) appear starting at 1200 K and peak around 1400 K. The ionization energies of formaldehyde, CO, and methanol are above the energy of the photons used so their absence is expected. The matching of theory and experiments gives motivation to continue both in tandem to further insights into the kinetics of oxygenate molecules. Further work is needed to calculate rate constants from these theoretical results using MESS to see how updated rates will affect the predictions shown in Figure 2.

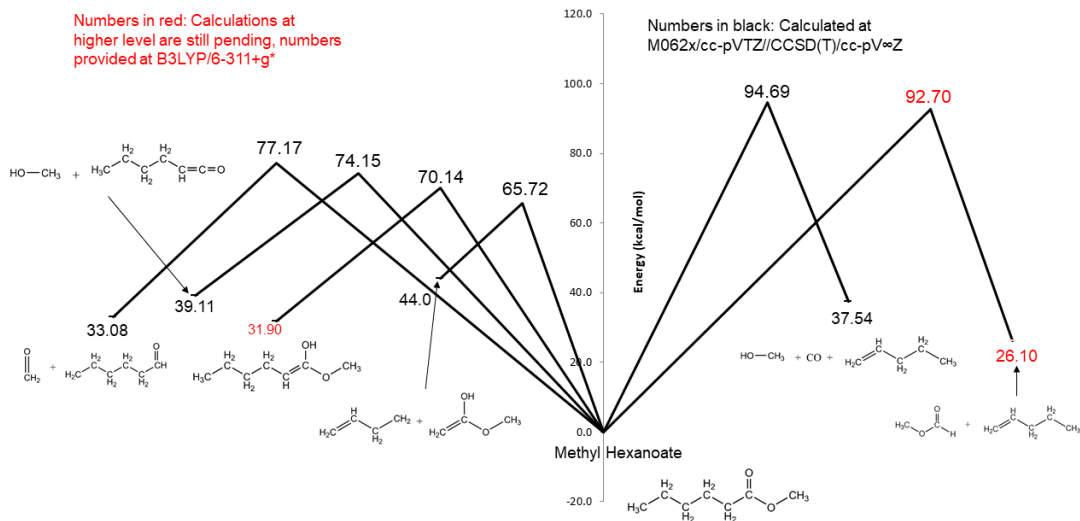


Figure 3: PES of methyl hexanoate thermal decomposition showing transition state reactions

Future Plans

In addition to wrapping up work on propionic acid/ethyl propanoate, the next year our goal is to focus primarily on the two methyl esters, methyl hexanoate and methyl hexenoate, as well as the two propanol isomers. For the methyl esters, our goal by next year is to complete experimental studies for both molecules in the microreactor as well as the JSR at Duisburg-Essen, and complete corresponding theoretical calculations to determine the fundamental reactions of both molecules. A similar study microreactor and theoretical will be completed for the two propanol isomers.

BES Sponsored Products (March 2018-present)

1. D. E. Couch, Q. L. Nguyen, D. D. Hickstein, H. C. Kapteyn, M. M. Murnane, and N. J. Labbe, "Detection of the Keto-Enol Tautomerization in Acetaldehyde, Acetone, Cyclohexanone, and Methyl Vinyl Ketone with a Novel VUV Light Source". *Proc. Combust. Inst.* (2020), *Under Review*
2. C. O. Rogers, K. S. Lockwood, Q. L. Nguyen, and N. J. Labbe, "Diol Isomer Revealed as the Source of Methyl Ketene from Propionic Acid". *Int. J. Chem. Kinetics* (2020), *Under Review*
3. C. O. Rogers, D. Kaczmarek, T. Kasper, and N. J. Labbe, "Probing the Low-Temperature Chemistry of Methyl Hexanoate: Insights from Oxygenate Intermediates". *Proc. Combust. Inst.* 38 (2020), *Under Review*
4. K. Lockwood, N. J. Labbe, "Insights on Keto-Hydroperoxide Formation from O₂ Addition to the Beta-Tetrahydrofuran Radical" *Proc. Combust. Inst.* 38 (2020), *Under Review*
5. C. Rogers, K. Cummins, J. Porterfield, J. W. Daily, G. B. Ellison, N. J. Labbe, "The Pyrolysis Chemistry of Propionic Acid and Ethyl Propionate in a Microreactor" Oral Presentation at the US National Combustion Meeting, Pasadena, CA, March 2019
6. C. Rogers, K. Cummins, J. Porterfield, J.W. Daily, G.B. Ellison, N.J. Labbe "The Pyrolysis Chemistry of Propionic Acid and Ethyl Propionate Revealed," International Conference on Chemical Kinetics, Orleans, France, June 2019. **[Invited Talk]**
7. C. Rogers, J.P. Porterfield, J.W. Daily, G.B. Ellison, N.J. Labbe. "Pyrolysis of Ethyl Esters in a Micro-Reactor," International Symposium on Molecular Spectroscopy, Champaign-Urbana, Illinois, June 2019.

SPECTROSCOPY AND DYNAMICS OF REACTION INTERMEDIATES IN COMBUSTION CHEMISTRY

Marsha I. Lester
Department of Chemistry
University of Pennsylvania
Philadelphia, PA 19104-6323
milester@sas.upenn.edu

I. Program Scope

Carbonyl oxides (Criegee intermediates, $R_1R_2C=O^+O^-$) with novel zwitterionic character are important intermediates in tropospheric hydrocarbon oxidation and some combustion reactions. The UV-vis spectroscopy, photoionization efficiency, unimolecular decay pathways, and bimolecular reactions of Criegee intermediates and related isomeric species are being examined.

II. Recent Progress

A. Electronic spectroscopy and photoinitiated dynamics

Recently, the Lester group generated and characterized two distinct four-carbon unsaturated Criegee intermediates for the first time.¹⁻³ The laboratory production involves photolysis of suitable precursors, synthesized by our organic colleagues, to generate resonance-stabilized monoiodoalkene radicals that react with O_2 . This approach has enabled production and characterization of methyl vinyl ketone oxide ($(CH_2=CH(CH_3)COO$, MVK-oxide) and methacrolein oxide ($(CH_2=C(CH_3))CHO$, MACR-oxide).¹⁻³ These four-carbon unsaturated Criegee intermediates are different than systems studied previously because the zwitterionic carbonyl oxide functional group ($C=O^+O^-$) is resonance stabilized with the vinyl side chain, influencing their UV-vis spectra, unimolecular decay dynamics, and bimolecular chemistry. They are also of particular significance because they are formed in the ozonolysis of isoprene, which is the most abundant non-methane hydrocarbon in the atmosphere. At Penn, we have examined the UV-vis spectra of MVK-oxide and MACR-oxide under jet-cooled conditions, along with their photochemical decay pathways.^{2,3} In collaboration with colleagues at Sandia, JPL, IAMS, Argonne, and Bristol (see below), we have probed the unimolecular decay dynamics and bimolecular reactions of MVK-oxide under thermal conditions⁴ with similar studies ongoing for MACR-oxide.

MVK-oxide and MACR-oxide are isomers, each composed of four conformers with similar ground state energies (within $3.3 \text{ kcal mol}^{-1}$). Under jet-cooled conditions, we expect that all four conformers are formed and stabilized. Under thermal conditions (298 K), we anticipate distinct *syn* and *anti* conformers (see Fig. 1), referring to the orientation of the methyl group with respect to the terminal O atom for MVK-oxide, while the orientation of the vinyl group, *cis* and *trans*, can rapidly interconvert about the C-C bond.

The UV-vis spectrum of MVK-oxide was initially recorded on its first $\pi^* \leftarrow \pi$ electronic transition under isolated conditions following supersonic jet cooling.² Resonant UV-vis laser excitation induces a ground state depletion and an associated reduction of the VUV (10.5 eV) photoionization signal on the m/z 86 parent mass. The strong depletion (up to 25%) of one or more of the four MVK-oxide conformers peaks at 388 nm in a one-photon absorption process. The experimental spectrum is broad and unstructured, spanning from 300 to 430 nm, with an asymmetric profile that falls off sharply on the long wavelength side as shown in Fig. 1 (upper panel). Additional velocity map imaging (VMI) experiments revealed prompt dissociation, assuring that the UV-vis spectrum obtained by the depletion method is equivalent to direct absorption. The vertical excitation energies (VEE) and oscillator strengths for *syn* and *anti* conformers of MVK-oxide (colored bars in Fig. 1; solid and dashed bars refer to *trans* and *cis*) were computed for the first $\pi^* \leftarrow \pi$ transition at 350-400 nm, in good accord with experiment.

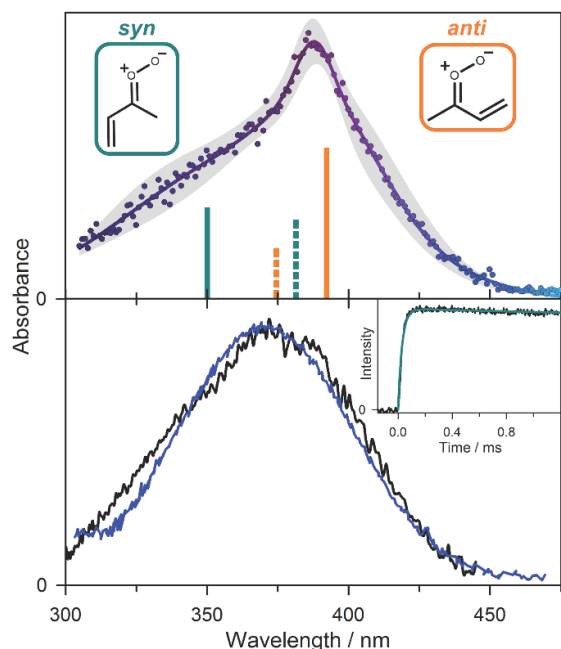


Fig. 1 (Upper) Electronic spectrum of MVK-oxide under jet-cooled conditions using depletion method with computed VEE and oscillator strengths (bars). (Lower) Transient absorption spectra of MVK-oxide at 298 K using Sandia (black) and IAMS (blue) instruments. (Inset) Kinetic time trace and simulated thermal decay (33 s^{-1}) is indicative of *syn*-conformers.

In collaboration with colleagues at Sandia, JPL, IAMS, Argonne, and Bristol, we have carried out experiments on MVK-oxide under thermal (298 K) conditions using the multiplexed photoionization mass spectrometer (MPIMS) at the Chemical Dynamics Beamline with tunable VUV radiation from the Advanced Light Source (ALS). We have also collaborated on transient absorption measurements at Sandia and with a group at IAMS in Taiwan, who performed similar transient absorption measurements. Together, these experiments have yielded important new results on the unimolecular decay and bimolecular reactions of MVK-oxide.⁴

The direct UV-vis absorption spectrum of the four-carbon, resonance-stabilized Criegee intermediate, MVK-oxide, has also been recorded under thermal conditions in two independent experiments (Fig. 1, lower panel). We observe broad absorption centered around 370 nm, in good agreement with our prior work,² with differences attributed to the different conformer distribution in the thermal (298 K) and jet-cooled experiments. The experimentally observed decay of MVK-oxide in the thermal experiments is consistent with *syn*-conformers (Fig. 1 inset), and substantiates very rapid removal decay of *anti*-conformers as predicted by our earlier calculations.¹

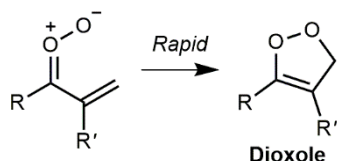
Computation and direct experimental kinetic measurements of bimolecular reactions of *syn*-MVK-oxide demonstrate slow *syn*-MVK-oxide removal in the presence of water, confirming recent theoretical predictions.^{9, 10} This means that MVK-oxide will survive in high-humidity environments and other bimolecular reactions may be important. Rapid reactivity with SO_2 and formic acid was observed and predicted theoretically, similar to previously studied C1 to C3 alkyl-substituted Criegee intermediates. Complementary MPIMS measurements of the products from SO_2 and formic acid reactions with MVK-oxide indicate the potential role of these reactions in particulate formation. SO_3 is observed from the reaction of *syn*-MVK-oxide with SO_2 , which plays a role in the formation of sulfuric acid. In addition,

The UV-vis spectrum of MACR-oxide on its first $\pi^* \leftarrow \pi$ electronic transition was similarly obtained under isolated conditions following jet cooling.³ Again, we utilized a depletion method, in which UV-vis excitation induces depletion of the ground state population of one or more of its four conformers and results in an associated decrease in the VUV (10.5 eV) photoionization signal on the $m/z=86$ parent mass channel. The resultant UV-vis spectrum peaks at 380 nm, spans across the 315-500 nm region, and exhibits weak oscillatory structure in the long wavelength region. Additional VMI experiments reveal anisotropic images of $\text{O } ^1\text{D}$ products, indicative of rapid dissociation and assuring that the electronic spectrum obtained by the depletion method is equivalent to a direct absorption method. The weak oscillatory structure of the MACR-oxide spectrum, which is analogous to an extended progression observed previously for CH_2OO ,^{5, 6} is likely due to short lived vibrational resonances in the excited $1^1\pi\pi^*$ state.^{7, 8} Finally, our complementary theoretical calculations predict strong vertical transitions for the four conformers in the 340-380 nm region.

B. Photoionization mass spectrometry and transient absorption studies of unimolecular and bimolecular chemistry

the net insertion of MVK-oxide into formic acid leads to formation of a highly oxygenated organic hydroperoxide.

In other experiments performed at the ALS in collaboration with Sandia, JPL, Argonne, and Bristol, we have obtained experimental evidence of a novel unimolecular decay pathway for specific conformational forms of MVK-oxide (*anti*) and MACR-oxide (*syn*) with the vinyl substituent adjacent to the terminal O atom.¹¹ These conformers can rapidly isomerize via an exothermic electrocyclic ring closure mechanism to form a five-membered cyclic peroxide, known as dioxole (Scheme 1; R and R' indicate the positions of the methyl group in MVK-oxide and MACR-oxide).^{1, 10, 12, 13}



Scheme 1. Electrocyclic ring closure mechanism for four-carbon unsaturated Criegee intermediates to form dioxole.

Dioxole is formed with sufficient internal excitation to undergo rapid unimolecular decay to oxygenated hydrocarbon radicals, producing acetyl and vinoxy radicals from MVK-oxide and formal and 2-methylvinoxy radicals from MACR-oxide.¹ In the presence of O₂ under our laboratory conditions, the newly formed radicals quickly react with O₂ in a barrierless exothermic reaction that yields peroxy radicals.¹⁴⁻¹⁶ The peroxy radicals undergo H-atom transfer to form QOOH intermediates that decay via submerged barriers to form carbonyl and HO_x products.¹⁴⁻¹⁶

The resultant stable carbonyl products were detected by MPIMS, providing the first experimental evidence of the dioxole unimolecular decay pathway for the four-carbon unsaturated Criegee intermediates. The main products (and associated relative abundances) originating from unimolecular decay of *anti*-MVK-oxide and subsequent reaction with O₂ are formaldehyde (88 ± 5%), ketene (9 ± 1%) and glyoxal (3 ± 1%). Those identified from the unimolecular decay of *syn*-MACR-oxide and subsequent reaction with O₂ are acetaldehyde (37 ± 7%), vinyl alcohol (9 ± 1%), methylketene (2 ± 1%), and acrolein (52 ± 5%).

III. Ongoing and Future Work

A new line of research is ongoing in our laboratory to generate hydroperoxyalkyl radicals (QOOH) in a pulsed supersonic expansion, and characterize them spectroscopically. In addition, we are continuing research at Penn and collaboratively at the ALS on the highly isomer- and conformer-specific chemistry of the four-carbon unsaturated carbonyl oxide intermediates. At Penn, we are examining the second $\pi^* \leftarrow \pi$ transition of MVK-oxide, which is principally associated with electronic excitation of the vinyl group. Key bimolecular reactions are also being examined at the ALS, including MVK-oxide with deuterated formic acid to reveal an acid-catalyzed pathway that forms a novel vinyl hydroperoxide species (2-hydroperoxybuta-1,3-diene).¹⁷ We are also characterizing the rates of bimolecular reaction and identifying products formed from MACR-oxide with water vapor, formic acid, and SO₂, many of which involve adduct formation.

Our Penn laboratory research was halted in mid-March 2020 due to COVID-19, and our ALS beamtime was lost due to COVID-19 (May 2020) and a power outage from wildfires (October 2019). Nevertheless, our DOE research is continuing with the team fully engaged in writing up papers, carrying out theoretical calculations, and planning future research. We are optimistic that a partial resumption of laboratory research at Penn will be possible this summer.

IV. References

1. V. P. Barber, S. Pandit, A. M. Green, N. Trongsrirawat, P. J. Walsh, S. J. Klippenstein and M. I. Lester, *J. Am. Chem. Soc.* **140**, 10866-80 (2018).
2. M. F. Vansco, B. Marchetti and M. I. Lester, *J. Chem. Phys.* **149**, 244309 (2018).
3. M. F. Vansco, B. Marchetti, N. Trongsrirawat, T. Bhagde, G. Wang, P. J. Walsh, S. J. Klippenstein and M. I. Lester, *J. Am. Chem. Soc.* **141**, 15058-69 (2019).
4. R. L. Caravan, M. F. Vansco, K. Au, M. A. H. Khan, Y.-L. Li, F. A. F. Winiberg, K. Zuraski, Y.-H. Lin, W. Chao, N. Trongsrirawat, P. J. Walsh, D. L. Osborn, C. J. Percival, J. J.-M. Lin, D. E.

- Shallcross, L. Sheps, S. J. Klippenstein, C. A. Taatjes and M. I. Lester, *Proc. Natl. Acad. Sci.*, Latest Articles (2020).
5. L. Sheps, *J. Phys. Chem. Lett.* **4**, 4201-5 (2013).
 6. W.-L. Ting, Y.-H. Chen, W. Chao, M. C. Smith and J. J.-M. Lin, *Phys. Chem. Chem. Phys.* **16**, 10438-43 (2014).
 7. R. Dawes, B. Jiang and H. Guo, *J. Am. Chem. Soc.* **137**, 50-3 (2015).
 8. M. F. Vansco, H. Li and M. I. Lester, *J. Chem. Phys.* **147**, 013907 (2017).
 9. J. M. Anglada and A. Solé, *Phys. Chem. Chem. Phys.* **18**, 17698-712 (2016).
 10. L. Vereecken, A. Novelli and D. Taraborrelli, *Phys. Chem. Chem. Phys.* **19**, 31599-612 (2017).
 11. M. F. Vansco, R. L. Caravan, K. Zuraski, F. A. F. Winiberg, K. Au, N. Trongsirawat, P. J. Walsh, D. L. Osborn, C. J. Percival, M. A. H. Khan, D. E. Shallcross, C. A. Taatjes and M. I. Lester, *J. Phys. Chem. A*, ASAP (2020).
 12. K. T. Kuwata, A. S. Hasson, R. V. Dickinson, E. B. Peterson and L. C. Valin, *J. Phys. Chem. A* **109**, 2514-24 (2005).
 13. K. T. Kuwata and L. C. Valin, *Chem. Phys. Lett.* **451**, 186-91 (2008).
 14. S. A. Carr, D. R. Glowacki, C.-H. Liang, M. T. Baeza-Romero, M. A. Blitz, M. J. Pilling and P. W. Seakins, *J. Phys. Chem. A* **115**, 1069-85 (2011).
 15. J. D. Weidman, R. T. Allen, K. B. Moore III and H. F. Schaefer III, *J. Chem. Phys.* **148**, 184308 (2018).
 16. M. M. Davis, J. D. Weidman, A. S. Abbott, G. E. Douberly, J. M. Turney and H. F. Schaefer III, *J. Chem. Phys.* **151**, 124302 (2019).
 17. M. Kumar, D. H. Busch, B. Subramaniam and W. H. Thompson, *Phys. Chem. Chem. Phys.* **16**, 22968-73 (2014).

V. Publications supported by this DOE project (2017-present)

1. R. L. Caravan, M. F. Vansco, K. Au, M. A. H. Khan, Y.-L. Li, F. A. F. Winiberg, K. Zuraski, Y.-H. Lin, W. Chao, N. Trongsirawat, P. J. Walsh, D. L. Osborn, C. J. Percival, J. Jr-M. Lin, D. E. Shallcross, L. Sheps, S. J. Klippenstein, C. A. Taatjes, and M. I. Lester, "Direct kinetic measurements and theoretical predictions of an isoprene-derived Criegee intermediate", *Proc. Natl. Acad. Sci.*, Latest Articles (2020). <https://doi.org/10.1073/pnas.1916711117>
2. M. F. Vansco, R. L. Caravan, K. Zuraski, F. A. F. Winiberg, K. Au, N. Trongsirawat, P. J. Walsh, D. L. Osborn, C. J. Percival, M. A. H. Khan, D. E. Shallcross, C. A. Taatjes, and M. I. Lester, "Experimental evidence of dioxole unimolecular decay pathway for isoprene-derived Criegee intermediates", *J. Phys. Chem. A*, ASAP (2020). <https://doi.org/10.1021/acs.jpca.0c02138>
3. M. F. Vansco, B. Marchetti, N. Trongsirawat, G. Wang, T. Bhagde, P. J. Walsh, S. J. Klippenstein, and M. I. Lester, "Synthesis, electronic spectroscopy and photochemistry of methacrolein oxide: A four carbon unsaturated Criegee intermediate from isoprene ozonolysis", *J. Am. Chem. Soc.* **141**, 15058–15069 (2019). <http://dx.doi.org/10.1021/jacs.9b05193>
4. M. F. Vansco, B. Marchetti, and M. I. Lester, "Electronic spectroscopy of methyl vinyl ketone oxide: A four-carbon unsaturated Criegee intermediate from isoprene ozonolysis", *J. Chem. Phys.* **149**, 244309 (2018). <https://doi.org/10.1063/1.5064716>
5. V. P. Barber, S. Pandit, A. M. Green, N. Trongsirawat, P. J. Walsh, S. R. Klippenstein, and M. I. Lester, "Four carbon Criegee intermediate from isoprene ozonolysis: Methyl vinyl ketone oxide synthesis, infrared spectrum, and OH production", *J. Am. Chem. Soc.* **140**, 10866–80 (2018). <https://pubs.acs.org/doi/abs/10.1021/jacs.8b06010>
6. M. F. Vansco, H. Li, and M. I. Lester, "Prompt release of O ¹D products upon UV excitation of CH₂OO Criegee intermediates", *J. Chem. Phys.* **147**, 013907 (2017). <http://aip.scitation.org/doi/full/10.1063/1.4977987>
7. C. A. Taatjes, F. Liu, B. Rotavera, M. Kumar, R. Caravan, D. L. Osborn, W. H. Thompson, and M. I. Lester, "Hydroxyacetone production from C₃ Criegee intermediates", *J. Phys. Chem. A* **121**, 16-23 (2017). <http://dx.doi.org/10.1021/acs.jpca.6b07712>

Advanced Nonlinear Optical Methods for Quantitative Measurements in Flames

Robert P. Lucht

School of Mechanical Engineering, Purdue University

West Lafayette, IN 47907-2088

Lucht@purdue.edu

I. Program Scope

Nonlinear optical techniques such as laser-induced polarization spectroscopy (PS), resonant wave mixing (RWM), and ultrafast coherent anti-Stokes Raman scattering (CARS) are techniques that show great promise for high-repetition-rate temperature measurements and sensitive measurements of transient gas-phase species, and diagnostic applications of these techniques are being pursued actively at laboratories throughout the world. The objective of this research program is to develop and test strategies for quantitative concentration and temperature measurements using nonlinear optical techniques in flames and plasmas. We have continued our fundamental theoretical and experimental investigations of these techniques. In recent years our theoretical and experimental efforts have been focused on investigating the potential of femtosecond (fs) laser systems for sensitive and accurate CARS measurements in gas-phase media. In the last few years we have demonstrated the acquisition of single-shot temperature measurements at data rates of 5 kHz in highly turbulent, swirl-stabilized methane-air flames and then in pilot-stabilized jet flames with both gaseous and liquid fuels (these measurements are described in Papers P2-P4) using N₂ chirped-probe-pulse (CPP) fs CARS. Our recent efforts have focused on the CPP fs CARS spectroscopy of other species such as CO₂ and O₂. We have also performed measurements on these species in a high-pressure, high-temperature gas cell and have observed very significant self-phase modulation of the pump and Stokes beams, with consequent significant impact on the CPP fs CARS spectra.

We are investigating the physics of both fs CARS and two-color PS by direct numerical integration (DNI) of the time-dependent density matrix equations for the resonant interaction. Significantly fewer restrictive assumptions are required using this DNI approach compared with the assumptions required to obtain analytical solutions. We are concentrating on the accurate simulation of two-photon processes, including Raman transitions, where numerous intermediate electronic levels contribute to the two-photon transition strength. Recent progress has been much more rapid in our modeling efforts after my PhD student Mingming Gu parallelized the time-dependent density matrix code with the assistance of my faculty colleague Prof. Carlo Scalo. Using this parallelized computer code, we have investigated in detail the effects of chirp in the pump and Stokes beams on the Raman excitation efficiency and on signal generation for chirped-probe-pulse (CPP) fs CARS.

We also have performed theoretical analysis of Raman transitions for molecules with non-¹Σ ground electronic levels, in particular pure rotational Raman transitions for NO and O₂. The theoretical analysis is based on the use of irreducible spherical tensors and Hund's case (a) basis states. The theoretical results for NO were compared with pure rotational CARS measurements performed several years ago on this project, and we have determined a new value for the anisotropic molecule-fixed tensor invariant that gives rise to the electronic Raman transition at 121 cm⁻¹ between the spin split ²Π_{1/2} and ²Π_{3/2} ground electronic levels. We are also starting to perform pure rotation O₂ CPP fs CARS spectroscopy, and the modeling of the ³Σ ground electronic level is necessary to model the spectra that we obtain.

We are continuing our investigation of two-color polarization spectroscopy. In particular, we are investigating collision-induced resonances in NO using this technique.

II. Recent Progress

A. Advances in CPP Fs CARS

Fs CARS offers several major potential advantages compared with nanosecond (ns) CARS; i.e., CARS as usually performed with nanosecond pump and Stokes lasers. These potential advantages include an elimination of collisional effects in the signal generation and the capability of performing real-time temperature and species measurements at data rates of 1 kHz or greater as compared to 10-50 Hz for ns CARS. Our Coherent ultrafast laser system operates at 5 kHz with a fundamental pulse width of 55-60 fs and pulse energy of over 2 mJ.

We have completed an investigation of the effects of moderate chirp in the pump and Stokes beams on the Raman excitation efficiency and signal generation for CPP fs CARS. The results are discussed in detail in Paper P7. The key result of our study of pump and Stokes chirp effects is that as long as the sign and magnitudes of the chirp are nearly equal for the pump and Stokes beams, the bandwidth of Raman excitation efficiency envelope decreases only slightly. We were able to model the decrease in the bandwidth of the Raman excitation efficiency using our parallelized time-dependent density matrix code. Our results indicate that inducing moderate levels of chirp appears to actually enhance slightly the temperature accuracy and precision of the CPP fs CARS technique.

In our most recent work we are exploring the potential for measuring temperature and concentrations from CPP fs CARS for species such as CO₂ and O₂. These studies are significant for future measurements in oxy-fuel flames or in pressure gain combustion devices where N₂ may not be present in high concentrations for CARS temperature measurements. The spectral models for both O₂ and CO₂ are much more complicated than for N₂, although the O₂ model is much more tractable than for CO₂. Some results of our initial experimental and theoretical results for combined O₂/CO₂ CPP fs CARS are shown in Fig. 1 from Paper P9. The CO₂ signal remains strong at much longer probe delays compared to O₂, as shown in Fig. 1c, due to the narrow bandwidth of the vibrational modes in the CO₂ Raman spectrum. Consequently CO₂ spectra can be obtained without interference from O₂, even in regions with high O₂ concentrations.

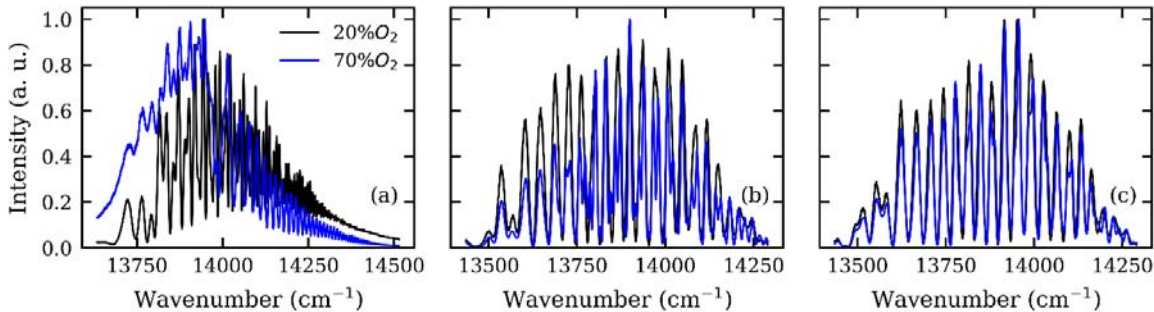


Fig. 1. CPP fs CARS spectra of O₂/CO₂ mixtures at room temperature and pressure at different probe time delays of (a) 0 ps, (b) 2 ps, and (c) 9 ps.

B. Self-Phase Modulation Effects in Femtosecond CARS

Several years ago we measured the CPP fs CARS spectra of methane and ethylene at room temperature and at pressures ranging from 1 to 7 bar. The methane spectrum was essentially unchanged as a function of pressure, but the ethylene spectrum changed drastically as the pressure was increased from 1 to 7 bar. We were not able to explain this effect at that time, but in 2018 we again started to investigate high-pressure effects for N₂, CO₂, O₂, CH₄ and C₂H₄ in a new high-pressure, high-temperature cell at pressures from 1 to 10 bar. We observed that at high pulse energies that the spectra of all of these species were very pressure dependent, even though the characteristic collisional times were much longer than the chirped probe pulse time duration of ~3 ps. We measured the spectra of the pump and Stokes beams before and after the cell and observed a drastic change in the spectrum

for high cell pressures due to self-phase modulation (SPM). We have been able to model these effects and to determine the nonlinear phase induced on the pump and Stokes beam as they traverse the gas cell. Using the nonlinear phase calculated at the probe volume, we are able to obtain good fits even for spectra that are affected significantly by SPM. The results are described in detail in Paper P6.

C. Pure Rotational Raman Spectroscopy of Nitric Oxide and Oxygen

Several years ago, we performed pure rotational CARS measurements mixture of nitric oxide and nitrogen at room temperature. The simultaneous acquisition of pure rotational CARS spectra from known mixtures of these two species will enable us to determine with excellent accuracy the pure rotational Raman cross section for nitric oxide, given that the pure rotational Raman cross section of nitrogen is so well known. The theoretical analysis of the pure rotational Raman process in nitric oxide is complicated because the ground electronic level is a $^2\Pi$ level rather than a $^1\Sigma$ level. This analysis is described in detail in Paper P8. The analysis of the O_2 pure rotational Raman transitions is proceeding in support of our investigation of pure rotational CPP fs CARS spectroscopy of O_2 .

D. Collision-Induced Resonances in Two-Color Polarization Spectroscopy of Nitric Oxide

We have continued our experimental and theoretical investigation of two-color polarization spectroscopy (TCPS) of the NO molecule. An energy level diagram and a comparison of theory and experiment are shown in Fig. 2. The circularly polarized pump beam for the TCPS process is tuned to the $R_{11}(11.5)$ transition. In the absence of transfer of Zeeman state anisotropy during rotational transfer collisions, only the $P_{11}(11.5)$ and $P_{11}(13.5)$ transitions, which share common lower and upper levels with the pump transition would be observed as the linearly polarized probe beam is scanned over the P-branch resonances. However, we observe significant signals from P-branch resonances that do not share the same levels with the pump transition, indicating that the pump-induced anisotropy is preserved to some extent during rotational transfer collisions. We are able to model the result using our time-dependent density matrix equation after incorporation of a detailed model for rotational transfer collisions.

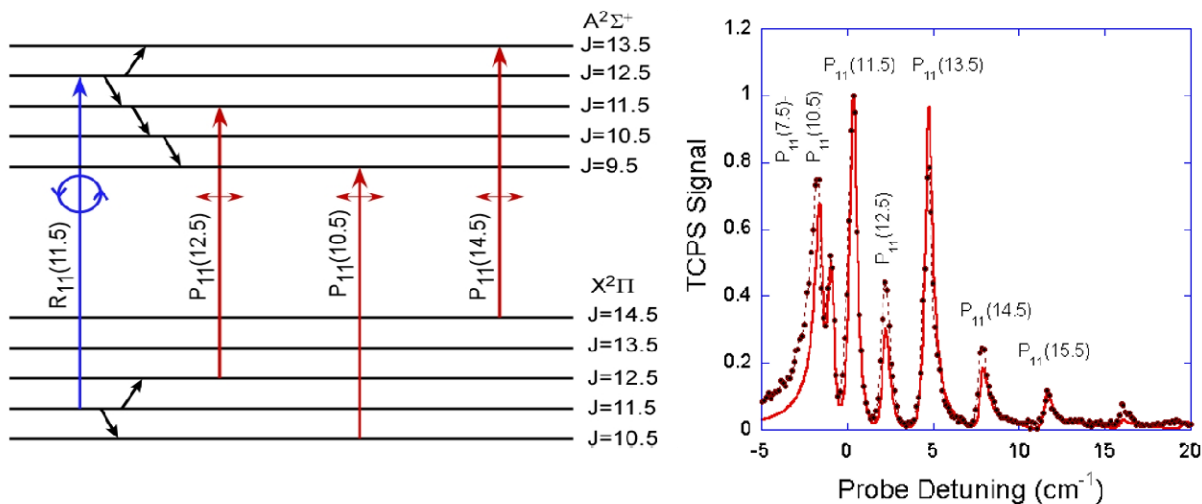


Figure 2. Generation and detection of collision-induced resonances for two-color NO polarization spectroscopy. The mixture was 1% NO in He buffer gas. The pump beam is tuned to the $R_{11}(11.5)$ transition as shown in the energy level diagram (left panel). The TCPS spectrum is shown in the right panel (experiment – filled symbols, dashed line; theory – solid red line).

III. Future Work

We will continue to perform fs CARS experiments using the Coherent ultrafast laser system. Our studies of temperature measurements using CPP fs CARS will continue. We continue to investigate the effect of laser system parameters on the CPP fs CARS spectrum to improve the

temperature accuracy of the technique. We will explore the potential for using CPP fs CARS for accurate concentration measurements for polyatomic species such as CO₂ and hydrocarbons. We will make full use of the high-temperature, high-pressure gas cell that we have fabricated for fundamental studies of the effects of temperature and pressure on CPP fs CARS spectra. We will explore further the effects of soot and droplets on the CPP fs CARS process, and use a Pockels cell between crossed polarizers as a fast electronic shutter for the 5 kHz fs CARS measurements.

Our theoretical studies of the physics of fs CARS will continue. The parallelization of our density matrix computer code will allow us to explore effects such as collisional narrowing that was simply not possible using the serial version of our code. The study of collisional narrowing requires communication between different computational nodes due to the transfer of coherence during collisions. We are still developing the numerical code for the collisional narrowing studies.

Our investigation of two-color PS and 6WM for species such as NO will continue. We will continue to explore collisional effects on the PS and 6WM processes in much more detail using a two-dye laser system. We will explore further the effects of buffer gas collisions on collision-induced resonances in single-photon, two-color PS of NO. We will continue to use the density matrix code to gain insight into the physics of the PS and 6WM processes.

Our theoretical studies of the physics of two-photon and Raman resonances will also continue. We will also initiate an investigation of ultrafast two-photon-induced fluorescence for species such as NO. The broadband excitation provide by fs pulses will be a significant advantage for these measurements. Although our initial ultrafast spectroscopy efforts have been focused on fs CARS, ultrafast laser systems will be useful for a wide range of future diagnostic techniques involving two-photon-induced processes including fluorescence, PS, and RWM.

IV. Refereed publications and submitted journal articles supported by this project 2018-2020

- P1. D. Han, J. Kim, A. Satija, J. P. Gore, and R. P. Lucht, "Experimental Study of CO₂ Diluted, Piloted, Turbulent CH₄/Air Premixed Flames using High-Repetition-Rate OH PLIF," *Combustion and Flame* **193**, 145–156 (2018). DOI: [10.1016/j.combustflame.2018.03.012](https://doi.org/10.1016/j.combustflame.2018.03.012)
- P2. A. Lowe, L. M. Thomas, A. Satija, R.P. Lucht, and A.R. Masri, "Chirped-Probe-Pulse Femtosecond CARS Thermometry in Turbulent Spray Flames," *Proceedings of the Combustion Institute* **37**, 1383-1391 (2019). DOI: [10.1016/j.proci.2018.06.149](https://doi.org/10.1016/j.proci.2018.06.149)
- P3. L. M. Thomas, A. Lowe, A. Satija, A.R. Masri, and R.P. Lucht, "5 kHz Thermometry in Turbulent Spray Flames Using Chirped-Probe-Pulse Femtosecond Coherent Anti-Stokes Raman Scattering, Part I: Processing and Interference Analysis," *Combustion and Flame* **200**, 405-416 (2019). DOI: [10.1016/j.combustflame.2018.11.004](https://doi.org/10.1016/j.combustflame.2018.11.004)
- P4. A. Lowe, L. M. Thomas, A. Satija, R.P. Lucht, and A.R. Masri, "Chirped-Probe-Pulse Femtosecond CARS Thermometry in Turbulent Spray Flames," *Proceedings of the Combustion Institute* **37**, 1383-1391 (2019). DOI: [10.1016/j.proci.2018.06.149](https://doi.org/10.1016/j.proci.2018.06.149)
- P5. A. Satija, Z. Chang, A. Lowe, L. M. Thomas, A. Masri, and R. P. Lucht, "CARS Thermometry in Laminar Sooting Ethylene-Air Co-Flow Diffusion Flames with Nitrogen Dilution," *Combustion and Flame* **208**, 37-44 (2019). DOI: [10.1016/j.combustflame.2019.06.025](https://doi.org/10.1016/j.combustflame.2019.06.025)
- P6. M. Gu, A. Satija, and R. P. Lucht, "Effects of Self-Phase Modulation (SPM) on Femtosecond Coherent Anti-Stokes Raman Scattering Spectroscopy," *Optics Express* **27**, 33955-33967 (2019). DOI: [10.1364/OE.27.033954](https://doi.org/10.1364/OE.27.033954)
- P7. M. Gu, A. Satija, and R. P. Lucht, "Impact of Moderate Pump-Stokes Chirp on Femtosecond Coherent Anti-Stokes Raman Scattering Spectra," *Journal of Raman Spectroscopy* **51**, 115-124 (2020). DOI: [10.1002/jrs.5754](https://doi.org/10.1002/jrs.5754)
- P8. A. Satija, N. Chai, M. T. Arendt, and R. P. Lucht, "Pure Rotational Coherent Anti-Stokes Raman Scattering Spectroscopy of Nitric Oxide: Determination of Raman Tensor Invariants," *Journal of Raman Spectroscopy* **51**, 807-828 (2020). DOI: [10.1002/jrs.5836](https://doi.org/10.1002/jrs.5836)
- P9. M. Gu, A. Satija, and R. P. Lucht, "CO₂ Chirped-Probe-Pulse Femtosecond CARS for Thermometry," *Proceedings of the Combustion Institute*, accepted for presentation (2021).

Thermal Decomposition of Cyclic, Oxygenated Hydrocarbons

Laura R. McCunn-Jordan
Chemistry Department, Marshall University
1 John Marshall Dr.
Huntington, WV 25755
mccunn@marshall.edu

Program Scope

The objective of this project is to elucidate how chemical structure affects the thermal decomposition mechanisms of cyclic, oxygenated hydrocarbons that are relevant to biofuels and combustion. The primary specific aim of the proposed experiments is to identify the thermal decomposition products of dihydro-2-furanone, dihydro-3-furanone, 2-cyclopentenone, 3-cyclopentenone, 2-pyrone, and 4-pyrone. A pulsed hyperthermal nozzle will be used to induce gas-phase pyrolysis at temperatures up to 1600 K. Product detection will be accomplished with a matrix-isolation FTIR spectrophotometer. A second specific aim of the project is to construct a mass spectrometer with tunable low-energy electron-impact ionization that can be used with the same hyperthermal nozzle. The introduction of a new detection technique will complement the FTIR experiments and provide a more complete characterization of the pyrolysis products, which is essential to the development of accurate thermal decomposition mechanisms.

The experiments are designed to probe the early steps in the pyrolysis mechanism, with the possibility of capturing radical intermediates. Two goals can be accomplished by this approach. First, the results will augment the existing body of knowledge created by shock-tube and static pyrolysis experiments, which typically probe the ultimate products of thermal decomposition on long time scales. Adding to the variety of techniques in the literature will clarify pyrolysis mechanisms, which can include dozens of elementary steps. Second, identifying pyrolysis products of compounds that are intermediates or by-products in the production or combustion of new fuels will enable the prediction of pollutants from these fuels. The experimental results will contribute to the elucidation of pyrolysis mechanisms and enable the assessment of the environmental impact of various fuels. The completed research will build a foundation of knowledge for overcoming challenges to the nation's energy supply and environmental quality.

Recent Progress

Construction of the Mass Spectrometer

The construction of the mass spectrometer is nearly complete. A vacuum chamber has been constructed with conflat hardware, two turbomolecular pumps and a custom skimmer flange to separate the source and detection regions. To integrate the laboratory's current pulsed, gas-phase pyrolysis source with the mass spectrometer, a custom, water-cooled mounting flange was procured. A support frame for the instrument was constructed and installed in the lab. Electrical upgrades were performed to support the additional vacuum pumps in the laboratory. Currently, the research group is awaiting installation of the software to control the quadrupole system and data collection, which has been delayed by the pandemic. Once the software is installed and delivered, testing of the instrument will commence.

Pyrolysis Experiments with Matrix-Isolation FTIR

Matrix-isolation FTIR experiments have been completed on several of the cyclic, oxygenated hydrocarbons targeted for study in this project. Pyrolysis was performed on four different molecules: dihydro-2-furanone; dihydro-3-furanone; 2-cyclopentenone; and 3-cyclopentenone. (Figure 1) Each molecule was mixed with argon at various dilute concentrations (0.02-0.4%) and subject to pyrolysis at a range of temperatures (900-1500 K). Products were identified with FTIR spectroscopy following matrix isolation.

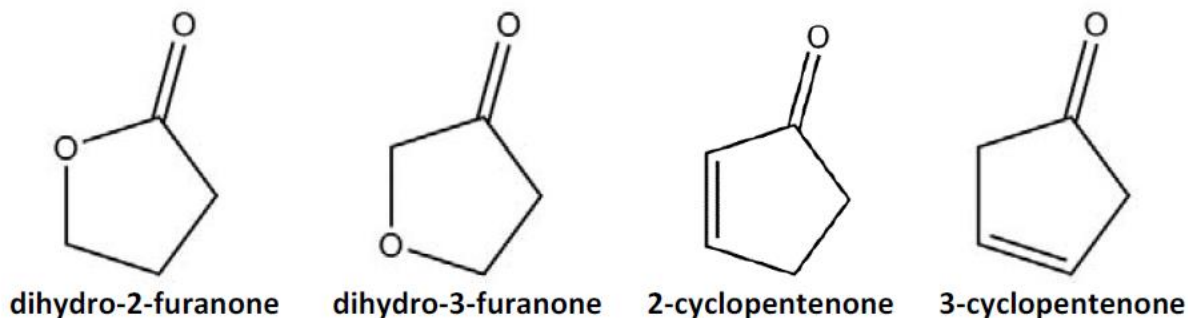


Figure 1. Cyclic, oxygenated hydrocarbons studied to date

Results for the four hydrocarbons studied thus far reveal several products that are commonly observed in the pyrolysis of oxygenated hydrocarbons: carbon monoxide, ketene, acetylene, and ethylene. Dihydro-2-furanone produces carbon dioxide, due to the placement of the oxygen atom in the ring. It also makes formaldehyde, a product that has not been observed with other techniques in the literature. The cyclopentenones are particularly interesting because they each produce propargyl radicals over a range of temperatures, indicating their possible contribution to soot formation when occurring in biofuels. The experiments on the cyclopentenones resulted in a few FTIR bands that have yet to be assigned, but are suspected to belong to substituted ketenes that have no benchmark spectra in the literature.

Computational study of pyrolysis reactions

During the first year of the project, the PI began a collaboration with Professor Carol Parish at the University of Richmond to use computational chemistry to understand the reactions that are relevant to the pyrolysis mechanism of the cyclic, oxygenated hydrocarbons being studied in this project. Geometry optimization and frequency calculations using Gaussian software are underway for dihydro-3-furanone, 2-cyclopentenone, and 3-cyclopentenone. Several intermediates and products have been identified, with transition states confirmed by intrinsic reaction coordinate calculations. The goal of this work is to map the energetics of all possible pathways for the unimolecular decomposition of these molecules. The frequency calculations are also proving helpful in identifying in the matrix-isolation FTIR spectra possible pyrolysis products for which no experimental spectra exist in the literature.

Future Plans

The second year of the project will focus on completing the implementation of the mass spectrometer and using it to study the pyrolysis of the various cyclic, oxygenated hydrocarbons that are the focus of this project. The mass spectra will confirm the product assignments already made from the FTIR spectra and will likely reveal a few unknown products as well. Additionally,

studies will begin of 2-pyrone and 4-pyrone (Figure 2), with both matrix-isolation FTIR and mass spectrometry detection of pyrolysis products. The computational studies will continue, and will likely be started for the pyrones as well.

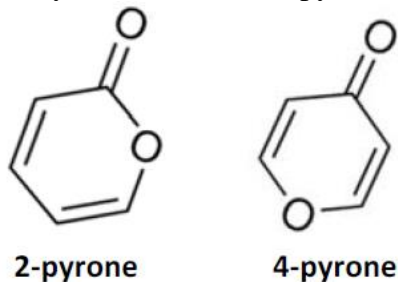


Figure 2. Remaining cyclic oxygenates to be studied.

Publications During Project Period

1. Brown, G.; Ellis, M.; Martin, T.; McCunn, L. R. Vibrational Bands of the 2-Butyn-1-yl Radical. *J. Phys. Chem. A*. In press (accepted April 29, 2020).

Machine Learning for Understanding Heavy Hydrocarbon Clustering

Habib Najm^{*1}, *Judit Zádor*¹, *Michael Eldred*², *Hope Michelsen*³

¹*Sandia National Laboratories, Livermore, CA*

²*Sandia National Laboratories, Albuquerque, NM*

³*University of Colorado, Boulder, CO*

Program Scope

The goal of this program is to use machine learning (ML) methods to advance the state of the art in our understanding of reaction processes in heavy hydrocarbon clustering, leading to incipient soot formation. We will do this by (1) building neural network (NN) potential energy surface (PES) representations for a class of hydrocarbon molecules, (2) using this construction to explore reaction processes among a set of initial C_mH_n molecules at concentrations typical in hydrocarbon flames, and (3) using stochastic sampling to estimate reaction probabilities and simulate growth leading to production of higher molecular weight hydrocarbons. Ultimately, our goal is to identify reaction processes that dominate molecular weight growth, and specifically explore the role of resonantly stabilized radicals (RSRs) in this process. Our NN training data will come from quantum chemistry computations at a range of levels of theory, and we will use the information thus gained from models of different fidelities in a multilevel-multifidelity (MLMF) formalism to efficiently attain requisite NN PES test accuracy. We will also rely on adaptive sampling following an active learning strategy to identify conditions for which additional quantum computations would provide maximal expected information gain, thereby again gaining computational efficiency. We will rely on KinBot [1] for exploration of the PES for generating geometries for training, and for exploring the trained NN PES to estimate reaction rates and expand the initial pool of molecules.

Recent Progress

We have made progress on a number of fronts this year, as outlined in the following.

Molecular Fingerprints:

The essential kernel of this work relies on the representation of the potential energy of an atomic system in a given geometry, using neural networks, as a function of atom locations and types. This is generally applicable to a collection of atoms, some, but not necessary all, of which may be bonded as molecules. The construction is to be used to represent the PES of different systems, each potentially composed of different numbers of atoms. In order to do this, and considering the NN representation for each atom type as some specific $y=f(x,w)$, with inputs x , and weights w , the n -long input (feature vector) x representing the geometry has to be the same size for any system considered. Accordingly, it has to be some suitable fingerprint, or summary, of the geometry. There is an extensive literature in this area, particularly on the use of the Behler and Parrinello symmetry functions (SFs) [2], which are used to construct the atomic environment vector (AEV) [3], which is the above input x , for each atom in the system. These SFs are of particular interest because of their translational, rotational, and permutational invariance. We implemented the algorithms for evaluating the AEV in Python and validated them on representative molecular systems.

AEV Construction:

The AEV construction involves design choices that control its spatial resolution in the representation of system geometry, and determine its resulting length n . Beyond this, the choice of underlying functional descriptors is also a design choice. Noting the availability of multiple options in this regard, the question arises as to optimal choices for our purposes. We have initiated a study in this regard employing a large database of hydrocarbon molecules in different geometrical configurations, and their associated energies [4]. This work is currently in progress.

* Principal Investigator. Address: P.O. Box 969, MS 9051, Livermore, CA 94551; Email: hnnajm@sandia.gov

Neural Network PES Construction:

We have developed Python software that leverages the PyTorch ML framework [5] for construction of feed-forward NNs for hydrocarbon molecule PES representation. Following [3], our construction employs an additive combination of NN PES predictions for each atom in the system, where one NN is employed for each atom type. Thus, for a system composed of, n C and m H atoms, its energy is represented as the sum of n forward predictions with the C NN, once for each of the n C atoms, and m forward predictions with the H NN, again once for each of the m H atoms. Each NN is composed of an input layer, several hidden layers, and an output layer. The width of the input layer is the dimension of the corresponding AEV, and the output layer contains a single node for the scalar-valued potential energy of the system. The number and widths of hidden layers, and their activation functions, are design choices, and natural targets for optimization. We currently use Gaussian functions, but others are available and will be considered.

Training the NN PES Construction:

As an initial demonstration we trained the above NN PES construction for (C,H) molecules with each of the two (C- and H-) NNs using 3 hidden layers with 128:128:64 node counts, and a 256-dimensional AEV. Each NN had ~58k parameters to be estimated, thus training optimization operated in a ~116k-dimensional space. The data extracted from [4] included computed energies for CH₄, C₂H₂, C₂H₄, C₂H₆, C₃H₄, C₃H₆, and C₃H₈ molecules, each in many different geometrical configurations. We used ~50k training points and ~12k testing points, randomly sampled from the available ~62k points for these 7 molecules in the database. Randomization of the training data was very effective in fast iterative reduction of training error.

We trained the NNs using mini-batched stochastic gradient descent (SGD), arriving at RMS errors of less than 1kcal/mole over both training and testing data. Maximum predictive errors of the trained system for rarely-sampled high-energy landscapes were significantly higher. Since only few samples at these energies were present in the database, this is understandable. This highlights the necessity for attention to density of samples in various regions of the configurational space, and the potential utility of weighted error norms or balanced sampling strategies. Our planned data generation with KinBot will generally involve non-uniform sampling, as we explore the PES, which will need to be taken into account in the subsequent choice of error norms and/or subsampling.

We explored the impact of hyperparameters on the training convergence rate, and observed particularly strong dependence on SGD batch-size, favoring small data batches. The batch size affects the noise in the gradient computed with SGD, with smaller batches leading to higher noise. In the high-dimensional (~116k) optimization objective function setting at hand, a crucial necessity is dealing with the preponderance of saddle point regions. The effectiveness of SGD comes in the presence of noise which helps the optimizer to escape these regions in the ongoing search for error minima. This was clearly evident in our results.

Training large NNs is computationally intensive, necessitating attention to computational resources and code optimization. As indicated, we have used Pytorch [5], which offers relatively easy migration to GPUs. While we have yet to use GPUs, we have worked on Python code optimization. We observed significant speedup by optimizing for-loop structures and data access, including maximizing use of C code underlying Python by avoiding for-loops where possible and relying on the underlying C handling of arrays, using advanced Pytorch libraries. These optimizations will be quite handy when we migrate to GPU utilization.

Proposed Work

Going forward, there are numerous lines of development/inquiry that we are actively working on.

KinBot:

KinBot is a recently developed open-source [1] tool to discover and characterize stationary points on reactive PESs. It casts the results in a form that lends itself directly to rate coefficient calculations. We will use KinBot to: (1) generate a large number of possible pathways for representative and relatively small

systems, to serve as a rich training data for the initial NN PES, and (2) explore many more pathways on the NN PES and turn the results of this exploration into rate coefficients.

Our first step will be to show that KinBot can produce full master equation (ME) representations of multiwell reactions relevant for RSR chemistry using *ab initio* evaluations for the PES. There is a very large literature of such reactions with known solutions, providing ample examples to benchmark our techniques. This benchmarking will guide the necessary improvements as large unsaturated and aromatic structures studied in this project create unique problems that need to be addressed. For instance, during a reaction path search, KinBot iteratively changes the geometry of the reactant to obtain initial guesses for reactive saddle points defined by KinBot's reaction types. However, KinBot does not have sufficient heuristics or other methods built into it to handle several rings or very rigid structures, and as a result, KinBot's transition-state templates tend to produce a lot of unrealistic saddle point guesses. In sync with other development plans for KinBot, we will also test and refine methods to automatically characterize barrierless reactions and the handling of regions of the PES with high multireference character.

We will also start coupling our code to the various elements of the project. In the output direction this will include routines to harvest the geometries explored by KinBot and methods to augment it, and to efficiently run the large number of calculations on DOE clusters. In the input direction, we will start designing an interface that allows KinBot to consume NN PES results in our framework.

Multilevel-Multifidelity (MLMF) Methods:

We will use MLMF methods [6] for incorporating data from quantum chemistry (QC) computations at different levels of theory to provide efficient means for NN training. We will start from traditional discrepancy-based emulation approaches for MLMF modeling, where we employ the NN PES formulations described above in a decoupled approach that decomposes the mapping from AEV into high-level theory predictions across multiple levels. Each level of QC theory adds a level to our modeling hierarchy, and starting from a NN PES for the lowest level of theory, we add additional NN models for each level of theory discrepancy until we additively emulate the highest-level QC theory. A key component to this approach is the use of varying amounts of training data, commensurate with the relative cost of the QC simulations.

Given initial promise from this basic MLMF approach, we will explore alternative NN architectures that can be adapted to more general graph relationships. In particular, we will explore the usage of recurrent NNs for general model sequences.

Our immediate steps in this regard, bringing together NNs and MLMF methods, will progress through model problems of increasing complexity. For initial exploration of MLMF NNs, we will investigate standard model problems based on discretization of elliptic PDEs. Given extensive MLMF benchmarking of these problems with Monte Carlo sampling and emulation with polynomial chaos, stochastic collocation, and function tensor train approximation, we will quickly assess MLMF NN performance characteristics.

Subsequently, as initial QC demonstrations, we will augment our current data with additional QC calculations at lower/higher levels of theory and demonstrate MLMF NN for molecular systems.

ML Capability Development:

Our immediate next goal with the NN training code will be adapting our Pytorch implementation towards GPU utilization. While Pytorch adaptation to use GPUs is relatively straightforward, achieving desirable performance gains will require significant attention to data locality and data movement. We will evaluate and improve training performance with utilization of single and multiple GPUs. We will also continue our current work on comparing and optimizing AEV design choices, and will proceed to variation and optimization of other hyperparameters including NN structure. We will also develop adaptive weighting of error norms to accommodate non-uniform distributions of data samples. We will also proceed to demonstrations of MLMF NN PES training with KinBot data for flame-representative molecules.

Validation Data:

Our ultimate scientific goal is to identify/test particle-inception mechanisms. We target the chemistry that leads to a transition from gas-phase species to condensed-phase particles. Such a transition can be identified when the properties (e.g., density, specific heat, and absorption and scattering cross sections) of the particle or cluster depart from those of the gas-phase species from which it is composed and begin to exhibit properties of a bulk material [7]. Many of the physical properties of incipient particles are not known, but experimental results have indicated these particles have elemental carbon-to-hydrogen (C/H) ratios of 1.5-2.5 [8-14]. As these particles further evolve at high temperature, they lose hydrogen, and their C/H ratios increase [15]. We will examine the role, and evaluate the importance, of resonance-stabilized radicals (RSRs) in high-temperature hydrocarbon growth processes. To accomplish this goal, we will analyze previously recorded measurements of particles extracted from flames and pyrolysis tubes using vacuum-ultraviolet photoionization mass spectrometry (VUV-AMS). These data provide observations of RSRs and other species produced over a wide range of high-temperature conditions that lead to soot inception.

References:

- [1] <https://github.com/zadorlab/KinBot>
R. Van de Vijver, J. Zádor, KinBot: Automated stationary point search on potential energy surfaces, *Computer Physics Communications*, Volume 248, March 2020, 106947.
- [2] J. Behler and M. Parrinello, Generalized Neural-Network Representation of High-Dimensional Potential-Energy Surfaces, *Physical Review Letters*, 98, 146401, 2007.
- [3] J. S. Smith, O. Isayev, and A. E. Roitberg. ANI-1: an extensible neural network potential with DFT accuracy at force field computational cost, *Chem. Sci.*, 8:3192–3203, 2017.
- [4] https://github.com/isayev/ANI1_dataset
- [5] <https://pytorch.org>
- [6] M.S. Eldred, L.W.T. Ng, M.F. Barone, and S.P. Domino, Multifidelity Uncertainty Quantification Using Spectral Stochastic Discrepancy Models, in *Handbook of Uncertainty Quantification*, pp. 1-45, Eds. R. Ghanem, D. Higdon, and H. Owhadi. Springer International Publishing, 2016..
- [7] P.A. Baron, K. Willeke, Aerosol fundamentals. In: P.A. Baron, K. Willeke, editors. *Aerosol Measurement: Principles, Techniques, and Applications*. 2nd ed. New York, NY: Wiley and Sons; 2001. p. 45-60.
- [8] S.J. Harris, A.M. Weiner, Chemical kinetics of soot particle growth, *Annu. Rev. Phys. Chem.*, 36 (1985) 31-52.
- [9] J.B. Howard, Carbon addition and oxidation reactions in heterogeneous combustion and soot formation, *Twenty-Third Symp. (Internat.) Combust.*, 23 (1990) 1107-1127.
- [10] A. D'Alessio, A. D'Anna, A. D'Orsi, P. Minutolo, R. Barbella, A. Ciajolo, Precursor formation and soot inception in premixed ethylene flames, *Proc. Combust. Inst.*, 24 (1992) 973-980.
- [11] R.A. Dobbins, H. Subramanian, *Soot precursors: Particles in flames*, in: H. Bockhorn (Ed.) *Soot Formation in Combustion*, Springer-Verlag, Berlin, 1994, pp. 290-301.
- [12] A. Ciajolo, R. Barbella, A. Tregrossi, L. Bonfanti, Spectroscopic and compositional signatures of PAH-loaded mixtures in the soot inception region of a premixed ethylene flame, *Proc. Combust. Inst.*, 27 (1998) 1481-1487.
- [13] J. Li, S. Yu, Soot particles analysis in laminar premixed propane/oxygen (C₃H₈/O₂) flame using published measurement data, *China Particuology*, 1 (2003) 168-171.
- [14] C. Russo, A. Tregrossi, A. Ciajolo, Dehydrogenation and growth of soot in premixed flames, *Proc. Combust. Inst.*, 35 (2015) 1803-1809.
- [15] H.A. Michelsen, Probing soot formation, chemical and physical evolution, and oxidation: A review of *in situ* diagnostic techniques and needs, *Proc. Combust. Inst.*, 36 (2017) 717-735.

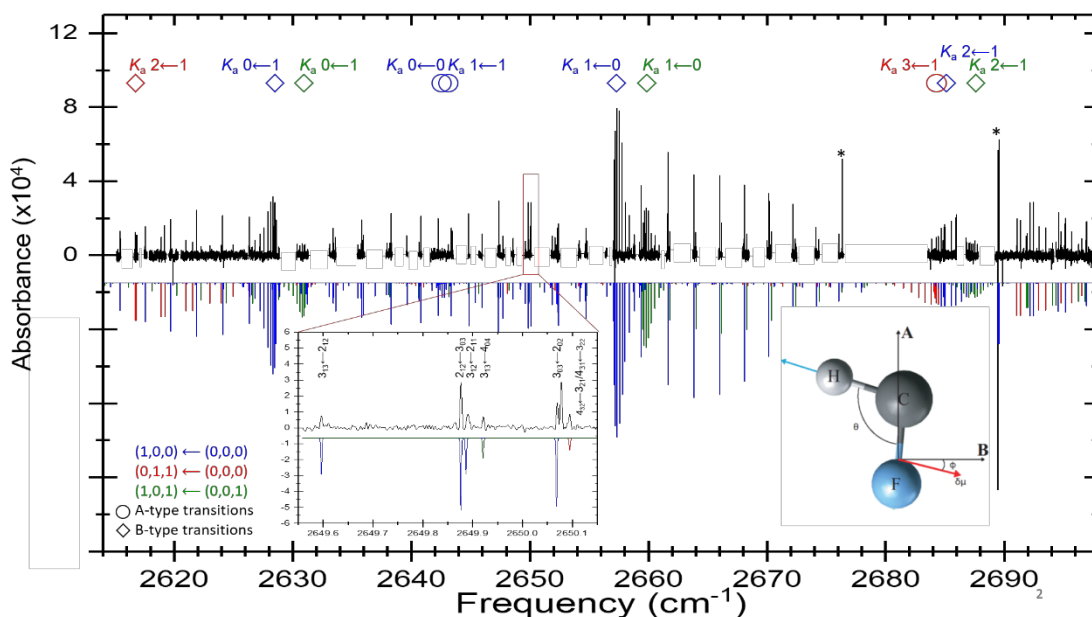
Spectroscopy, Kinetics and Dynamics of Combustion Radicals

David. J. Nesbitt

Our research program involves experimental and theoretical study of transient chemical species relevant to fundamental combustion and atmospheric chemical processes. The work focuses on spectroscopy and unimolecular/bimolecular dynamics of highly reactive radical intermediates, combining i) high-resolution direct IR laser absorption methods with quantum shot noise limited detection, ii) high densities (10^{12} - 10^{14} #/cm³) of jet-cooled hydrocarbon radicals and molecular ions in slit supersonic discharge expansions, accompanied by iii) high-level *ab initio* potential surface and multidimensional quantum mechanics calculations. Advantages of the slit discharge expansion techniques are i) generation of high concentrations of chemically reactive species yet ii) rapid subsequent cooling of these transient intermediates to $T_{\text{rot}} \approx 15$ -30 K in a collisionally collimated multipass geometry ideal for “reduced-Doppler” direct absorption spectroscopy with quantum shot-noise limited detection sensitivity. Over the past year, our group has explored multiple jet-cooled transients such as i) highly reactive singlet carbenes (e.g., HCF), ii) Criegee intermediate precursor halocarbon radicals (e.g., CH₂Br), and iii) H atom radical catalyzed oxyhydrocarbon isomerization dynamics (e.g., *trans*- to *cis*-formic acid) via high-resolution IR laser spectroscopy. Highlights from the first two topics are briefly discussed below, with papers resulting from both these projects chosen as “Editor’s Picks” in the Journal of Chemical Physics.^{1,2}

A. High-resolution infrared spectroscopy of HCF in the CH stretch region

Halogenated molecules are of importance to their involvement in commercial products, atmospheric and interstellar chemistry, and organic synthesis.^{3,4} In particular, halogen containing complex organic molecules (COMs, e.g., CH₃Cl) can be formed as the byproduct of biological activity and have been proposed as biomarkers in exoplanet atmospheres.⁵ However, the recent observation of CH₃Cl towards a sun-like star forming region and in the comet 67P/Churyumov-Gerasimenko indicates that there are non-biological formation mechanisms in the interstellar medium (ISM).⁶ One such mechanism is by halogen atom (X) incorporation into simple molecules and COMs in irradiated ice mantles of dust grains, including sequential H-atom addition to CX.^{4,7} In order to better understand how halogenated molecules are formed in the ISM, a complete understanding of the reaction-pathway intermediates and their relative abundances is needed. This requires gas-phase laboratory spectra with which to make unambiguous molecular assignments in astronomical observations of possible halogen containing molecules in the reaction network. To date, the pure rotational transitions of three fluorinated molecules have been detected in astronomical spectra: CF⁺ and HF, in diffuse and translucent clouds; HF, in dense sources;⁸⁻¹¹ and HF and AlF, in circumstellar envelopes of carbon rich stars.^{12,13} HF has also been observed in absorption in interstellar gas through its infrared rovibrational transitions, $\nu = 1 \leftarrow 0$ R(0) and R(1).¹⁴ Since the interstellar formation mechanism for CH₃F, like CH₃Cl, is thought to be dominated by grain surface reactions starting from CF, with the diradical halocarbene HCF as an intermediate,⁴ and given that the interstellar abundance of F is comparable to Cl,¹⁵ it is highly likely that CH₃F and its simpler radical derivatives,



e.g., HCF, also exist in astronomical environments. However, detection of fluorinated molecules with more than two atoms is currently hampered by limited laboratory-based high-resolution spectroscopic data.

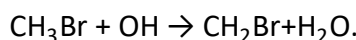
Over the past year we have obtained results from a high-resolution infrared study of jet-cooled singlet monofluorocarbene (HCF) in the CH stretch region near 2600 cm⁻¹, with the absorption signals recorded using near quantum shot noise limited laser absorption methods (see sample spectral region above). The fully resolved absorption spectra of the CH stretch (ν_1) fundamental band and a partial progression of transitions of the HCF bend plus CF stretch ($\nu_2 + \nu_3$) combination band are observed, and show clear evidence of a strong rovibrational coupling between the ν_1 $K_a^i = 2$ and $\nu_2 + \nu_3$ $K_a^i = 3$ manifolds, including the observation of “dark state” transitions. A detailed perturbation analysis of a c-type Coriolis interaction is carried out for these two coupled vibrational states, providing experimental determination of precise rovibrational constants. A combined ground state combination difference fit of the transitions to the ν_1 and $\nu_2 + \nu_3$ vibrational states in this study with previously reported LIF $\tilde{A}(0,0,0) \leftarrow \tilde{X}(0,0,0)$ data has been done to increase the accuracy of the ground state rotational constants. Moreover, we report for the first time hot band ($\nu_1 + \nu_3 \leftarrow \nu_3$) transitions due to vibrationally excited HCF in the CF stretch mode, ν_3 . The high-resolution results for all vibrational frequencies and rotational constants are in good agreement with and significantly extend the analysis of the rovibrational manifold of HCF.¹⁶ The present ground state and ν_3 spectroscopic parameters now permit improved predictions for pure rotational and ν_3 fundamental transitions to aid spectral searches for HCF in the laboratory and the interstellar medium.

B. High-resolution infrared spectroscopy of jet cooled CH₂Br radicals:

Ever since their initial prediction over 50 years ago, the spectroscopy and quantum dynamics of diradical carbonyl oxides (so-called Criegee intermediates) have become increasingly significant topics because of their relevance to atmospheric and combustion chemistry, particularly with the recent demonstration that gas phase synthesis of Criegee

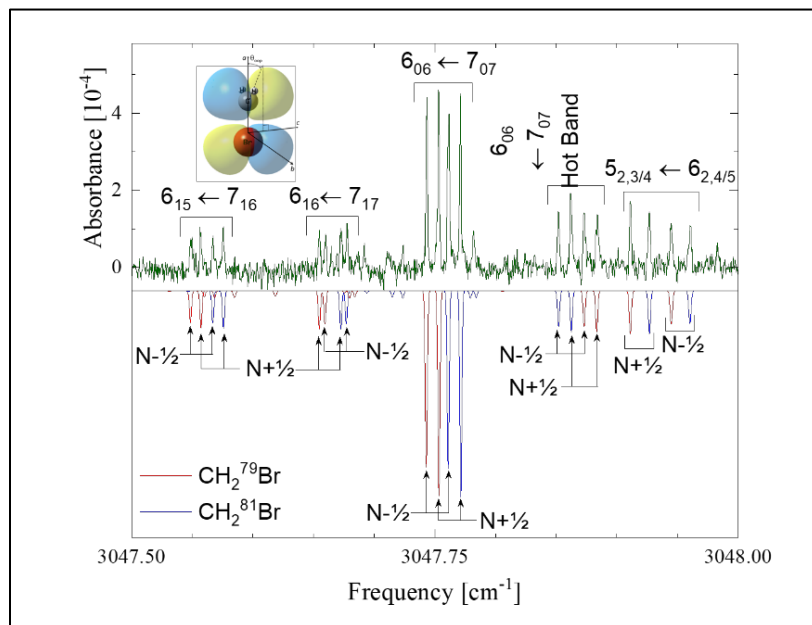
intermediates R_1R_2COO can be made relatively simply by the addition of O_2 to mono-iodohydrocarbon radicals.¹⁷ This approach has been quite recently extended to mono-bromohydrocarbon radicals by Nakajima and Endo¹⁸ in Fourier-transform microwave spectroscopy (FTMS) measurements, based on dissociating CH_2Br_2 in a O_2 doped discharge and collisionally stabilizing the subsequent Criegee species ($CH_2Br + O_2 \rightarrow CH_2OO + Br$) in a supersonic expansion. Given the important role of CH_2Br in the chemical formation of Criegee intermediates, we have chosen to explore the infrared rovibrational spectroscopy of the jet cooled radical CH_2Br as a first step towards spectroscopic study of CH_2OO itself.

Beyond utility in generating Criegee intermediates, the CH_2Br radical is of fundamental interest in both atmospheric and interstellar chemistry (ISC). For example, methyl bromide (CH_3Br) is known to have a relatively long residence time (roughly two years¹⁹) in the atmosphere, with the primary removal process by hydroxyl radical abstraction reaction to form CH_2Br , i.e.,



Once the CH_2Br radical is generated, it can undergo solar photodissociation and production of free radical Br atoms, known to be a strong catalytic species in the destruction of stratospheric ozone.^{20,21} Natural sources of CH_2Br include evolution of CH_3Br from biological activity in the marine environments, with less benign anthropomorphic sources of CH_3Br due to fumigant use still permitted by the Montreal Protocol.²² From the perspective of ISC, halogen-containing complex organic molecules (COMs) such as CH_3Br on earth are predominantly formed as the byproduct of biological activity and have therefore also been proposed as potential biomarkers in exoplanetary atmospheres.⁵ However, recent observational data for halogenated organic molecules in comets and sun-like star forming regions suggests that there might also be *non-biological* formation pathways in the interstellar medium (ISM),⁶ such as halogen incorporation into COMs via irradiation of ice mantles on dust grains.²³ In order to better characterize the formation of halogenated molecules in the ISM, therefore, a more complete understanding of the underlying brominated hydrocarbon reaction intermediates and their high resolution infrared (IR) spectroscopic signatures would be extremely helpful, toward which the efforts in the current paper have been directed.

Direct laser absorption of a slit supersonic discharge expansion provides the first high-resolution spectroscopic results on symmetric CH stretch excitation (ν_1) of bromomethyl (CH_2Br) radical in the ground electronic state. Narrowband (< 1 MHz) mid-infrared radiation is produced by difference frequency generation of two visible lasers beams, with the open shell halohydrocarbon radical generated by electron associative detachment of CH_2Br_2 in a discharge and rapidly cooled to $T_{rot} =$



18 ± 1 K in the subsequent slit-jet supersonic expansion. Rovibrational structure in the radical spectrum is fully resolved, as well as additional splittings due to spin-rotation effects and $^{79}\text{Br}/^{81}\text{Br}$ isotopologues in natural abundance. Spectroscopic constants and band origins are determined by fitting the transition frequencies to a non-rigid Watson Hamiltonian, yielding results consistent with a vibrationally averaged planar radical and an unpaired electron in the out-of-plane p_π orbital. Additionally, extensive satellite band structure from a vibrational hot band is observed and analyzed. This hot band is compared to CFOUR/VPT2 (CCSD(T)cc-pVQZ) ab initio anharmonic predictions of the vibration rotation alpha matrix. This permits unambiguous assignment of this band to CH_2 symmetric stretch excitation built on the singly excited CH_2 out-of-plane bending mode ($\nu_1+\nu_4 \leftarrow \nu_4$). Longitudinal cooling of the Doppler width in the slit jet expansion geometry also reveals partially resolved hyperfine structure on transitions from the lowest angular momentum states which is in excellent agreement with predictions based on microwave studies. High level ab initio MOLPRO calculations (CCSD(T)-f12b/VnZ-f12 (n=3, 4, CBS) are also performed with explicitly correlated f12 electron methods for the out-of-plane CH_2 bending mode over the halogen series CH_2X (X = F, Cl, Br, I), which clearly reveals a non-planar geometry for X = F (with a $\Delta E \approx 0.3$ kcal/mol barrier) and yet planar equilibrium geometries for X = Cl, Br, and I. Finally, a detailed Boltzmann analysis of the transition intensities provides support for negligible collisional equilibration of the entangled H atom nuclear spin states on the few hundred microsecond time scale and high collision densities of a slit supersonic expansion.

- 1 K. D. Doney *et al.*, J. Chem. Phys. (in press, 2020, Editor's Pick).
- 2 A. Kortyna *et al.*, J. Chem. Phys. (in press, 2020, Editor's Pick).
- 3 S. Elliott and F. S. Rowland, J. Chem. Educ. **64**, 387 (1987).
- 4 K. Acharyya and E. Herbst, Astrophys. J. **850** (2017).
- 5 E. W. Schwieterman *et al.*, Astrobiology **18**, 663 (2018).
- 6 E. C. Fayolle *et al.*, Nat. Astron. **1**, 703 (2017).
- 7 M. Kama *et al.*, Astron. Astrophys. **574** (2015).
- 8 D. A. Neufeld *et al.*, Astrophys. J. **488**, L141 (1997).
- 9 D. A. Neufeld *et al.*, Astron. Astrophys. **454**, L37 (2006).
- 10 T. G. Phillips *et al.*, Astron. Astrophys. **518** (2010).
- 11 P. Sonnentrucker *et al.*, Astrophys. J. **806** (2015).
- 12 J. Cernicharo and M. Guelin, Astron. Astrophys. **183**, L10 (1987).
- 13 M. Agundez *et al.*, Astron. Astrophys. **533** (2011).
- 14 N. Indriolo *et al.*, Astrophys. J. **764** (2013).
- 15 M. Asplund *et al.*, in *Annual Review of Astronomy and Astrophysics, Vol 47*, edited by R. Blandford, J. Kormendy, and E. VanDishoeck (Annual Reviews, Palo Alto, 2009), Vol. 47, pp. 481.
- 16 M. Kakimoto *et al.*, J. Mol. Spectrosc. **88**, 300 (1981).
- 17 C. A. Taatjes *et al.*, J. Am. Chem. Soc. **130**, 11883 (2008).
- 18 M. Nakajima and Y. Endo, J. Chem. Phys. **139**, 101103 (2013).
- 19 A. Mellouki *et al.*, Geophys. Res. Lett. **19**, 2059 (1992).
- 20 S. C. Wofsy *et al.*, Geophys. Res. Lett. **2**, 215 (1975).
- 21 Y. L. Yung *et al.*, J. Atmosph. Sci. **37**, 339 (1980).
- 22 S. W. J. Johnson, S. Gerik, in *Outlooks on Pest Management* (2012), Vol. 23, pp. 53.
- 23 M. Kama *et al.*, Astron. Astrophys. **574**, A107 (2015).

Fundamental Molecular Spectroscopy and Chemical Dynamics

Stephen R. Leone and Daniel M. Neumark

Lawrence Berkeley National Laboratory and Departments of Chemistry and Physics, University of California, Berkeley, California 94720 (510) 643-5467 srl@berkeley.edu, 510-642-3502

dmneumark@berkeley.edu

Scope of the Project: Decades of research into molecular dynamics, including branching fractions, dissociation dynamics, and energetics, have vastly improved our fundamental understanding of chemical processes. Measurements of radical spectroscopy, ions and excited state dynamics comprise key future goals of the effort, especially the development of new ways to probe excited-state dynamics and photoproducts in the program of Leone and Neumark. The Leone group has pioneered femtosecond time-resolved table-top x-ray spectroscopic investigations of chemical dynamics at sufficiently high photon energies to access the carbon K-edge. Ultrafast x-ray transient absorption spectroscopy based on this methodology investigates transition states and products. The Neumark program uses a suite of experimental methods aimed at the spectroscopy and photodissociation dynamics of reactive free radicals: slow electron velocity-map imaging of cryogenically cooled anions (cryo-SEVI), a high resolution variant of photoelectron spectroscopy, and fast radical beam (FRBM) studies of radical photodissociation, in which a beam of radicals is generated by negative ion photodetachment. A crossed molecular beam apparatus formerly used for gas phase experiments is being re-purposed for liquid jet scattering experiments.

Recent Progress:

Femtosecond Soft X-ray Transient Absorption Experiments A unique femtosecond soft x-ray transient absorption spectroscopy apparatus with x-ray probe energies up to 300 eV is used to characterize the electronic structure of transient intermediates of chemical reactions. Previously, the ultrafast photoinduced ring-opening reaction of 1,3-cyclohexadiene – a fundamental prototype of photochemical pericyclic reactions – was measured, the ring opening of an organic heterocycle – furfural – was investigated, and the photodissociation of CH_2ICl was explored, each documented by previous in-depth publications. The non-adiabatic dynamics of acetylacetone (pentane-2,4-dione) singlet-to-triplet transfer was directly observed upon 266 nm excitation. At this wavelength, the enolic tautomer of the molecule is excited to the S_2 ($^1\pi\pi^*$) electronic state, from which it undergoes internal conversion to the lower-lying singlet states and intersystem crossing to the triplet states. Currently the photochemistry of hexafluoroacetylacetone is being explored. Preliminary measurements show a similar, but slightly slower deactivation pathway from the initially excited state. Computations are being carried out using a square gradient minimization algorithm that obtains spin-pure restricted open-shell Kohn-Sham energies. Ultrafast electron diffraction measurements at SLAC will also be used to study the early time dynamics of acetylacetone and the hexafluoro analog (run time granted, but currently postponed).

A new type of experiment involves the ability to acquire detailed x-ray spectra of ions for the first time. Two-photon (1+1) ionization with 266 nm is used to prepare benzene cations in the ground state cation. The ionization from the degenerate highest occupied π orbitals of neutral benzene leads to two cations, $\text{Bz}^+(\text{B}_{2g})$ and $\text{Bz}^+(\text{B}_{3g})$, with different geometries compared to the neutral benzene. This leads to a splitting of the π^* orbitals that is observed in the x-ray spectra, as well as the partially open π orbitals. The results are confirmed by theoretical calculations by a collaboration of A. Krylov at USC and S. Coriani at DTU (Denmark). The theoretical results present the possibility of future observations of Jahn-Teller splitting in the x-ray domain, when higher spectral resolution will be possible, and the results provide insight into the electronic structure of benzene and its cation.

Pyrazine is a photophysically rich molecule and represents a benchmark example of vibronic coupling between S_2 ($^1\pi\pi^*$) and S_1 ($^1n\pi^*$) electronic states. In this way, the ~ 20 fs S_2 to S_1 internal conversion has been thoroughly characterized both experimentally and theoretically. However, experimental limitations hindered the observation in real time of electronic deexcitation to the ground state. Carbon

K edge spectroscopy sheds light on the early photochemical changes in pyrazine after 266 nm excitation. Preliminary results point to the presence of a major deactivation channel on ~ 200 fs time scale that can be interpreted as internal conversion to the vibrationally excited ground state, raising fundamental questions on the photostability of pyrazine. In the ongoing collaboration, the groups of A. Krylov and S. Coriani carry out quantum mechanical simulations to determine the nature of the observed deactivation channel and the possible isomerization channels to pyrimidine and pyridazine.

In order to access even shorter time electronic dynamics – such as passage through conical intersections – a new beamline, provided by combined NSF, campus, and LBNL funds, has been designed for attosecond and few-femtosecond soft x-ray transient absorption experiments. In this new laboratory, 1300 nm pulses are compressed down to 12 fs few-cycle pulses and used to generate a soft x-ray continuum up to 375 eV. The brightness of this beamline allows the measurement of absorption spectra in a few seconds, an order of magnitude improvement compared to existing apparatuses that provide photon continua in this energy range. Few-cycle pulses centered at 800 nm are simultaneously produced at a millijoule level and can be used as a pump pulse for strong-field ionization or impulsive stimulated Raman scattering. The cross-correlation between the soft x-ray pulses and near-IR pulses is measured to be 11 fs, thus opening many possibilities for the observation of ultrafast chemical dynamics on this timescale.

In a first time-resolved experiment with the new attosecond carbon K edge apparatus, a vibrational wavepacket superposition of states was observed, produced by impulsive stimulated Raman scattering in sulfur hexafluoride. The superposition is observed through six different sulfur core-excited states of the molecule (170-240 eV). The vibrational period for the ν_1 mode (symmetric stretching of S-F bonds) of 43 fs is well resolved in the time domain. The x-ray transition energies are very sensitive to small changes in internuclear distances, here of the order of a few 0.01 Å. Each core-excited state responds differently to the same vibrational wavepacket, shifting the transition energy by a certain amount. This allows determining experimentally the gradients of the core-excited state potential energy surfaces. Calculations of the potential energy surfaces in the E. Neuscammann group (UC Berkeley) are ongoing to compare to the experimental results. In a follow-up experiment, carbon dioxide was vibrationally excited by impulsive stimulated Raman scattering. A multimode vibrational wavepacket superposition composed of the ν_1 and $2\nu_2$ modes of the well-known CO₂ Fermi resonance is excited and observed via the C 1s electronic transitions at 293 eV. The temporal resolution of the experiment allows observing a ~ 22 fs vibrational motion in the time-domain. This result demonstrates the ability of the apparatus to resolve very short ultrafast molecular dynamics at the carbon K-edge, and the probing of such superposition states connects directly to quantum coherence properties important in molecular dynamics.

Free radical spectroscopy and dynamics The spectroscopy and photodissociation dynamics of several free radicals are studied using slow photoelectron velocity-map imaging of cryogenically cooled anions (cryo-SEVI) and fast radical beam (FRBM) dissociation. In cryo-SEVI, mass-selected anions are stored in a radio-frequency ion trap at T=5 K and cooled by collisions with a low-pressure buffer gas. Ions are then extracted and photodetached, and the resulting slow photoelectrons are selectively analysed with velocity-map imaging, yielding photoelectron spectra with energy resolution as high as 1-2 cm⁻¹ for complex species. This experiment was used to obtain isomer-specific, high-resolution photoelectron spectra of the *para*-, *ortho*-, and *meta*-pyridinide anions, yielding electron affinities and detailed vibrational structure for the three neutral pyridyl radical isomers. Strong isomeric variations in the photoelectron angular distributions were explained by a model approximating the anion orbitals from which detachment occurs as superpositions of *s*-, *p*-, and *d*-like hydrogenic wavefunctions.

On the FRBM experiment, photofragment translational spectroscopy was used to probe the unimolecular photodissociation of the indenyl radical (C₉H₇). The radicals were generated by photodetachment of the C₉H₇⁻ anion and photodissociated at 248 and 193 nm. Two- and three-body channels were seen at both wavelengths: C₂H₂ + C₇H₅, C₂H₂ + C₃H₃ + C₄H₂, and C₂H₂ + C₂H₂ + C₅H₃. The three-body channels are not energetically accessible by one photon excitation at either

dissociation wavelength. This observation, in combination with calculated dissociation rates and laser power studies, implies that all dissociation in this experiment occurs exclusively by multiphoton processes in which the C₉H₇ radical absorbs two photons sequentially prior to dissociation to two or three fragments. The translational energy distributions for each product channel peak will be below the maximum available energy for two-photon absorption and are largely independent of dissociation wavelengths. These results suggest that all observed channels occur via internal conversion to the ground electronic state followed by dissociation.

Future Plans: The UV-pump, soft x-ray-probe apparatus will be used to spectroscopically investigate fundamental photochemical processes including radical formation, decomposition of carbonyl compounds, predissociation of aromatic systems, and isomerization of heterocyclic rings. Future investigations include cyclopentadiene, pentamethylcyclopentadiene, benzaldehyde, pyridine and heptatriene, involving characterization of rapid return to internally excited ground states and H migration. Significant progress to date in the production of femtosecond 200 nm pump light promises a much wider pool of systems that will become accessible for investigation. Future efforts will extend the soft x-ray probe to obtain energy-tunable pulses covering the nitrogen K-edge (410 eV) as well as the temporal resolution to achieve few-femtosecond timescales. The new attosecond soft x-ray apparatus will be combined with a short UV pump to provide the temporal resolution to resolve excited state dynamics through conical intersections in, e.g., methyl iodide, pyrazine and thymine. Coherent wave packet dynamics will be explored to detail the impact of vibrational wave packets on x-ray core-level absorption spectroscopy with attosecond resolution.

The molecular beam instrument in Neumark's laboratory, which was previously also used to investigate free radical photodissociation, is being modified to investigate the elastic, inelastic, and reactive scattering of atoms and reactive free radicals from flat liquid jets of water and other volatile solvents. The incorporation of flat jet technology into the molecular beam scattering instrument will build on the pioneering liquid scattering experiments carried out by Nathanson and co-workers. The proposed experiments will provide unprecedented insights into how the well-understood binary interactions that govern gas phase collision dynamics are modified when one of the scattering partners is a liquid. In addition, the flat jet geometry is suitable for carrying out transient absorption experiments in liquids at photon energies at or above the carbon K-edge, so mastering this technology will enable time-resolved x-ray experiments that will also be of interest in the CPIMS and AMO programs in the DOE Basic Energy Sciences portfolio.

Recent Publications Acknowledging DOE GPCP Support (2016-2019):

- L. Barreau, A. D. Ross, S. Garg, P. M. Kraus, D. M. Neumark and S. R. Leone, "*Efficient table-top dual-wavelength beamline for ultrafast transient absorption spectroscopy in the soft X-ray region*," *Sci. Rep.* 10, 5773 (2020).
- " J. A. DeVine, M. C. Babin, K. Blackford, D. M. Neumark, "*High-resolution photoelectron spectroscopy of the pyridinide isomers*," *J. Chem. Phys.* 151, 064302 (2019).
- E. N. Sullivan, B. Nichols, S. von Kugelgen, G. da Silva, D. M. Neumark, "*Multiphoton dissociation dynamics of the indenyl radical at 248 nm and 193 nm*," *J. Chem. Phys.* 151, 174303 (2019).
- E. N. Sullivan, B. Nichols, D. M. Neumark, "*Fast beam photofragment translational spectroscopy of the phenoxy radical at 225 nm, 290 nm, and 533 nm*," *Phys. Chem. Chem. Phys.* **21**, 14720 (2019).
- I. Ramphal, C. Lee, D. M. Neumark, "*Photodissociation dynamics of the methylsulfinyl radical at 248 nm*," *Molec. Phys.* **117**, 3043 (2019).
- K. Schnorr, A. Bhattacharjee, K. J. Oosterbaan, M. G. Delcey, Z. Yang, T. Xue, A. R. Attar, A. S. Chatterley, M. Head-Gordon, S. R. Leone, and O. Gessner, "*Tracing the 267 nm-Induced Radical Formation in Dimethyl Disulfide Using Time-Resolved X-ray Absorption Spectroscopy*," *J. Phys. Chem. Lett.* 10, 1382–1387 (2019).

- A. Bhattacharjee, and S. R. Leone, "*Ultrafast X-ray Transient Absorption Spectroscopy of Gas-Phase Photochemical Reactions - A New Universal Probe of Photoinduced Molecular Dynamics*," *Acc. Chem. Res.* 51, 3203–3211 (2018).
- Z. Yang, K. Schnorr, A. Bhattacharjee, P. L. Lefebvre, M. Ephstein, T. Xue, J. F. Stanton, and S. R. Leone, "*Electron-withdrawing effects in the photodissociation of CH₂ICl to form CH₂Cl radical, simultaneously viewed through the carbon K and chlorine L_{2,3}X-ray edges*," *J. Am. Chem. Soc.* 140, 13360 (2018).
- A. Bhattacharjee, K. Schnorr, S. Oesterling, Z. Yang, T. Xue, R. Vivie-Riedle, and S. R. Leone, "*Photoinduced heterocyclic ring opening of furfural: distinct open-chain product identification by ultrafast X-ray transient absorption spectroscopy*," *J. Am. Chem. Soc.* 140, 12538 (2018).
- P. M. Kraus, M. Zürich, S. K. Cushing, D. M. Neumark, and S. R. Leone, "*The ultrafast X-ray spectroscopic revolution in chemical dynamics*," *Nat. Rev. Chem.* 2, 82 (2018).
- E. N. Sullivan, B. Nichols, D. M. Neumark, "*Photodissociation dynamics of the simplest alkyl peroxy radicals, CH₃OO and C₂H₅OO, at 248 nm*," *J. Chem. Phys.* 148, 033409 (2018).
- B. Nichols, E. N. Sullivan, M. Ryazanov, C. M. Hong, D. M. Neumark, "*Investigation of the two- and three-fragment photodissociation of the tert-butyl peroxy radical at 248 nm*," *J. Chem. Phys.* 147, 134304 (2017).
- J. A. DeVine, M. L. Weichman, M. C. Babin, Daniel M. Neumark, "*Slow photoelectron velocity-map imaging of cold tert-butyl peroxide*," *J. Chem. Phys.* 147, 013915 (2017).
- M. L. Weichman, L. Cheng, J. B. Kim, J. F. Stanton, D. M. Neumark, "*Low-lying vibronic level structure of the ground state of the methoxy radical: Slow electron velocity-map imaging (SEVI) spectra and Koppel-Domcke-Cederbaum (KDC) vibronic Hamiltonian calculations*," *J. Chem. Phys.* 146, 224309 (2017).
- Z. Wang, D. M. Popolan-Vaida, B. Chen, K. Moshhammer, S. Y. Mohamed, H. Wang, S. Sioud, M. A. Raji, K. Kohse-Höinghaus, N. Hansen, P. Dagaut, S. R. Leone, and S. M. Sarathy, "*Unraveling the structure and chemical mechanisms of highly oxygenated intermediates in oxidation of organic compounds*," *PNAS* 114, 13102 (2017).
- I. A. Ramphal, M. Shapero, C. Haibach-Morris, D. M. Neumark, "*Photodissociation dynamics of fulvenallene and the fulvenallenyl radical at 248 and 193 nm*," *Phys. Chem. Chem. Phys.* 19, 29305 (2017).
- A. Bhattacharjee, C. D. Pemmaraju, K. Schnorr, A. R. Attar, and S. R. Leone, "*Ultrafast intersystem crossing in acetylacetone via femtosecond x-ray transient absorption at the carbon K-edge*," *J. Am. Chem. Soc.* 139, 16576 (2017).
- Z. Wang, D. M. Popolan-Vaida, B. Chen, K. Moshhammer, S. Y. Mohamed, H. Wang, S. Sioud, M. A. Raji, K. Kohse-Höinghaus, N. Hansen, P. Dagaut, S. R. Leone, and S. M. Sarathy, "*Unraveling the structure and chemical mechanisms of highly oxygenated intermediates in oxidation of organic compounds*," *PNAS* 114, 13102 (2017).
- S. Chambreau, D. Popolan-Vaida, G. Vaghjiani, and S. R. Leone, "*Catalytic decomposition of hydroxylammonium nitrate ionic liquid: enhancement of NO formation*," *J. Phys. Chem. Lett.* 8, 2126 (2017).
- S. D. Chambreau, D. M. Popolan-Vaida, G. L. Vaghjiani, S. R. Leone, "*Catalytic Decomposition of Hydroxylammonium Nitrate Ionic Liquid: Enhancement of NO Formation*," *J. Phys. Chem. Lett.* 8, 2126-2130 (2017).
- A. R. Attar, A. Bhattacharjee, C. D. Pemmaraju, Kirsten Schnorr, Kristina D. Closser, David Prendergast, and S. R. Leone, "*Femtosecond x-ray spectroscopy of an electrocyclic ring-opening reaction*," *Science* 356, 54 (2017).
- B. Nichols, E. N. Sullivan, M. Ryazanov, D. M. Neumark, "*Photodissociation dynamics of the i-methylvinoxy radical at 308, 248, and 225 nm using fast beam photofragment translational spectroscopy*," *J. Phys. Chem. A* 121, 579 (2017).
- J. A. DeVine, M. L. Weichman, S. J. Lyle, D. M. Neumark, "*High-resolution photoelectron imaging of cryogenically cooled α - and β -furanil anions*," *J. Mol. Spec.* 332, 16 (2017).

State-to-State Molecular Reactions in the Ultracold Regime

Kang-Kuen Ni

Department of Chemistry and Chemical Biology, Harvard University

12 Oxford St., Cambridge, MA 02138

ni@chemistry.harvard.edu

Research Scope:

We aim to gain state-to-state experimental data for both the $AB + CD$ and $AB + C$ types of reactions that can be compared to advanced theoretical calculations and elucidate the role of quantum mechanics in the processes of bond breakage and formation. Our approach is to conduct experiment with reactants prepared at ultracold temperatures ($< 1\mu K$) such that quantum effects of translational motion are an important factor. Specific examples of the potassium-rubidium metathesis reaction $KRb + KRb \rightarrow K_2 + Rb_2$ and the atom exchange reaction $K + KRb \rightarrow K_2 + Rb$ are chosen because the technology of quantum internal and motional state control of these types of molecules is ripe. We have constructed a new quantum degenerate gas apparatus that integrates ion detection and velocity map imaging capabilities and began to explore the bimolecular reaction. Reactions in this regime will serve as a sensitive probe to compare to high accuracy *ab initio* potentials and quantum scattering calculations. This work will advance both our intuition about and ability to perform chemistry at ultracold temperatures and to control chemistry at the most basic quantum level.

Recent Progress:

For the funding period since last year, our efforts in studying bimolecular reactions of KRb molecules at sub-microkelvin temperatures have yielded two key results. 1. We directly observed the reaction transient intermediate complex, $K_2Rb_2^*$, and the products[1] via photo-ionization detection. 2. We studied the complex lifetime and its photo-excitation properties [2].

The observation of the intermediate complex without resorting to ultrafast techniques was a pleasant surprise. An important element to the observation was the preparation of rovibronic ground-state KRb molecules at sub-microkelvin temperatures, which energetically minimizes the number of product channels available for the complexes to dissociate, and thus resulting in long-lived complexes. To look for these complexes, we probed a cloud of reacting KRb molecules using a nanosecond pulsed UV ionization laser whose wavelength ranges from 285 to 356 nm. The first experimental signature of the $K_2Rb_2^*$ complex came in the form of K_2Rb^+ and KRb_2^+ ions (determined by time-of-flight mass spectrometry), which we attributed to the single-photon dissociative ionization of $K_2Rb_2^*$ based on the dependence of their characteristic kinetic energies (measured via velocity map imaging) on the ionization photon energy. The threshold energy for $K_2Rb_2^*$ to dissociate into a KRb_2^+ ion and a K atom is determined to be $2.9 \times 10^4 \text{cm}^{-1}$ (corresponding to a wavelength of 345 nm), in good agreement with the theoretically calculated value. Using an ionization laser wavelength of 356 nm, which targets below the dissociation threshold, we observed a

strong signal of K_2Rb_2^+ in the mass spectrum, which resulted from the single-photon ionization of K_2Rb_2^* .

Being able to catch these fleeting complexes in their act using nanosecond laser pulses indicate that their lifetime is at least of similar order of magnitude, which is unusual for systems of only a few particles. The natural next steps are to investigate the possible consequences of such a long-lived complex, and make a direct measurement of its lifetime. To this end, we discovered that the

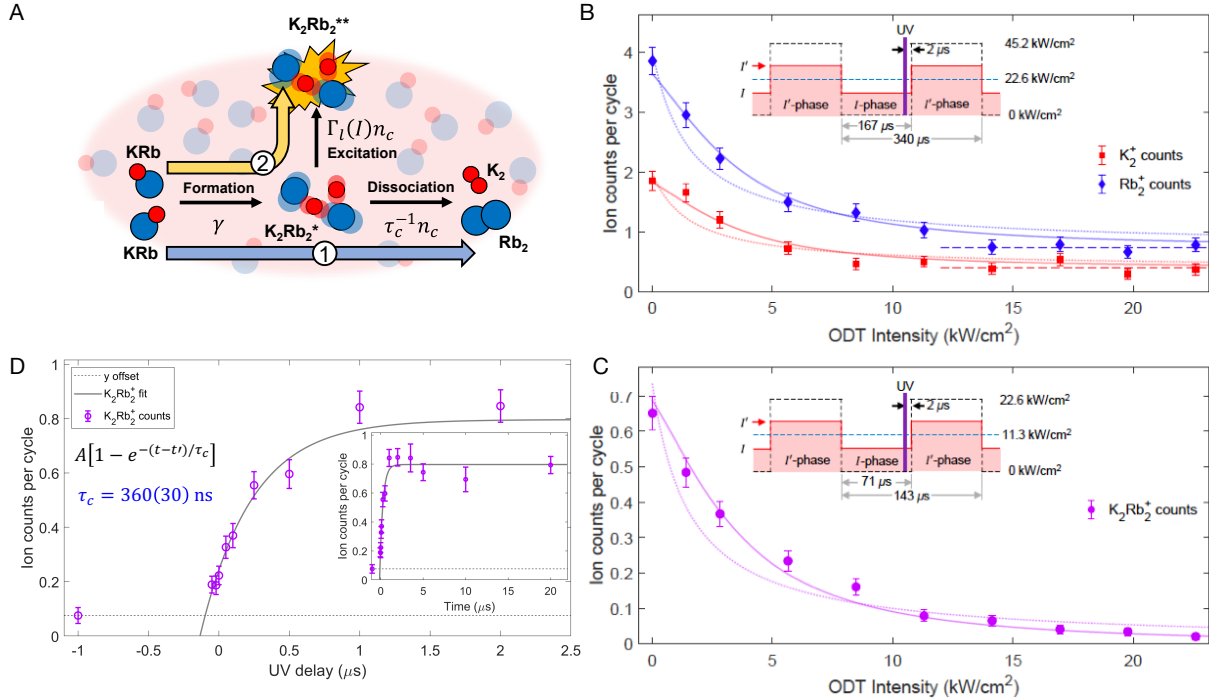


Figure 1: Photo-excitation of reaction intermediate and its lifetime. **A**, Two pathways for bimolecular KRb reactions. Both pathways involve the formation of a long-lived intermediate complex K_2Rb_2^* . ① indicates the ground state pathway $\text{KRb} + \text{KRb} \rightarrow \text{K}_2\text{Rb}_2^* \rightarrow \text{K}_2 + \text{Rb}_2$, which is the only pathway in the absence of the confining optical dipole trap (ODT) light; ② indicates the excited state pathway $\text{KRb} + \text{KRb} \rightarrow \text{K}_2\text{Rb}_2^* \rightarrow \text{K}_2\text{Rb}_2^{**}$, which is dominant at high ODT intensity. **B**, Steady-state K_2^+ (red squares) and Rb_2^+ (blue diamonds) ion counts at various ODT light intensities, normalized by the number of experimental cycles (~ 80 for each data point). **C**, Steady-state K_2Rb_2^+ (purple circles) ion counts at various ODT light intensities, normalized by the number of experimental cycles (~ 290 for each data point). The data in **B** and **C** are simultaneously fitted using the function that contains both linear and quadratic dependencies on intensity. (Insets) Timing schemes for the ODT (red) and the pulsed UV ionization laser (purple) used for the product and complex measurements. The blue dashed line represents the time-averaged intensity level, while the black dashed line represents the ODT intensity envelope for full depth modulation. **D**, K_2Rb_2^+ ion counts (purple circles) measured at different UV ionization delays with respect to the off edge of the “kill” pulse. The solid line shows a fit to the entire data set that yields a complex lifetime $\tau_c = 360 \pm 30$ ns.

complexes live long enough to be electronically excited by the very light (at 1064 nm) we use to confine the reactant KRb molecules. By studying the reaction in the presence of varying levels of the optical dipole trap (ODT) light intensity, we found that, in addition to the observed ground state reaction pathway (labeled as ① in Fig. 1A), there is a competing excited pathway (labeled as ②). Experimental evidence for this excitation is shown in Fig. 1B and C, where both the complex and product ion counts decrease monotonically as the ODT light intensity is increased. At a typical ODT intensity of 11.3 kW/cm^2 , the reaction is ~ 8 times as likely to proceed via the excited-state pathway as the ground-state pathway. This observation not only sheds light on the origin of the two-body loss widely observed in ultracold molecule experiments [3–7], but also provides an excellent way for us to directly measure the complex lifetime. Specifically, we first strongly reduce the complex population by exposing the KRb cloud to an intense 1064 nm light (“kill” beam), and then monitor its growth to a new steady-state value after the light is quickly switched off. In this case, the $1/e$ saturation time for the growth directly yields the complex lifetime, which we determined to be $360 \pm 30 \text{ ns}$ (see Fig. 1D). This agrees well to the calculated lifetime of $170 \pm 60 \text{ ns}$ based on RRKM theory using full-dimensional ab initio potential energy surfaces from our collaborators, Tijs Karman (Harvard ITAMP) and Hua Guo (UNM). The long complex lifetime, coupled with the observed photo-excitation pathway, opens up the possibility to spectroscopically probe the structure of the complex with high resolution and further elucidating the reaction dynamics.

Future Plans:

On the reaction products front, we are working towards a complete picture of how the products emerge from the chaos during the intermediate complex stage, with the goal of gaining information about the reaction dynamics complementary to what can be learned directly from the complex. Specifically, we are interested in whether the various product channels in our reaction will be populated in a statistical or non-statistical fashion. Here, a product channel denotes a specific partitioning of the energy release by the reaction into the products’ external and internal degrees of freedom. While the expected chaotic motion of the complex seems to suggest a statistical picture, the nuclear spin statistics and the orbital angular momenta of the products may lead to non-statistical outcomes [8]. The question can be answered by measuring both the kinetic and rotational energy distributions of K_2 and Rb_2 (vibrational excitations in the products are forbidden due to the low exothermicity of the reaction). We are working to map out the rotational energy/state distribution of the products in a quantum-state-specific manner using resonantly-enhanced multi-photon ionization.

References to publications of DOE sponsored research:

- (1) M.-G. Hu*, Y. Liu*, D. D. Grimes, Y.-W. Lin, A. H. Gheorghe, R. Vexiau, N. Bouloufa-Maafa, O. Dulieu, T. Rosenband, and K.-K. Ni. Direct Observation of Bimolecular Reactions of Ultracold KRb Molecules, *Science* 366, 1111 (2019)
- (2) Y. Liu*, D. D. Grimes*, M.-G. Hu*, K.-K. Ni Probing Ultracold Chemistry using Ion Spectrometry, *Phys. Chem. Chem. Phys.* 22, 4861-4874 (2020)
- (3) Y. Liu*, M.-G. Hu*, M. A. Nichols, D. D. Grimes, Tijs Karman, Hua Guo, K.-K. Ni. Steering ultracold reactions through long-lived transient intermediates, arXiv:2002.05140 (2020) [currently

under journal review]

Reference

- [1] M-G Hu, Y Liu, DD Grimes, Y-W Lin, AH Gheorghe, R Vexiau, N Bouloufa-Maafa, O Dulieu, T Rosenband, and K-K Ni. Direct observation of bimolecular reactions of ultracold krb molecules. Science, 366(6469):1111–1115, 2019.
- [2] Yu Liu, Ming-Guang Hu, Matthew A Nichols, David D Grimes, Tijs Karman, Hua Guo, and Kang-Kuen Ni. Steering ultracold reactions through long-lived transient intermediates. arXiv:2002.05140, 2020.
- [3] S Ospelkaus, K-K Ni, D Wang, MHG De Miranda, B Neyenhuis, G Quéméner, PS Julienne, JL Bohn, DS Jin, and J Ye. Quantum-state controlled chemical reactions of ultracold potassium-rubidium molecules. Science, 327(5967):853–857, 2010.
- [4] Tetsu Takekoshi, Lukas Reichsöllner, Andreas Schindewolf, Jeremy M Hutson, C Ruth Le Sueur, Olivier Dulieu, Francesca Ferlaino, Rudolf Grimm, and Hanns-Christoph Nägerl. Ultracold dense samples of dipolar rbc molecules in the rovibrational and hyperfine ground state. Physical review letters, 113(20):205301, 2014.
- [5] Xin Ye, Mingyang Guo, Maykel L González-Martínez, Goulven Quéméner, and Dajun Wang. Collisions of ultracold $^{23}\text{Na}^{87}\text{Rb}$ molecules with controlled chemical reactivities. Science advances, 4(1):eaq0083, 2018.
- [6] Philip D Gregory, Matthew D Frye, Jacob A Blackmore, Elizabeth M Bridge, Rahul Sawant, Jeremy M Hutson, and Simon L Cornish. Sticky collisions of ultracold rbc molecules. Nature communications, 10(1):1–7, 2019.
- [7] Jee Woo Park, Sebastian A Will, and Martin W Zwierlein. Ultracold dipolar gas of fermionic $^{23}\text{K}^{40}\text{Ca}$ molecules in their absolute ground state. Physical review letters, 114(20):205302, 2015.
- [8] David J. Nesbitt. Toward state-to-state dynamics in ultracold collisions: Lessons from high-resolution spectroscopy of weakly bound molecular complexes. Chemical Reviews, 112(9):5062–5072, 2012.

Chemical Kinetic Modeling of Combustion Chemistry

William J. Pitz, Charles K. Westbrook

Lawrence Livermore National Laboratory, P.O. Box 808, Livermore, CA 94550

pitz1@llnl.gov

1. Program Scope

We develop chemical kinetic reaction models to describe the combustion of hydrocarbons and other related fuels, including bio-derived fuels. The models also describe reactions important for the formation of emissions such as PAHs. These models are validated through comparisons between simulated and experimental results in carefully controlled laboratory-scale facilities including shock tubes, stirred reactors, flow reactors, premixed flames, diffusion flames, and rapid compression machines. After validation, these models are then used to understand more complex combustion phenomena in practical combustion systems. We identify particularly sensitive parts of these models and provide that information to other DOE/GPCP researchers who can use theory and new experiments to refine the kinetic models. We try to anticipate kinetic modeling needs of the DOE combustion community, so other researchers can have accurate models to assist in their own research projects. Our kinetic models are freely available at <https://combustion.llnl.gov/> and provide a valuable service to the combustion community.

2. Recent Progress

Our work has focused on developing and improving the chemical kinetic models of transportation fuels, including the formation of PAHs which are important precursors in the formation of soot emissions.

Development of an improved PAH model: An accurate and validated chemical kinetic model for PAHs is needed for use in simulating soot formation from the combustion of hydrocarbon and alternative fuels. At LLNL, a PAH mechanism was recently developed [1] with formation of aromatics up to 4 aromatic rings.

The updated PAH model was compared to experiments performed by Nils Hansen [1] in a counterflow burner at 700 Torr at Sandia National Laboratory. Allene and propyne flames are studied because hydrogen-abstraction reactions from these hydrocarbons lead to resonance-stabilized propargyl radical (C_3H_3), which has been identified as a main precursor for aromatic species in combustion processes. The flame structure was measured with a quartz microprobe and analyzed using high-resolution mass spectrometry with single-photon ionization employing synchrotron-generated vacuum-ultraviolet radiation. Results of the kinetic model are compared to measurements of benzene, and 2-4 ring PAHs in Fig. 1. The new PAH model simulates reasonably well the peak heights of these PAH species in allene and propyne flames.

One of the interesting findings of the study was the importance of the reaction of phenyl with propargyl radicals (C_3H_3) in the formation of indene and indenyl (Fig. 2-left). The rate constant expression for this key reaction was taken from the recent work of Morozov and Mebel [2]. The indenyl radical formed subsequently leads to the formation of naphthalene (Fig. 2-right) through methyl assisted ring expansion reactions. Reactions of PAH radicals with propargyl radical, followed by methyl assisted ring expansion facilitate formation of PAH's with six-member rings. Figure 3 shows the pathways for formation of phenanthrene from naphthalene from this reaction sequence.

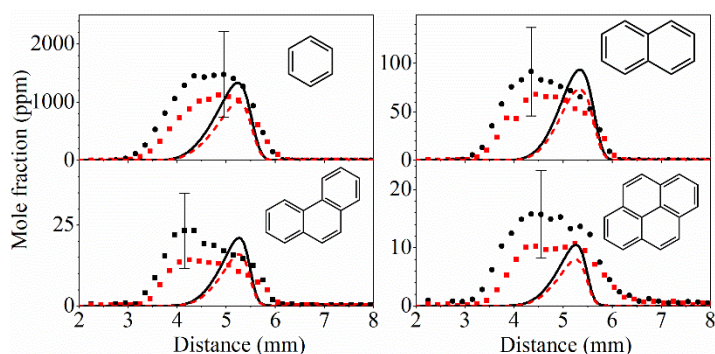


Figure 1: Comparison of the simulated (curves) and measured (symbols) mole fractions of isomers of benzene, naphthalene, phenanthrene, and pyrene in allene (black) and propyne (red) counter flow diffusion flames [1].

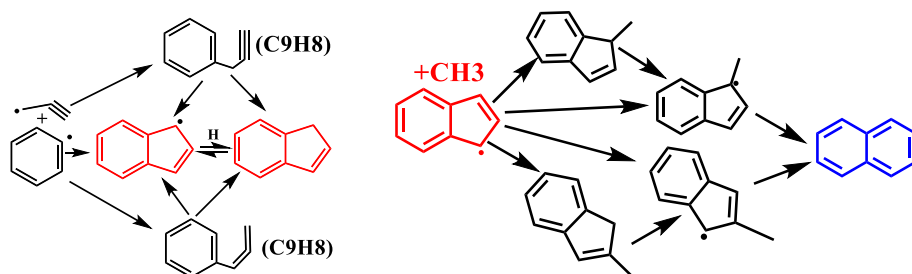


Figure 2: Formation of C_9H_8 (indene) and C_9H_7 (indenyl) from $C_6H_5 + C_3H_3$ reactions, and subsequent ring expansion reactions of indenyl radical with CH_3 to produce naphthalene.

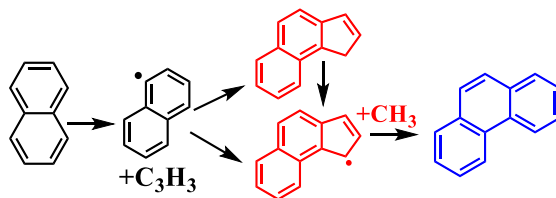


Figure 3: Pathways for formation of phenanthrene from naphthalene.

Development of accurate reaction-rate rules for the low temperature chemistry for alkanes:
 We are working on developing a more accurate description of the low temperature reaction paths and associated rate constants of alkanes. One potential missing part of these pathways is the network of reactions associated with the 3rd addition of O_2 . Most current mechanisms include two successive additions of O_2 , but not a 3rd addition. In a combined experimental, theoretical and kinetic-modeling study of Hansen et al. [3], we have added the reaction network of 3rd addition of O_2 to a neo-pentane kinetic model based on Bugler et al. [4] and simulated its effect in neo-pentane in a flow reactor, jet-stirred reactor (JSR), shock tube and rapid compression machine (RCM). Neo-pentane was chosen because of its unique symmetric molecular structure which results in only single keto-hydroperoxide (KHP) and keto-dihydroperoxide (KDHP) isomers. This feature helped to enable their identification in photoionization mass spectrometry experiments. We added reactions to include the formation of the dihydroperoxy-alkylperoxy radicals $[O_2P(OOH)_2]$ produced from 3rd O_2 additions to the kinetic model of neo-pentane. The rates used for formation and consumption of $O_2P(OOH)_2$ radical and KDHP are taken from analogous rates in [4]. The kinetic model predictions compared well with a quantitative analysis of KHP and the time-resolved

signal traces of KPH in the flow reactor. Also, computed KHP/KDHP mole fraction ratios from the model compared well with the experimentally determined signal ratios in the JSR. However, calculations showed that inclusion of the 3rd O₂ addition appears to be not substantially important for accurately predicting ignition delay times in a shock tube and RCM.

Reactions and thermodynamic properties for further fundamental study: Our work has identified reactions for further fundamental experimental and theoretical studies by DOE/GPCP and other researchers. For PAH chemistry, the following reactions need further study. The reaction of o-xylyl radical with acetylene is needed to evaluate how methyl substitutions at ortho position affect PAH growth. The reaction rates of 1-naphthyl radicals with ethylene should be determined for producing 1,2-dihydroacenaphthylene or vinyl naphthalene. The reaction of 1-methylnaphthalene radicals with acetylene needs to be investigated to understand the formation of phenalene-like species. A study on oxidation of phenyl acetylene and its radical with OH, O and O₂ radicals is warranted to examine the oxidation chemistry of ethynyl-PAHs. Reaction rates of acenaphthylene radicals with O and O₂ are needed to investigate the oxidation chemistry of cyclopentafused PAHs (e.g. acenaphthylene) produced from HACA mechanism.

3. Future Plans

In the future, we plan to continue our development of chemical kinetic models for fuel components present in gasoline, diesel and alternative fuels. We also will continue our work on the development of an accurate PAH kinetic model and soot model, and we plan to focus on the oxidation reactions of PAHs. Additionally, we intend further studies of allylic radicals.

Acknowledgements

This work was performed under the auspices of the U.S. Department of Energy by Lawrence Livermore National Laboratory under Contract DE-AC52-07NA27344.

References

1. G. Kukkadapu, S. W. Wagnon, W. J. Pitz and N. Hansen, "Identification of the Molecular-Weight Growth Reaction Network in Counterflow Flames of the C₃H₄ Isomers Allene and Propyne," Proc. Combust. Inst. (2020).
2. A.N. Morozov, A. Mebel, Theoretical Study of the Reaction Mechanism and Kinetics of the Phenyl+ Propargyl Association, Phys. Chem. Chem. Phys., (2020).
3. N. Hansen, G. Kukkadapu, B. Chen, S. Dong, H. J. Curran, C. A. Taatjes, A. J. Eskola, D. L. Osborn, L. Sheps, W. J. Pitz, K. Moshhammer, A. W. Jasper, W. Chen, J. Yang and Z. Wang, "The Impact of the Third O₂ Addition Reaction Network on Ignition Delay Times of neo-Pentane," Proc. Combust. Inst. (2020).
4. J. Bugler; B. Marks; O. Mathieu; R. Archuleta; A. Camou; C. Gregoire; K.A. Heufer; E.L. Petersen; H.J. Curran, An ignition delay time and chemical kinetic modeling study of the pentane isomers. Combust. Flame 163 (2016) 138-156.

Published papers in 2018 to 2020

1. G. Kukkadapu, S. W. Wagnon, W. J. Pitz and N. Hansen, "Identification of the Molecular-Weight Growth Reaction Network in Counterflow Flames of the C₃H₄ Isomers Allene and Propyne," Proc. Combust. Inst. (2020).

2. N. Hansen, G. Kukkadapu, B. Chen, S. Dong, H. J. Curran, C. A. Taatjes, A. J. Eskola, D. L. Osborn, L. Sheps, W. J. Pitz, K. Moshhammer, A. W. Jasper, W. Chen, J. Yang and Z. Wang, "The Impact of the Third O₂ Addition Reaction Network on Ignition Delay Times of neo-Pentane," *Proc. Combust. Inst.* (2020).
3. S. S. Nagaraja, J. Power, G. Kukkadapu, S. Dong, S. W. Wagnon, W. J. Pitz and H. J. Curran, "A single pulse shock tube study of pentene isomer pyrolysis," *Proc. Combust. Inst.* (2020).
4. C. Saggese, S. W. Wagnon, G. Kukkadapu, S. Cheng, S. S. Goldsborough and W. J. Pitz, "An improved detailed chemical kinetic model for butanol isomers and their blends with gasoline for engine-relevant conditions," *Proc. of The Combust. Inst.* (2020).
5. S. Cheng, D. Kang, S. S. Goldsborough, C. Saggese, S. Wagnon and W. J. Pitz, "Experimental and modeling study of C2-C4 alcohol autoignition at intermediate temperature conditions," *Proc. Combust. Inst.* (2020).
6. S. Dong, K. Zhang, P. K. Senecal, G. Kukkadapu, S. W. Wagnon, S. Barrett, N. Lokachari, S. Panigaphy, W. J. Pitz and H. J. Curran, "A comparative reactivity study of 1-alkene fuels from ethylene to 1-heptene," *Proc. Combust. Inst.* (2020).
7. G. Issayev, K. Djebbi, G. Kukkadapu, M. Mehl, S. W. Wagnon, W. J. Pitz and A. Farooq, "Experimental and kinetic modeling study of tetralin: a naphtho-aromatic fuel for gasoline, jet and diesel surrogates," *Proc. Combust. Inst.* (2020).
8. Fang, R., Kukkadapu, G., Wang, M., Wagnon, S.W., Zhang, K., Mehl, M., Westbrook, C.K., Pitz, W.J., and Sung, C.-J., "Fuel molecular structure effect on autoignition of highly branched iso-alkanes at low-to-intermediate temperatures: iso-octane versus iso-dodecane", *Combust. Flame* 214, 152-166 (2020).
9. Zhang, K., Lokachari, N., Ninnemann, E., Khanniche, S., Green, W. H., Curran, H. J., Vasu, S. S. and Pitz, W. J., "An Experimental, Theoretical, and Modeling Study of the Ignition Behavior of Cyclopentanone," *Proceedings of the Combustion Institute* 37 (1) (2019) 657-665.
10. Ahmed, A., Pitz, W. J., Cavallotti, C., Mehl, M., Lokachari, N., Nilsson, E. J. K., Wang, J.-Y., Konnov, A. A., Wagnon, S. W., Chen, B., Wang, Z., Kim, S., Curran, H. J., Klippenstein, S. J., Roberts, W. L. and Sarathy, S. M., "Small Ester Combustion Chemistry: Computational Kinetics and Experimental Study of Methyl Acetate and Ethyl Acetate," *Proc. Combustion Inst.* 37 (1) (2019) 419-428.
11. Kim, Doohyun, Westbrook, C.K., and Violi, A., "Two-stage ignition behavior and octane sensitivity of toluene reference fuels as gasoline surrogate", *Combust. Flame* 210, 100-113 (2019).
12. Westbrook, C. K., Mehl, M., Pitz, W. J., Kukkadapu, G., Wagnon, S. and Zhang, K., "Multi-Fuel Surrogate Chemical Kinetic Mechanisms for Real World Applications," *Physical Chemistry Chemical Physics* 20 (16) (2018) 10588-10606. An invited "Perspective" paper.
13. Wagnon, S. W., Thion, S., Nilsson, E. J. K., Mehl, M., Serinyel, Z., Zhang, K., Dagaut, P., Konnov, A. A., Dayma, G. and Pitz, W. J., "Experimental and Modeling Studies of a Biofuel Surrogate Compound: Laminar Burning Velocities and Jet-Stirred Reactor Measurements of Anisole," *Combustion and Flame* 189 (2018) 325-336.
14. Zhang, K., Banyon, C., Burke, U., Kukkadapu, G., Wagnon, S. W., Mehl, M., Curran, H. J., Westbrook, C. K. and Pitz, W. J., "An Experimental and Kinetic Modeling Study of the Oxidation of Hexane Isomers: Developing Consistent Reaction Rate Rules for Alkanes," *Combustion and Flame*, 206 (2019) 123-137.
13. Guzman, J., Kukkadapu, G., Brezinsky, K. and Westbrook, C., "Experimental and Modeling Study of the Pyrolysis and Oxidation of an Iso-Paraffinic Alcohol-to-Jet Fuel," *Combustion and Flame* 201 (2019) 57-64.
14. Westbrook, C. K., Sjöberg, M. and Cernansky, N. P., "New Chemical Kinetic Method of Determining RON and MON Values for Single Component and Multicomponent Mixtures of Engine Fuels," *Combust. Flame* 195 (2018) 50-62.
15. Padilla, R. E., Escofet-Martin, D., Pham, T., Pitz, W. J. and Dunn-Rankin, D., "Structure and Behavior of Water-Laden CH₄/Air Counterflow Diffusion Flames," *Combustion and Flame* 196 (2018) 439-451.

INVESTIGATION OF NON-PREMIXED TURBULENT COMBUSTION

Grant: DE-FG02-90ER14128

Stephen B. Pope & Perrine Pepiot
Sibley School of Mechanical & Aerospace Engineering
Cornell University, Ithaca, NY 14853
s.b.pope@cornell.edu, pp427@cornell.edu

1 Scope of the Research Program

The goal of this work is the development of computational approaches that allow our detailed knowledge of chemical kinetics to be applied to modeling and simulation of combustion devices. Towards realizing this goal, we have proposed a pre-partitioned adaptive chemistry methodology (PPAC) for use in LES/PDF simulations. PPAC generates a set of reduced models in an offline preprocessing stage, which are dynamically utilized at runtime based on the local composition. The methodology has been demonstrated in the context of a piloted turbulent diffusion flame. Research is currently focused on examining methods for generating the initial database used in the offline preprocessing stage to generate the reduced models. A related endeavor is the development of an online error control strategy to improve the robustness of PPAC for cases where the initial database is not completely representative of the compositions encountered at runtime.

2 Recent Progress

2.1 Development and performance characterization of a coupled PPAC-ISAT LES/PDF solver

Previously, we have combined PPAC with ISAT and showed that the combination gave encouraging results in the simplified Partially Stirred Reactor (PaSR) context [1]. In this work, we have proposed and implemented the steps necessary for the holistic integration of PPAC-ISAT in a LES/PDF framework. We show that PPAC-ISAT can be used to accelerate LES/PDF simulations of turbulent combustion within and beyond the reaction fractional step. More specifically, the computation of resolved scalar fields is modified to take into account the sparsity of the species mass fraction vector, the load balancing strategy is tailored to the specific case of multiple chemical representations, and the neglect of locally significant species is investigated and shown to be acceptable in this setting. The performance of the coupled PPAC-ISAT was examined in two different configurations used for simulating Sandia Flame D. A smaller simulation of domain was utilized to quantify the efficiency and accuracy of PPAC-ISAT in detail by examining the relative time, conservation and incurred errors for five different reduction error thresholds. Then, the performance of PPAC-ISAT was examined in a full-scale LES/PDF simulation for a single reduction threshold (Fig. 1). We showed that the coupled PPAC-ISAT LES/PDF captures the resolved mean and RMS profiles of temperature and major species mass fractions to within 2% and OH to within 5%, with a reduction in the average simulation wall clock time per time step of 39% over an ISAT implementation using the detailed mechanism.

2.2 Database generation

The efficient generation of a representative initial database is crucial to the success of PPAC. We recall that PPAC assumes that the samples included in the database are representative of the compositions encountered at runtime. Hence, there is a need for computationally efficient surrogate configurations, which can generate compositions similar to those encountered in turbulent combustion simulations. In this work, we have examined whether canonical 0D/1D models such as counterflow flames, which are used in conventional offline reduction, satisfy this requirement of emulating the compositions encountered in turbulent combustion simulations. Towards this end, we have developed a simple approach based on ISAT to quantify similarity between two sets of compositions. This technique has been utilized to examine whether a set of compositions extracted from a series of direct numerical simulations can be emulated by canonical 0D/1D simulations. Figure 2 shows quantitative results for whether compositions encountered in turbulent combustion simulations can be emulated using 1D counterflow flames and PaSR. Overall, we observe that a large fraction of compositions in the turbulent combustion simulation can be emulated by simple 1D counterflow flames. However, there are still some compositions in the turbulent combustion simulations that are not captured by such simple and efficient surrogates, indicating a need for on-the-fly error control.

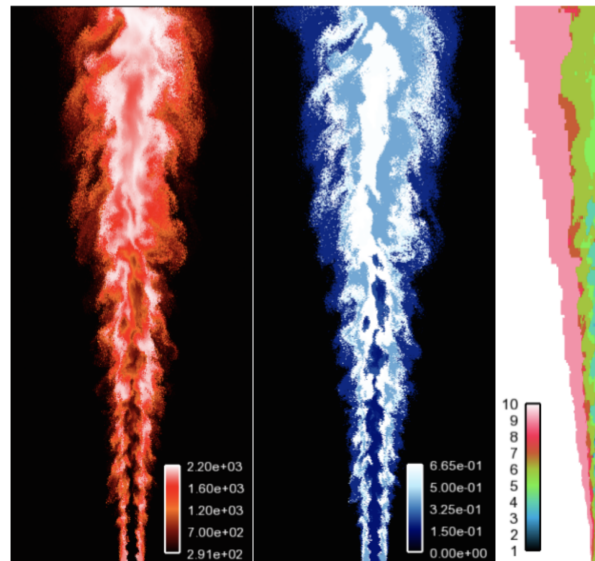


Figure 1: PPAC-ISAT simulation of Sandia Flame D - Instantaneous particle distribution in a cut of the Flame D domain, passing through the axis, colored by the particle temperature (left) and active reaction fraction (middle); most frequently used model at each combination of axial and radial grid locations for the same time instant, shown on a 2D cut plane passing the axis (right).

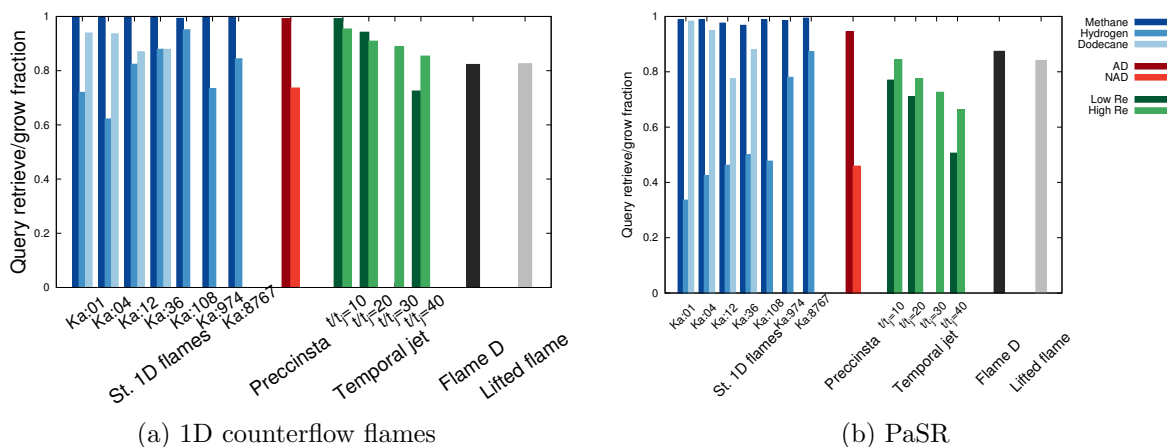


Figure 2: Quantitative estimates on whether compositions from turbulent combustion simulations can be emulated using simple canonical models such 1D counterflow flames (left) and PaSR (right).

2.3 Online error control strategy

We are working towards an online error control strategy based on the same aforementioned approach based on ISAT. Specifically, during the runtime stage, the ISAT-based approach is utilized to determine whether an encountered composition is similar to a sample in the database used in the offline stage. If this is the case, the usual PPAC approach is followed to resolve the encountered composition. However, if the composition is deemed to be dissimilar, the encountered composition is integrated using the detailed mechanism. We have tested this error control strategy in a simple PaSR context. The offline stage of PPAC is performed using a database generated with a mixing to residence time ratio of 0.1. This set of reduced models coupled with the

online error control strategy are tested for a PaSR with a mixing to residence time ratio of 0.25. The results for this test for the original PPAC implementation and error-controlled PPAC using different ISAT error tolerances are shown in Fig. 3, which shows the error incurred at runtime versus the reduction error threshold specified in the offline stage. We observe that without error control, PPAC incurs errors larger the threshold specified in the offline stage, whereas the error control strategy using the ISAT based approach is able to maintain the errors at runtime below the pre-specified threshold.

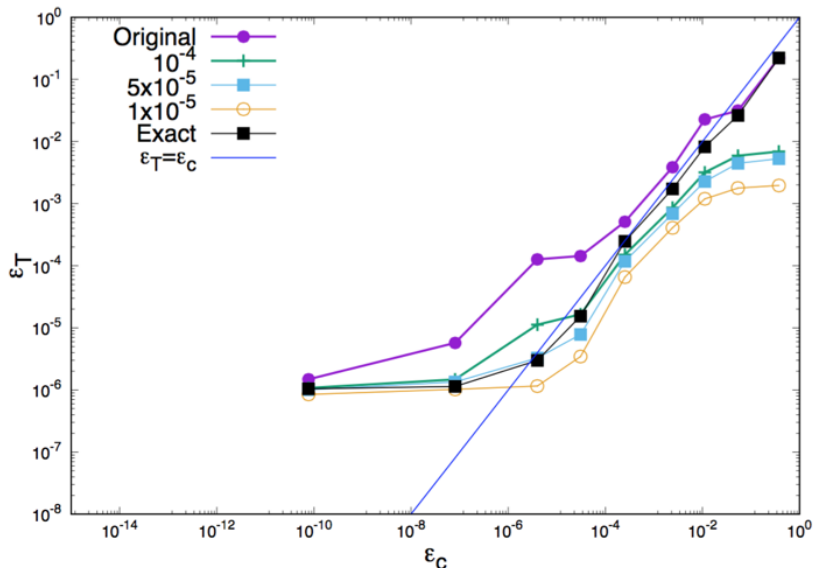


Figure 3: Incurred error at runtime versus the reduction error threshold specified in the offline preprocessing stage for the original implementation without error control and for PPAC coupled with an online error control strategy using ISAT based approach for different ISAT error tolerances.

3 Future Plans

Overall, we note that the efficient generation of the initial database coupled with an online error control strategy makes PPAC a highly capable and general technique that can enable predictive LES/PDF computations at a significantly reduced computational cost. Future work will be geared towards a more in-depth exploration of these two avenues. The specific aspects that are the focus of ongoing work are detailed below:

3.1 Database generation

As part of this work thus far, we have only examined a single metric for the similarity for the entire database. A closer examination is being pursued to gauge the type of the composition

in the turbulent combustion simulations that cannot be emulated using simple canonical 0D/1D simulations and possibly exploring the reasons for this lack of similarity.

3.2 Error-control

The use of the detailed mechanism for integrating the dissimilar compositions is a viable strategy only if the number of such compositions is small and they can be accurately identified without severe safety margins. Ongoing work is focused on refining the ISAT-based approach to accurately identify dissimilar compositions. Finally, the error control strategy needs to be generalized for cases where the database is not at all representative of the compositions encountered at runtime. In other words, a large fraction of the compositions encountered at runtime are dissimilar to the database. A possible recourse in this scenario is redoing the offline stage of PPAC using compositions collected at runtime. Although based on current evidence, such a scenario can be avoided by wisely choosing the initial database, a recourse for such an eventuality is necessary to make the error control strategy fail safe and universally applicable.

4 Publications from DOE Research 2018-2020

- A.S. Newale, S.B. Pope, P. Pepiot (2020) Computationally-efficient and accurate particle PDF simulations of turbulent combustion using coupled pre-partitioned adaptive chemistry and tabulation, Proceedings of the Combustion Institute, *accepted for presentation*.
- A.S. Newale, Y. Liang, S.B. Pope, P. Pepiot (2019) “A combined PPAC-RCCE-ISAT methodology for efficient implementation of combustion chemistry”, *Combust. Th. Modell.*, 23(6):1021–1053.
- A. Felden, B. Cuenot, L. Esclapez, P. Pepiot, E. Riber (2018) “Including analytically reduced chemistry (ARC) in CFD applications”, *Acta Aeronautica*, *accepted*.
- F. Tagliante, T. Poinso, L.M. Pickett, P. Pepiot, L.-M. Malbec, G. Bruneaux, C. Angelberger (2019) “A conceptual model of the flame stabilization mechanisms for a lifted Diesel-type flame based on direct numerical simulation and experiments”, *Combust. Flame* 201, 65 – 77.
- Jaravel, T., Riber, E., Cuenot, B., Pepiot, P. (2018) “Large Eddy Simulation of the Sandia flame D using reduced mechanism for accurate pollutant prediction”, *Combust. Flame* 188, 180 – 198.

References

- [1] A.S. Newale, Y. Liang, S.B. Pope, and P. Pepiot. *Combust. Theory and Modelling*, 2019.

OPTICAL PROBES OF ATOMIC AND MOLECULAR DECAY PROCESSES

S.T. Pratt
Building 200, B-125
Argonne National Laboratory
9700 South Cass Avenue
Lemont, Illinois 60439
E-mail: spratt@anl.gov

PROGRAM SCOPE

The study of molecular photoabsorption, photoionization, and photodissociation dynamics can provide insight into how energy and angular momentum flow among the electronic, vibrational, and rotational degrees of freedom in isolated, highly energized molecules. This project is focused on these dynamics in small molecules, with the goal of determining the mechanisms of these decay processes and their product branching distributions. In addition to intramolecular dynamics, a second aspect of this work involves the determination of absolute photoabsorption and photoionization cross sections, as well as the general principles that determine them. The experimental approach uses both laboratory-based laser techniques for single- and multiphoton excitation of valence-shell processes, and facilities-based vacuum-ultraviolet (VUV) and x-ray techniques for the excitation of both valence-shell and inner-shell processes. The detection methods include mass spectrometry, photoion- and photoelectron-imaging, high-resolution photoelectron spectroscopy, photoelectron-photoion coincidence techniques, and VUV Fourier-transform absorption spectroscopy. Photoelectron imaging is also being explored for circular dichroism studies of photoelectron angular distributions as a means to characterize chiral molecules. Finally, time-domain experiments enabled by new VUV and x-ray free electron laser sources are being performed to complement ongoing frequency-domain work.

RECENT PROGRESS

The current effort is focused on three general areas: the photoabsorption and photoionization of alkynes and alkynyl radicals; the photoabsorption and photoionization of molecular nitrogen; and inner-valence and inner-shell spectroscopy of small polyatomic molecules, in particular species relevant to time-resolved studies using free-electron lasers. Over the past year, new experiments have been performed in the laboratory at Argonne and at the SOLEIL and MAX IV synchrotron facilities. The work at SOLEIL and MAX IV is performed with the team of researchers acknowledged below. I have also begun to develop collaborations to broaden my research to include time-resolved photoionization and photodissociation studies.

Photoabsorption and Photoionization of Alkynes and Alkynyl Radicals

In previous years, we have studied the photoionization of the resonance stabilized CH_3CCCH_2 isomer of C_4H_5 by using F atoms to abstract H atoms from 2-butyne, and characterizing the C_4H_5 by using imaging-photoelectron photoion coincidence techniques at the SOLEIL synchrotron. This past year, we extended this work to two additional resonance stabilized C_4H_5 radicals: $\text{CH}_2\text{CHCCH}_2$ (i- C_4H_5), and CH_3CHCCH . This work builds on and complements earlier studies of the C_4H_5 radicals by N. Hansen et al. [J. Phys. Chem. A **110**, 3670 (2006)] and M. Lang et al. [J. Phys. Chem. A **119**, 3995 (2015)]. Interestingly, when combined with our previous work, we find that H atom abstraction from 1-butyne, 2-butyne, and 1,3-butadiene leads to relatively pure preparations of CH_3CHCCH , CH_3CCCH_2 , and $\text{CH}_2\text{CHCCH}_2$, respectively, and thus we can record "pure" slow photoelectron spectra (SPES) and photoionization mass spectra (PIMS) for each of these isomers.

In contrast to the other precursors, H atom abstraction from 1,2-butadiene ($\text{CH}_3\text{CHCCH}_2$) can directly produce all three resonance-stabilized C_4H_5 radicals. As a result, the corresponding SPES and PIMS of C_4H_5 from 1,2-butadiene corresponds to a linear combination of the individual isomer spectra. In principle, the coefficients of these linear combinations could be used to extract the relative rates of the three H-atom abstraction reactions from 1,2-butadiene. However, the absolute photoionization cross sections of the three radicals are necessary to extract these rates. We have measured the photoionization cross section of the

CH₃CCCH₂ in our early study [Hrodmarsson et al., J. Phys. Chem. A **123**, 1521-1528 (2019)]. Unfortunately, for the precursors used to produce the CH₃CHCCH and CH₂CHCCH₂ radicals, F-atom addition to the precursor competed with H atom abstraction, precluding the use of our method to determine the absolute photoionization cross sections. Theoretical values for these cross sections exist [C. Huang et al., Combust. Flame **198**, 334-341 (2018)], but the calculated cross sections only include the direct ionization process, and the experiments show evidence for significant resonance structure. Because the inclusion of resonance structure in such calculations is quite challenging, our findings reinforce the need to develop and improve experimental methods for the determination of these cross sections.

We have also continued the study of closed shell alkyne molecules. In previous years, we have recorded a set of comprehensive absorption spectra of C2 to C6 alkynes. We are currently analyzing a set of spectra corresponding to the four isomers of hex-1-yne. These spectra show some striking trends that carry over to analogous sets of molecules, such as the four isomers of butanol, that contain the four different butyl groups. In the past year, Jasper and Harding have performed new calculations to aid the assignment of the spectra, and to help rationalize the systematics of the observations. While the theoretical predictions reproduce the observed systematic trends in the spectra, we are still working to develop qualitative arguments to explain the observed trends. We hope to complete this work later this year.

Photoionization of Molecular Nitrogen

I continue to work on the comprehensive analysis of the valence-shell photoabsorption and photoionization of molecular nitrogen. This work combines data from double-resonance studies in my laboratory at Argonne, synchrotron studies using photoabsorption and photoelectron-photoion coincidence techniques, and theoretical studies in collaboration with Ch. Jungen (Orsay). In collaboration with Ubachs (Amsterdam) and Jungen, experiments were planned to use the VUV Fourier Transform Spectrometer at SOLEIL to record the absorption spectrum of isotopically substituted ¹⁵N₂ across a broad energy range spanning the Rydberg manifold below the first ionization threshold and extending to above the N₂⁺ B ²Σ_u threshold. The combination of high resolution and accurate intensities afforded by this instrument will provide a valuable complement to our work on ¹⁴N₂, and enhance our ability to assign all of the structure in both isotopes. Beamtime had been approved and scheduled for March, 2020, but the SOLEIL facility was shut down days before the start of our run. We expect this beamtime will be rescheduled once operations resume. Travel restrictions have also slowed the collaboration on the theoretical aspects of this work.

In a collaboration with K. Ueda et al., we continue to analyze time-resolved pump-probe data on N₂ recorded at the FERMI free-electron laser. In this work, we prepared a wavepacket made up of several bound Rydberg states, and probed the wavepacket evolution as a function of time delay by using photoelectron imaging. This approach provided both the time-resolved electron energy and angular distributions. Working with A. Stolow (University of Ottawa) and his group, we completed a related study of electronic coherences in NH₃. In both cases, high-resolution photoabsorption data from our experiments at SOLEIL have aided the assignment and interpretation of the time-resolved data.

Inner-shell and inner-valence processes in methyl iodide and xenon difluoride

I have continued my collaboration with D. Holland (STFC, UK) and R. Forbes (SLAC) on the photoelectron spectroscopy of the inner-shell and inner-valence shells of methyl iodide. New papers were published on valence and 4d subshells, and on the Auger spectroscopy and shake-up satellites near the C 1s⁻¹ edge. The new experiments on XeF₂ focused on the Xe 3d⁻¹ and 4d⁻¹ absorption edges, and were motivated by our studies near the corresponding I edges of CH₃I, with a particular focus on how the different ligand geometries affected the structure in the ion-yield spectra and the photoelectron angular distributions. As an exploration of a new research direction, we also performed new measurements using high-resolution electron spectroscopy at the MAX IV synchrotron on the imidazole molecule. Imidazole is an aromatic five-member ring with two nitrogen atoms, and is present in many important biological building blocks, such as the amino acid histidine. Our initial work focused on the inner and outer valence-shell electronic structure and photoionization dynamics of imidazole between 20 and 100 eV, and included high-resolution measurements of photoelectron energy distributions and angular distributions. The goal of the work will be to try to unravel the vibronic interactions that mix the outermost electronic states of the molecule. This

work should have more general relevance for this whole class of bio-relevant molecules. Preliminary spectra were also recorded at the C $1s^{-1}$ and N $1s^{-1}$ edges. The data look very promising and we are planning on extending this work to the methyl-imidazoles in the future.

FUTURE PLANS

I will continue to investigate the photoionization of alkynes and small alkynyl radicals. In our previous studies on C_4H_5 , we saw evidence for the sequential abstraction of two or more H atoms from the precursor, and we have significant data on the SPES and PIMS of C_4H_4 and C_4H_3 species that has yet to be fully analyzed. New experiments, in which the conditions are optimized for the production of those species, should result in better signal-to-noise experiments and allow a more complete interpretation of the data. As discussed above, F addition reactions were also observed in the previous experiments, and more detailed studies may allow us to characterize these reactions more fully and subsequently allow us to determine the absolute photoionization cross sections of the C_4H_5 isomers. This work should also allow us to compare the absolute photoionization cross sections of the different C_4H_5 isomers. There appears to be a growing general interest in absolute photoionization cross sections of radicals. While theoretical cross sections are valuable, they typically only account for direct photoionization, and small radicals often have considerable resonant structure. We will explore cross section measurements in our laboratory at Argonne on C_4H_5 and other small radicals.

I will continue to work on a more comprehensive analysis of the photoabsorption and photoionization spectra of molecular nitrogen, bringing together results from laser-based double-resonance spectroscopy, synchrotron studies, and theory. As discussed above, new photoabsorption measurements on the $^{15}N_2$ isotope should provide considerable new insight into the analysis of many bands in the spectra. At this time, my collaboration with Jungen should be particularly valuable, as his multichannel quantum defect theory calculations will ultimately be essential for a global assignment of the data.

We will complete our analysis of our results on the inner-valence and inner-shell photoionization of XeF_2 . We have completed a series of papers on the inner-valence and inner-shell photoionization of CH_3I , and we expect that this work will be useful in the interpretation of time-resolved studies with free-electron lasers. Our work near the C $1s^{-1}$ absorption edge raised questions about the role of spin-orbit interactions in the production of shake-up satellites. New experiments near the C $1s^{-1}$ edge of CH_3Cl and CH_3Br are planned to try to elucidate these spin-orbit effects. in the same region. Beamtime was scheduled in July, 2020, to use the soft x-ray, high-resolution photoelectron spectrometer at the PLEIADES beamline at SOLEIL perform these studies. Unfortunately, it now appears that this beamtime will also require rescheduling.

This past year, I led a proposal for beamtime at the FERMI free-electron laser. The unique aspects of this FEL, as compared to the LCLS and other FEL user facilities, is that it is focused on much lower photon energies, and that the beam is seeded. Our proposal is to characterize the evolution of electronic structure in acetylene following excitation to the A state of acetylene by using time-resolved photoelectron spectroscopy with the FEL as the probe. This work will begin to bring together our work on the photoabsorption and photoionization of alkynes with our developing interest in time-resolved techniques. The A state will be excited around 200 nm, and can decay by internal conversion to high vibrational levels of the electronic ground state, intersystem crossing into the triplet manifold, or isomerization to the vinylidene structure. The use of a 16 eV probe enabled by the FEL should allow the observation of all of these potential decay channels, and provide new insight into the dynamics of this fundamental molecule. The proposal process is highly competitive, as beamtime is limited, but our proposal was recently approved. Unfortunately, the facility is currently shut down, and it is not clear when the beamtime will be scheduled. Nevertheless, we are excited about the prospects for these experiments when we are able to perform them.

ACKNOWLEDGEMENTS

I have been fortunate to collaborate with several teams of people on the experiments at SOLEIL, MAX IV, and FERMI. Work at Soleil was performed in collaboration with S. Boyé-Péronne and B. Gans (Institut des Sciences Moléculaires d'Orsay), J. -C. Loison (University of Bordeaux), D. M. P. Holland (STFC,

Daresbury), R. Forbes (SLAC), I. Powis (Nottingham), J. Bozek (SOLEIL), G. Garcia (SOLEIL), L. Nahon (SOLEIL), and N. de Oliveira (SOLEIL). Work at MAX IV was performed with Holland, Powis, and M. Patanen (University of Oulu). The previous work at FERMI was performed in collaboration with a large international group of researchers led by K. Ueda (Tohoku University, Japan). Theoretical work on N₂ was performed in collaboration with Ch. Jungen (Laboratoire Aimé Cotton). This work was supported by the U.S. Department of Energy, Office of Science, Office of Basic Energy Sciences, Division of Chemical Sciences, Geosciences, and Biological Sciences under contract No. DE-AC02-06CH11357.

DOE-SPONSORED PUBLICATIONS SINCE 2018

1. R. Forbes, A. De Fanis, C. Bomme, D. Rolles, S. T. Pratt, I. Powis, N. A. Besley, S. Nandi, A. R. Milosavljević, C. Nicolas, J. D. Bozek, J. G. Underwood, and D. M. P. Holland, Auger electron angular distributions following excitation or ionization of the I 3d level in methyl iodide, *J. Chem. Phys.* **149**, 094304 (2018).
2. R. Forbes, A. De Fanis, C. Bomme, D. Rolles, S. T. Pratt, I. Powis, N. A. Besley, M. Simon, S. Nandi, A. R. Milosavljevic, C. Nicolas, J. D. Bozek, J. G. Underwood, and D. M. P. Holland, Photoionization of the iodine 3d, 4s and 4p orbitals in methyl iodide, *J. Chem. Phys.* **149**, 144311 (2018).
3. A. Sen and S. T. Pratt, Double-resonance studies of electronically autoionizing states of molecular nitrogen, *Mol. Phys.* **117**, 2930-2940 (2019). DOI: [10.1080/00268976.2018.1544672](https://doi.org/10.1080/00268976.2018.1544672)
4. H. R. Hrodmarsson, J.-C. Loison, U. Jacovella, D. M. P. Holland, S. Boyé-Péronne, B. Gans, G. A. Garcia, L. Nahon, and S. T. Pratt, Valence-shell photoionization of the C₄H₅ radical, *J. Phys. Chem. A* **123**, 1521-1528 (2019).
5. B. Gans, G. A. Garcia, S. Boyé-Péronne, S. T. Pratt, J.-C. Guillemin, A. Aguado, O. Roncero, and J.-C. Loison, Origin band of the first photoionizing transition of hydrogen isocyanide, *Phys. Chem. Chem. Phys.* **21**, 2337-2344 (2019).
6. O. J. Harper, M. Hassenfratz, J.-C. Loison, G. A. Garcia, N. de Oliveira, H.R. Hrodmarsson, S. T. Pratt, S. Boyé-Péronne, and B. Gans, Quantifying the photoionization cross section of the hydroxyl radical, *J. Chem. Phys.* **150**, 141103 (2019) DOI: 10.1063/1.5091966
7. A. B. Trofimov, A. M. Belogolova, S. A. Serebrennikova, R. Forbes, S. T. Pratt, and D. M. P. Holland, An experimental and theoretical study of the C 1s ionization satellites in CH₃I, *J. Chem. Phys.*, **150**, 224303 (2019).
8. V. Makhija, K. Véyrinas, A. E. Boguslavskiy, R. Forbes, I. Wilkinson, R. Lausten, S. P. Neville, S. T. Pratt, M. S. Schuurman, and A. Stolow, Ultrafast molecular frame electronic coherences from lab frame scattering anisotropies, *J. Phys. B* (in press).
9. R. Forbes, S. T. Pratt, A. De Fanis, A. R. Milosavljević, C. Nicolas, J. D. Bozek, N. A. Besley, and D. M. P. Holland, Photoabsorption, photoionization, and auger processes at the carbon K-edge in CH₃I, *Phys. Rev. A* (in press).
10. R. Forbes, A. De Fanis, D. Rolles, S. T. Pratt, I. Powis, N. A. Besley, A. R. Milosavljević, C. Nicolas, J. D. Bozek, and D. M. P. Holland, Photoionization of the I 4d and valence orbitals of methyl iodide *J. Phys. B* (in press).

Reaction Mechanisms Studied with Chirped-Pulse Rotational Spectroscopy

Kirill Prozument
Argonne National Laboratory
Chemical Sciences and Engineering Division
Lemont, IL 60439
prozument@anl.gov

1. Scope of the Program

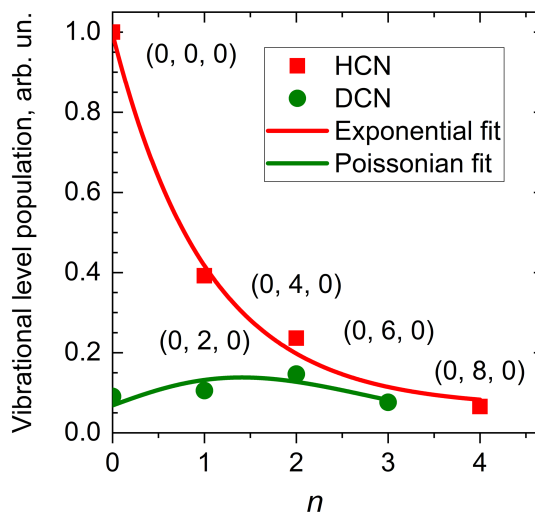
The goal of the Program is to gain detailed understanding of the dynamical processes that govern chemical reactivity. Oftentimes, the rates predicted for even simple reactions are in disagreement with experimental observations. The discrepancy may arise because such effects as roaming dynamics, tunneling reaction mechanism, lack of thermal equilibration of reaction intermediates and others are often neglected in kinetics models. We investigate the pyrolysis and photolysis reactions that help us reveal these mechanisms. We aim at generalizing our findings to broad classes of reactions. The experimental approach in this Program is based on chirped-pulse Fourier transform millimeter-wave (CP-FTmmW) spectroscopy. The reaction products are detected non-destructively, with quantum state specificity and time resolution. Because CP-FTmmW spectroscopy is also quantitative, branching ratios are measured and can be compared with theoretical models. The versatility of the CP-FTmmW technique is sufficient for its application to a wide range of experiments in reaction dynamics and kinetics in the gas phase. The program is currently focused of two experimental directions: i) investigation of pyrolysis chemistry in the microtubular reactor at 1000–1800 K, and ii) *in situ* time-resolved chirped-pulse spectroscopy of photoproducts at room temperature. The third direction of the Program is development of the Artificial Intelligence (AI) methods for automation of spectroscopic assignment. The need for that component is pressing as vast amounts of potentially useful spectroscopic data are generated in broadband rotational experiments, but rarely are fully analyzed. The goal of the AI thrust is that vast amounts of *spectroscopic* data becomes the *chemical* information, ready for reaction mechanisms discovery.

2. Recent Progress

Photodissociation Transition States Characterized by CP-FTmmW Spectroscopy

The transition state (TS), a hypersurface dividing the reactants and products in the phase space, is the most hidden aspect of a chemical reaction. Molecules are never stabilized at the TS and spend only $\sim 10 - 100$ fs in its vicinity. Yet, the structure of the potential energy surface near TS determines reaction rates, product branching, and energy distribution between the degrees of freedom of those products. The latter two observables are measured in our CP-FTmmW experiments with the goal of “back-engineering” some properties of the TS.

In this work, which is based on the spectra obtained by the PI in the group and under the supervision of Prof. Robert W. Field at MIT, we analyze the distributions of vibrational population between the levels of HCN and DCN that are the photolysis products of CH₂CHCN and CH₂CDCN, respectively.¹ In the Figure, one can see that the vibrational population distributions (VPDs) have obviously distinct behaviors. The HCN VPD is well approximated by an exponent, while the DCN VPD follows the Poisson-like function. The abscissa is $n = k/2$, where k is the number of quanta in the bending vibration of HCN or DCN. Deuteration of the parent vinyl cyanide helps revealing different mechanisms of the unimolecular elimination of DCN and HCN, which is evident from their distinct distributions of vibrational population in the bending mode (see the Figure).



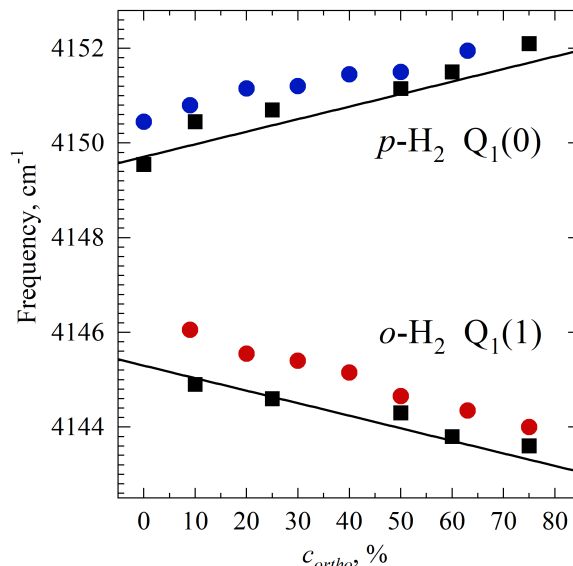
Why are these two VPD curves so different? We argue that they imprint the Franck-Condon-type overlap between the geometries of the H(D), C, N atoms (i) at the TS within the parent molecule and (ii) as a part of the linear H(D)CN molecule. For example, excess in the $\nu_2 = 4$ ($n = 2$) DCN bending mode population compared to its ground $\nu_2 = 0$ state population indicates that the D, C, N atoms are in a bent geometry ($\angle DCN < 180^\circ$) in the TS. Indeed, calculations point to existence of at least two such TS in 193 nm photodissociation of vinyl cyanide. On the other hand, $\nu_2 = 0$ is the most populated state in the HCN photoproducts. That is consistent with a near-linear position of the H, C, N atoms in that TS, the identity of which remains unknown. We speculate that the HCN responsible for the exponential VPD is a product of a bimolecular reaction in the jet.¹

Mixed ortho-H₂/para-H₂ clusters supercooled to 1–2 K investigated by vibrational Coherent anti-Stokes Raman Spectroscopy

Superfluidity is a fascinating macroscopic quantum effect that has been discovered by Kapitza in liquid helium-4 in 1938. Molecular hydrogen can be in two nuclear spin configurations, para-H₂ ($I = 0$), and ortho-H₂ ($I = 1$), both species being bosons. In 1972, Ginzburg and Sobyanin proposed a possibility of superfluidity in para-hydrogen if it is cooled below 6 K. Experimental evidence for superfluidity has been found in para-H₂ clusters using a probe OCS molecule by Vilesov and co-workers in 2000. During his Ph.D. studies, the PI has applied non-linear Raman spectroscopy to directly probe the state of para-H₂ clusters. If expanded with He gas, these clusters avoid freezing, which occurs at 13.8 K in bulk samples, and remain fluid even at 1 – 2 K.²

Here we have analyzed the data on ortho-H₂ clusters obtained by the PI at the University of Southern California under the supervision of Prof. Andrey F. Vilesov. The ortho-hydrogen nuclear spin configuration is a boson and can, in principle, be superfluid. Stronger interaction between the *o*-H₂ molecules and their higher degeneracy compared to *p*-H₂, diverted attention from *o*-H₂ in the search for molecular superfluidity. In this work, we show the evidence that ortho-hydrogen is also supercooled during the expansion with helium to 1 – 2 K, which is the realm of predicted superfluidity.³

The blue and red circles in the Figure show the vibrational frequencies of para-H₂ and ortho-H₂ molecules in supercooled clusters, respectively as measured by coherent anti-Stokes Raman scattering (CARS) spectroscopy.³ The squares are the corresponding frequencies in frozen clusters and the lines – those in the bulk. The data is given for different percentages of *o*-H₂ in the mixed *o*-H₂/*p*-H₂ clusters. The vibrational frequencies in both *p*-H₂ and *o*-H₂ in supercooled clusters are clearly blue-shifted from the frozen cluster (expansion without helium), which we attribute to their fluid state. This work does not provide an evidence of superfluidity in these *o*-H₂/*p*-H₂ clusters, but shows an experimental pathway to search for it. Also, in this work we have characterized the phases of these mixed clusters by analyzing the CARS spectra at various c_{ortho} . While the interior is comprised of uniformly mixed *o*-H₂ and *p*-H₂, there is an evidence that the outer shell is formed almost exclusively by *p*-H₂. These findings may serve as a benchmark for theoretical models aimed at describing many-body quantum systems.



Automated Identification of Molecules in Broadband Rotational Spectra

Previously, the PI and his postdoctoral associate Daniel Zaleski have demonstrated the potential of using machine learning to extract the rotational constants from broadband rotational spectra.⁴ The next challenge is to find an efficient way of predicting the likely chemical identity from those constants. While a molecular geometry gives rise to a unique rotational spectrum, we started an inquiry into whether a rotational spectrum may be attributed, within a given uncertainty, to more than one molecule. If the answer is no, or if the number of candidates is not large, then it is conceivable to use a machine learning tool trained on vast molecular databases to predict that unique molecule or a set of candidates from a rotational spectrum. The results obtained by the current postdoctoral associate Nathan Seifert and the PI suggest that for molecules containing up to 9 heavy atoms, but not taking into the account the conformers, and with a 2% uncertainty in the rotational constants ($B + C$), ($B - C$), A , and in the dipole moment, there is a unique molecular identity for a given rotational spectrum.

3. Future Plans

Continuing the time-resolved kinetic chirped-pulse (TReK-CP) experiments,⁵ we have extended the present spectrometer to 260 – 290 GHz range. With the new spectrometer, we plan to initiate H-atom abstraction reactions by OH or CN radicals (193 nm photolysis of H₂O₂ or NCCN) from hydrocarbons, alcohols, or aldehydes. Because rotational and vibrational relaxations can be directly observed and may play an important role in products branching, we anticipate a close collaboration with Ahren Jasper on this project.

We have established a collaboration with Michael Davis and are interested in exploring the optimal transport method developed by Davis to rapidly compare rotational spectra. Included in this work is the molecular inversion problem: extracting molecular specific information from spectra. Although there are some important projects underway elsewhere, we feel that optimal transport may provide a useful and more direct approach and its utility will be investigated.

References

¹ K. Prozument, J. H. Baraban, P. B. Changala, G. B. Park, R. G. Shaver, J. S. Muentner, S. J. Klippenstein, V. Y. Chernyak, and R. W. Field. Photodissociation transition states characterized by chirped pulse millimeter wave spectroscopy. *Proc Natl. Acad. Sci. U.S.A.* **117**, 146 (2020)

² K. Kuyanov-Prozument, and A. F. Vilesov. Hydrogen clusters that remain fluid at low temperature. *Phys. Rev. Lett.* **101**, 205301 (2008)

³ K. Prozument, B. G. Sartakov, and A. F. Vilesov. Mixed ortho-H₂ and para-H₂ clusters studied by vibrational coherent anti-Stokes Raman spectroscopy. *Phys. Rev. B*, accepted (2020)

⁴ D. P. Zaleski, and K. Prozument. Automated assignment of rotational spectra using artificial neural networks. *J. Chem. Phys.* **149**, 104106 (2018)

⁵ D. P. Zaleski, L. B. Harding, S. J. Klippenstein, B. Ruscic, and K. Prozument. Time-Resolved Kinetic Chirped-Pulse Rotational Spectroscopy in a Room-Temperature Flow Reactor. *J. Phys. Chem. Lett.* **8**, 6180 (2017)

DOE-Sponsored Publications Since 2018

D. P. Zaleski, and K. Prozument. Automated assignment of rotational spectra using artificial neural networks. *J. Chem. Phys.* **149**, 104106 (2018)

P. J. Weddle, C. Karakaya, H. Y. Zhu, R. Sivaramakrishnan, K. Prozument, and R. J. Kee. Boundary-Layer Model to Predict Chemically Reacting Flow within Heated, High-Speed, Microtubular Reactors. *Int. J. Chem. Kinet.* **50**, 473 (2018)

K. Prozument, J. H. Baraban, P. B. Changala, G. B. Park, R. G. Shaver, J. S. Muentner, S. J. Klippenstein, V. Y. Chernyak, and R. W. Field. Photodissociation transition states characterized by chirped pulse millimeter wave spectroscopy. *Proc Natl. Acad. Sci. U.S.A.* **117**, 146 (2020)

K. Prozument, B. G. Sartakov, and A. F. Vilesov. Mixed ortho-H₂ and para-H₂ clusters studied by vibrational coherent anti-Stokes Raman spectroscopy. *Phys. Rev. B*, accepted (2020)

ULTRAFAST CHEMISTRY: PROBES OF NON-ADIABATIC DYNAMICS

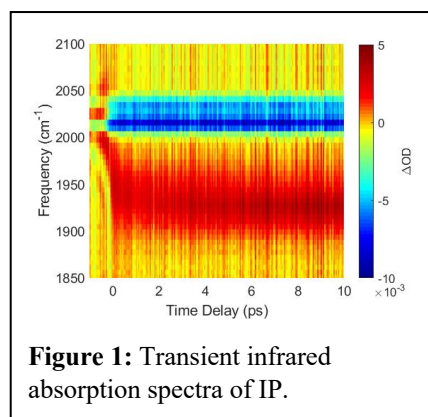
Krupa Ramasesha, Laura M. McCaslin, Leonid Sheps, Christopher J. Kliewer, Nils Hansen, Habib Najm
Combustion Research Facility, Mail Stop 9055; Sandia National Laboratories, Livermore, CA 94550
kramase@sandia.gov, lmmcass@sandia.gov, cjkliew@sandia.gov, lsheps@sandia.gov,
nhansen@sandia.gov, hnnajm@sandia.gov

I. Program Scope

This program aims to apply ultrafast spectroscopy to follow fundamental gas-phase chemical dynamics. The work develops probes to follow coupled electronic and nuclear motion on femtosecond to picosecond timescales in gas-phase molecules. The work in this task has strong connections to the laser spectroscopy investigated under the “Ultrafast Physics: Nonlinear Optical Spectroscopy and Diagnostics” task, and the high photon-energy techniques developed in the “Advanced Diagnostics” task. The coupling of electronic and nuclear degrees of freedom, representing a breakdown of the Born-Oppenheimer approximation, gives rise to complex pathways of non-radiative energy dissipation in electronically excited molecules, often involving participation of several electronic states. Identifying the motions that couple electronic states, the timescales and dynamics of excited state population relaxation, and the role of coupled vibrational modes of a molecule in guiding energy flow is crucial to our understanding of non-equilibrium dynamics, and it forms the mainstay of this program. This task extends the “Chemical Dynamics Methods and Applications” work down to the fundamental timescales of vibrational or electronic motion. *Ultrafast Chemistry* is one of the synergistic research themes of CSGB and this work addresses two key aspects of the Grand Challenges for Basic Energy Sciences: (1) investigating the nature of electronic excited states, and (2) exploring the breakdown of the Born-Oppenheimer approximation.

II. Recent Progress

Photodissociation dynamics of iron pentacarbonyl: Iron pentacarbonyl (IP, $\text{Fe}(\text{CO})_5$), a prototypical organometallic system, exhibits an optically bright electronic transition involving the transfer of an electron from the Fe 3d orbital to the CO π^* orbital, a metal-to-ligand charge transfer (MLCT). It is well known that MLCT excitation of gas phase IP at 266 nm causes rapid elimination of CO. A long-standing controversy has existed as to whether the CO is eliminated concertedly or sequentially following MLCT excitation.¹⁻² In an attempt to develop an unambiguous description of the photodissociation mechanism in IP, we performed ultrafast transient infrared absorption spectroscopy of gas phase IP following MLCT excitation at 260 nm. Infrared spectroscopy is particularly sensitive to the coordination state of IP because frequencies of the CO stretching vibrations of IP and smaller iron carbonyls are predicted to be different, with the vibration shifting to lower frequencies with every reduction in coordination.³ Furthermore, the frequency of free CO vibration of 2143 cm^{-1} is starkly different from the CO coordinated to iron. Transient infrared absorption spectra at different UV pump – IR probe time delays are displayed in Figure 1. Bleach at 2019 cm^{-1} and 2038 cm^{-1} appear immediately upon excitation. The 2019 cm^{-1} vibration corresponds to the equatorial CO stretching vibration, while the 2038 cm^{-1} feature corresponds to the axial CO stretching vibration. The bleach in this region is consistent with loss of ground state IP. An induced absorption is also seen that exhibits a frequency shift to lower frequencies with increasing pump-probe time delay. The broad lineshape centered at 1953 cm^{-1} at early times evolves to a narrow lineshape centered at 1930 cm^{-1} at longer times. The timescale for this evolution is 4.3 ps. *Ab initio* molecular dynamics (AIMD) calculations will predict the mechanisms and timescales for CO loss. These dynamical trajectories will be used to identify key structures along the reaction pathway for anharmonic vibrational analysis.



III. Future Work

Ultrafast photodissociation of dimethyl disulfide: Dimethyl disulfide (DMDS, CH_3SSCH_3) is a model system for the disulfide (S–S) bond, an important moiety in protein structure.⁴ Despite its central role in maintaining the structural integrity of proteins, the disulfide bond is photolabile with several electronic excited states proposed to be dissociative along the S–S and C–S bonds (see Figure 1).⁵⁻⁶ Photodissociation studies on the first excited state, $S_1(n\sigma^*_{\text{s-s}})$, of DMDS have found exclusive S–S bond fission⁷ with a dissociation lifetime of $\tau = 120$ fs.⁸ However, relatively little work has been done on the photochemistry of the higher lying electronic excited states near the DMDS absorption maximum at 195 nm. Photoexcitation of DMDS to these higher-lying states results in both S–S and C–S fission⁵ with final product state distributions indicative of at least some dissociation occurring on an electronic excited state.^{7,9} We have been awarded beam time at the MeV-UED facility at SLAC to probe the competing pathways of ultrafast photodissociation of DMDS following 200 nm excitation. This facility provides a unique opportunity to observe the rates of competing ultrafast bond dissociation in a molecule without interference from probe-induced fragmentation. The specific aims of this experiment are to determine the timescales of competing C–S and S–S bond fission in photoexcited DMDS, determine the relative quantum yields of each dissociation pathway, and explore the structural changes that drive internal conversion from the higher-lying electronic excited states to the lower-lying $n\sigma^*_{\text{s-s}}$ electronic states.

Intramolecular charge transfer in donor-bridge-acceptor systems: Excited-state dynamics in large conjugated molecules with extended π -orbitals are sensitive to the molecular structure, the nature of participating electronic orbitals, and interactions among electronic states and the surrounding environment. They often involve large-amplitude motion of atoms, coupled to intramolecular charge transfer (ICT). New computational approaches are being developed that include advanced functionals¹⁰ or ab initio methods, which treat both ICT and locally-excited states accurately, such as equation-of-motion coupled cluster (EOM-CC).¹¹⁻¹² These methods require validation by comparison to experiments that probe key regions of the excited-state PES and quantify the effects of electron correlation and non-adiabatic coupling. We propose measurements in jet-cooled molecules to map out the PESs and vibronic couplings of model compounds. As a platform for these studies we choose two prototypical push-pull molecules, para-nitroaniline (PNA) and 4-dimethylamino-4'-nitro-stilbene (DANS), both of which have donor-bridge-acceptor architecture with delocalized, partially overlapping molecular orbitals. Both molecules have nearly planar, polar S_0 states with dipole moments $\mu \sim 6.3$ and ~ 8 D. Both have excited states with local minima in which the NO_2 acceptor group is turned 90° out-of-plane, resulting in very strong charge transfer character (twisted ICT, or TICT).¹³ This coupling of large-range molecular motion to strong charge transfer implies numerous avoided crossings of electronic states with differing charge distribution. We will probe the excited-state ICT dynamics in PNA and DANS using femtosecond time-resolve photoelectron spectroscopy (TRPES) and core-level X-ray absorption spectroscopy. We will compare the experimental time-resolved photoelectron spectra and PADS to calculated values using advanced theoretical methods. A highly accurate theoretical description of the Franck-Condon region, including energy levels and PADS will be computed with EOM-CC methods¹¹⁻¹² in the program ezDyson.¹⁴ Core-level spectra will be calculated via EOM-CC methods with core-valence separation.

Probing cyclic azide formation: The azide radical (N_3) is the smallest polynitrogen compound and its $^2\Pi_g$ ground state has been quite extensively studied experimentally and theoretically.¹⁵⁻¹⁸ Other stationary points also exist on the ground doublet surface of N_3 , the most remarkable being a *cyclic*- N_3 (2B_1) minimum, 30.3 kcal mol⁻¹ above the $X^2\Pi_g$ state.^{16,19} *cyclic*- N_3 is an interesting molecule: It is a stable isomer needing 33.1 kcal mol⁻¹ of energy to dissociate into $\text{N}(^2D) + \text{N}_2(X^1\Sigma_g^+)$ and 31.9 kcal mol⁻¹ to overcome the barrier for isomerization to linear N_3 . There is accumulating experimental evidence concerning the formation of the *cyclic*- N_3 by photolysis of a suitable precursor.²⁰⁻²¹ Wodtke and coworkers observed the formation of N_3 products from CIN_3 photodissociation using velocity map ion imaging and photofragment translational spectroscopy. Synchrotron-based experiments revealed an

ionization energy of the high-energy form of N₃ 0.4-0.5 eV below the ionization of 11.06(±0.01) eV of the *linear*-N₃,²² in agreement with *ab initio* calculations of 10.595 eV for the *cyclic*-N₃.²³ We will apply ultrafast electron diffraction at SLAC for probing the structural evolution to *cyclic*-N₃ following UV photolysis of ClN₃, from the initial photodissociation to the isomerization of the N₃ radical to the cyclic conformation.

Statistical modeling of ultrafast electron diffraction: We propose to use statistical methods and theoretical computations for analysis and interpretation of experimental ultrafast electron diffraction (UED) measurements. We will use Bayesian statistical modeling of the system, and make use of associated hypothesis testing methods to aid interpretation of planned measurements with UED of dimethyl disulfide. Successful modeling of the experiment would provide means to progress towards optimal experimental design of future measurement campaigns with this instrument.

Treatment of Non-Adiabatic Effects in Ab Initio Molecular Dynamics: The difficulty of accurately treating molecular dynamics involving multiple electronic states is a well-known problem in chemical theory. When two or more electronic states are close in energy at a given molecular configuration, the Born-Oppenheimer (BO), or adiabatic, approximation breaks down, presenting many challenges for theories that rely on it. In the field of *ab initio* molecular dynamics (AIMD), a system's energy and nuclear forces are calculated on a single BO surface from *ab initio* electronic structure methods and the nuclear coordinates are propagated forward in time using Newton's equations of motion. In regions of the potential energy surface where multiple potential energy surfaces become close in energy, theories that can treat many surfaces must be used. An approach called “exact factorization” exactly separates the electronic and nuclear degrees of freedom of the wavefunction²⁴ without use of the BO approximation. This new formulation of the time-dependent Schrodinger equation can be approximated for semi-classical treatment of the nuclei, leading to a scalable non-adiabatic molecular dynamics approach. Proposed here is the development of a software package that uses the high-accuracy methods of equation-of-motion coupled cluster (EOM-CC) for on-the-fly AIMD,²⁵ which is not available in current non-adiabatic dynamics program packages. Initial studies will employ multiple spawning techniques for treatment of non-adiabatic effects due to the large computational expense of calculating derivative coupling elements. Exact factorization methods in the form of MQC-MD will be integrated into this software and employed for calculating chemical reaction mechanisms as well as quantitative reaction yields and timescales, as described in previous sections. In order to extend the system sizes and timescales studied, neural networks will be employed to fit the energies, gradients, and couplings of the relevant potential energy surfaces.

IV. References

1. Trushin, S.; Fuss, W.; Kompa, K.; Schmid, W., Femtosecond dynamics of Fe (CO) 5 photodissociation at 267 nm studied by transient ionization. *The Journal of Physical Chemistry A* **2000**, *104* (10), 1997-2006.
2. Banares, L.; Baumert, T.; Bergt, M.; Kiefer, B.; Gerber, G., The ultrafast photodissociation of Fe (CO) 5 in the gas phase. *The Journal of chemical physics* **1998**, *108* (14), 5799-5811.
3. Weitz, E., Transient infrared spectroscopy as a probe of coordinatively unsaturated metal carbonyls in the gas phase. *The Journal of Physical Chemistry* **1994**, *98* (44), 11256-11264.
4. Huxtable, R. J., Thiols, disulfides, and thioesters. In *Biochemistry of sulfur*, Springer: 1986; pp 199-268.
5. Larsen, M. A.; Skov, A. B.; Clausen, C. M.; Ruddock, J.; Stankus, B.; Weber, P. M.; Sølling, T. I., Putting the Disulfide Bridge at Risk: How UV-C Radiation Leads to Ultrafast Rupture of the S-S Bond. *ChemPhysChem* **2018**, *19* (21), 2829-2834.
6. Luo, C.; Du, W.-N.; Duan, X.-M.; Liu, J.-Y.; Li, Z.-S., Theoretical study on the excited states and photodissociation mechanism of dimethyldisulfide. *Chemical Physics Letters* **2009**, *469* (4-6), 242-246.

7. Lee, Y.; Chiu, C.; Lin, S.-M., Ultraviolet photodissociation study of CH₃SCH₃ and CH₃SSCH₃. *The Journal of chemical physics* **1994**, *100* (10), 7376-7384.
8. Schnorr, K.; Bhattacharjee, A.; Oosterbaan, K. J.; Delcey, M. G.; Yang, Z.; Xue, T.; Attar, A. R.; Chatterley, A. S.; Head-Gordon, M.; Leone, S. R., Tracing the 267 nm-induced radical formation in dimethyl disulfide using time-resolved x-ray absorption spectroscopy. *The journal of physical chemistry letters* **2019**, *10* (6), 1382-1387.
9. Nourbakhsh, S.; Liao, C. L.; Ng, C., A 193 nm laser photofragmentation time-of-flight mass spectrometric study of CH₃SSCH₃, SSCH₃, and SCH₃. *The Journal of chemical physics* **1990**, *92* (11), 6587-6593.
10. Autschbach, J., Charge-Transfer Excitations and Time-Dependent Density Functional Theory: Problems and Some Proposed Solutions. *ChemPhysChem* **2009**, *10* (11), 1757-1760.
11. Krylov, A. I., Equation-of-motion coupled-cluster methods for open-shell and electronically excited species: The hitchhiker's guide to Fock space. *Annual review of physical chemistry* **2008**, *59*, 433-462.
12. Stanton, J. F.; Bartlett, R. J., The equation of motion coupled-cluster method. A systematic biorthogonal approach to molecular excitation energies, transition probabilities, and excited state properties. *Journal of chemical physics* **1993**, *98* (9), 7029-7039.
13. Grabowski, Z. R.; Rotkiewicz, K.; Rettig, W., Structural changes accompanying intramolecular electron transfer: focus on twisted intramolecular charge-transfer states and structures. *Chemical reviews* **2003**, *103* (10), 3899-4032.
14. Gozem, S.; Krylov, A. I. ezDyson. <http://iopenshell.usc.edu/downloads/ezdyson>.
15. Haas, T.; Gericke, K. H., HIGH-RESOLUTION SPECTROSCOPY OF N₃ BY LASER-INDUCED FLUORESCENCE. *Berichte Der Bunsen-Gesellschaft-Physical Chemistry Chemical Physics* **1991**, *95* (10), 1289-1292.
16. Kerkines, I. S. K.; Wang, Z.; Zhang, P.; Morokuma, K., Structures and energies of low-lying doublet excited states of N-3 from accurate configuration interaction calculations. *Molecular Physics* **2009**, *107* (8-12), 1017-1025.
17. Wasilewski, J., Stationary points on the lowest doublet and quartet hypersurfaces of the N-3 radical: A comparison of molecular orbital and density functional approaches. *Journal of Chemical Physics* **1996**, *105* (24), 10969-10982.
18. Continetti, R. E.; Cyr, D. R.; Osborn, D. L.; Leahy, D. J.; Neumark, D. M., PHOTODISSOCIATION DYNAMICS OF THE N₃ RADICAL. *Journal of Chemical Physics* **1993**, *99* (4), 2616-2631.
19. Zhang, P.; Morokuma, K.; Wodtke, A. M., High-level ab initio studies of unimolecular dissociation of the ground-state N-3 radical. *Journal of Chemical Physics* **2005**, *122* (1).
20. Hansen, N.; Wodtke, A. M.; Goncher, S. J.; Robinson, J. C.; Sveum, N. E.; Neumark, D. M., Photofragment translation spectroscopy of ClN₃ at 248 nm: Determination of the primary and secondary dissociation pathways. *Journal of Chemical Physics* **2005**, *123* (10).
21. Samartzis, P. C.; Lin, J. J. M.; Ching, T. T.; Chaudhuri, C.; Lee, S. H.; Wodtke, A. M., The simplest all-nitrogen ring: Photolytically filling the cyclic-N-3 well. *Journal of Chemical Physics* **2007**, *126* (4).
22. Samartzis, P. C.; Lin, J. J. M.; Ching, T. T.; Chaudhuri, C.; Lee, Y. T.; Lee, S. H.; Wodtke, A. M., Two photoionization thresholds of N-3 produced by ClN₃ photodissociation at 248 nm: Further evidence for cyclic N-3. *Journal of Chemical Physics* **2005**, *123* (5).
23. Mozhayskiy, V. A.; Babikov, D.; Krylov, A. I., Conical and glancing Jahn-Teller intersections in the cyclic trinitrogen cation. *Journal of Chemical Physics* **2006**, *124* (22).
24. Abedi, A.; Maitra, N. T.; Gross, E. K., Exact factorization of the time-dependent electron-nuclear wave function. *Physical review letters* **2010**, *105* (12), 123002.
25. Malrieu, J. P.; Caballol, R.; Calzado, C. J.; de Graaf, C.; Guihery, N., Magnetic interactions in molecules and highly correlated materials: physical content, analytical derivation, and rigorous extraction of magnetic Hamiltonians. *Chemical reviews* **2014**, *114* (1), 429-492.

Photoinitiated Reactions of Molecules and Radicals in Molecular Beams

Hanna Reisler

Department of Chemistry, University of Southern California

Los Angeles, CA 90089-0482

reisler@usc.edu

Program Scope

The UV photochemistry of organic molecules is a fundamental process that governs reactions in the atmosphere, synthetic chemistry, organic aerosols, and biological damage in living tissues. The ensuing dynamics usually involve pathways that are in competition, such as direct dissociation on excited states, couplings to lower potential energy surfaces, isomerization, and secondary dissociation of products. This program is focused on detailed photochemical mechanisms of alpha-keto carboxylic acids. In the atmosphere, they are destroyed mainly by solar radiation but studying their photochemistry has been surprisingly difficult because of the complexity of their excited electronic states, the many energetically allowed dissociation pathways, and the effects of collisions and secondary reactions on final outcomes.

Recent Progress

Photodissociation of Pyruvic Acid at 193 nm

Pyruvic acid (PA), like other alpha-keto carboxylic acids, comprises a carbonyl, a carboxylic group, and an alkyl group, with the carbonyl serving as chromophore. Its most stable conformer, cis-keto, has an internal hydrogen bond that influences the evolution of its unimolecular decomposition. It is also known to have keto and enol tautomers. In a previous study we reported the dissociation dynamics of PA on the S_2 state in molecular beams using velocity map imaging (VMI). Here we describe a comprehensive study of the photodissociation dynamics of PA on the S_3 state carried out at 193 nm. Understanding the complex UV photochemistry of PA requires the use of different experimental approaches, and for this project we have used two complementary methods: (i) The time-sliced VMI instrument at USC is exploited to determine kinetic energy release of fragments, fast dissociation timescales, and internal state distributions of fragments for which Resonance Enhanced Multiphoton Ionization (REMPI) schemes exist; and (ii) The multiplexed photoionization mass spectrometer (MPIMS) setup developed at the Sandia Combustion Research Facility is used for product discovery (including isomers and tautomers), achieved by exploiting tunable narrowband VUV radiation at the Advanced Light Source (ALS), and to follow in time the subsequent unimolecular and bimolecular reactions of the products. The experiments described below have been performed in collaboration with Dr. David Osborn, Sandia Combustion Research Facility.

The MPIMS instrument, which employs tunable photoionization, allows the detection of products that are stable for longer than about a millisecond and enables quantitative determination of their mole fraction yields. The VMI technique is used to identify nascent products created in the collision-free environment of molecular beams but has been limited in this case to H and CO photofragments, which have efficient REMPI detection schemes. Using these two techniques, we have succeeded in observing all the major photodissociation products of PA: CO_2 , CO, H, OH, HCO, CH_2CO , CH_3O and CH_3 . Acetaldehyde and vinyl alcohol are minor products, but products that are known to arise from their dissociation, such as HCO, H_2CO and CH_4 , have been identified and their yields quantified. In Figures 1 and 2 we show representative examples, obtained with the MPIMS instrument, of ionization spectra of products and the kinetic time behavior of reactive radical products.

By using a multivariate analysis method to fit the percent mole fraction yields of 17 products, we are able to achieve a comprehensive description of the complicated photoinitiated chemistry of PA at 193 nm, albeit with some necessary simplifications to account for a few unobserved products. We recognize that a full kinetic model, which addresses all the intermediates and their bimolecular reactions with PA and

other photoproducts, is needed to capture the full reaction kinetics that takes place in the MPIMS flow tube. However, we believe that the twenty energetically allowed dissociation reactions that were used in the multivariate analysis to fit the products' yields provide the most complete reaction scheme proposed to date for the photodissociation of PA initiated on the S_3 state. See Table 1 for a list of contributing reactions and proposed mechanisms.

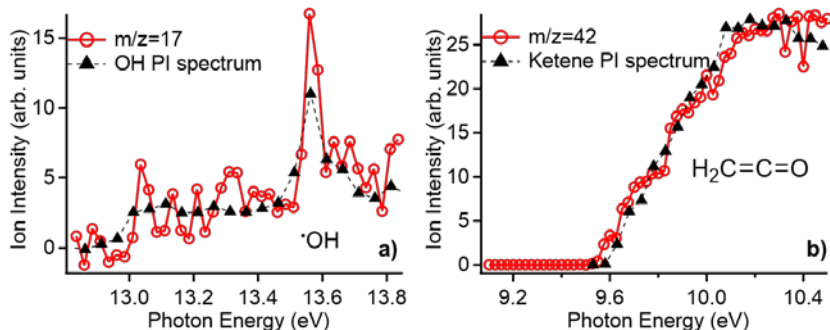


Fig. 1. Photoionization spectrum of (a) $m/z = 17$, and (b) $m/z = 42$ referenced to published spectra of the hydroxy radical and ketene.

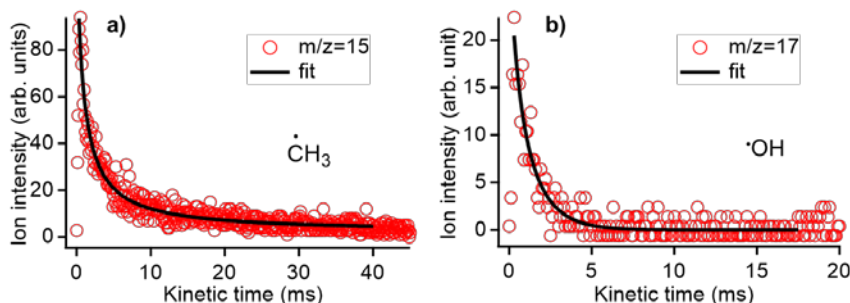


Fig. 2. Kinetic time traces and their decay fits of (a) methyl radical at 10.25 eV, and (b) hydroxyl radical at 13.25 eV.

The dissociation reactions that best fit most of the observed products and yields are rationalized on the basis of three dissociation mechanisms: (i) decarboxylation terminating in CO_2 primary products; (ii) Norrish type I dissociation typical of carbonyls; and (iii) O-H and C-H bond fission reactions generating H atoms. Consistent with previous observations, we also detected small yields of water and acetic acid but the mechanisms of their formation remain unclear.

One of the main conclusions of our work is that most of the participating dissociation reactions have more than two products. This is not surprising considering the large excitation energy of the 193 nm photon ($\sim 51,800 \text{ cm}^{-1}$), and fairly low energy required for the decarboxylation pathway ($14,000 \text{ cm}^{-1}$) and breaking the $\text{CH}_3\text{C}(\text{O})\text{-C}(\text{O})\text{OH}$ bond ($28,000 \text{ cm}^{-1}$). In addition, the low dissociation energies of CH_3CO , HOCO , and methylhydroxycarbene (CH_3COH), which are the major products of two-body fragmentation processes, facilitate their further dissociation. The underlying mechanisms (i) – (iii) are involved in three-body (and sometimes even four-body) fragmentation processes through (1) sequential dissociation of one or both primary products and (2) synchronous (or asynchronous) three-body dissociation of PA. Experiments with partially deuterated PA (CH_3COCOOD) support the interpretations.

The dissociation on S_3 is fast, as indicated by the angular anisotropy measurements of the CO ($v=1$) products displayed in Figure 3, but the roles of internal conversion and intersystem crossing to lower states are yet to be assessed. An intriguing issue concerns the probability of H-transfer from the carboxylic group to the ketonic CO group followed by decarboxylation, which is implicated in dissociation on S_0 and requires a 5-member cyclic transition state. If the dissociation on S_3 is fast and the available energy is

large, then H-transfer via a tight transition state would be less likely than synchronous (or asynchronous) three-body fragmentation processes. Dynamical calculations initiated on the S_3 potential energy surface are needed to determine the exact contributions of the proposed dissociation reactions and clarify the roles of lower electronic states.

Table 1: Reaction mechanisms, primary two-body steps, and final fragmentation reactions, their ΔH_{rxn} values, and percent contributions. A 193 nm photon supplies $51,800 \text{ cm}^{-1}$ of energy.

	Primary step	Fragmentation reaction	ΔH_{rxn} (cm^{-1})	% contribution
<i>Decarboxylation</i>	$\text{CH}_3\text{COH} + \text{CO}_2$	$\text{Ac} + \text{CO}_2$	-3,200	51
		$\text{VA} + \text{CO}_2$	890	
		$\text{CH}_4 + \text{CO} + \text{CO}_2$	-5,020	
		$\text{CH}_2\text{CO} + \text{H}_2 + \text{CO}_2$	5,900	
		$\text{CH}_3 + \text{HCO} + \text{CO}_2$	25,800	
		$\text{C}_2\text{H}_2 + \text{H}_2\text{O} + \text{CO}_2$	9,800	
		$\text{C}_2\text{H}_4 + \text{O}({}^3\text{P}) + \text{CO}_2$	35,700	
		$\text{CH}_2 + \text{H}_2\text{CO} + \text{CO}_2$	34,600	
<i>Norrish Type I Bond fission</i>	$\text{CH}_3\text{COCO} + \text{OH}$	$\text{CH}_2 + \text{CO} + \text{H}_2 + \text{CO}_2$	33,900	27
		$\text{CH}_3\text{CO} + \text{HOCO}$	28,600	
		$\text{CH}_3 + \text{CO} + \text{HOCO}$	31,400	
		$\text{CH}_3 + \text{CO} + \text{H} + \text{CO}_2$	32,000	
		$\text{CH}_3 + \text{CO} + \text{CO} + \text{OH}$	39,000	
<i>H fragmentation</i>	$\text{H} + \text{CH}_2\text{COCO} + \text{H}$	$\text{CH}_3\text{CO} + \text{CO} + \text{OH}$	37,600	9
		$\text{H} + \text{CH}_2\text{CO} + \text{H} + \text{CO}_2$	43,800	
		$\text{H} + \text{CH}_2\text{CO} + \text{HOCO}$	43,200	
<i>Others</i>	$\text{CH}_3\text{COCOO} + \text{H}$	$\text{CH}_3\text{CO} + \text{CO}_2 + \text{H}$	29,200	13
		$\text{CH}_3\text{COOH} + \text{CO}$	-1,000	
		$\text{CH}_2\text{CO} + \text{CO} + \text{H}_2\text{O}$	10,300	
		$\text{CH}_2 + \text{CO} + \text{CO} + \text{H}_2\text{O}$	37,300	

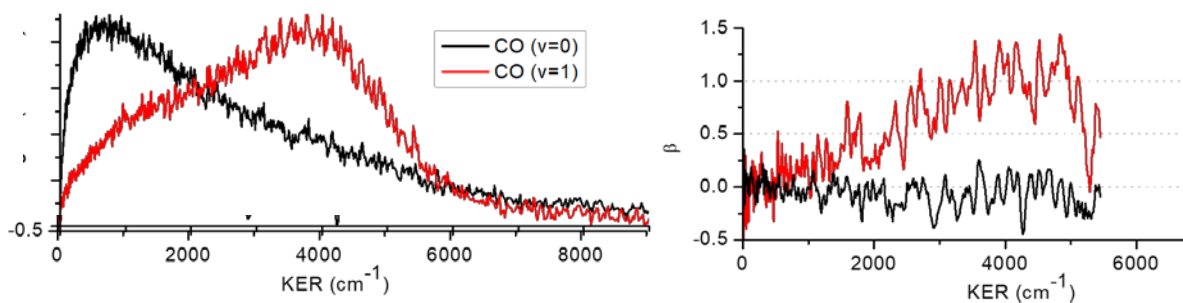


Fig. 3. KER distributions (left) and corresponding recoil anisotropy parameters β (right) of CO fragments in $v=0$ (black) and $v=1$ (red).

Future work

The work on the photodissociation of pyruvic acid will continue, and in the next year we will focus on analyzing the data and publishing the results acquired in experiments carried out at the ALS. These projects include a comprehensive study of the photodissociation of PA and partially deuterated PA at 351 nm, and the first identification of the elusive and short-lived methyldihydroxycarbene primary product and its more stable isomers, vinyl alcohol and acetaldehyde. PA is known to slowly react with water, and we plan to study this reaction, as well as other collisional effects. We will determine bimolecular reaction rates of short-lived species and detect reaction products by using tunable VUV at the ALS. The lifetime of the excited S_1 state will be determined using time-resolved fluorescence detection.

Publications 2017-2020

1. S. Sutradhar, B.R. Samanta, A.K. Samanta, and H. Reisler, "Temperature dependence of the photodissociation of CO_2 from high vibrational levels: 205-230 nm imaging studies of $CO(X^1\Sigma^+)$ and $O(^3P, ^1D)$ products", *J. Chem. Phys.* **147**, 013916 (2017).
2. B.R. Samanta, S. Sutradhar, R. Fernando, A.I. Krylov, A. I. and Reisler, "Electronic structure and Rydberg-core interactions in hydroxycarbene and methyldihydroxycarbene", *J. Phys. Chem. A* **122**, 6176-6182 (2018).
3. S. Sutradhar, B.R. Samanta, R. Fernando, and H. Reisler, "Spectroscopy and two-photon dissociation of jet-cooled pyruvic acid", *J. Phys. Chem. A* **123**, 5906-5917(2019).
4. B.R. Samanta, R. Fernando, D. Rösch, H. Reisler, and D.L. Osborn, "Looking at the bigger picture: Identifying the photoproducts of pyruvic acid at 193 nm" (submitted, 2020).

Ultrafast Transient Absorption Spectroscopy of Hydrocarbon Radicals

Melanie Reber
Department of Chemistry
University of Georgia, Athens, GA 30602
mreber@uga.edu

Project Scope

We aim to i) complete an ultrafast cavity-enhanced transient absorption spectrometer and incorporate two sources of radicals in molecular beams and ii) study the excited state dynamics of vinyl radical and allyl radical. The spectrometer consists of a home-built Ytterbium fiber laser frequency comb and Ytterbium fiber chirped-pulse amplification system that will generate ultrafast (about 100 fs pulse duration) pulses across much of the visible region. This light will be split into pump and probe beams and coupled into enhancement cavities housed in a vacuum chamber. Lock-in detection and noise subtraction techniques will be used during signal detection. With the increase in signal-to-noise with these techniques, it will be possible to perform ultrafast transient absorption spectroscopy in the visible and near-IR spectral regions of radical intermediates in molecular beams. The first goal is to demonstrate the ability to take ultrafast transient absorption spectroscopy of the electronically excited states of radical intermediates.

The second goal is to study the excited state dynamics of vinyl, C_2H_3 , and allyl, C_3H_5 , radicals. The first excited state of allyl radical exhibits a broad absorption and is thought to connect to the ground state through several conical intersections. The upper state lifetime is less than 5 ps and excitation of this state results in the release of a hydrogen atom through an unknown mechanism. Direct, time-resolved absorption spectroscopy could elucidate this mechanism. Similarly, the first excited state of vinyl radical has picosecond lifetimes, with a decrease in lifetimes with higher vibrational excitation. The frequency-resolved spectroscopy has the signature of ultrafast predissociation from the ground state. We hope to gain insight into these processes in vinyl radical with ultrafast transient absorption spectroscopy. This work will advance our knowledge of excited state processes in combustion intermediates and reactive species.

Recent Progress

We report on the progress since the funding period began in fall 2019. The major activities for this reporting period included i) design calculations and purchase of an excimer laser and associated optics, ii) design of differential pumping system, iii) molecular beam design, iv) completion of laser system, and v) completion of cavity-enhanced spectrometer. All of these activities are necessary to complete the first goal of the project of building an ultrafast transient absorption spectrometer to study radicals in molecular beams.

The combustion radicals will eventually be generated through photolysis, pyrolysis, and electrical discharge as a way to identify the desired signal. The photolysis source will be the first source implemented and the design is complete; the excimer laser and optical setup will be purchased with DOE support. The excimer laser will have about 100 mJ/pulse and 100 Hz repetition rate at 193 nm. It will pass through a window into the vacuum chamber as it is lightly focused on the molecular beam. This pulse power and repetition rate allow for sufficient flexibility for future photolysis experiments after generating vinyl and allyl radical for these studies.

The chamber that holds the optics needs to be maintained at near microTorr pressure levels to prevent contamination of optics and minimize cavity dispersion. The optical region is therefore

pumped by a turbomolecular pump. To accommodate the high gas flow of a molecular beam, the nozzle region will be pumped by a Roots blower. Then enhancement cavity beams must enter the molecular beam interaction region through small holes, rather than windows, to maintain the high-finesse of the optical cavity and minimize dispersion. The differential pumping system calculations and mechanical design are nearly complete and are being drawn up in Solidworks for fabrication by the UGA instrument shop. A cartoon version of the design is in Figure 1. There are multiple rectangular slit openings between the turbomolecular-pumped region and the Roots-blower pumped region. The slits are large enough to accommodate the multiple laser beams of the crossed enhancement cavities, but small enough to keep the pressure in the optical chamber near 10^{-5} Torr. The nozzle actuators are motorized to enable optimization of the molecular beam and cavity overlap while the system is under vacuum and are adjustable in the x-, y-, and z-directions. The photolysis nozzle is a continuous pinhole nozzle with switchable nozzle diameters.

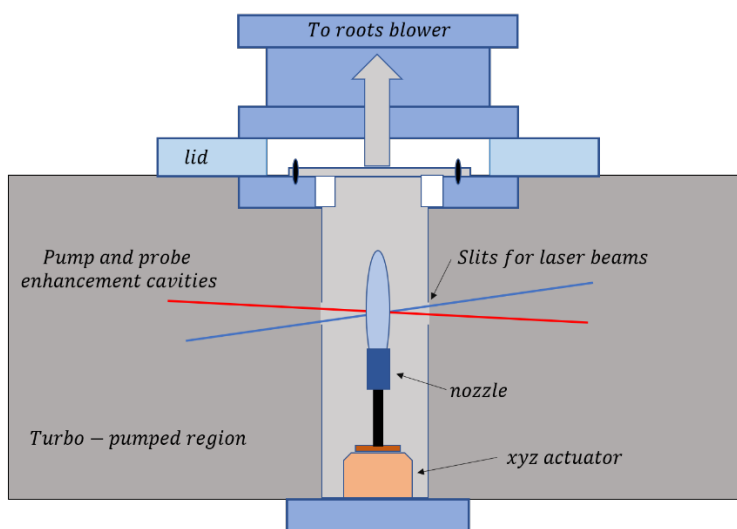


Figure 1. General layout of differential pumping system and molecular beam apparatus

The Ytterbium fiber laser system and chirped-pulse amplification system is operational and we are preparing a paper on a new feature of the Yb: fiber laser. We have frequency doubled the light and are optimizing the spectral broadening in a fiber. We therefore have the necessary visible light for first experiments on vinyl and allyl radical and are working on getting broader tunability. The cavity-enhanced spectrometer includes two enhancement cavities, locking electronics, and the detection scheme. While the locking electronics have been tested and the cavity is set up, they require the vacuum chamber to be complete before testing can finish.

Future Plans:

The ultrafast cavity-enhanced transient absorption spectrometer, once coupled with a photolysis source for generating combustion radicals, will be a powerful new tool for understanding combustion intermediates. Completion of the first phase of the spectrometer is expected within the next few months. We will then start with studying the time-resolved excited state spectroscopy of vinyl and allyl radical. Experiments with a wide range of combustion radicals are planned for the future as well as increasing the spectral range of the spectrometer to include the infrared and mid-infrared region.

Active Thermochemical Tables

Branko Ruscic
Chemical Sciences and Engineering Division, Argonne National Laboratory,
9700 South Cass Avenue, Lemont, IL 60439
ruscic@anl.gov

Program Scope

The *spiritus movens* of this program is anchored to the need of providing the scientific community with accurate and reliable thermochemical information on chemical species that are relevant in energy-generating chemical processes or play prominent roles in subsequent environmental chemistry. Detailed knowledge of thermodynamic parameters for a broad array of stable and ephemeral chemical species is pivotal to chemistry and essential in many industries. In particular, the availability of accurate, reliable, and internally consistent thermochemical values is a *conditio sine qua non* in kinetics, reaction dynamics, formulation of plausible reaction mechanisms, and construction of predictive models of complex chemical environments. In addition, the availability of accurate thermochemical values has historically been the prime driver for steady advancements of increasingly sophisticated electronic structure theories.

The aim of this program is to bring substantial innovations to the field of thermochemistry by developing new methodologies and utilizing them to the fullest in order to systematically improve both the quality and quantity of available thermochemical data relevant to energy-producing processes. In order to achieve the stated goals, this program has developed a novel approach that is centered on analyzing and optimally utilizing the information content of *all available* thermochemically relevant determinations, irrespective of whether they originate from experiment or from state-of-the-art theory. The aim is not only to dynamically produce the best currently possible thermochemical parameters for the targeted chemical species, but also to allow efficient updates when new knowledge becomes available, properly propagating its consequences through all affected chemical species, as well as to provide critical tests of new experimental or theoretical data, and generate pointers to new determinations that are most likely to efficiently improve the overall thermochemical knowledge base. In order to provide a broad perspective of this area of science, the effort of this program is synergistically coordinated with related experimental and theoretical efforts within the Gas-Phase Chemical Dynamics Group at Argonne.

Recent Progress

Over the past year we have continued the development of Active Thermochemical Tables (ATcT). Tersely, ATcT are a new paradigm for developing accurate and reliable thermochemical values for stable and reactive chemical species. Thermochemically relevant determinations, such as reaction enthalpies, equilibrium constants, bond dissociation energies, etc., by definition involve several chemical species, and thus define the enthalpy of formation of the target chemical species *relative* to other species. Consequently, rather than being directly measured quantities *per se*, enthalpies of formation are defined indirectly via complex manifolds of thermochemical dependencies. Historically, extracting the enthalpies of formation from intertwined (and frequently inconsistent) dependencies was an intractable proposition, resulting in a simplified *sequential* approach of inferring the enthalpies of formation one at the time (A begets B, B begets C, etc.), delivering static sets of derived values that contain hidden progenitor-progeny relationships and cannot be updated with new knowledge without introducing inconsistencies. The success of ATcT is rooted in treating the intertwined thermochemical determinations as a network of simultaneous dependences that is amenable to mathematical and statistical manipulation, converting the originally intractable problem to an information-rich environment that produces a quantum leap in the quality and reliability of the resulting thermochemistry. The underlying Thermochemical Network (TN) corresponds to a system of qualified constraints that must be simultaneously satisfied in order to produce enthalpies of formation that correctly reflect the epistemic content of the TN. Because of the unavoidable presence of determinations with ‘optimistic’ uncertainties (a.k.a. erroneous determinations), ATcT first performs an iterative statistical analysis, which isolates them and brings the TN to self-consistency. Once self-consistency is achieved, ATcT proceeds to solve the TN simultaneously for all included species.

Undeniably, the most significant vehicle for disseminating the ATcT results is the ATcT website, ATcT.anl.gov, which keeps growing in popularity as a reliable source of enthalpies of formation for species relevant in combustion and atmospheric chemistry, as well as other areas. Incidentally, ATcT now emerges as the top result (ahead of the venerable JANAF Tables) when the web is searched for “thermochemical tables” using Google. The number of website visitors is also steadily growing, currently attracting – with modest seasonal variations – a stream of 20,000 – 30,000 monthly visitors.

During the last year, we have publicly released two new versions of ATcT results. (Please note that all ATcT results are strictly versioned, and public versions that were released earlier remain permanently available on the website.) The most recent public version, ATcT TN ver. 1.122g, which was released in September 2019, covers 1617 chemical species. This version has been obtained by refinement of the predecessor ver. 1.122e, which was achieved by the inclusion of the results centered on the very accurate determination of the appearance energy of the methylium (CH_3^+) fragment from methane (collaborative effort with C.-Y. Ng, UC Davis). This significantly increased the accuracy by which $\text{D}_0(\text{H}-\text{CH}_3)$ is now known, enhancing - through various intertwined determinations in the TN - the overall accuracy of a significant number of other related thermochemical quantities in ATcT. Ver. 1.122e of the ATcT results has been in turn obtained by expansion of ver. 1.122d (1414 species), which was largely driven by the needs of a collaborative study that were related to combined experimental and theoretical activities involving the thermal decomposition of ester biofuels (using methyl acetate and methyl butanoate as examples), and which involved the members of the ATcT Task Force One (J. F. Stanton and his group at UF, T. L. Nguyen at UF, G. B. Ellison at UC Boulder, B. Changala at JILA, J. Baraban at Ben-Gurion).

Of course, during the past year we have continued to expand the coverage of the ATcT TN. The current developmental version, 1.122t, recently surpassed 2200 species, for an increase of more than 200 species with respect to the previous year. In order to define the thermochemistry of all these species, the TN now includes >27,000 active determinations (both from experiment and from high-level theory), as well as several thousand additional determinations that have been rendered obsolescent during previous ATcT TN analyses and improvements.

In parallel to the expansion of coverage of the ATcT TN, another important activity during the last year relates to improving the thermophysical properties (i.e. properties derivable directly from the partition function, such as heat capacity, entropy, enthalpy increment) of the species included in the ATcT TN. While the ubiquitous RRHO model is in many cases acceptable for approximate conversions of thermochemical properties between 0 and 298.15 K, it is demonstrably inadequate for extending these properties to temperatures relevant in combustion. We are currently in the process of systematically substituting the RRHO thermophysical properties with NRRAO properties. The latter rely on a two-pronged strategy that includes corrections accounting for the effects of vibrational anharmonicity, vibration-rotation interaction, centrifugal stretching, resonances, as well as low-temperature effects, using lengthy, but otherwise explicit expressions for rigid vibrational modes, and direct counts for large-amplitude motions. We are also exploring the possibility of making good use of classical phase-space integral approaches developed by other members of the Chemical Dynamics Group at ANL (A. Jasper).

We have also continued the activity related to cases where ostensibly extremely accurate experimental determinations (an illustrative example being combustion calorimetry of the condensed phase, combined with a determination of the vaporization enthalpy from vapor pressure measurements) imply a gas-phase enthalpy of formation that differs significantly from the prevailing theoretical value(s). In some cases, the nominal (though actually unwarranted) high accuracy of the suspect experimental data may overcome the cumulative statistical weight of mid-accuracy composite methods (such as G4, CBS-APNO, W1), thus dominating the final ATcT result. During the ATcT analysis, the red flag is typically raised by a tell-tale stubborn discrepancy between experiment and multiple theory, warranting further research. In two such recent cases (oxalic acid and hydrazine), the problem was resolved by performing additional highly accurate state-of-the-art composite electronic structure approaches (collab. with D. Feller, WSU).

We have a broad range of ongoing collaborations, both outside (nationally and internationally) and inside the Gas-Phase Chemical Dynamics Group at ANL. Here we would like to mention three collaborative

groups organized as ATcT Task Forces. The most active of the three is Task Force One (J. Stanton et al., UF, B. Ellison, UColorado), which maintains weekly meetings and was mentioned earlier in this abstract. Task Force Two (collab. with K. Peterson, WSU) is aiming to expand ATcT into actinides. The thermochemistry of uranium and the other actinides is particularly relevant for the separation techniques related to generation of nuclear power. Historically, the associated thermochemistry relied on difficult and frequently inconsistent experimental determination. However, with the advent of highly improved theoretical approaches for electronic structure computation of species containing heavy and ultra-heavy elements, ATcT is now in an excellent position to synergistically combine new theoretical determination with extant experimental measurements. Task Force Three (R. Dawes, MST) is aiming to help the systematic computational expansion of the ATcT TN to species relevant in combustion and atmospheric chemistry in a more efficient way than hitherto possible.

Future Plans

Future plans of this program pivot around further development and expansion of the Active Thermochemical Tables approach, continuing to provide accurate thermochemistry to the scientific community, and driving targeted thermochemically-relevant theoretical and experimental investigations of radicals and transient species that are intimately related to combustion and post-combustion atmospheric processes. A significant part of the effort will be focused on continued ‘finalization’ and dissemination of the resulting ATcT thermochemistry, typically involving groups of related chemical species. One important component of this process, focused on their enthalpies of formation, consists of testing and analyzing the TN dependencies, using tools such as the variance/covariance decomposition approach and analyses of the influence of relevant determinations via the hat-matrix, followed by improving the connectivity within the TN and adding new high-quality results (either virtual, i.e. computational, or actual, i.e. experimental) to coerce the resulting thermochemistry toward stable, ‘release quality’ values. This iterative process unavoidably results in an expansion of the TN with new related chemical species, which is an added benefit. Another equally important component focuses on enhancing the accuracy of the partition functions, typically by upgrading RRHO partition functions to NRRAO partition functions, which, as described above, is a currently ongoing effort. Future plans invariably incorporate a continuation of the current effort of expanding our web site (ATcT.anl.gov) that displays the ATcT thermochemistry together with pertinent metadata. The ever expanding set of metadata aims to accomplish a number of things, including the adequate documentation of the provenance of each thermochemical value, entailing a variance decomposition analysis for each of the chemical species. These, as well as other related activities may also become necessary in order to fully comply with the drafted characteristics of DOE SC Public Research Data Sets, given that ATcT is being currently considered as a candidate for this designation.

This work is supported by the U.S. Department of Energy, Office of Basic Energy Sciences, Division of Chemical Sciences, Geosciences, and Biosciences, under Contract No. DE-AC02-06CH11357.

Publications resulting from DOE sponsored research (2017 – present)

- *Active Thermochemical Tables (ATcT) Enthalpies of Formation Based on version 1.122g of the Thermochemical Network*, B. Ruscic and D. H. Bross, Argonne National Laboratory, Argonne, Ill. (2019); URL: <https://atct.anl.gov/Thermochemical%20Data/version%201.122g/>
- *High-Accuracy Extrapolated ab initio Thermochemistry. IV. A Modified Recipe for Computational Efficiency*, J. H. Thorpe, C. A. Lopez, T. L. Nguyen, J. H. Baraban, D. H. Bross, B. Ruscic, and J. F. Stanton, *J. Chem. Phys.* **150**, 224102/1-16 (2019); DOI: 10.1063/1.5095937
- *An Automated Thermochemistry Protocol Based on Explicitly Correlated Coupled-Cluster Theory: The Methyl and Ethyl Peroxy Families*, B. K. Welch, R. Dawes, D. H. Bross, and B. Ruscic, *J. Phys. Chem. A* **123**, 5673-5682 (2019); DOI: 10.1021/acs.jpca.9b04381
- *Active Thermochemical Tables: The Partition Function of Hydroxymethyl (CH₂OH) Revisited*, D. H. Bross, H.-G. Yu, L. B. Harding, and B. Ruscic, *J. Phys. Chem. A* **123**, 4212-4231 (2019); DOI: 10.1021/acs.jpca.9b02295 (*Hanna Reisler Festschrift*)
- *Thermochemistry*, B. Ruscic and D. H. Bross, *Comp. Aided Chem. Eng.* **45**, 3-114 (2019); DOI: 10.1016/B978-0-

- 444-64087-1.00001-2 (Ch. 1 in *Mathematical Modelling of Gas-Phase Complex Reaction Systems: Pyrolysis and Combustion*, T. Faravelli, F. Manenti, and E. Ranzi, Eds., Elsevier: Amsterdam 2019)
- *Active Thermochemical Tables (ATcT) Enthalpies of Formation Based on version 1.122e of the Thermochemical Network*, B. Ruscic and D. H. Bross, Argonne National Laboratory, Argonne, Ill. (2019); <https://atct.anl.gov/Thermochemical%20Data/version%201.122e/>
 - *Enthalpy of Formation of C₂H₂O₄ (Oxalic Acid) from High-Level Calculations and the Active Thermochemical Tables Approach*, D. Feller, D. H. Bross, and B. Ruscic, *J. Phys. Chem. A* **123**, 3481-3496 (2019); DOI: 10.1021/acs.jpca.8b12329
 - *A Master Equation Simulation for the •OH + CH₃OH Reaction*, T. L. Nguyen, B. Ruscic, and J. F. Stanton, *J. Chem. Phys.* **150**, 084105/1-8 (2019); DOI: 10.1063/1.5081827
 - *Toward Accurate High Temperature Anharmonic Partition Functions*, D. H. Bross, A. W. Jasper, B. Ruscic, and A. F. Wagner, *Proc. Combust. Inst.* **37**, 315-322 (2019); DOI: 10.1016/j.proci.2018.05.028
 - *Unimolecular Reaction of Methyl Isocyanide to Acetonitrile: A High-Level Theoretical Study*, T. L. Nguyen, J. H. Thorpe, D. H. Bross, B. Ruscic, and J. F. Stanton, *J. Phys. Chem. Lett.* **9**, 2532-2538 (2018); DOI: 10.1021/acs.jpcllett.8b01259
 - *Active Thermochemical Tables (ATcT) Enthalpies of Formation Based on version 1.122d of the Thermochemical Network*, B. Ruscic and D. H. Bross, Argonne National Laboratory, Argonne, Ill. (2018); URL: <https://atct.anl.gov/Thermochemical%20Data/version%201.122d/>
 - *Modeling Nitrogen Chemistry in Combustion*, P. Glarborg, J. A. Miller, B. Ruscic, and S. J. Klippenstein, *Progress Energy Combust. Sci.* **67**, 31-68 (2018); DOI: 10.1016/j.peccs.2018.01.002
 - *Time-Resolved Kinetic Chirped-Pulse Rotational Spectroscopy in a Room-Temperature Flow Reactor*, D. P. Zaleski, L. B. Harding, S. J. Klippenstein, B. Ruscic, and K. Prozument, *J. Phys. Chem. Lett.* **8**, 6180-6188 (2017); DOI: 10.1021/acs.jpcllett.7b02864
 - *Post-Transition State Dynamics and Product Energy Partitioning Following Thermal Excitation of the F··HCH₂CN Transition State: Disagreement with Experiment*, S. Pratihar, X. Ma, J. Xie, R. Scott, E. Gao, B. Ruscic, A. J. A. Aquino, D. W. Setser, and W. L. Hase, *J. Chem. Phys.* **147**, 144301/1-15 (2017); DOI: 10.1063/1.4985894
 - *Active Thermochemical Tables: The Adiabatic Ionization Energy of Hydrogen Peroxide*, P. B. Changala, T. L. Nguyen, J. H. Baraban, G. B. Ellison, J. F. Stanton, D. H. Bross, and B. Ruscic, *J. Phys. Chem. A* **121**, 8799-8806 (2017); DOI: 10.1021/acs.jpca.7b06221 (highlighted on the journal cover, see <https://pubs.acs.org/toc/jpcafh/121/46#>)
 - *Ab Initio Computations and Active Thermochemical Tables Hand in Hand: Heats of Formation of Core Combustion Species*, S. J. Klippenstein, L. B. Harding, and B. Ruscic, *J. Phys. Chem. A* **121**, 6580-6602 (2017); DOI: 10.1021/acs.jpca.7b05945
 - *Enthalpy of Formation of N₂H₄ (Hydrazine) Revisited*, D. Feller, D. H. Bross, and B. Ruscic, *J. Phys. Chem. A* **121**, 6187-6198 (2017); DOI: 10.1021/acs.jpca.7b06017
 - *Thermal Decomposition of Potential Ester Biofuels, Part I: Methyl Acetate and Methyl Butanoate*, J. P. Porterfield, D. H. Bross, B. Ruscic, J. H. Thorpe, T. L. Nguyen, J. H. Baraban, J. F. Stanton, J. W. Daily, and G. B. Ellison, *J. Chem. Phys. A* **121**, 4658-4677 (2017); DOI: 10.1021/acs.jpca.7b02639 (Veronica Vaida Festschrift)
 - *An Experimental and Theoretical Study of the Thermal Decomposition of C₄H₆ Isomers*, J. P. A. Lockhart, C. F. Goldsmith, J. B. Randazzo, B. Ruscic, and R. S. Tranter, *J. Phys. Chem. A* **121**, 3827-3850 (2017); DOI: 10.1021/acs.jpca.7b01186
 - *A Vacuum Ultraviolet laser Pulsed Field Ionization-Photoion Study of Methane (CH₄): Determination of the Appearance Energy of Methylum From Methane with Unprecedented Precision and the Resulting Impact on the Bond Dissociation Energies of CH₄ and CH₄⁺*, Y.-C. Chang, B. Xiong, D. H. Bross, B. Ruscic, and C. Y. Ng, *Phys. Chem. Chem. Phys.* **19**, 9592-9605 (2017); DOI: 10.1039/c6cp08200a (part of 2017 PCCP Hot Articles collection)
 - *Bond Dissociation Energies for Diatomic Molecules Containing 3d Transition Metals: Benchmark Scalar-Relativistic Coupled-Cluster Calculations for Twenty Molecules*, L. Cheng, J. Gauss, B. Ruscic, P. Armentrout, and J. Stanton, *J. Chem. Theory Comput.* **13**, 1044-1056 (2017); DOI: 10.1021/acs.jctc.6b00970
 - *Active Thermochemical Tables (ATcT) Enthalpies of Formation Based on version 1.122b of the Thermochemical Network*, B. Ruscic and D. H. Bross, Argonne National Laboratory, Argonne, Ill. (2017); URL: <https://atct.anl.gov/Thermochemical%20Data/version%201.122b/>

SPECTROSCOPIC INVESTIGATIONS OF MOLECULAR SYMMETRY BREAKDOWN

Trevor J. Sears

Department of Chemistry, Stony Brook University, Stony Brook, NY 11794-3400

trevor.sears@stonybrook.edu

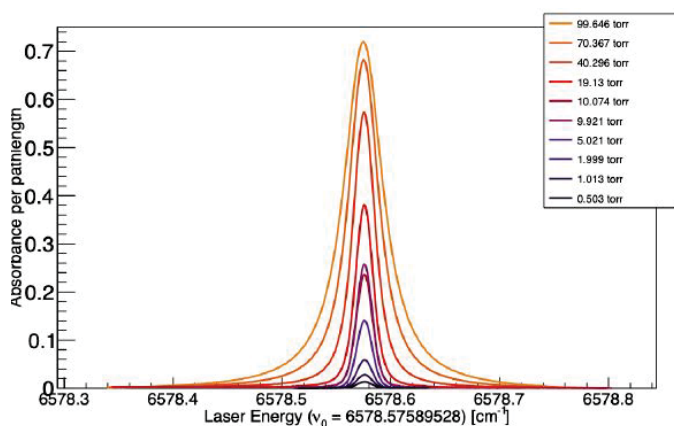
Program Scope

This project aims to make precise measurements of the spectra of small molecules to address fundamental questions in chemical physics in the realm of nuclear spin symmetries and their breakdown in molecules, and parity non-conservation caused by the weak nuclear force. Nuclear spin symmetry is intimately connected to parity in symmetrical molecules and plays a central role in the physical and chemical properties of symmetric molecules, their collisional relaxation, and the establishment of thermodynamic equilibrium in an ensemble. Such effects are present in every molecular system or process, but their small size means they are often only directly observable under special conditions. However, their measurement is of fundamental, and often practical importance, and strongly relates to the themes of coherence in light and matter in the recent Basic Energy Sciences Advisory Committee (BESAC) report “Challenges at the Frontiers of Matter and Energy: Transformative Opportunities for Discovery Science”.

I. Recent Progress

Precision Line Shape Measurements and Analysis

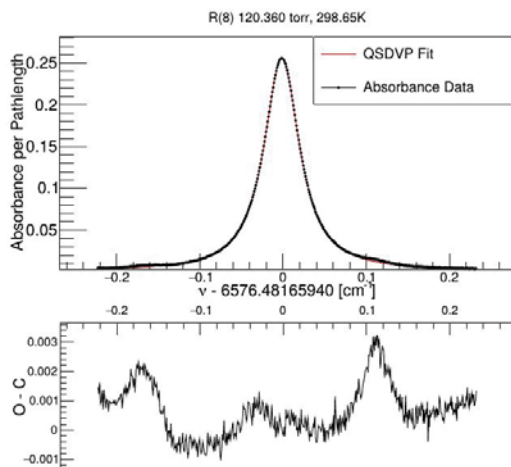
Following the report by Iwakuni et al. [Phys. Rev. Letts. **117**, 143902 (2016); **119**, 069402 (2017)]



of large (10%) alternation in the magnitudes of self-pressure broadening coefficients between the ortho- and para- nuclear spin states (odd and even J values) of ground state acetylene, we have remeasured the self-pressure broadening of the R(8) – R(13) rotational lines of the $\nu_1 + \nu_3$ band of pure acetylene gas in question. As described in more detail in last year’s report, the effect is possible if resonant rotational energy transfer between pairs of molecules in levels separated by $\Delta J = \pm 2$ have a significantly larger cross section than other inelastic interactions, and these can only occur in

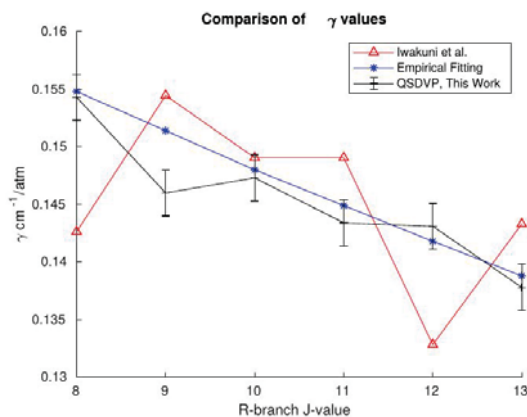
para-para or ortho-ortho collisions. Since population statistics favor the ortho-spin states, the total pressure broadening can be larger for ortho molecules. In the report, the R-branch lines we have measured showed the largest effects, hence our choice. Most of the new data was recorded using a free-running extended cavity diode laser as the spectroscopic source, but multiple calibration measurements were made with the same laser locked to a component of a frequency comb resulting in absolute frequencies and long-term optical frequency stability good to a few parts in 10^{11} . For the purposes of this work, the data recorded using a free-running laser were found to be adequate. Examples of the data for R(9) at a sequence of pressures are shown in the figure above. All the data were recorded in transmission at (measured) ambient temperatures. The figure shows the measured data converted to absorbance per pathlength in cm.

To analyze the new measurements, the effects of weak background absorption lines were subtracted out using line strengths from the Hitran database [I. Gordon, et al. *J. Quant. Spectros. Rad. Transf.* **203**, 3 – 69 (2017)] and assuming Voigt profiles. These hotband and low abundance isotopic lines have intensities of up to a few percent of the main lines in this region. A suite of Python programs was written to read the data files, collate files by transition, fit the data to a normalized line shape function, and present the resulting line profile parameters. The new code was based on previously published work from our group [D. Forthomme, et al. *J. Quant. Spectrosc. Rad. Transf.* **165**, 28–37 (2015)]. To gauge the effects of approximate models, various line profile models were used, from the simple Voigt convolution (VP) of a Gaussian (Doppler) and Lorentzian (pressure) profiles used by Iwakuni et al., to



a full Hartmann-Tran line profile (HTP) [H. Tran, et al. *J. Quant. Spectrosc. Radiat. Transf.* **129** 199–203 (2013)]. The HTP model has the advantage of including six physically meaningful parameters accounting for pressure broadening, shift, speed-dependent corrections to these quantities, and the frequency of velocity-changing collisions (VCCs) and a correlation between VCCs and hard (broadening) collisions in addition to the line strength factor. The model permits a sequential introduction or reduction of the smaller parameters to permit gradual and physically meaningful additions or reductions to the accuracy of the line profile model used, depending on the quality of the experimental measurements. After investigating the parameter space, we found the new data were adequately fitted using a

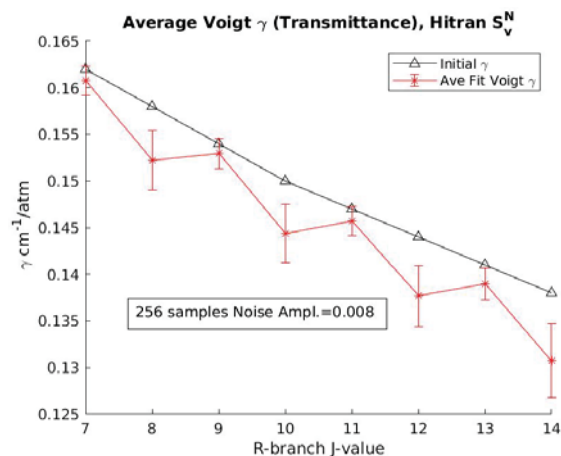
quadratic speed-dependent Voigt profile (QSDVP) which includes the broadening and shift parameters for the most probable molecular speed and quadratic (in speed)-dependent corrections to these two parameters, although the speed-dependent correction to the shift was found to be negligible for these data. The VP contains just the average broadening and shift parameters, and the additional parameter(s) in the QSDVP most importantly allow for the collisional narrowing, missing in the VP. Global fits of the sets of data corresponding to the same vibration-rotational transition at varying pressures and pathlengths were performed to extract the line profile parameters, in particular the broadening coefficients to compare to the controversial report of an ortho- para- variation.



An example of the data is shown in the figure above. The effects of inexact accounting for weak background line absorptions are easily seen and can be corrected by small adjustments to the (assumed) line strength factors. The resulting broadening parameters for the transitions in question, in units of $\text{cm}^{-1}/\text{atm}$ are plotted in comparison to those reported by Iwakuni et al. in red on the figure on the left. The dramatic “sawtooth” variation between odd (ortho- nuclear spin symmetry) and even (para-) rotational quantum number levels is not reproduced by our analysis.

The question arises as to how the data and/or the analysis of the original report could have led to the apparent variation in the broadening coefficient. The answer seems to lie in the approximate line shape model used in the analysis [Hartman and Tran, *Phys. Rev. Letts.* **119**, 069401 (2017)]. We have

investigated this further by using smoothly varying QSDVP line shape parameters to simulate the data of Iwakuni et al including the exact reported pressures and path lengths used in that work. Random Gaussian noise at a level estimated from the figures in their reports was added to the simulated spectrum and it was then fitted to a VP in the same way as in the original work. The calculations were repeated 256 times with new random errors of the same amplitude, applied to the data on each cycle. The fitted average VP broadening parameter (γ) and its RMS deviation is shown in the graph in comparison to the one (γ_0) appearing in the QSDVP simulated data. It is clear that the use of the



approximate VP results in the kind of ortho-para-broadening alternation reported. The effect is exacerbated by the extremely strong peak absorptions observed under the pressure and pathlength conditions of the work.

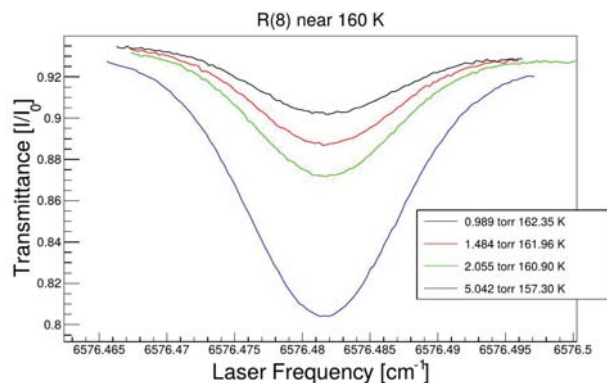
II. Future Work

A. Continued analysis of C₂H₂ Broadening Data

The frequency comb was repaired in late summer 2019 and the data recorded in the investigation of potential ortho- para- variations in pressure broadening coefficients discussed above is being augmented by new measurements at lower

temperatures. The temperature dependence of the broadening is of interest for both practical and theoretical reasons. We have built a new absorption cell that is cooled by a closed cycle helium refrigerator and some preliminary data for the same transitions has already been recorded, but work has come to a halt due to the Covid-19 pandemic.

Improvements to the spectrometer including more accurate pressure measurement, lower noise detectors and deeper laser amplitude modulation are in hand. An example of some recent low temperature data for the R(8) transition shown above at ambient temperature is shown in the figure on the left.



B. Nuclear Rotation-Vibration Splittings in CH₄

The development of the cryogenically-cooled cell mentioned above opens the way to beginning the work on methane in the near-IR proposed last year. Assuming the Covid-19 restrictions are at

least partially lifted in the summer, we plan to begin a series of measurements of the cold spectrum of CH₄ and mixtures of CH₄ in nitrogen that have relevance to the atmosphere of Titan, a satellite of Saturn. Aside from this practical interest, the low temperature data of methane will permit investigations of nuclear spin effects, such as differences in self-pressure broadening in the spectrum that have not been observed in ambient temperature spectra, despite decades of extensive high resolution studies,

As mentioned last year, we also propose to frequency measure nuclear spin splittings for the low-J transitions in the strong Q-branches of the 1.65 μm CH₄ 2 ν_3 band using the comb-referenced sub-Doppler saturation dip technique we demonstrated in our earlier work on NH₃. [Twagirayezu et al. *J. Chem. Phys.* **145**, 144302 (2016)] These new measurements will provide accurate rest frequencies

for features hidden under the Doppler profile in conventional spectra that are needed for accurate line shape modeling of observed spectra and remote sensing observations. They also lay the groundwork for higher resolution spectroscopic and dynamical measurements because the frequencies provide the information needed for experiments to produce and investigate non-equilibrium nuclear spin-state distributions. The targeted transitions in CH₄ have line strengths comparable to those for which extensive sub-Doppler measurements have been made in NH₃, so that the existing spectrometer can be used with minimal upgrades. Future improvements to the spectrometer such as installing higher quality cavity mirrors to permit more sensitive detection, will be carried out in parallel with these proposed measurements.

III. Publications related to this project since 2018

¹ Frequency measurements and self-broadening of sub-Doppler transitions in the $\nu_1 + \nu_3$ band of acetylene,

S. Twagirayezu, G. E. Hall and T. J. Sears, *J. Chem. Phys.*, **149**, 154308 (2018).

² Re-evaluation of ortho-para-dependence of self-pressure broadening in the $\nu_1 + \nu_3$ band of acetylene

E. C. Gross,¹ K. A. Tsang, and T. J. Sears, *J. Chem Phys*, (under review, April 2020).

Theoretical Studies of Potential Energy Surfaces and Computational Methods

Ron Shepard

Chemical Sciences and Engineering Division,
Argonne National Laboratory, Lemont, IL 60439
[email: shepard@tcg.anl.gov]

Program Scope: This project involves the development, implementation, and application of theoretical methods for the calculation and characterization of potential energy surfaces (PES) involving molecular species that occur in combustion, atmospheric, and general gas-phase chemistry. An accurate and balanced treatment of reactants, intermediates, and products for both ground and excited electronic states is required. This difficult challenge is met with general multiconfiguration self-consistent field (MCSCF) and multireference configuration interaction (MRCI) methods [see *Chem. Rev.* **112**, 108 (2012)]. More recently, the *graphically contracted function* (GCF) method has been developed to address some of the practical limitations of the traditional MCSCF and MRCI approaches, including the number of active electrons that may be accommodated and the overall expense associated with the study of larger molecular systems [see *J. Chem. Phys.* **141**, 064105 (2014) and references therein]. These methods are developed and maintained within the COLUMBUS Program System.

Recent Progress: GCF METHOD: In the GCF method the wave function is written as a linear combination of GCFs, and each GCF in turn is formally equivalent to a linear combination of configuration state functions (CSFs) that comprise an underlying linear expansion space of dimension N_{CSF} . The CSF coefficients that define the GCFs are nonlinear functions of a smaller number of essential variables $N_{\phi} \ll N_{\text{CSF}}$, and the formulation results in computational effort that depends only on the nonlinear parameters, not on the potentially much larger linear dimension. This nonlinear formulation has allowed, for example, expansions of $N_{\text{CSF}} > 10^{200}$ to be considered in the context of spin-density computation [*Int. J. Quantum Chem.* **109**, 3552 (2009)]. A fundamental difficulty with such large wave function expansions is that it is impractical to generate the complete list of CSF coefficients in order to analyze various features of wave functions and of molecular properties. We have in the past developed alternative analysis methods based on *arc density* and *node density* graphs [*Theor. Chem. Acc.* **133**, 1512 (2014)]. We are also examining approaches to extract the dominant CSFs from these large expansions. This is described in the next section.

Max-Flow Algorithm: An algorithm for computing the maximum-flow path in a network is applied to the identification of the dominant CSFs in a GCF wave function. The algorithm loops over the nodes of the arc density at each level, and, for each node, loops over its incoming arcs, of which there are at most four, determining an upper bound to the maximum possible incoming flow for that node. The maximum squared CSF coefficient is identified with the maximum possible incoming flow. A candidate walk with flow corresponding to the CSF is generated by backtracking from the graph head to the graph tail. The arc density contributions for that CSF walk are removed from the graph, and the

This work was performed under the auspices of the Office of Basic Energy Sciences, Division of Chemical Sciences, Geosciences, and Biosciences, U.S. Department of Energy, under contract number DE-AC02-06CH11357.

algorithm is applied to this updated graph. Each step of this process requires typically $O(n \log n)$ computational effort for n orbitals. This produces a sequence of CSF walks, usually in decreasing order of coefficient magnitudes. This list of generated walks can be partitioned using max-min bounds in order to guarantee the largest walks have been identified.

This max-flow algorithm has been applied to three states of the dissociation $C_2(X^1\Sigma_g^+, B^1\Delta_g, B'^1\Sigma_g^+) \rightarrow 2C(X^3P)$. The ACME MCSCF method [GPCP Abstracts, 163 (2019)] was used to optimize the core and valence orbitals. The 28^8 full-CI and 8^8 valence-full-CI curves, along with the dominant CSF curves are shown in Fig. 1. The valence-full-CI energies were computed by fully converging the GCF wave functions with respect to the facet counts. The dominant CSFs were extracted from the GCF wave functions at each bond distance, and the energies were computed and sorted in increasing order. Seven CSFs

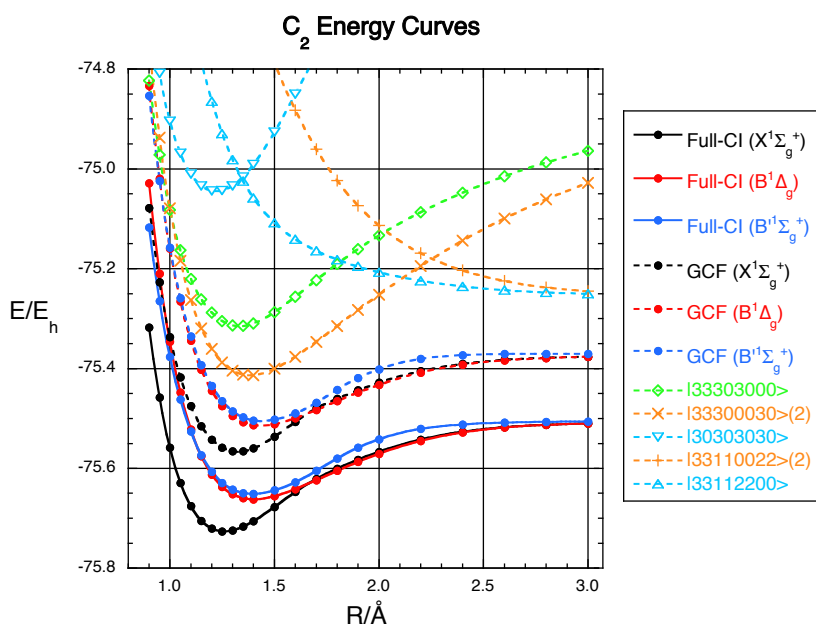


Fig. 1. 28^8 Full-CI curves, 8^8 Valence-Full-CI curves, and the dominant CSF curves with step-vector notation. The core orbitals are $(1\sigma, 1\sigma^*)$, and the valence orbitals are ordered as: $2\sigma, 2\sigma^*, \pi_x, \pi_x^*, \pi_y, \pi_y^*, 3\sigma, 3\sigma^*$.

were identified. The state energy curves may be divided into three regions. For $R < 1.15\text{\AA}$, the states are ordered from lowest to highest as X, B', and B. For $1.15\text{\AA} < R < 1.70\text{\AA}$, the states are ordered as X, B, and B'; this region includes the R_c distances for all three states. For $1.70\text{\AA} < R$, the states are ordered as B, X, and B', although the lower two states are almost degenerate in this region, and all three states approach exact degeneracy as $R \rightarrow \infty$. These regions may be understood from the crossings of the dominant CSFs. In particular, the crossing of the $|33303000\rangle$ CSF and the degenerate $|33300030\rangle$ and $|33003030\rangle$ CSFs accounts for the state ordering at short R distances. Then, the crossing of the $|33303000\rangle$ and $|33112200\rangle$ CSFs results in an avoided crossing of the $1\Sigma_g^+$ states; this crossing results in anomalous spacings of the vibrational energy levels for the X and B' states. Finally, the CSF crossing between the degenerate pair $|33300030\rangle$ and $|33003030\rangle$ and the degenerate pair $|33110022\rangle$ and $|33001122\rangle$ at $R = 2.25\text{\AA}$ results in the state ordering in the long R region. After this crossing occurs, the lowest energy CSFs in the long R region are completely distinct from the lowest energy CSFs in the R_c region. This gives rise to the asymptotic behaviors of the three states, and it shows that it is impossible to identify a

single CSF that could serve reliably as the reference wave function for a single-reference-based electronic structure calculation.

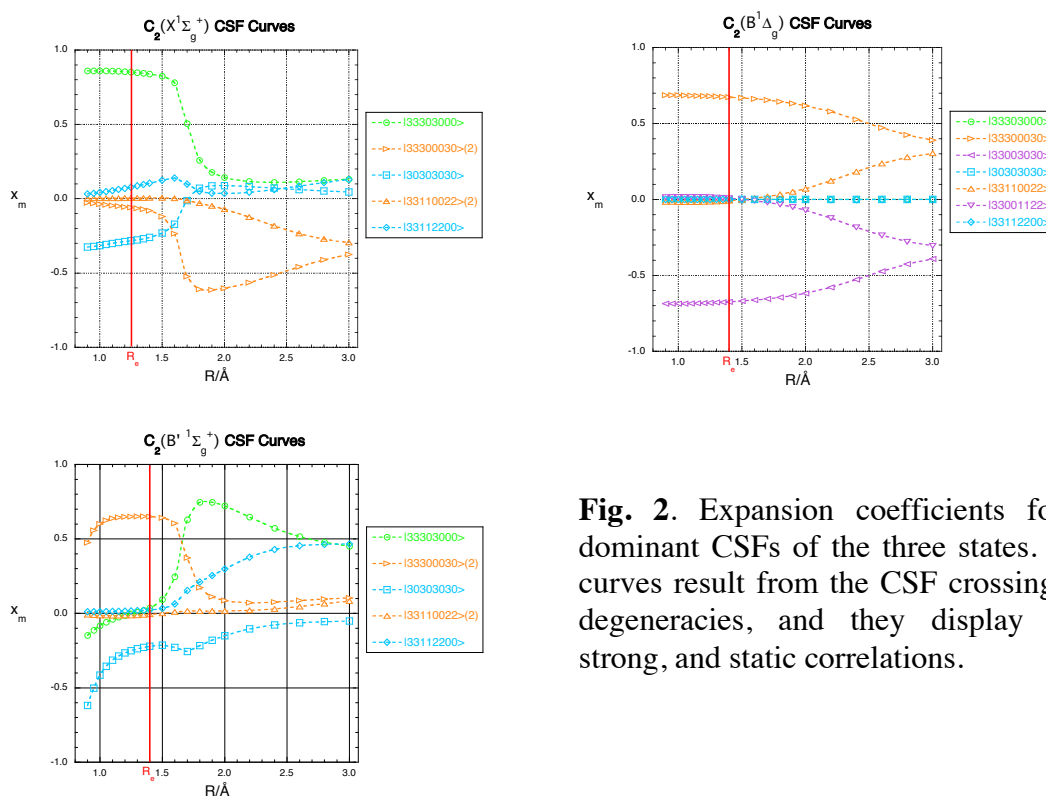


Fig. 2. Expansion coefficients for the dominant CSFs of the three states. These curves result from the CSF crossings and degeneracies, and they display weak, strong, and static correlations.

The CSF coefficients for the three states are shown in Fig. 2. The X state curves display strong correlation effects in the R_e region, the avoided crossing in the stretched R region, and static correlation in the long R region. The $|30303030\rangle$ coefficient is large in the short R region. This configuration becomes the dominant electronic configuration ($1s^2 2s^2 2p_x^2 2p_y^2 2p_z^2 3s^2$) of the Mg(X^1S) atom ground state, the 12-electron united-atom limit, but due in part to large ionic character, its importance decreases significantly at larger R distances.

The B state curves show a smooth transition from the Δ combination of the degenerate CSFs in the R_e region to the static correlation in the long R region. As for the other states, this static correlation is required for the correct description of the $2C(X^3P)$ fragments.

The B' state coefficients are complementary to the X state coefficients, which is partly a consequence of the orthogonality of the two states. In particular, the $|33303000\rangle$ coefficient in the R_e region is large for the X state and small for the B' state, and the Σ combination of the degenerate $|33300030\rangle$ and $|33003030\rangle$ CSFs is small for the X state and large for the B' state. At stretched R values, the importance of these configurations switches between the two states. The $|30303030\rangle$ coefficient is large at small R , but with

opposite sign relative to the degenerate pair compared to the X state, and as for the X state, its importance decreases at larger R distances. Static correlation is seen for long R values.

All of these max-flow results were verified with traditional CSF expansions. However, all of the steps involved in these calculations, the ACME MCSCF optimization of the orbitals, the optimization of the GCF wave function, and the application of the max-flow algorithm to extract the dominant CSFs, can be applied in principle to larger molecular systems with large valence orbital spaces that are too large to be practical, or even possible, for traditional MCSCF and MRCI electronic structure methods. This application to C_2 dissociation is a proof-of-principle calculation to demonstrate the capabilities of these new nontraditional methods. Further work is required to refine the CSF generation steps of the max-flow algorithm, and the compilation of the data necessary for Figs. 1-2 should require less manual effort.

Publications:

- “Recent Developments with the Multifacet Graphically Contracted Function Electronic Structure Method,” R. Shepard, Scott Brozell, Gergely Gidofalvi, *Abstracts of Papers of the American Chemical Society* **253**, 212-COMP (2017).
- “On the All Configuration Mean Energy Condition,” 59th Sanibel Symposium in Honor of Klaus Ruedenberg Proceedings, (2019).
- “The All Configuration Mean Energy Multiconfiguration Self-Consistent-Field Method I. Equal Configuration Weights,” R. Shepard and S. R. Brozell, *Mol. Phys.* **117**, 2374-2390 (2019). DOI: 10.1080/00268976.2019.1635275.
- “The All Configuration Mean Energy (ACME) MCSCF Method,” R. Shepard, S. R. Brozell, G. Gidofalvi, 7th Annual OpenMolcas Developers’ Workshop Book of Abstracts, 27 (2019).
- “Some Recent Applications of the Graphical Unitary Group Approach,” R. Shepard, S. R. Brozell, G. Gidofalvi, *The Utah Workshop on Quantum Methods in Molecular and Solid-State Theory Abstracts*, (2019).
- “Representations of Shavitt Graphs Within the Graphical Unitary Group Approach,” R. Shepard, S. R. Brozell, and G. Gidofalvi, *J. Computational Chem.* **41**, 129-135 (2020). DOI: 10.1002/jcc.26080.
- “An Arc Density Maximum Flow Algorithm,” R. Shepard, S. R. Brozell, J. Larson, P. Hovland, and S. Leyffer, 60th Sanibel Symposium Abstracts (2020).
- “The Generality of the GUGA MRCI Approach in COLUMBUS for Treating Complex Quantum Chemistry,” H. Lischka, R. Shepard, T. Müller, P. G. Szalay, R. M. Pitzer, A. J. A. Aquino, M. M. A. do Nascimento, M. Barbatti, L. T. Belcher, J.-P. Blaudeau, I. Borges Jr., S. R. Brozell, E. A. Carter, A. Das, G. Gidofalvi, L. Gonzalez, W. L. Hase, G. Kedziora, M. Kertesz, F. Kossoski, F. B. C. Machado, S. Matsika, S. A. do Monte, D. Nachtigallova, R. Nieman, M. Oppel, C. A. Parish, F. Plasser, R. F. K. Spada, E. A. Stahlberg, E. Ventura, D. R. Yarkony, Z. Zhang, *J. Chem. Phys.* **152**, 134110 (2020). DOI: 10.1063/1.5144267.
- “Wave Function Analysis with a Maximum Flow Algorithm,” R. Shepard, S. R. Brozell, J. Larson, P. Hovland, and S. Leyffer, (*submitted*, 2020).

Mechanisms and Models for Simulating Gas Phase Chemical Reactivity

Raghu Sivaramakrishnan
Chemical Dynamics Group, Chemical Sciences & Engineering Division
Argonne National Laboratory, Argonne, IL 60439
raghu@anl.gov

I. Program Scope

Mechanisms describing the chemical reactivity of small gas phase species can be complex involving a myriad of unimolecular and bimolecular elementary steps. The primary scope of this program is to develop and validate detailed chemical kinetics mechanisms and models for use in predictive simulations of high temperature gas phase reactivity. Kinetics modeling has been used predominantly as an engineering tool for making predictions for practical applications in combustion and chemical conversions. However, within the context of the chemical physics BES program we have also utilized the highly coupled nature of sequences of elementary reactions in our kinetics models along with associated theoretical and experimental efforts in our group to highlight interesting problems pertinent to gas phase chemical reactivity. In such a context, modeling combustion chemistry provides access to a wide range of relevant physical (pressures, temperatures and gradients in these), chemical environments (small gas phase hydrocarbon species to particulate matter), internal energies, and timescales to allow us to highlight the role of quantum effects such as tunneling, anharmonic thermochemistry, and chemically activated molecules and nonthermal reactions among others.

II. Recent Progress

A. Path Analyses in Low-Temperature Propane Oxidation

Inspired by the modeling, experiment, and theoretical efforts to understand propane oxidation as part of the HPCC program we initiated path flux analyses on this chemical system using the “Sum over Histories Representation”^{1,2,3,4} in collaboration with M. J. Davis and Rex Skodje (Univ. of Colorado-Boulder). The SOHR method allows time-dependent kinetic observables to be computed using an expansion over global chemical pathways that follow chemical moieties as they move through a complex reaction network such as in propane oxidation.⁵ In particular, by decomposing the kinetics into individual chemical pathways with well-defined probabilities a quantitative mechanistic picture is obtained for the ignition process in propane-air mixtures at high pressures. Merchant et al.⁵ concluded the early stages of the ignition process in propane can be understood as a catalytic process with the OH-radical serving as the catalytic center. The present study using SOHR⁶ identified additional pathways apart from the primary cycles identified in ref. 5 for OH production. In particular, propylperoxy radical reactions were identified as sinks that impeded OH production from the primary pathways. The kinetics of these reactions are poorly characterized⁷ at conditions relevant to auto-ignition regimes and therefore experimental and theoretical studies may be warranted under such conditions. Theoretical efforts are in progress (see ab-initio chemical kinetics section) to improve our understanding of the reactions of peroxy radicals.

B. Ring Opening in Cycloheptane and the Associated Thermal Dissociation of 1-Heptene

Cycloalkanes and alkenes are important components of real fuels but there is little kinetic and mechanistic data on the dissociation of most large cyclic and olefinic molecules at elevated temperatures. Consequently, a series of systematic experimental studies on cyclopentane and cyclohexane along with their primary products, 1-pentene and 1-hexene respectively, have been performed by Kiefer et al.⁸ and Tranter et al.⁹ in prior shock tube studies. The present work on cycloheptane initiated by Tranter¹⁰ is a continuation of these studies to characterize the role of size and ring-strain in the thermal dissociation of cycloalkanes. The potential energy surface (PES) for cycloheptane isomerization to 1-heptene and other potentially competing processes was characterized using electronic structure theory at the CCSD(T)/cc-pV ∞ Z//M06-2X/cc-pVTZ level. The lowest energy pathway in cycloheptane is ring opening leading to the formation of a diradical which has a low barrier for subsequent hydrogen transfer to form 1-heptene.

The direct process for cycloheptane isomerization has a much higher barrier and therefore is not expected to be relevant to the formation of 1-heptene. VLPP studies on cycloheptane pyrolysis¹¹ suggest that C-H fission and formation of cycloheptene are potentially relevant channels. However, the current calculations show large barriers for these processes, thereby rendering them irrelevant to the unimolecular kinetics of cycloheptane dissociation. The present calculations provide convincing support for the diradical mechanism that is known to be the dominant kinetic process in other similar sized cycloalkanes such as cyclopentane^{9,12} and cyclohexane.⁸ The lowest energy bond fission process in 1-heptene leads to the formation of the resonance stabilized allyl radical and n-butyl radical. Six-center retro-ene elimination pathways¹³ are known to be active in such molecules, and in 1-heptene this is the energetically most favorable pathway forming propene and 1-butene with a barrier 55.3 kcal/mol. Despite the lower barrier for the molecular process, the tight nature of the TS leads to lower A-factors and at high temperatures (T>1000 K) this process is expected to be a minor channel.

Master equation calculations were performed with VARIFLEX¹⁴ using the ab-initio based energetics and molecular properties to obtain theoretical rate constants for the relevant cycloheptane and 1-heptene dissociation channels. The transition state partition functions are evaluated using Phase Space Theory (PST) for the C-H bond fission in cycloheptane and the dominant barrierless bond fission channel in 1-heptene whereas a conventional transition state theory (TST) treatment was employed for ring-opening in cycloheptane and the six-center retro-ene molecular channel in 1-heptene. The coefficient for the inverse sixth power potential in the PST calculations was varied to match the capture rate constants for C₃H₅ recombination¹⁵ which is a reasonable approximation to the C₃H₅ + n-C₄H₉ capture rate constants forming 1-heptene. In cycloheptane, this coefficient in the PST calculations was varied to match capture rate constants for H + c-C₇H₁₃ that were assumed to be $\sim 1.5 \times 10^{-10} \text{ cm}^3 \text{ molecule}^{-1} \text{ s}^{-1}$. Pressure dependent rate constants were calculated over the temperature range 800–2000 K. An exponential down model was used for energy transfer. For ring-opening in cycloheptane, $\langle \Delta E_{\text{down}} \rangle = 1000 \text{ cm}^{-1}$ provided a good fit to the experimental data. In 1-heptene, a temperature dependent $\langle \Delta E_{\text{down}} \rangle = 200 (T/298)^{0.85} \text{ cm}^{-1}$, which is a reasonable estimate,¹⁶ provided a best fit with the present experimentally determined rate constants at 30 – 120 torr for the bond fission channel. The PST calculations confirm that C-H fission is a negligible process (<2% of total flux) in cycloheptane dissociation. In 1-heptene, TST calculations confirm that the retro-ene reaction is indeed a minor channel and contributes less than 5% to the total flux at T > 1100 K and P > 30 torr. Consequently, C-H fission in cycloheptane and the retro-ene channel in 1-heptene have not been included in simulating the present experiments.

C. Siloxane Chemistry

As part of a DOE funded project, Tranter and Wooldridge (Univ. of Michigan) are pursuing experimental studies relevant to siloxane oxidation and combustion. Preliminary measurements¹⁷ in a Rapid Compression Machine (RCM) indicated that doping small quantities of hexamethyldisiloxane (HMDSO) and trimethylsilanol (TMSO) accelerated ignition in syngas-air mixtures. With a view to understanding the chemistry responsible for ignition enhancement we have initiated theoretical studies to determine thermochemistry for the various siloxane species as well as characterize the PES's for HMDSO decomposition and oxidation (R + O₂ and other reactions). Two molecular channels are active and have energies below the lowest energetically accessible bond fission channel (CH₃ loss) in the HMDSO decomposition PES. The two molecular processes have barriers above 75 kcal/mol effectively ruling out significant decomposition at temperatures relevant to the syngas autoignition studies. However, it is interesting to note that the energetics for these processes are similar to that observed in disilane.¹⁸ The lowest energy saddle point for dissociation to (CH₃)₃SiOH + (CH₃)₂Si=CH₂ is lower in energy than the separated products calling for the application of a two transition state model for the kinetics of this lowest energy process. The kinetics for these channels will be calculated to aid in interpreting shock tube experiments performed by Tranter and for use in models to simulate the ignition delay data.

D. Radical-Radical Reactions – Competition between Multiple Channels

In prior studies²⁰ we have highlighted the role of chemically activated adducts in radical-radical reactions and emphasized the role of unaccounted for pathways that can be accessed through such

energized adducts to explain the evolution of species in flames. Most detailed chemical kinetics models often consider only the recombination process (and often at the high-pressure limit) in a radical-radical reaction for C₄ and larger hydrocarbons. For H + alkyl and CH₃ + alkyl radical reactions, prior theoretical studies^{21,22} have determined high-pressure limiting rate constants for the recombination processes in selected straight and branched chain alkyl radicals. However, the presumption that recombination will be the dominant process may not hold good since steric effects may dictate large contributions from disproportionation processes. Additionally, at elevated temperatures there is an increased likelihood to access higher energy channels. Tranter has performed experiments to determine rate constants for such self-reactions of all four butyl radical isomers (n, sec, iso, and tert). In collaboration with theoretical predictions for capture rates from Jasper, we have simulated these experiments²³ to determine the role of addition vs disproportionation in these bimolecular processes. In the experimental conditions accessed (700-1300K) by Tranter, these alkyl radicals also dissociate predominantly^{24,25,26} via,



and lead to reactive H, CH₃, and C₂H₅ radicals in each of these radical systems. Proper interpretation of the experiments also requires consideration of reactions of these reactive atoms/radicals with the parent butyl radicals, i. e. H + tert-C₄H₉, CH₃ + iso-C₄H₉/sec-C₄H₉ and C₂H₅ + n-C₄H₉. Again, as with the self-reactions of butyl radicals, addition and disproportionation processes occur in these reaction systems. Additionally, energetically accessible addition-elimination radical products can also be accessed in these reactions. While detailed kinetics models consider recombination to be the dominant channel²⁷ (or the only channel²⁸) for these reactions, our preliminary results indicate that even for the larger C₂H₅ + n-C₄H₉ system at T > 1000 K and P = 1 bar there is significant contribution (~20%) to addition-elimination leading to n-C₃H₇ + n-C₃H₇. At higher temperatures and lower pressures and for the other three smaller C₃ and C₄ radical systems, recombinations are even less important.

Another area of interest in such radical-radical reactions is the role of the roaming transition state mediating direct abstraction such that this may be the dominant kinetic process at low temperatures and pressures. In collaboration with Klippenstein we plan on initiating theoretical and modeling studies to characterize this in the C₂H₅ + C₂H₅ system. This reaction also plays a crucial role in a recent low-temperature study²⁹ of the C₂H₅ + HBr reaction, and if disproportionation is favored over recombination, then this may lead to a re-interpretation of these very low pressure studies on R + HX that are at odds with other literature studies on the kinetics for these reactions. Lastly, we were highlighted to this problem by Ruscic and Bross who have been developing accurate thermochemical functions for C₂H₅. The R + HX (HBr and HI) kinetic equilibrium studies described above have also been used to determine heats of formation for the alkyl radicals of interest. The recent work of Leplat et al.²⁹ concluded from their results and a third law analysis that the heat of formation of the C₂H₅ radical needs to be lower which is inconsistent with current ATcT recommendations. Reinterpreting these very low pressure bromination and iodination studies may also have an implication for the derived experimental thermochemistry of C₂H₅ and other alkyl radicals.

III. Acknowledgements

This work was supported by the U.S. Department of Energy, Office of Science, Office of Basic Energy Sciences, Division of Chemical Sciences, Geosciences, and Biosciences under Contract No. DE-AC02-06CH11357.

IV. References

1. S. R. Bai, D. Y. Zhou, M. J. Davis, R. T. Skodje, *J. Phys. Chem. Lett.* 6, 183 (2015).
2. S. R. Bai, M. J. Davis, R. T. Skodje, *J. Phys. Chem. A* 119, 11039 (2015).
3. S. R. Bai, R. T. Skodje, *Int. Rev. Phys. Chem.* 35, 539 (2016).
4. S. R. Bai, R. T. Skodje, *J. Phys. Chem. Lett.* 8, 3826 (2017).
5. S. S. Merchant, C. F. Goldsmith, A. G. Vandeputte, M. P. Burke, S. J. Klippenstein, W. H. Green, *Combust. Flame* 162, 3658 (2015).
6. S. Bai, M. J. Davis, R. Sivaramakrishnan, R. T. Skodje, *Comb. and Flame* 202, 154 (2019).

7. R. Atkinson, D. L. Baulch, R. A. Cox, J. N. Crowley, R. F. Hampson, R. G. Hynes, M. E. Jenkin, M. J. Rossi and J. Troe, *Atmos. Chem. Phys.* 6, 3625 (2006) and references within.
8. J.H. Kiefer, K.S. Gupte, L.B. Harding, S.J. Klippenstein, *J. Phys. Chem. A* 113 (2009) 13570–13583.
9. J.B. Randazzo, C.J. Annesley, K. Bell, R.S. Tranter, *Proc. Combust. Inst.* 36 (2017) 273–280.
10. T. Sikes, K.B. Burdett, R.L. Speth, C.F. Goldsmith, R. Sivaramakrishnan, R.S. Tranter, In Press, *Proc. Combust. Inst.* (2020).
11. L.E. Gusel'nikov, V. V. Volkova, P.E. Ivanov, S. V. Inyushkin, L. V. Shevelkova, G. Zimmermann, U. Ziegler, B. Ondruschka, *J. Anal. Appl. Pyrolysis*. 21 (1991) 79–93.
12. B. Sirjean, F. Buda, H. Hakka, P.A. Glaude, R. Fournet, V. Warth, F. Battin-Leclerc, M. Ruiz-Lopez, *Proc. Combust. Inst.* 31 (2007) 277–284.
13. A.T. Blades, H.S. Sandhu, *Int. J. Chem. Kinet.* 3 (1971) 187–193.
14. S.J. Klippenstein, A.F. Wagner, R.C. Dunbar, D.M. Wardlaw, S.H. Robertson, J.A. Miller, VARIFLEX 2.03m, Unpublished Information, (2010).
15. Y. Georgievskii, J.A. Miller, S.J. Klippenstein, *Phys. Chem. Chem. Phys.* 9 (2007) 4259–4268.
16. J.A. Miller, S.J. Klippenstein, *Phys. Chem. Chem. Phys.* 6 (2004) 1192–1202.
17. R. A. Schwind, M. S. Wooldridge, R. S. Tranter, Spring Technical Meeting CSSCI, March 2018.
18. K. Matsumoto, S. J. Klippenstein, K. Tonokura, M. Koshi, *J. Phys. Chem. A* 109 (2005) 4911–4920.
19. R. A. Schwind, M. S. Wooldridge, R. Sivaramakrishnan, Paper 2A06, 11th US National Combustion Meeting, Pasadena, CA, March 2019.
20. N. J. Labbe, R. Sivaramakrishnan, S. J. Klippenstein, *Proc. Combust. Inst.* 35, 447 (2015).
21. L. B. Harding, Y. Georgievskii, S. J. Klippenstein, *J. Phys. Chem. A* 109, 4646 (2005).
22. S. J. Klippenstein, Y. Georgievskii, L. B. Harding, *Phys. Chem. Chem. Phys.* 8, 1133 (2006).
23. J. B. Randazzo, R. Sivaramakrishnan, A. W. Jasper, T. Sikes, P. T. Lynch, R. S. Tranter, In Review, *Phys. Chem. Chem. Phys.* (2020).
24. V. D. Knyazev, I. A. Dubinsky, I. R. Slagle, D. Gutman, *J. Phys. Chem.* 98, 5279 (1994).
25. V. D. Knyazev, I. A. Dubinsky, I. R. Slagle, D. Gutman, *J. Phys. Chem.* 98, 11099 (1994).
26. V. D. Knyazev, I. R. Slagle, *J. Phys. Chem.* 100, 5318 (1996).
27. H. Wang, X. You, A.V. Joshi, S.G. Davis, A. Laskin, F. Egolfopoulos, C.K. Law, USC Mech Version II.
28. W.K. Metcalfe, S.M. Burke, S.S. Ahmed, H.J. Curran, *Int. J. Chem. Kin.* 45 (2013) 638-675.
29. N. Leplat, A. Wokaun, M. J. Rossi, *J. Phys. Chem. A* 117, 11383 (2013).

V. Journal articles supported by this project 2018-2020

1. P. J. Weddle, C. Karakaya, H. Zhu, R. Sivaramakrishnan, K. Prozumant, R. J. Kee, “Boundary-layer Model to Predict Chemically Reacting Flow within Heated, High-Speed, Micro-tubular Reactors”, *Int. J. Chem. Kin.* **50** (2018) 473-480.
2. G. Magnotti, Z. Wang, W. Liu, R. Sivaramakrishnan, S. Som, M. J. Davis, “Sparsity Facilitates Chemical-Reaction Selection for Engine Simulations”, *J. Phys. Chem. A* **122** (2018) 7227-7237.
3. S. Bai, M. J. Davis, R. Sivaramakrishnan, R. T. Skodje, “A Chemical Pathway Perspective on the Kinetics of Low-Temperature Ignition of Propane”, *Comb. and Flame* 202 (2019) 154-178.
4. T. Sikes, K. B. Burdett, R. L. Speth, C. F. Goldsmith, R. Sivaramakrishnan, R. S. Tranter, “Ring Opening in Cycloheptane and Dissociation of 1-heptene at High Temperatures”, In Press, *Proc. Combust. Inst.* (2020).
5. J. B. Randazzo, R. Sivaramakrishnan, A. W. Jasper, T. Sikes, P. T. Lynch, R. S. Tranter, “An Experimental and Theoretical Study of the High Temperature Reactions of the Four Butyl Radical Isomers”, In Review, *Phys. Chem. Chem. Phys.* (2020).
6. D. P. Zaleski, R. Sivaramakrishnan, H. R. Weller, D. H. Bross, B. Ruscic, K. B. Moore, S. N. Elliott, A. V. Copan, C. Cavallotti, Y. Georgievskii, H. F. Schaefer, S. J. Klippenstein, R. W. Field, K. Prozumant, “Keto-enol Tautomerization and its Role in Driving Primary and Secondary Reactions in The High Temperature Pyrolysis of Acetone” In Preparation (2020).
7. N. J. Labbe, A. W. Jasper, S. J. Klippenstein, J. A. Miller, R. Sivaramakrishnan, B. Ruscic, “From Anharmonic Partition Functions to Flame Chemistry: High Accuracy Thermochemical Kinetics for $H + CH_3 (+M) \rightleftharpoons CH_4 (+M)$ ”, In Preparation, *J. Phys. Chem. A* (2020).

Quantum Chemistry of Radicals and Reactive Intermediates

John F. Stanton
Quantum Theory Project
Departments of Chemistry and Physics
University of Florida
Gainesville, FL 32611
johnstanton@ufl.edu

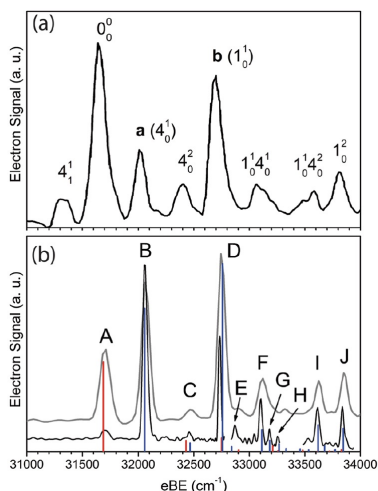
Scope of Research

My research group works in the area of theoretical chemical physics, especially on the properties and chemistry of organic radicals and other reactive intermediates. This research follows a number of paths, including first-principles calculation of bond energies and other thermochemical information (as well as development of methodology needed for such calculations), methods for the simulation and analysis of molecular spectra (especially those relevant to experiments that can be used to glean thermochemical information), the development of *ab initio* quantum chemical methods needed for the accurate treatment of fundamental aspects of electronic structure and potential energy surfaces, and computational kinetics including semiclassical transition state theory and master equation modeling of chemical reactions.

Summary of Selected Recent Accomplishments

- Our longstanding interest in the often-perplexing nitrate (NO_3) radical has continued, with a major finding reported in the last year. While the accepted vibrational assignment¹ of this prototype delocalized radical had been questioned (first reported in 2007 and then supported by a number of follow-up calculations), no consensus had emerged even a year ago. That is, theory rather consistently gave one answer, and experiments gave conflicting answers. However, in collaboration with the Neumark group at Berkeley (part of the GPCP program), a joint experimental-theoretical study was carried out using very high-level equation-of-motion coupled cluster theory and the technique of slow-electron velocity map imaging (SEVI) anion photoelectron (photodetachment) spectroscopy. Quite conspicuous energy dependence in the cross-sections of the major peaks in the spectrum convincingly demonstrated that the 2007 interpretation of the vibrational level structure of the ground state is indeed correct, and showed that a later (2012) simulation of the anion photoelectron spectrum was correct in all details (see Figure). This work draws to a close one of the most controversial subjects in small-molecule molecular spectroscopy, which has been a subject of intense debate each year at the International Symposium for Molecular Spectroscopy since 2008. It further shows what can be done by combining the excellent resolution of SEVI with high-level quantum chemistry calculations to study the energy level structure of transient molecules.

¹T. Ishiwata, I. Tanaka, K. Kawaguchi and E. Hirota *J. Chem. Phys.* 82, 2196 (1985).



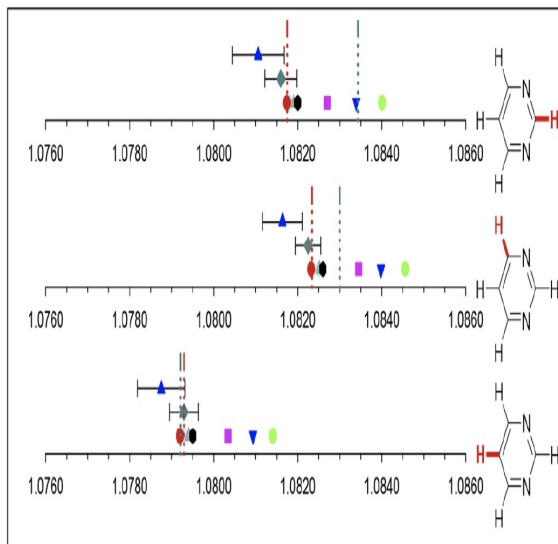
Photoelectron spectra of the nitrate ion. The top is a relatively low-resolution survey scan, while the latter is a composite of several SEVI spectra recorded at photon wavelengths near various threshold regimes in the spectrum. The stick spectra come from EOMIP-CCSDT calculations combined with *ab initio* photodetachment cross-sections². The red peaks correspond to Franck-Condon allowed transitions that terminate on totally symmetric vibrational levels of the neutral, while the black peaks derive their intensity from vibronic coupling to the excited $\tilde{B}E'$ electronic state. The peak just about 32700 cm^{-1} is seen to be dominated by vibronic (Herzberg-Teller) effects, as is clearly consistent with the more recent interpretation of the vibrational energy level structure of the neutral.

- Together with the Zwier group at Purdue (also part of the GPCP program), we have worked on a combined experimental theoretical study of the prototype phenoxy radical, an important intermediate in combustion and relevant to processes involving the oxidation of aromatic compounds. The study used a combination of the hyperthermal nozzles popularized by Peter Chen (Harvard, then ETH in Europe) and Barney Ellison (Boulder, part of the GPCP program) and chirped-pulse microwave spectroscopy. Through study of a number of isotopically substituted phenoxy radicals generated by thermolysis of appropriate precursors, a molecular structure was determined – experimentally – for the first time. Quantum chemical calculations and predictions guided the search for the isotopic species in the spectrum, and provided insight into the distribution of unpaired spin in this species.

In related work that was found to be particularly satisfying to me, we collaborated with the group at Wisconsin led by Robert J. McMahon and R. Claude Woods to determine the molecular structure of the pyrimidine molecule (see figure) to *unprecedented* precision for a polyatomic molecule. While the procedure used in this work was not novel – the structure was determined by combining experimental ground-state rotational constants with calculated corrections for rotation-vibration interaction (as well as the fact that the electronic contribution to the mass of a molecule cannot simply be subsumed into the atomic masses at the corresponding nuclear positions) – the results were simply extraordinary. The combinations of specialties here – McMahon is an outstanding synthetic chemist specializing in reactive species and isotopically-labeled molecules, Woods has had a truly impressive career in the area of microwave spectroscopy, and our ability to carry out quantum-chemical calculations relevant to rotational spectroscopy – led to the availability of high-quality data (driven by Woods’ expertise) for several isotopic species (McMahon) that was processed and analyzed with very high-quality coupled-cluster calculations. The apparent quality of the resulting equilibrium structure is astounding; it seems that bond lengths are determined to a few *ten-thousandths* of an Angstrom, sufficiently precise that the effects of the adiabatic correction (also known as the diagonal Born-Oppenheimer correction, which results in isotope-dependent potential energy surfaces) begin to come into play in the refinement of structural parameters. A paper presenting these initial results has been published³, and additional work is ongoing in the Stanton group to investigate the effects of the adiabatic correction as well as to calculate various spectroscopic constants that have been fit to the very high-quality datasets. These include the vibrational state dependence of quartic centrifugal distortion constants (which have been reliably measured and exhibit a quasilinear dependence on $(n + \frac{1}{2})$), and octic centrifugal distortion constants. Indeed, the data from the Madison laboratory provides a fertile source of inspiration for

³Cited at end of report.

the development of spectroscopic theory.



CH bond lengths of the pyrimidine molecule. Relevant here are the green points with (2σ) error bars, determined from extensive rotational line positions for eleven distinct isotopic species. High-level quantum chemical calculations include those done at the CCSD(T) level with the cc-pCV5Z basis sets (1100 basis functions, designed by red circles) and a more refined estimate that takes into account residual electron correlation beyond CCSD(T), basis set effects beyond cc-pCV5Z, and relativistic effects. It is clear that the experimental determinations are accurate to nearly 0.0001 Angstrom, which is comparable to a nuclear diameter. Agreement for the heavy atom distances nearly as good. The interested reader can refer to the published paper for additional details.

- In addition, with Ruscic, we have been working on several projects associated with the Active Thermochemical Tables (ATcT) paradigm that has had a major impact on the quality and precision of thermochemical data. Amongst these, currently being written up for publication, is an accurate thermochemical study of the formamide molecule ($\text{H}_2\text{NC}(\text{O})\text{H}$), the simplest molecule that contains a “peptide” bond. Formamide is an interesting molecule for reasons other than “biological-relevance”, as the potential governing inversion of the amino group is remarkably flat. While chemists are trained to think of the H-N-C=O linkage in these molecules as decisively planar, this does not turn out to be true for formamide, as has been known for a long time. From the standpoint of thermochemical calculations, this largely affects the determination of the vibrational zero-point energy (and, for elevated temperatures, the partition function). To address this issue, we have collaborated with P.B. Changala at Boulder, whose NITROGEN program for vibrational calculations (it specializes in large-amplitude motions such as that in formamide) was essential for this work. Other work going on with the ATcT task force that we belong to include molecules relevant to radical-radical reactions associated with the generation of larger cyclic hydrocarbons, and chlorine oxides (ClOCl , ClOO , Cl-ClO_2 and ClO_2), this latter area also being done in collaboration with Okumura’s group at Caltech.

- We have embarked on a study of “slow” reactions in the atmosphere, inspired by Ravishankara at Colorado State. It is now accepted that the nitrous oxide (N_2O) molecule – generated a number of ways, naturally, *via* agriculture and also *via* fossil-fuel combustion is destined to become the major ozone-depleting substance in the 21st century atmosphere. N_2O , which is similar to CO_2 electronically, is also very similar in terms of stability. While it can be destroyed by reactions with singlet oxygen atoms in and above the stratosphere, there are currently no known mechanisms for its destruction that involve “fast” chemical reactions. As the experimental study of “slow” reactions ranges from difficult to impossible, depending on just how “slow” they are, Ravishankara has appealed to us to use theoretical methods to study such processes. Here, where atmospheric half-lives of a century or so are “important”, it appears that modeling will ultimately require high-quality theoretical rate constants. To this end, we have continue to develop methodology for rate calculations; my associate T. Lam Nguyen – the kinetics expert in my group – has been working on various master-equation models to describe the effect of rotation on the outcomes of multiwell reactions.

• Additional information about our DOE-supported research can be found in the publications listed at the end of this document.

Students and Postdoctoral Supported:

T.L. Nguyen (postdoc, Florida)

C.A. Lopez (student, Austin)

J.T. Thorpe (student, Florida)

M.B. Bentley (student, Florida)

References from 3/2018-3/2019 acknowledging DE-FG02-07ER15884

Z.N. Heim, B.K. Amberger, B.J. Esselman, J.F. Stanton, R.C. Woods and R.J. McMahon Precise Equilibrium Structure Determination of Pyrimidine (m-C₄H₄N₂) by Millimeter Wave Spectroscopy *J. Chem. Phys.* 152, 104303 (2020).

L.T. Nguyen and J.F. Stanton Pragmatic Solution for a Fully-Resolved E,J Master Equation, *J. Phys. Chem. A* 124, 2907 (2020).

M.C. Babin, J.A. Devine, M. DeWitt, J.F. Stanton and D.M. Neumark High-Resolution Photoelectron Spectroscopy of Cryogenically-Cooled NO₃- *J. Phys. Chem. Lett.* 11, 395 (2020).

L.T. Nguyen, M.N. Romanias, A. R. Ravishankara, A.M. Zaras, P. Dagaut, and J.F. Stanton The Atmospheric Impact of the Reaction of N₂O with NO₃: a Theoretical Study *Chem. Phys. Lett.* 731, 136605 (2019).

S.M. Rabidoux, R.J. Cave and J.F. Stanton A Non-adiabatic Investigation of the Spectroscopy of trans-1,3-butadiene *J. Phys. Chem. A* 123, 3255 (2019).

J.H. Thorpe, C.A. Lopez, T.L. Nguyen, J.H. Baraban, D.H. Bross, B. Ruscic and J.F. Stanton High-Accuracy Extrapolated ab initio Thermochemistry. IV. Modified Recipes for Computational Efficiency *J. Chem. Phys.* 150, 224102 (2019).

A.O. Hernandez-Castillo, C. Abeysekara, J.F. Stanton and T.S. Zwier Structural Characterization of Phenoxy Radical with Mass-Correlated Broadband Microwave Spectroscopy *J. Phys. Chem. Lett.* 10, 2919 (2019).

T.L. Nguyen and J.F. Stanton Accurate Rate Coefficients for H + NH₃ → H + NH₂ from High-Level Theoretical Calculations, *Int. J. Chem. Kin.*, 51, 321 (2019).

Universal and State-Resolved Imaging Studies of Chemical Dynamics

Arthur G. Suits

Department of Chemistry, University of Missouri, Columbia MO 65211
suitsa@missouri.edu

I. Program Scope

The focus of this program is on combining universal ion imaging probes providing global insight with high-resolution state-resolved probes providing quantum mechanical detail, to develop a molecular-level understanding of chemical phenomena. Particular emphasis is placed upon elementary reactions involving transient species and in revealing new aspects of reaction mechanisms and the dynamical behavior of molecules. Much of the current effort here is in generalizing the lessons from simple systems as we investigate the behavior of larger polyatomic molecules and radical-molecule reactions. The results of these investigations can then be used to help bring order to the tens of thousands of reactions that take place in practical systems from combustion environments at high temperature, atmospheric conditions near room temperature, or interstellar clouds approaching absolute zero. This research is conducted using state-of-the-art molecular beam machines, photodissociation, reactive scattering, and vacuum ultraviolet lasers in conjunction with velocity map ion imaging and other techniques we develop. A major focus of our effort remains crossed-beam reactive scattering of polyatomic molecules. New directions in time-resolved studies of photochemical processes are also underway.

II. Recent Progress

Multichannel bimolecular reaction dynamics. The differing reactivity of primary vs. secondary hydrogen atom sites is a first step toward chemical complexity, but the detailed dynamics of this have only been studied for atomic reactants and only then yielding limited insight. We have recently combined direct quasiclassical trajectory calculations with crossed molecular beam velocity map imaging to reveal the distinct dynamics for primary vs. secondary hydrogen abstraction in *n*-butane for a *molecular radical*, OH, for the first time. Normal butane is a prototypical straight-chain alkane that possesses two main sites (primary and secondary sites) for hydrogen abstraction, providing us opportunity to directly study and compare their different dynamics under same conditions. We have collaborated with theorist Diego Troya at Virginia Tech, who applied a highly accurately specific-reaction-parameter Hamiltonian to run direct quasiclassical trajectory calculations on such a high-dimensionality system. The synergy between crossed-beam imaging and trajectories opens door to detailed dynamics of ever-complex multidimensional, multichannel reactions.

Using an unfocused laser, vacuum ultraviolet (VUV) single photon ionization at 157 nm unequivocally probed the 2-butyl product from the $\text{OH} + n\text{-butane} \rightarrow 2\text{-butyl} + \text{H}_2\text{O}$ secondary reaction channel at a collision energy of 7.7 kcal/mol (Fig. 1). This showed a strongly backward-scattered angular distribution with mild translation energy release. Excellent agreement with experiment was captured by trajectory calculations on both the backward nature of the angular distribution and the modest translational energy release distributions. Using a loosely focused 157 nm probe laser then enabled us to detect both 2-butyl product from the secondary H abstraction channel and 1-butyl product from the primary H abstraction channel under the same conditions as we have shown previously, although the ionization energy of the 1-butyl radical is slightly above

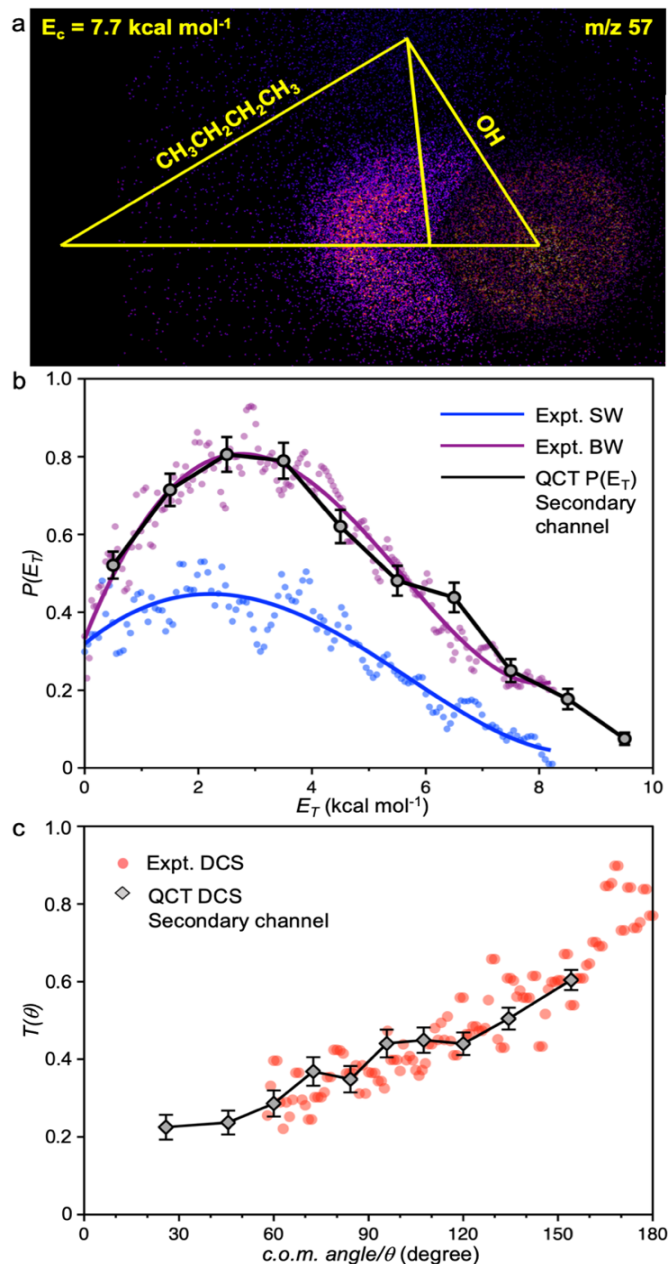


Figure 1. DC sliced images (a) of the butyl products (m/z 57) from OH + *n*-butane reaction under collision energy of $7.7 \text{ kcal mol}^{-1}$ with Newton diagram superimposed. Photochemical background is masked by the black shaded area in the forward direction. Plots (b) and (c) are the corresponding translational energy release and angular distributions, compared to QCT results of the H abstraction secondary channel. The experimental translational energy release is shown with the sideways (SW, in blue) and backward (BW, in purple) components, and its angular distribution is shown with red filled circles. All calculated QCT results are shown in black with error bar indicated.

mentioned above. Our experimental observations showed backward angular distribution and low translational energy release. This work is also in collaboration with Diego Troya. In addition to

the photon energy. The contour map analysis of the concurrent 1-butyl and 2-butyl signals showed markedly different angular distribution, less backward than that of secondary reaction channel. Trajectory calculations further refined this by a predominantly backward scattering for the secondary channel, and an enhanced sideways component for the primary one. The differing angular distributions are correlated with the opacity functions of each channel. Reaction at the secondary sites occurs preferentially with low impact parameters that leads to rebound dynamics, however, reaction at the more peripheral primary sites can occur at longer impact parameters that does not confine products with backward propensity. While the two reaction channels have distinct angular distributions, they both exhibited modest product translational energy release, which was excellently captured by trajectory calculations. Further trajectory analysis indicated a substantial amount of the available energy is diverted into the water product internal excitation, and very little excitation into the organic fragment, for both reaction channels. The comparable reaction cross sections for the two reactive sites suggested $\sim 70\%$ greater reactivity for the secondary H atoms given their fewer number. We have concluded this work and submitted it for publication.

OH + *i*-butane. At the same time, we have carried out a crossed-beam imaging study on the OH + *i*-butane reaction in order to compare with the OH + *n*-butane reaction system. Isobutane contains one unique tertiary H site and nine primary H sites. This allows us to explore the tertiary hydrogen abstraction reaction dynamics, which provides a complement to the reaction dynamics on different hydrogen sites as

obtain dynamics information for this OH + *i*-butane reaction, more generalized potential energy surfaces are aimed to be derived for understanding the hydrogen abstraction dynamics with different H atom sites in hydrocarbons. This will aid to improve the theoretical modeling in the atmospheric and combustion chemistry.

Progress in Multi-mass and time resolved imaging. As described in last year's abstract, we are pursuing time-resolved studies of photochemical processes, with the goal to use Coulomb Explosion Imaging (CEI) to probe nuclear dynamics in real time. We rebuilt a molecular beam apparatus for this purpose that will take advantage of the principal tool for our time-resolved experiments, a KMLabs Wyvern 1000 femtosecond laser system. Unfortunately, in the past year this laser has had some issues with reliability, so progress has been slower than hoped. However, we have successfully demonstrated CEI in methyl iodide, a well-studied system, and used covariance mapping to reveal the ion-ion correlations, finding good agreement with the literature. Our approach involves multi-mass imaging based on the 3D method of Wen Li and co-workers. We have recognized that background gases are a significant issue with strong-field CEI, and we are currently implementing additional cryopumping to reduce this interference. During the current laboratory shutdown, the team is improving the data acquisition for the challenging time-resolved CEI measurements we hope to acquire when the laboratories are reopened.

III. Future Directions

OH + alkenes. Alkenes are a significant class of volatile organic compounds emitted to the earth's troposphere from a wide range of biogenic and anthropogenic sources. The competition between the direct H abstraction and the addition–elimination mechanism in OH alkene reactions is a largely unexplored question. Competing pathways have been observed in the Cl + isobutene reaction, where direct H abstraction is more important at high collision energy and addition–elimination pathway play a role at low collision energy. We will study analogous bimolecular reaction dynamics for the OH + isobutene reaction. In preliminary crossed-beam experiments, we successfully detected the H abstraction product from the reaction of OH and isobutene under collision energy of 8 kcal/mol. More interestingly, the angular distribution is nearly isotropic possibly indicating an addition–elimination mechanism. Initial OH addition into the double bond can result in the stabilization energy of 27-30 kcal/mol. Thus, we must ask what the reaction pathway looks like from the long-lived adduct to the H₂O and C₄H₇ products. In addition, a related question is the possible competition between direct H abstraction and addition–elimination. We will perform crossed-beam experiments at various collision energies to look into these questions, and pursue high-level characterization of stationary points on the potential energy surface. Another interesting aspect of the OH + alkenes reaction is the formation of enols following the OH addition to the double bond. Our probe laser is more sensitive to detect alkyl radicals, so 3-methyl-1-butene will be a good target alkene to check the enol route since in that case the isopropyl radical that we can readily detect is the coproduct with ethanol.

OH + alcohols. Alcohols are pursued as potential biofuels that are renewable and carbon-neutral to offer a long-term fuel-source with less impact on the air pollution and climate change than petroleum-based transportation fuels. We are thus planning to extend our OH radical investigations to alcohols. We have studied the related reactions, O(³P) + propanol isomers, using our crossed-beam DC sliced velocity map imaging technique, showing backward angular distribution and

modest translational energy release. Most product internal excitation indicated here was further analyzed by quasi-classical trajectory calculations, suggesting a significantly larger portion of the available energy diverted to the hydroxypropyl organic product. However, in our recent work mentioned above, the OH + *n*-butane reaction gave the opposite result, in which a substantial amount of the available energy is released into the water product internal excitation rather than the organic radical. Therefore, a detailed check on the reaction dynamics of the OH + propanol isomers will be one of our future targets. This will provide further information on whether simple kinematics or exit channel interactions play a major role in controlling product energy disposal on such high dimensional reactions.

Time-resolved nuclear dynamics at the Ultrafast Electron Diffraction (MeV UED) facility at LCLS. In parallel with our efforts to achieve time-resolved CEI in our own laboratory, we have been interested in the possibility of using ultrafast electron diffraction to achieve similar ends, and thus recently submitted a successful proposal to the MeV UED facility at LCLS. The goal of the initial study was to revisit a system that we had studied many years ago that exhibited novel photochemical decay dynamics. The molecule oxalyl chloride, (ClCO)₂, was shown by state-resolved imaging of the CO product to give four fragments following absorption of a single photon in the UV. Using ultrafast electron diffraction, we plan to study the photodissociation dynamics of oxalyl chloride by measuring the evolution of the diffraction patterns and pair distribution functions after excitation. The initial experiments suggested a two-stage process producing high- and low-velocity fragments, but more recent work proposed that short excitation wavelengths instead induce a concerted dissociation. We intend to image the process at multiple wavelengths to determine whether the pair distances do increase in a step-wise fashion, and whether this changes with photon energy. Product fragments are also generated with significant rotational excitation, which we hope to observe in the diffraction experiments. The beamtime was scheduled for late Spring, but this has been interrupted by the COVID pandemic. We look forward to our first beamtime as soon as it can be rescheduled.

IV. DOE Publications 2017-present

A. Kamasah, H. Li, J. Onvlee, A. van der Avoird, D. H. Parker, and A. G. Suits, "Imaging the inelastic scattering of vibrationally excited NO(*v*=1) with Ar," *Chem. Phys. Lett.* (2018) **692**, 124-128. DOI: 10.1016/j.cplett.2017.12.016

A. G. Suits, "Invited Review Article: Photofragment Imaging," (2018) 89, 111101 DOI: [10.1063/1.5045325](https://doi.org/10.1063/1.5045325)

H. Li, A. Kamasah, S. Matsika and A. G. Suits, "Intersystem Crossing in the Exit Channel," *Nature Chem* (2018) DOI:10.1038/s41557-018-0186-5

H. Li, A. Kamasah, and A. G. Suits, "Imaging H abstraction dynamics in crossed molecular beams: O(³P) + propanol isomers," *Phys Chem Chem Phys*, (2018) DOI:10.1039/C8CP06351F.

H. Li and A. G. Suits, "Universal Crossed Beam Imaging Studies of Polyatomic Reaction Dynamics," *Phys Chem Chem Phys*. (2020) DOI: 10.1039/D0CP00522C.

Multiscale Interaction of Turbulence, Temperature, and Soot Formation: Measurements for Critical Assessments of Chemical Kinetics and Mechanisms

Jeffrey A. Sutton
Department of Mechanical and Aerospace Engineering
Ohio State University
Columbus, OH 43210
sutton.235@osu.edu

Project Scope

This program targets an improved understanding of how turbulence affects soot formation chemistry (directly and indirectly) with a particular focus on detailing the multiscale coupling between flow turbulence, mixing, thermal transport, and soot formation kinetics in gas-phase reacting systems. There is ample evidence that soot formation and growth is strongly affected by turbulence. This is due to the fact that soot formation chemistry is characterized by slow time scales and thus surrounding fluid mechanic and mixing time scales not only influence the kinetic processes, but may dictate them. In this manner, the assessment of soot formation and the resulting chemical kinetic mechanisms for application under turbulent conditions must be benchmarked against measurements in turbulent reacting flows. This project targets simultaneous, quantitative multi-dimensional velocity, soot volume fraction, and gas-phase temperature imaging in turbulent non-premixed sooting flames to elucidate the relative effects of fluid kinematics, mixing, thermal processes, and turbulence/scalar time/length scales on soot formation chemistry and topology. The local gas-phase temperature field is critically important to further understand soot formation under turbulent conditions because of its direct linkage between turbulence (i.e., thermal and molecular mixing) and chemical kinetics (i.e., temperature-dependent reaction rates). In this program, a new implementation of filtered Rayleigh scattering (FRS) is applied for quantitative 2D temperature measurements in turbulent sooting non-premixed flames. The combined velocity (via PIV), soot volume fraction (via LII), and gas-phase temperature imaging will provide a previously unavailable database concerning turbulence-temperature-soot interaction. From these measurements, novel multi-parameter statistics will be derived that detail the coupling and importance of various kinematic and thermal parameters. This analysis is necessary for understanding relevant formation pathways, transport mechanisms, and developing soot mechanisms to be applied under turbulent conditions.

Recent Progress

Development of Quantitative Temperature Imaging in Sooting Flames

While the implementation of laser-induced incandescence (LII) and particle imaging velocimetry (PIV) is difficult in sooting environments, the methods have been successfully applied [e.g., 1-4] and thus represent known measurement strategies under sooting conditions. The primary diagnostic challenge lies in developing and applying a robust and accurate temperature imaging methodology that can be applied in sooting turbulent non-premixed flames and simultaneously with LII and PIV. Of the numerous laser-based thermometry approaches that exist, few are applicable in the presence of soot or PIV tracer particles due to the scattering/interference from the particles. In the current program, the targeted method for temperature measurements is filtered

Rayleigh scattering (FRS). FRS is a variant of the traditional laser Rayleigh scattering (LRS) technique which uses the combination of a spectrally narrow laser and an atomic or molecular filter (cell filled with an absorbing species such as molecular iodine, I₂) placed in front of the detector [5]. This combination rejects interference that is spectrally identical to the incident laser light (i.e., scattered light from particles), while collecting gas-phase information. In this program we have developed particular fuel combinations for sooting flames such that the measured FRS signal is a known function of temperature. This allows quantitative single-shot temperature measurements using only an FRS measurement.

In the last reporting period, we presented results showing our methodology in turbulent non-sooting flames (and in the presence of PIV particles). This work served (i) as a demonstration of the ability to determine accurate temperature measurements in particle-laden flow and (ii) to develop a series of non-sooting flames for direct comparison to the targeted sooting flames to examine the effect of soot on flow turbulence and mixing. In this reporting period we present results demonstrating accurate temperature measurements in turbulent sooting flames.

The signal collected from an FRS experiment can be written as

$$S_{FRS} = AI_o n \sum X_i \sigma_i \int_{\nu} \mathfrak{R}_i(\nu) T(\nu) \quad (1)$$

where A is an optical constant; I_o is the incident laser intensity; n is the gas number density; X_i , σ_i , and \mathfrak{R}_i are the mole fraction, differential Rayleigh scattering, and Rayleigh-Brillouin scattering lineshape, respectively, for each species; $T(\nu)$ is the frequency-dependent transmission of the I₂ cell, and ν is the spectral frequency over which the RBS light and I₂ absorption bands are distributed. If Eq. (1) is normalized by a reference measurement at known conditions and rearranged, the FRS signal is written as

$$\frac{S_{FRS}}{S_{ref}} = \frac{T_{ref}}{T} \times \frac{\sum X_i \sigma_i \psi_i(T)}{\sigma_{air} \psi_{air}(T)} \times \frac{\sigma_{air} \psi_{air}(T)}{\sigma_{air} \psi_{air}(T_{ref})} \quad (2)$$

where $\psi_i = \int_{\nu} \mathfrak{R}_i T(\nu)$. Through fuel tailoring, we specify unique fuel mixtures such that the second term on the right hand side is near unity (with acceptable error) such that temperature is determined from FRS using

$$T = T_{ref} \times \frac{S_{ref}}{S_{FRS}} \times \frac{\psi_{air}(T)}{\psi_{air}(T_{ref})} \quad (3)$$

and the temperature dependence is imbedded in the third term on the RHS which is calculated using the Tenti S6 model [5]. This approach has been utilized previously by our research group in non-sooting flames [6, 7].

The fuel design led to a mixture of 12% C₂H₂, 45% H₂, and 43% Ar by volume. An additional benefit of this flame is that it has a nearly constant Rayleigh scattering cross section over the full thermochemical space such that traditional LRS can be used as an assessment of the FRS-based temperature measurements in non-sooting regions. For these preliminary measurements, C₂H₂/H₂/Ar non-premixed jet flames were stabilized on the Sandia piloted burner (pilot off). Figure 1 shows a set of results at axial locations of $x/d = 20$ and $x/d = 40$ in a $Re = 11,000$ turbulent flame. At $x/d = 20$, the soot is highly intermittent in its appearance and thus the majority of results are soot-free and the FRS results can be evaluated by LRS for comparison. Figure 1 shows two simultaneous LRS/FRS images and extracted temperature profiles at $x/d = 20$. The excellent agreement between the two sets of images indicates highly accurate FRS temperature measurements in non-sooting regions. Furthermore, the images are of very high quality,

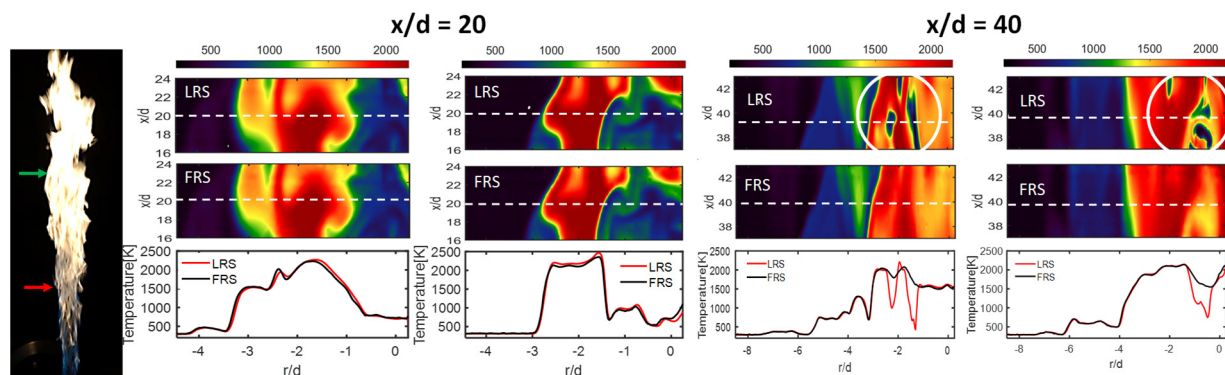


Figure 1: (Left) photograph of $C_2H_2/H_2/Ar$ flame with measurement locations. (Middle) Simultaneous LRS/FRS images and extracted temperature profiles at $x/d = 20$. (Right) Simultaneous LRS/FRS images and extracted temperature profiles at $x/d = 40$.

demonstrating high resolution and signal-to-noise ($SNR > 50$ at highest temperatures). The right side images of Fig. 2 shows a set of results at $x/d = 40$ in the $Re = 11,000$ turbulent flame. LRS and FRS results are almost indistinguishable in the soot-free regions (see profiles), giving further confidence in the FRS-based temperature fields. Regions of soot (marked with white circles) are easily identified in the LRS images due to the high scattering and resulting artificially “low” temperature. At these same locations, the FRS images are free from soot interference and by all visual indications of the surrounding temperature field topology, yield accurate temperature information in the presence of soot. While we have not compared to other techniques (i.e., CARS) in turbulent flames, additional measurements in laminar flames show accurate FRS-based thermometry in sooting flames. In addition, an algorithm was derived to identify “soot structures” from the LRS images. The correlation coefficient between the LRS- and FRS-derived temperatures in the high sooting regions approached zero, while the correlation coefficient between LRS- and FRS-derived temperatures in the non-sooting regions was near unity. Thus, there appears to be no detrimental effects from soot scattering on the FRS-based temperature measurements.

Additional Progress

We also have refined our in-house Rayleigh Brillouin scattering (RBS) spectroscopic model to include sooting fuels such as acetylene and ethylene and performed a systematic testing of the accuracy of the Tenti S6 model for CH_4 , C_2H_2 , C_2H_4 , C_3H_8 , and C_4H_{10} . Accurate interpretation of the measured FRS signal requires accurate modeling of the RBS spectral lineshape of the hydrocarbon fuels. Results showed that the Tenti model accuracy predicts the RBS lineshape for CH_4 , C_2H_2 , and C_2H_4 , but exhibits error for C_3H_8 , and C_4H_{10} . The sources of the error are unknown and will continue to be investigated. The results have been submitted for publication.

Future Plans

Near-term work includes the combining of FRS, PIV, and LII in sooting flames. Previously, we have demonstrated accurate measurements of velocity and temperature using PIV and FRS in non-sooting flames [7] and the current work demonstrates accurate temperature measurements under sooting conditions. When laboratories re-open, the first joint FRS-PIV-LII studies will begin. A series of turbulent sooting flames have been developed for study that span a broad range of Reynolds and Damköhler numbers. A key focus of the initial sets of experiments is to characterize

accuracy and precision of all measurements when combined together to examine “crosstalk” effects.

With the simultaneous temperature-velocity-soot volume fraction database, longer-term work includes a detailed statistical characterization of the flames including statistical moments, integral scales, and joint statistics. A significant utility of the simultaneous LII-PIV-FRS imaging lies in the ability to formulate a set of joint statistics (including bivariate correlations, joint PDFs, conditional statistics, and multi-variate correlations) between multiple parameters with a particular focus on examining the relative roles of turbulent and thermal transport on soot formation. Finally, an investigation of the relative roles of flow kinematics and thermal variations on soot topology will be investigated.

References

- [1] Narayanaswamy, V., Clemens, N.T., *Combust. Flame*, 2013, 34, 1455-1463.
- [2] Köhler, M., Geigle, K.P., Meier, W., Crosland, B.M., Thomson, K.A., Smallwood, G.J., *Appl. Phys. B*, 2011, 104, 409-425.
- [3] Park, O., Burns, R.A., Buxton, O.R.H., Clemens, N.T., *Proc. Combust. Inst.*, 2017, 36, 899-907
- [4] Köhler, M., Boxx, I., Geigle, Meier, W., *Appl. Phys. B*, 2011, 103, 271.
- [5] Tenti, G., Boley, C.D., Desai, R.C., *Can. J. Phys.*, 1974, 52(4), 285-290.
- [6] McManus, T.A., Sutton, J.A., *Appl. Opt.*, 2019, 57(11), 2936-2947.
- [7] McManus, T.A., Sutton, J.A., accepted, *Exp. Fluids*, 2020.

Publications Supported by this DOE Project (2016 – present)

McManus, T.A., Sutton, J.A., “Simultaneous 2D Filtered Rayleigh Scattering Thermometry and Stereoscopic Particle Image Velocimetry Measurements in Turbulent Non-Premixed Flames”, accepted for publication in *Experiments in Fluids*, 2020.

Elementary Reactions of PAH Formation

Robert S. Tranter

Chemical Sciences and Engineering Division, Argonne National Laboratory

Argonne, IL-60439

tranter@anl.gov

I. Program Scope

This program is focused on the experimental determination of kinetic and mechanistic parameters of elementary reactions, in particular those involved in the formation and destruction of the building blocks for aromatic species. The program also encompasses dissociation of novel fuels such as ethers and cyclic species and their dissociation products that are representative of intermediates in combustion mechanisms. Thermal sources of radicals are investigated and characterized for use in more complex reaction systems where secondary chemistry can be significant. Recently, the scope has been increased to include thermally initiated roaming reactions. The approach involves a diaphragmless shock tube (DFST) equipped with laser schlieren densitometry (LS) and a time-of-flight mass spectrometer (TOF-MS). The combination of these techniques accesses a wide range of reaction temperatures and pressures. Finally, x-ray diagnostics are exploited to study flows in hostile environments to provide targets for simulations and develop better understanding of the environment in common experiments..

II. Recent Progress

A. Aromatics: Pyrolysis of Styrene

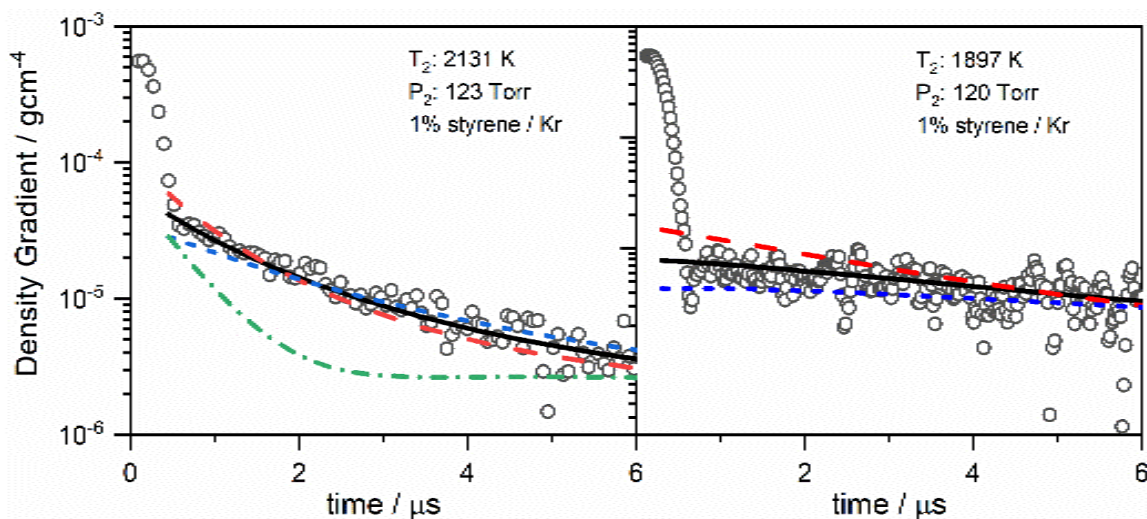


Figure 1: Semi-log plots of absolute density gradients (points) and simulations (lines). Solid black line: current model with styrene = $o\text{-C}_6\text{H}_4 + \text{C}_2\text{H}_4$, reaction 2, as the dominant channel. Broken red and blue lines show the effect of increasing and decreasing k_2 by a factor of two. Green dash-dot line, left plot only, simulation assuming that reaction (1), $\text{C}_8\text{H}_8 = \text{C}_6\text{H}_6 + \text{C}_2\text{H}_2$ is the main decomposition path for styrene as the literature suggests.

The reactions of aromatic molecules and radicals and resonantly stabilized radicals (RSRs) are important in the formation of polycyclic aromatic hydrocarbons (PAH) and particulate matter. We have previously studied recombination reactions of allyl,¹ 2-methyl allyl² and phenyl radicals³ in combined experimental and theoretical studies, and dissociation of o -benzyne experimentally.⁴ We are continuing our investigations of the pyrolysis of aromatics with an investigation of styrene, the smallest substituted benzene with an double bonded side chain.

Styrene is a major industrial product, which is predicted to be produced in 33 Mt/yr by 2023.⁵ Consequently, disposal of the main product, polystyrene, is a critical issue and upcycling of waste material as opposed to simple incineration would be desirable (see for example Ref. 6). Thermal decomposition of polystyrene yields significant amounts of styrene and benzene.⁷ Styrene is also formed in the oxidation of many aromatic species, for example *n*-alkyl benzenes,⁸ and combustion of biomass, for example from wildfires.⁹ Consequently, detailed insights into the elementary mechanistic steps for pyrolysis of styrene, and the subsequent roles the products play in PAH formation, are important for developing strategies for reducing pollution from incineration and upcycling waste material.

To investigate the early stages of styrene pyrolysis we have conducted laser schlieren densitometry (LS) experiments in a diaphragmless shock tube. The shock tube is also coupled via molecular beam sampling to a time-of-flight mass spectrometer (TOF-MS) with electron impact ionization (EI). The LS experiments were conducted behind incident shock waves and span 1700-2300 K and 120 Torr. The TOF-MS experiments cover 1650 – 1950 K and 450 -700 Torr and were performed behind reflected shock waves. As usual, the LS experiments examine only the first few microseconds of reaction, whereas the TOF-MS studies probe up to 1000 μ s with snapshots of composition every 10 μ s. The low pressure studies were augmented by photoionization (PI) mass spectrometry studies at 10 bar and similar pressures by work performed under the Argonne/Sandia Consortium on High Pressure Combustion Chemistry. We have also collaborated with Comandini (CNRS-Orleans), who studied pyrolysis of styrene at 20 bar in a single pulse shock tube with reaction times of 3 – 4 ms. Thus, between the various studies we should be able to develop a mechanism for styrene pyrolysis which will also form a firm foundation for oxidation mechanisms.

To simulate the LS experiments a simplified mechanism was taken from prior work by Comandini and co-workers.¹⁰ Similar to styrene oxidation mechanisms from other groups, they assumed that the primary dissociation channel was reaction (1) forming benzene and vinylidene. Under the conditions of this work, vinylidene immediately isomerizes to acetylene. However, as shown in the left hand panel of Fig. 1 it was not possible to simulate the density gradients from the LS experiments with this model. Alternate decomposition paths such as H-atom loss, reaction 3, and a ring contraction/elimination path are much more endothermic and at first glance would not be expected to be competitive. Reaction 2 has not been previously suggested for decomposition of styrene. However, there is some evidence for it from a study of ethylene addition to *o*-C₆H₄.¹¹ With reaction (2) as the dominant channel, good simulation of the LS experiments was achieved over the complete experimental range, Fig. 2.

		$\Delta H_{r,298\text{ K}}$
(1)	$\text{C}_8\text{H}_8 = \text{benzene} + \text{H}_2\text{CC}$	82.7
(2)	$\text{C}_8\text{H}_8 = \text{oC}_6\text{H}_4 + \text{C}_2\text{H}_4$	87.1
(3)	$\text{C}_8\text{H}_8 = \text{aC}_8\text{H}_7 + \text{H}$	104.3
(4)	$\text{C}_8\text{H}_8 = \text{c-C}_5\text{H}_5 + \text{C}_3\text{H}_3$	111.5

However, the mass spectra appear to indicate a different story to the LS results. Both the EI (~600 Torr) and PI TOF-MS (~ 10 bar) show strong peaks for benzene and acetylene at $T < 2000$ K. There are only small peaks at m/z 76 (*o*-C₆H₄) in both sets of mass spectra and peaks at m/z 28 (C₂H₄) are also minor. Additionally, a strong peak is observed at m/z 102 (phenylacetylene) in the PI spectra and a small peak at m/z 102 in the low pressure mass spectra, which are suggestive of styryl being formed in reaction 3 and rapidly decomposing by H-elimination. Finally, in both sets of spectra the actual products formed show a marked change between low temperature and high temperature with the aromatic species being replaced by polyynes, up to C₈H₂ at 10 bar. The shift is more evident in PI studies which extend to higher temperatures and above 2100 K essentially the only major products are C₂H₂ or polyynes. The LS and TOF-MS results are apparently contradictory. To simulate the LS results, a mechanism that strongly favors dissociation via reaction 2 is currently necessary. However, the low temperature mass spectra suggest that reaction 1 is dominant. As temperature is increased, the mass spectra suggest an apparent large shift in mechanism to one that favors polyne formation. Additional complications exist because the ratios of C₂H₂:C₄H₂:C₆H₂

are not consistent with production simply through dissociation of *o*-benzynes⁴ and we have not previously observed C₈H₂ in studies of aromatics. The ratio C₈H₂:C₆H₂ appears to be too large for it to be formed by addition of C₂ species to C₆H₂. The experimental results point to some interesting and complicated chemistry that was not expected based on literature studies, mainly oxidation, of styrene. Currently, we are developing a mechanism that can reconcile the apparently contradictory experimental results and accommodate the change in reaction paths that occur with temperature. We will also collaborate with Sivaramakrishnan and Goldsmith to develop a theoretical model for the initial dissociation of styrene.

B. X-ray fluorescence measurements of temperatures in sooting flames

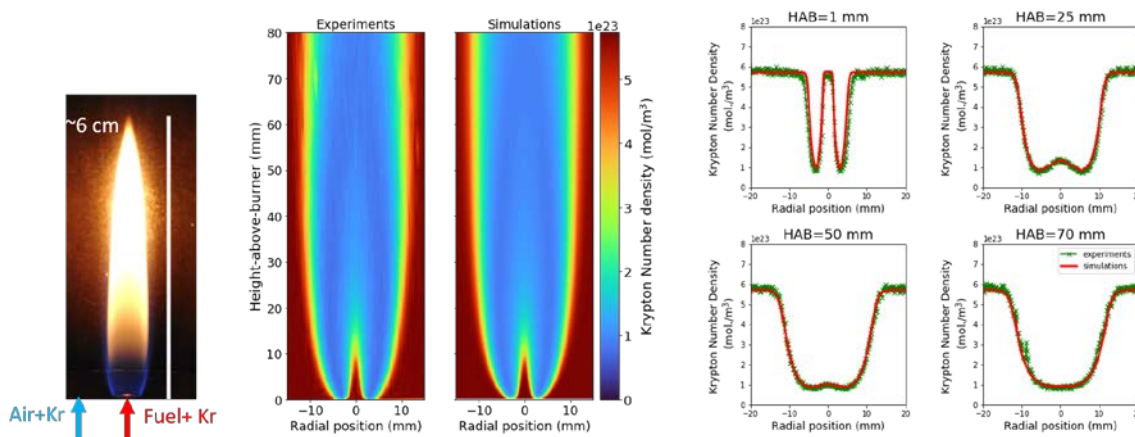


Figure 2: Comparison of temperatures from Kr/ x-ray fluorescence measurements in an atmospheric pressure sooting methane/air co-flow diffusion flame and 2D CFD simulations of the flame. Fuel flow: CH₄ 330 mL/min, Kr 8.0 mL/min (2.37%); Oxidizer co-flow: Air 50 L/min, Kr 1206.9 mL/min (2.38%). The flame is shown on the left. The middle images show the two dimensional temperature fields from the experiment and simulation. The quad plot on the right shows slices of the fluorescence signal and simulation at various heights above the burner, HAB.

Accurate and spatially resolved measurements of temperatures are challenging to make in combustion systems, particularly in sooting regions of flames. However, such measurements are necessary for testing the performance of models that simulate the flames. We have previously reported, with Hansen, temperatures determined in rich low-pressure ethylene flames seeded with krypton atoms.¹² The number density of the krypton atoms was measured by x-ray fluorescence (XRF) and converted to temperature with the ideal gas law. These experiments yielded detailed maps of the temperature fields and revealed the large distortions created by quartz sampling cones immersed in the flame on the temperature fields.¹² Recently, in collaboration with McEnally (Yale) and Xuan (Penn State), we have applied the XRF method to mapping temperatures throughout atmospheric pressure, fuel-rich methane flames. The experiments were performed at the 7-BM-B beamline at the Advanced Photon Source. X-rays of 15 keV were focused to a 6 x 7 μ m cross section at the center of the flame. Fluorescence photons were collected orthogonal to the x-ray beam. Methane/air diffusion flames were produced by a co-flow burner with a geometry that is widely used for testing numerical models of soot formation. Fuel was introduced via a central tube and air formed the outer co-flow. The krypton concentration was \sim 2.4% by mole and Kr could be added to either or both the fuel and oxidizer streams. Fluorescence signals were collected in a raster scan style, in both the horizontal and vertical planes, by translating the burner around the x-ray beam. A wide range of experiments were performed with different stoichiometries, C:O ratio and Kr in both flows and individual flows. The fluorescence measurements provided a comprehensive dataset which also allowed phenomena such as diffusion and mixing between the flows to be studied. A key goal of the experiments was to obtain high-fidelity data to test simulations against prior to using the simulations as a basis for in depth studies of chemistry within the flames. Consequently, 2D CFD models of the flames were developed to reproduce the temperature fields. An example of the experimental and simulation results for one flame is shown in Fig.

2. The agreement between the simulations and the experimental data is extremely good and provides confidence in using the model for future studies with this flame. The complete set of experimental data will provide a solid test group for future developments in flame simulations.

C. Future work

The DFST/TOF-MS/LS studies of aromatics and resonantly stabilized radicals are being expanded to include reactions between radicals and oxygen molecules. Organonitrites will be exploited as sources of a broad range of radicals including unsaturated ones, resonantly stabilized and aromatic radicals. These will allow key processes in formation of polyaromatic hydrocarbons to be tested and characterized. These experiments will be supplemented with photoionization mass spectrometry experiments in the miniature high repetition rate shock tube, discussed elsewhere. Michael's high purity shock tube will be converted to a DFST and optical diagnostics including ARAS and UV-OH absorption will be implemented to complement the DFST/TOF-MS/LS experiments.

III. References

- 1) P. T. Lynch, C. J. Annesley, C. J. Aul, X. Yang and R. S. Tranter, *J. Phys. Chem. A*: 117, 4750-4761 (2013).
- 2) R. S. Tranter, A. W. Jasper, J. B. Randazzo, J. P. A. Lockhart, and J. P. Porterfield, *Proc. Combust. Inst.* 36, 211-218 (2017)
- 3) R. S. Tranter, S. J. Klippenstein, L. B. Harding, B. R. Giri, X. Yang, and J. H. Kiefer, *J. Phys. Chem. A* 114, 8240-8261 (2010)
- 4) P. T. Lynch, C. J. Annesley and R. S. Tranter, *Proc. Combust. Inst.* 35, 145-152 (2015)
- 5) Williams & Marshall Strategy, The Global Styrene Mark
- 6) Report of the Basic Energy Sciences Roundtable on Chemical Upcycling of Polymers, Bethesda, Maryland, April 30–May 1, 2019.
- 7) J. Li, J. Cai, T. Yuan, H. Guo, F. Qi, *Rapid Commun. Mass Spectrom.* 23 (2009) 1269–1274.
- 8) K. Brezinsky, G.T. Linteris, T.A. Litzinger, I. Glassman, *Proc. Combust. Inst.* 21 833–840 (1988).
- 9) B. Gullett, A. Touati, L. Oudejans, *Atmos. Environ.* 42 (2008) 7997–8006.
- 10) A. Comandini, G. Pengloan, S. Abid, N. Chaumeix, *Combust. Flame.* 173 (2016) 425–440.
- 11) G. Friedrichs, E. Goos, J. Gripp, H. Nicken, J.-B. Schönborn, H. Vogel, F. Temps, *Zeitschrift Für Phys. Chemie.* 223 (2009) 387–407.
- 12) N. Hansen, R. S. Tranter, J. B. Randazzo, J. P. A. Lockhart, A. L. Kastengren, *Proc. Combust. Inst.* 37, 1401-1408 (2019)

IV. Publications and submitted journal articles supported by this project 2018-2020

- 1) Sikes T, Bell Burdett K., Speth R. L., Goldsmith C. F., Sivaramakrishnan R., Tranter R. S., 'Ring opening in cycloheptane and dissociation of 1-heptene at high temperatures' *Proc. Combust. Inst.* **2020** accepted.
- 2) Randazzo J.B., Sivaramakrishnan R., Jasper A. W., Sikes T., Lynch P. T., and Tranter R. S., 'An Experimental and Theoretical Study of the High Temperature Reactions of All Four Butyl Radical Isomers' *Phys. Chem. Chem. Phys.* **2020** submitted.
- 3) Fuller M. E., Skowron M., Tranter R. S. and Goldsmith C. F. 'A modular, multi diagnostic, automated shock tube for gas-phase chemistry' *Rev. Sci. Instrum.* **2019**, 90, 064104
- 4) Randazzo J. B., Fuller M. E., Goldsmith C. F. and Tranter R. S. 'Thermal Dissociation Of Alkyl Nitrites And Recombination Of Alkyl Radicals' *Proc. Combust. Inst.* **2019**, 37,703-710.
- 5) Hansen N., Tranter R. S., Randazzo J. B., Lockhart J. P. A., and Kastengren A. L. 'Investigation of Sampling-Probe Distorted Temperature Fields with X-Ray Fluorescence Spectroscopy' *Proc. Combust. Inst.* **2019**, 37, 1401-1408.
- 6) Tranter R. S., Randazzo J. B., Lockhart J. P. A., Chen X. and Goldsmith C. F. 'High Temperature Pyrolysis of 2-Methyl Furan' *Phys. Chem. Chem. Phys.* **2018**, 20, 10826 – 10837.

Probing Nonvalence Excited States of Anions Using Photodetachment and Photoelectron Spectroscopy

Lai-Sheng Wang

Department of Chemistry, Brown University, Providence, RI 02912

Email: lai-sheng_wang@brown.edu

Program Scope

This program is aimed at providing energetic, electronic, and vibrational information about radical species important in combustion using novel anion spectroscopic techniques. Negative ions do not possess Rydberg states, but highly diffuse nonvalenced excited states can exist for anions as a result of long-range forces between an electron and a molecule, including charge-dipole, charge-quadrupole, or charge and induced-dipole interactions. A major goal of this project is to probe this class of anionic excited states that exist in polycyclic aromatic hydrocarbon (PAH) molecules or functionalized PAH molecules. The weakly-bound nature of these nonvalence excited states implies that vibrational excitation in the neutral core can induce autodetachment via vibronic coupling. We have developed a high-resolution electrospray photoelectron imaging apparatus equipped with a cryogenically-controlled ion trap, which is ideal to probe this class of nonvalence anionic excited states. Photodetachment spectroscopy is used to search for the nonvalence excited states of cold anions via resonant two-photon detachment or vibrational autodetachment. The autodetachment process is investigated by resonantly-enhanced photoelectron spectroscopy. The combination of photodetachment spectroscopy and resonant photoelectron spectroscopy can probe the dynamics of the vibronic interactions leading to autodetachment, as well as detailed energetic, electronic, and vibrational information about the underlying neutral radicals. Three types of anionic species are investigated: 1) O-containing PAH anions with dipole-bound excited states; 2) O- and/or N-functionalized PAH anions with quadrupole-bound excited states; and 3) PAH and fullerene anions with polarization-bound excited states.

Recent Progress

Resonant Two-Photon Photoelectron Imaging and Intersystem Crossing from Excited Dipole-Bound States of Cold Anions.

We investigated cryogenically-cooled deprotonated 4,4'-biphenol anion (bPh^-) using high resolution photoelectron imaging and photodetachment spectroscopy. The electron affinity and rich vibrational information of the bPh radical were obtained. We observed a dipole-bound state (DBS) 659 cm^{-1} below the electron detachment threshold of bPh^- and nineteen of its lowest vibrational levels. Interestingly, resonant two-photon photoelectron imaging (R2P-PEI) via the vibrational levels of the DBS displayed a sharp peak with a constant binding energy. This observation indicated vertical detachment from the vibrational levels of the DBS to the corresponding neutral levels

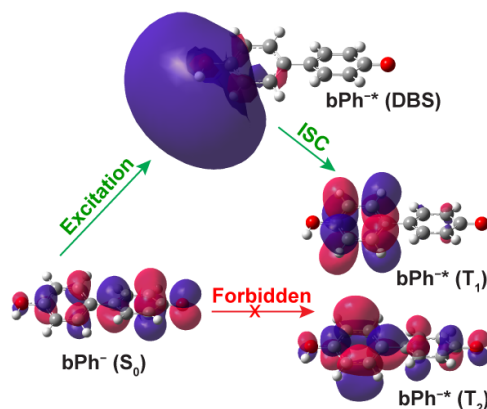


Fig. 1 Schematics showing the excitation from the ground state of the bPh^- anion to the DBS, and intersystem crossing from the DBS to the valence-bound excited states of bPh^- , T_1 and T_2 .

with the conservation of the vibrational energy, suggesting that the highly diffuse electron in the DBS has little effect on the neutral core. Surprisingly, the R2P-PEI spectra also exhibited two features at lower binding energies, which came from intersystem crossings from the DBS to two lower-lying valence-bound triplet excited states of bPh^- (see Fig. 1). This study disclosed the first R2P-PEI spectra from vibrational excited states of a DBS and direct spectroscopic evidence of transitions from a DBS to valence-bound states of an anion.

Probing the Critical Dipole Moment to Support Excited Dipole-Bound States in Valence-Bound Anions. The critical dipole moment to support dipole-bound states (DBSs) was an interesting quantum

mechanical problem, but rather complicated for molecular systems. To probe the critical dipole moment for DBS would require molecular systems with similar size, but varying dipole moments. We conducted a photodetachment spectroscopy and high-resolution photoelectron imaging study on a series of *para*-halogen substituted

phenoxide anions, $p\text{-XC}_6\text{H}_4\text{O}^-$ ($X = \text{F}, \text{Cl}, \text{Br}, \text{I}$). The dipole moments of the $p\text{-XC}_6\text{H}_4\text{O}$ neutral radicals increase from 2.56 to 3.19 D for $X = \text{F}$ to I ,

providing a series of similar molecules to allow the examination of charge-dipole interactions by minimizing molecule-dependent effects. Excited DBSs ($[p\text{-XC}_6\text{H}_4\text{O}]^{*-}$) were observed for the four anions with binding energies of 8, 11, 24, and 53 cm^{-1} , respectively, for $X = \text{F}$ to I , below their respective detachment thresholds. The binding energies exhibited a linear correlation with the dipole moments of the neutral radicals, extrapolating to a critical dipole moment of 2.5 D for zero binding energy (Fig. 2). Because of the small binding energy of the excited DBS of $[\text{FC}_6\text{H}_4\text{O}]^{*-}$, rotational autodetachment was observed to compete with vibrational autodetachment in the resonant photoelectron spectra, resulting in electrons with near zero kinetic energies.

High-Resolution Photoelectron Imaging and Resonant Photoelectron Spectroscopy via Noncovalent-Bound Excited States of Cryogenically-Cooled Anions. Valence-bound anions with polar neutral cores ($\mu > \sim 2.5$ D) can support dipole-bound excited states below the detachment threshold (see Fig. 2). These dipole-bound states (DBSs) are highly diffuse and the weakly bound electron in the DBS can be readily autodetached via vibronic coupling. Excited DBSs can be observed in photodetachment spectroscopy using a tunable laser. Tuning the detachment laser to above-threshold vibrational resonances yields vibrationally-enhanced resonant photoelectron spectra, which are highly non-Franck-Condon with much richer vibrational information. An invited perspective article was published, describing recent advances

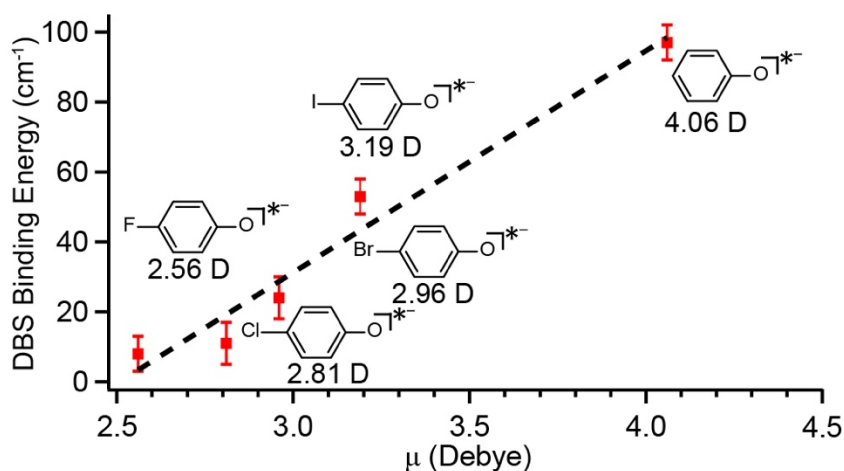


Fig. 2 The DBS binding energies of the electronically excited DBSs of $[p\text{-XC}_6\text{H}_4\text{O}]^{*-}$ as a function of the dipole moments of the neutral $p\text{-XC}_6\text{H}_4\text{O}$ cores. The binding energies (BEs) are found to be linearly dependent on the dipole moments for this set of molecules. The dashed line is a linear fit with a R^2 value of 0.96 and $\text{BE} = 63.4\mu - 159.0$. The linear curve is extrapolated to a critical dipole moment of 2.5 D at zero binding energy.

in the studies of excited DBSs of cryogenically cooled anions using high-resolution photoelectron imaging (PEI) and resonant photoelectron spectroscopy (rPES) primarily from the PI's group. The basic features of dipole-bound excited states and the highly non-Franck-Condon resonant photoelectron spectra were discussed. The power of rPES to yield rich vibrational information beyond conventional PES were highlighted, especially for low-frequency and Franck-Condon-inactive vibrational modes, which are otherwise not accessible from non-resonant conventional PES. Mode-selectivity and intra-molecular rescattering were observed during the vibrationally-induced autodetachment. Conformer-specific rPES was possible due to the different dipole-bound excited states of molecular conformers with polar neutral cores. For molecules with $\mu \ll 2.5$ D or without dipole moments, but large quadrupole moments, excited quadrupole-bound states can exist, which can also be used to conduct rPES.

Observation of a *p*-Type Dipole-Bound State in Molecular Anions. For an electron in a fixed dipole field, an infinite number of dipole-bound states (DBSs) were found above a critical dipole moment, similar to the

solutions of the H atom (an electron in a Coulombic field). However, in molecular systems, usually only a finite number of DBSs exist, usually just one. We have conducted high resolution photoelectron imaging and photodetachment spectroscopy (Fig. 3) study of cryogenically cooled deprotonated 9-anthrol molecular anions ($9AT^-$) to obtain energetic and vibrational information of the O-containing polycyclic aromatic hydrocarbon radical ($9AT$). A

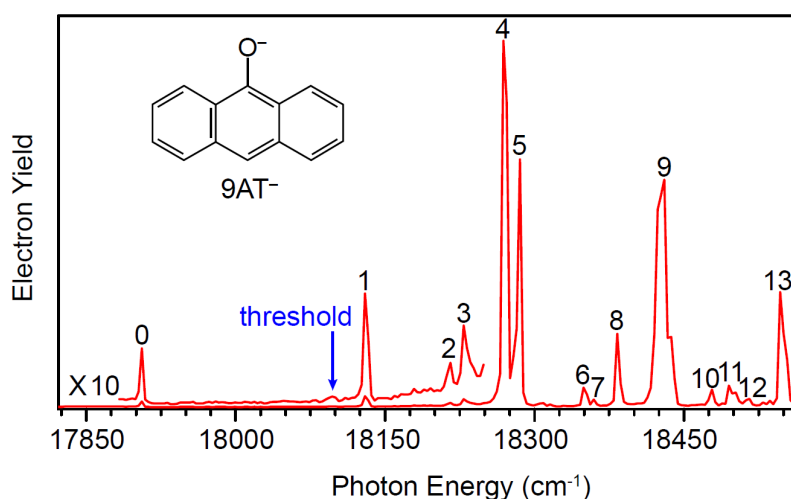


Fig. 3 The photodetachment spectrum of $9AT^-$ by measuring the total electron yield as a function of photon energy near the detachment threshold. The blue arrow indicates the detachment threshold at 18097 cm^{-1} .

DBS was indeed observed below the detachment threshold, represented by peak 0 in Fig. 3. Although the lowest DBS of $9AT^-$ was calculated to be an *s*-like diffuse orbital with no angular nodes (see Fig. 1 for example), we observed experimentally a *p*-type DBS (*p*-DBS) in resonant two-photon photoelectron imaging. The DBS was determined to be 191 cm^{-1} below the detachment threshold of $9AT^-$ (Fig. 3) and the existence of the *p*-DBS was revealed by a distinct (*s*+*d*)-wave photoelectron angular distribution. The *p*-DBS was found to be stabilized by the large anisotropic in-plane polarizability of $9AT$. The population of the dipole-forbidden *p*-DBS was proposed to be due to bifurcation from the dipole-allowed *s*-type DBS mediated by molecular rotations.

Future Plans

Experiments on dipole-bound excited states will be continued on polycyclic aromatic hydrocarbon (PAH) anions. Specifically, we plan to move to larger deprotonated O-containing PAHs. Preliminary data have been obtained on the naphthoxide anions already and will be

written up for publication. We plan to study three- or four-phenyl ring PAHs. We will also investigate more complex O-containing PAHs, such as the C-linked biphenol oxide anions and phenoxide with complex substituents.

Work supported by the BES-GPCP program (2018- present)

1. G. Z. Zhu, Y. Liu, Y. Hashikawa, Q. F. Zhang, Y. Murata, and L. S. Wang. Probing the Interaction between the Encapsulated Water Molecule and the Fullerene Cages in $\text{H}_2\text{O}@C_{60}^-$ and $\text{H}_2\text{O}@C_{59}\text{N}^-$. *Chem. Sci.* **9**, 5666-5671 (2018). (DOI: 10.1039/C8SC01031E)
2. G. Z. Zhu, C. H. Qian, and L. S. Wang. Dipole-Bound Excited States and Resonant Photoelectron Imaging of Phenoxide and Thiophenoxide Anions. *J. Chem. Phys.* **149**, 164301 (2018). (DOI: 10.1063/1.5049715)
3. G. Z. Zhu, C. H. Qian, and L. S. Wang. Tautomer-Specific Resonant Photoelectron Imaging of Deprotonated Cytosine Anions. *Angew. Chem. Int. Ed.* (2019). (DOI: 10.1002/anie.201903444)
4. J. Czekner, L. F. Cheung, G. S. Kocheril, and L. S. Wang. Probing the Coupling of A Dipole-Bound Electron with the Molecular Core. *Chem. Sci.* **10**, 1386-1391 (2019). (DOI: 10.1039/c8sc04771e)
5. G. Z. Zhu, L. F. Cheung, Y. Liu, C. H. Qian, and L. S. Wang. Resonant Two-Photon Photoelectron Imaging and Intersystem Crossing from Excited Dipole-Bound States of Cold Anions. *J. Phys. Chem. Lett.* **10**, 4339-4344 (2019). (DOI: 10.1021/acs.jpcclett.9b01743)
6. C. H. Qian, G. Z. Zhu, and L. S. Wang. Probing the Critical Dipole Moment to Support Excited Dipole-Bound States in Valence-Bound Anions. *J. Phys. Chem. Lett.* **10**, 6472-6477 (2019). (DOI: 10.1021/acs.jpcclett.9b02679)
7. G. Z. Zhu and L. S. Wang. High-Resolution Photoelectron Imaging and Resonant Photoelectron Spectroscopy via Noncovalent-Bound Excited States of Cryogenically-Cooled Anions. *Chem. Sci.* **10**, 9409-9423 (2019) (Invited article). (DOI: 10.1039/C9SC03861B)
8. D. F. Yuan, Y. Liu, C. H. Qian, Y. R. Zhang, B. M. Rubenstein, and L. S. Wang. Observation of a *p*-Type Dipole-Bound State in Molecular Anions. submitted (2020).

Fundamental chemical kinetics of siloxane and silicon compounds

DOE BES Grant #18SC503179

Margaret S. Wooldridge (PI)

University of Michigan, Department of Mechanical Engineering, 2350 Hayward St., Ann Arbor, MI, 48109-2125, mswool@umich.edu

Andrew B. Mansfield

Eastern Michigan University Mechanical, Engineering, College of Technology, Ypsilanti, MI, 48197, amansfi3@emich.edu,

Robert S. Tranter

Chemical Sciences and Engineering Division, Argonne National Laboratory, Argonne, IL, 60439, tranter@anl.gov

Program Scope

Siloxanes and other silicon compounds play significant roles as impurities in land-fill gas and as primary feedstock materials for high-value and large-volume products, yet the fundamental reaction chemistry of gas-phase silicon compounds remains largely unexplored. The proposed work integrates two complementary experimental efforts to significantly advance the science of gas-phase silicon reaction chemistry. The primary research focus is on the elementary thermal reactions of siloxanes and their decomposition products with a progression in the chemical structure of the compounds studied to elucidate the effects of bond structure. An additional area of interest is the interaction of gas-phase species with silica nanoparticles that are formed naturally as products of the thermal reactions of siloxanes and during oxidation.

Methodology

Experiments have been conducted using the University of Michigan (UM) rapid compression facility (RCF) and the diaphragmless shock tube (DFST) and the high-repetition rate shock tube (HRRST) at the Argonne National Laboratory (ANL). The combination of experimental approaches allows a broad and complementary range of state conditions to be studied with temperatures in the range of 700-2000 K and pressures of 0.1-50 bar. With the RCF studies, rapid gas-sampling coupled with gas-chromatography and mass spectrometry will be applied to measure stable intermediates and products allowing reaction pathways to be identified and limiting elementary rate coefficients to be determined. Narrowline laser absorption measurements will be used to measure the formation of the OH radical in the RCF systems as well as to measure the interaction of OH with silicon nanoparticles. Elementary rate coefficients and mechanisms of the thermal decomposition reactions will be determined in studies at ANL with a combination of optical measurements and online mass spectrometry. In addition, photoionization mass spectrometry (PIMS) experiments have been conducted using the Advanced Light Source (ALS) at Lawrence Berkeley National Laboratory with the portable HRRST and at ANL using electron impact ionization mass spectrometry (EIMS) measurements with the DFST. Together the UM and ANL data sets have provided the foundation for developing an accurate understanding of gas-phase silicon chemistry over a wide range of state conditions. These are the first measurements to systematically address such a large spectrum of fundamental gas-phase silicon chemistry. Successful outcomes of this work include multiple categories of pioneering data, and directly address the two **DOE BES Grand Challenges** of *Synthesizing new forms of matter with tailored properties* and *Understanding and controlling material properties emerging from complex atomic and electronic interactions*.

Recent Progress

The ignition studies using the UM RCF of trimethylsilanol (TMSO) and hexamethyldisiloxane (HMDSO) have been completed, and the results are summarized in Schwind and Wooldridge (2019). The experimental data were used to propose and test hypotheses for siloxane reaction pathways important for this class of compounds. Importantly, the experimental data indicate significant reactivity at combustion conditions that may be attributed to, in part, increased production of the OH radical pool. However, the results also indicate direct reactions with the siloxane compounds or silicon-containing intermediates are necessary to explain the observed behaviors. Our current work includes developing the experimental strategy for fast gas sampling during siloxane ignition and thermal decomposition experiments using the RCF. Towards these goals, we have adapted an atmospheric-pressure Hencken burner for siloxane addition to a methane/air flame. Gas sampling experiments using the burner, followed by gas chromatography (GC) for speciation and quantification of stable intermediates, will complement the RCF and shock tube data. The burner will be used for particle sampling studies as the one-dimensional system provides a clear quantitative understanding of the time history of the particles produced from the siloxanes. The time-resolved particle database provides a foundation to interpret findings from particles sampled from the RCF and shock tube studies.

During the past year, several series of shock tube on the thermal decomposition of TMSO, HMDSO and hexamethylcyclotrisiloxane (HMCTSO) experiments were completed using the ANL DFST with laser schlieren densitometry to determine overall thermal decomposition rates and EIMS measurements of intermediate species were also made. All three siloxane compounds were also studied using the HRRST/PIMS. The data from these experiments are still being analyzed; however, the initial analysis indicates unexpected behavior and new trends and understanding of siloxane chemistry. Some interesting observations are highlighted here.

Previous work in the literature predicted that HMDSO would thermally decompose to produce larger linear and cyclic siloxanes. However, the major products identified in the ANL DFST study were smaller organic species such as methane, ethylene, and acetylene, as well as hydrogen. No prior studies have been conducted on the thermal decomposition of TMSO. **Figure 1** presents typical EIMS results from the DSTF studies of TMSO. The data indicate TMSO also produces small organic species. However, mass spectra data from the HRRSTF studies (not shown here) indicate TMSO produces larger siloxane species (based on peaks observed at m/z ratios of ~ 207 to 209) in addition to producing small organic species. Importantly, ethane was not observed in the spectra which has been predicted to be a major product of TMSO thermal decomposition.

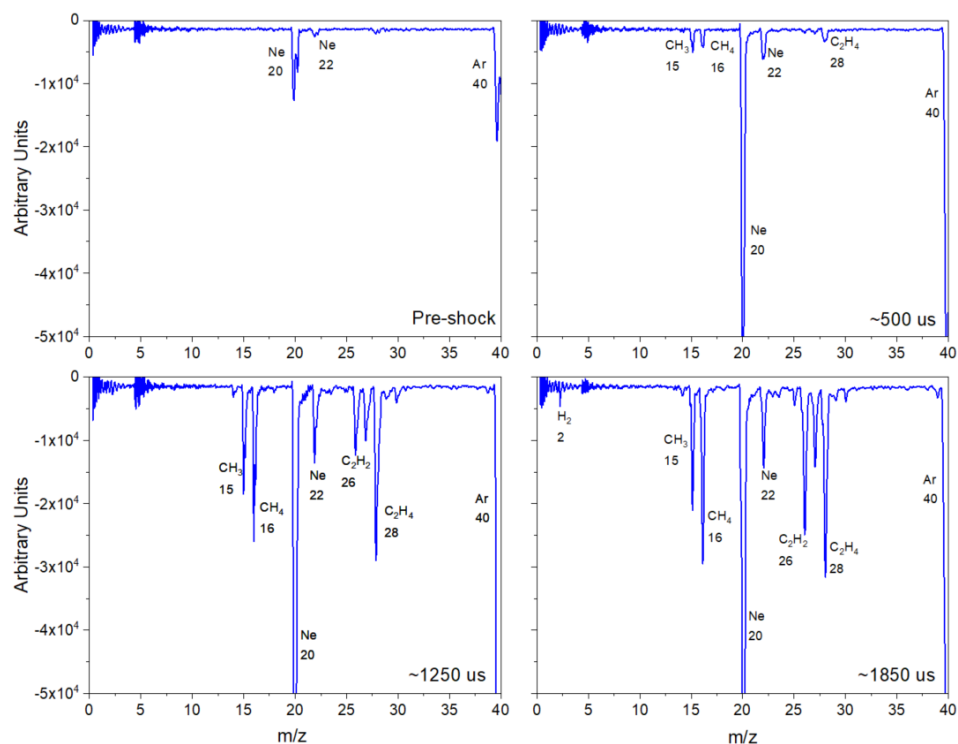


Figure 1. Average time of flight mass spectra from 10 TMSO thermal decomposition experiments conducted in the ANL-DSTF. The experimental conditions were 1410 K and 0.2 atm with 0.5% TMSO in 2% Ar and the balance Ne. Four representative reaction times are shown: Pre-shock, 500 μ s post-shock, 1250 μ s post-shock, and 1850 μ s post-shock. The longest times are in the quench phase where recombination is enhanced.

The ANL DFST schlieren data directly correspond to the exothermicity or endothermicity of the siloxane thermal decomposition reactions. **Figure 2** shows some of the laser schlieren results for HMDSO. In the figure, each row presents results from experiments at the same pressure, with temperature increasing from left to right. Pressure increases from the top row to the middle and bottom rows. A key observation for all experiments is that the density gradients are always positive, indicating radical recombination reactions to stable species, e.g., $\text{CH}_3 + \text{CH}_3 = \text{C}_2\text{H}_6$ ($\Delta H_{r,298\text{ K}} \cong -90$ kcal/mol), are negligible. Thus, the laser schlieren and electron impact ionization mass spectra results are consistent. Essentially no ethane is seen in the EIMS results, and the distributions of C_2H_4 and C_2H_2 are not consistent with prior DFST/EIMS experiments on CH_3 recombination. These observations all imply that insertion/elimination mechanisms are significant for the thermal decomposition of these siloxane compounds.

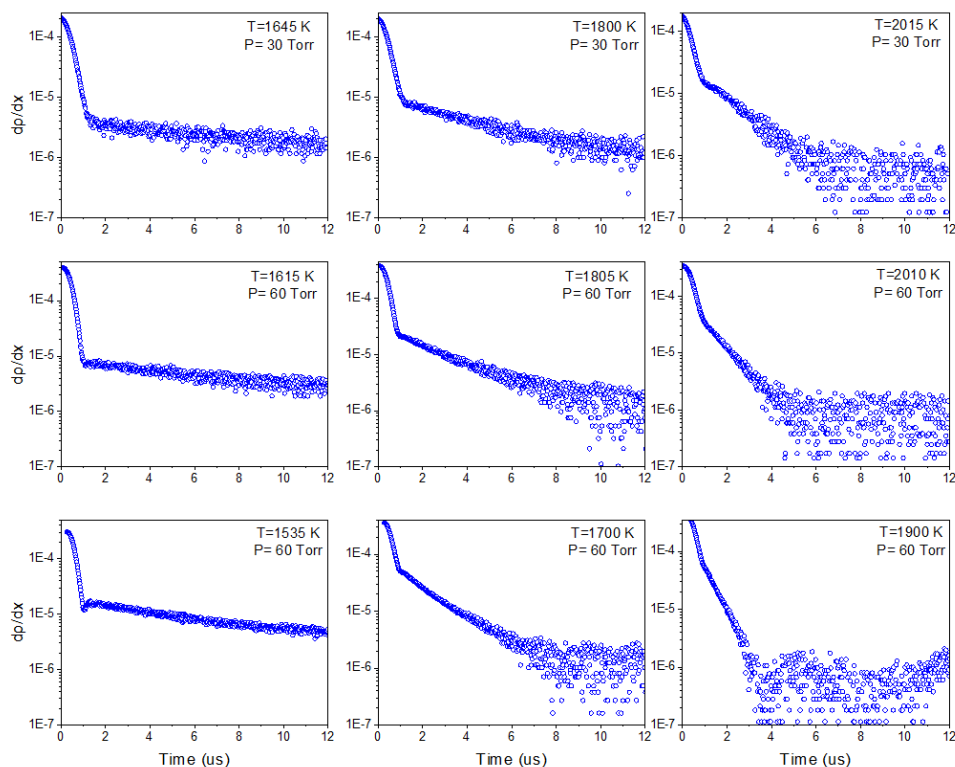


Figure 2. Density gradients obtained from laser schlieren measurements during DFST studies of 0.5% HMDSO in Kr for temperatures $T = 1535$ K to 2015 K and pressures $P = 0.04$ and 0.08 atm.

Future Plans

The ANL DFST and HRRST data are the first of their kind, and provide a sound experimental basis for developing detailed understanding of siloxane reaction chemistry. Current and future work includes particle formation experiments using the one-dimensional burner and RCF (described above), as well as OH measurements in shock tube and RCF studies of HMDSO, TMSO and ring siloxane compounds. We continue to work with Dr. Raghu Sivaramakrishnan (ANL) to develop siloxane thermochemistry to allow further insights into the elementary reactions controlling siloxane combustion. Additionally, Dr. Rachel Schwind, who worked with Tranter at ANL and LBNL on these siloxane studies as part of her dissertation research, recently graduated from the University of Michigan and is currently a post-doctoral scholar working with Prof. Franklin Goldsmith at Brown University. Prof. Goldsmith and Dr. Schwind are collaborating with us on additional computational development of the siloxane thermochemistry.

DOE publications supported by this project

Schwind, R. A., 2019, *Understanding the Combustion Chemistry of Siloxanes: Reaction Kinetics and Fuel Interactions*, Ph.D. Thesis, University of Michigan, Ann Arbor.

Schwind, R., Wooldridge, M. S., (2019) "Effects of Organic Silicon Compounds on Syngas Auto-ignition Behavior," *Combustion and Flame*, 212 pp. 234-241.

Schwind, R. A., Wooldridge, M. S., Sivaramakrishnan, R., (2019) "Understanding Siloxane Combustion Chemistry: Computational and Experimental Studies of Hexamethyldisiloxane (HMDSO)," 11th National Meeting of the U.S. Sections of the Combustion Institute, Paper No. 1A18, Pasadena, CA.

Nonadiabatic Photochemistry

Hua Guo¹, Donald G. Truhlar,² and David R. Yarkony³

¹Department of Chemistry and Chemical Biology, University of New Mexico, Albuquerque, New Mexico 87131. ²Department of Chemistry, University of Minnesota, Minneapolis, Minnesota 55455. ³Department of Chemistry, Johns Hopkins University, Baltimore, Maryland 21218

Program Scope:

This project involves the development and application of methods for treating electronically nonadiabatic processes with the emphasis on photochemical dynamics studied on accurate coupled diabatic potential energy surfaces fit to accurate electronic structure data (ESD) generated from accurate, quantum mechanical wavefunctions.

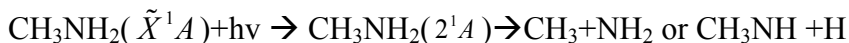
Recent progress:

David R. Yarkony

During the present performance period we have addressed three aspects of conical intersections, a ubiquitous topographical feature of the potential energy landscape.

We have developed a completely new version of our algorithm (SURFGEN),¹ which simultaneously fits and diabaticizes *ab initio* adiabatic ESD. It replaces the molecular functions, bond angles and dihedral angles used in SURFGEN with feed forward Neural Network (NN) functions. This algorithm (NN-SURFGEN) employs permutation invariant polynomials (PIPs)² which unlike molecular functions can be symmetry equivalent atoms, in the CNPI group,³ without treating multidimensional irreducible representations. Our previous representations of ESD have focused on the coupled potentials energy surfaces (PESs). Interactions with the electric field, dipole and transition dipole and the spin-orbit interaction were not considered. As part of other funded research, we have developed algorithms to fit dipole and transition dipole moments⁴ and spin-orbit interaction.⁵ This will allow us to handle problems not usually treated with the fit representation of ESD approach. In particular we hope to treat processes in which the electromagnetic fields shift the locus of the conical intersection seam⁶ and in which intersystem crossing competes with internal conversion.⁷

We studied the photodissociation of methylamine,⁸



a deceptively simple methyl derivative of NH₃. It might appear that both the methyl and hydrogen channels of the above photodissociation would be produced by a similar mechanism. But that is not the case, as the excited 2¹A state barrier and 1-2¹A conical intersection relevant to the methyl channel are sufficiently high in energy to preclude direct production of that channel. Rather, the methyl channel is produced indirectly via the 1¹A state equilibrium structure. This required us to develop a representation of the ESD that could describe both direct and statistical, long time propagation, dissociation. Long time propagation dynamics requires fit ESD as opposed to on-the-fly ESD. In future work we will compare the long-lived trajectories with the predictions of statistical models.

With Guo we are studying the effects of the conical intersections on product energy disposal in the nonadiabatic photodissociation of phenol

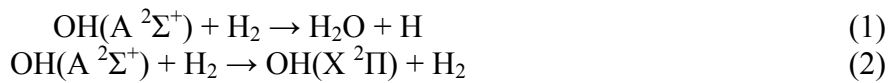


The primacy of the **g** and **h** modes,⁹ defining the branching space in the vicinity of a conical intersection, is well established. Here **g** and **h** are 2 of the 3 disappearing modes. However, the

role of the remaining modes is less well studied/understood. A key question is: how is energy redistributed into and among these modes during photodissociation. The assignment of the line positions and intensities in the observed H-atom kinetic energy release (KER) spectrum¹⁰ is computationally challenging since the process involves two nonadiabatic steps. Guo has carried out¹¹ a series of 1,2,3¹A state reduced 4-internal coordinate (3 disappearing modes and one phenoxyl mode), coupled adiabatic state simulations of the measured KER spectrum. It is gratifying that the diabatic potential energy matrix (DPEM) used in these calculations is the one we determined over 4 years ago as part of a previous DoE BES grant.^{1, 12} Guo's results challenged prior interpretations of the measured KER spectra. In the coming performance period, the dynamical model will be extended to incorporate additional degrees of freedom, yielding a more accurate representation/understanding of the photodissociation.

Donald G. Truhlar

The reactions



provide enticing targets for theoretical study because of the detailed experimental data available, dating back to the pioneering experimental studies in the Lester, Crosley, and Heard laboratories. Upon the A²Σ⁺-X²Π excitation of isolated OH, only radiative decay is conceivable, but collisions with other molecules open nonradiative de-excitation pathways, such as reactions (1) and (2). Understanding these competitive pathways is necessary to fully interpret the LIF measurements. In addition, the OH₃ system has established itself as the four-body system most widely studied by quantum mechanical dynamics calculations; in particular, OH₃ is a prototype for four-body quantum dynamics in a similar way to how H₃ is a prototype for three-body quantum dynamics.

We have employed extended multi-configuration quasidegenerate perturbation theory, fourfold-way diabatic molecular orbitals, and configurational uniformity to develop a global three-state diabatic representation of the PESs and their couplings for the electronically nonadiabatic reaction (1).¹³ To achieve sign consistency of the computed diabatic couplings, we developed a GPU-accelerated algorithm called the cluster-growing algorithm. Having obtained consistent signs of the diabatic couplings, we fit the diabatic matrix elements (which consist of the diabatic potentials and the diabatic couplings) to analytic representations. Adiabatic PESs are generated by diagonalizing the 3 × 3 DPEM. The comparisons between the fitted and computed DPEM elements and between the originally computed adiabatic PESs and those generated from the fits indicate that the fit is accurate enough for semiclassical dynamics calculations, although further adjustments are necessary for quantal dynamics calculations that require energies over a broader range of geometries than are accessed in the classical trajectories explored during the parametrization.

Photodissociation of thiophenol produces a phenylthiyl radical in which the singly occupied molecular orbitals (SOMOs) for the both the ground and first excited states are dominated by the occupied 3*p* orbital on sulfur. Photoinduced bond fission processes proceeding via an n_π σ* excited state are prototypes of electronically nonadiabatic reactions. The photodissociation of thiophenol is a representative of these n_π σ*-mediated reactions that has been extensively studied both experimentally and theoretically. The photo-induced S-H fission of thiophenol mainly involves the ground state and the first two excited singlet states; these singlet states are labeled as ¹π π, ¹π π*, and ¹n_π σ* in the diabatic representation and as S₀, S₁, and S₂ in the

adiabatic representation. The $^1n_{\pi} \sigma^*$ state is repulsive along the S–H dissociation coordinates and intersects the $^1\pi \pi^*$ and $^1\pi \pi$ states; the conical intersections are $(3N - 8)$ -dimensional subspaces of these $(3N - 7)$ -dimensional diabatic crossings. We have constructed a set of full-dimensional PESs and state couplings for thiophenol in the diabatic representation.¹⁴ The DPEMs are obtained by electronic structure calculations including dynamic correlation via excitations into the virtual space of a three-state multi-configuration self-consistent field calculation. The resulting DPEM is a function of all the internal coordinates of thiophenol. The DPEM as a function of the S–H bond stretch and C–C–S–H torsion and the diabatic couplings along two in-plane bend modes and nine out-of-plane distortion modes are computed using extended multi-configurational quasi-degenerate perturbation theory followed by the fourfold way determination of diabatic molecular orbitals and model space diabatization by configurational uniformity, and this dependence of the DPEM is represented by general functional forms. Potentials along 31 tertiary internal degrees of freedom are modeled with system-dependent, primary-coordinate-dependent nonreactive molecular mechanics-type force fields that are parametrized by Cartesian Hessians calculated by generalized Kohn-Sham density functional theory. These component fits are joined together by the anchor points reactive potential (APRP) scheme developed in our group. The resulting full-dimensional potentials and state couplings are functions of all 33 internal degrees of freedom of thiophenol. Adiabatic PESs and nonadiabatic couplings are obtained by a transformation of the DPEM. The topography of the APRP PESs is characterized by vertical excitation energies, equilibrium geometries, vibrational frequencies, and conical intersections, and we find good agreement with available reference data. This analytic DPEM is suitable for full-dimensional electronically nonadiabatic molecular dynamics calculations of the photodissociation of thiophenol with analytic gradients in either the adiabatic or diabatic representation.

We pointed out an angular momentum conservation problem that exists in widely used mixed quantum–classical nonadiabatic dynamics algorithms, including trajectory surface hopping (TSH), semiclassical Ehrenfest (SE), and coherent switching with decay of mixing (CSDM). We found that none of these dynamical methods conserve angular momentum when using the nonadiabatic coupling vectors (NAC) directly computed from the electronic structure theory codes usually employed in on-the-fly nonadiabatic dynamics. We proposed a projection operator to apply to the NAC to project out the translational and rotational contributions. We demonstrated that the projected NAC conserves angular momentum very well for TSH, SE, and CSDM dynamics.¹⁵

Electron momentum spectroscopy, scanning tunneling microscopy, and photoelectron spectroscopy provide unique information about electronic structure, but their interpretation has been controversial. We discussed a framework for interpretation stressing that these experiments provide information about how the electron distribution changes upon ionization, not how electrons behave in the pre-ionized state.¹⁶

We studied the effects of anharmonicity on reaction dynamics and reaction kinetics.¹⁷⁻²⁵

Hua Guo

Two invited reviews of our (Yarkony and Guo) recent work on geometric phase effects in nonadiabatic unimolecular reactions are published.^{26, 27}

In collaboration with the Zhang (UCR), Dawes (MUST), and Xie (Nanjing) groups, we have investigated the nonadiabatic dynamics in photodissociation of HCO, in which the CO product state distribution exhibits strong oscillation.²⁸ We have identified the origin of such

oscillation as the interference between different reaction paths on the ground state PES. Furthermore, we have made significant progress in understanding the nonadiabatic photodissociation dynamics of hydroxymethyl using a full-dimensional quantum model on the global DPEM developed by Yarkony.²⁹ The quantum dynamical calculations revealed the initial dynamics in the Franck-Condon region and helps to assign the features in the absorption spectrum. In a more recent work with Yarkony, the energy disposal in phenol photodissociation was investigated using reduced dimensional models and the results challenged the original assignment of the KER.¹¹

In collaboration with Yarkony, we have also explored various approaches to constructing high accuracy DPEM using NN approaches.^{8, 30, 31}

We have been continuing our investigation of dynamics of bimolecular scattering and reactions. These studies include the $O(^3P) + HCCH$ reaction,³² the $F + CH_3OH$ reaction,^{33, 34} the nonadiabatic quenching of $C(^1D)$ by N_2 ,³⁵ the isomerization between $HCCH$ and H_2CC ,³⁶ the $NO + Ar$ scattering,³⁷ the $OH + O_2$ scattering,³⁸ and $HO + HO_2$ reaction.³⁹

Future plans:

David R. Yarkony

In the coming performance period, we will extend the current work as noted above, including using our emerging tools to study the competition between spin-conserving and spin-nonconserving nonadiabatic dynamics and energy transfer into and within the complement of the branching plane. With the growing importance of diabatic representations in nonadiabatic dynamics, it is important to juxtapose distinct approaches for constructing diabatic representations. Our tripartite collaboration provides just such an opportunity using the archetypical HO_3 system. For reactive and nonreactive quenching processes reaction (1) and reaction (2) Truhlar's group has recently reported a 3 state diabatization based on his symmetry adapted 4-fold way. We are currently preparing for submission a four state representation constructed using our SURFGEN algorithm. This same ESD will be used to construct a 3-state coupled diabatic state representation using our NN-SURFGEN algorithm. The resulting DPEMs will be compared with the published results of Truhlar and used for quantum dynamics by Guo.

Donald G. Truhlar

In the coming period we will carry out dynamics calculations on $OH(A) + H_2$ nonadiabatic collisions and photodissociation of C_6H_5SH – in both cases using PESs and couplings developed on this grant in 2019.

We will present a full-dimensional DPEM for photodissociation of the N–H bond in methylamine. The electronic state space will include the ground and first excited singlet state. Input for the fit will be calculated by extended multi-state complete active space second-order perturbation theory (XMS-CASPT2) with diabatization using the dipole–quadrupole (DQ) diabatization method into which we will incorporate a coordinate-dependent weighting scheme for the contribution of the quadrupole moments. To make the resulting potential energy surfaces semiglobal, we will extend the APRP method.

The OH_3 and CH_3NH_2 projects mentioned in the two previous paragraphs provide excellent opportunities for intraproject collaboration as they were chosen because they are well suited for study by the quantal wave packet methods developed by the Guo group.

A primary area of advance in methodology is development of improved methods and programs for semiclassical dynamics methods. We will put our coherent switching with decay-

of-mixing method into the SHARC program developed by a team in the group of Prof. González at the Institute of Theoretical Chemistry at the University of Vienna, Austria. This program is not as general as our own ANT program, but it has advantages for direct dynamics. We are also developing a way to make the coherent switching with decay-of-mixing semiclassical algorithm much more efficient for direct dynamics by changing the approximation to the nonadiabatic coupling vector, and we will incorporate this into SHARC.

Hua Guo

We will be focusing on the nonadiabatic dynamics for the OH(A) + H₂ reaction dynamics, which includes the reactive and nonreactive quenching channels, using the newly developed DPEMs from both the Yarkony and Truhlar groups. Both reduced dimensional quantum and full-dimensional trajectory surface hopping calculations will be carried out to explore the reactive and non-reactive quenching channels. Quantum dynamical calculations will also be carried out for several prototypical systems, such as methylamine, hydroxymethyl, and thiophenol, that DPEMs have been constructed. Particular attention will be paid to the use of the MCTDH approach. In addition, we will explore the possible impact of diabatic singularities on nonadiabatic dynamics.

References (publications from the last funding period are marked by *)

1. X. Zhu and D. R. Yarkony, *J. Chem. Phys.* **144**, 024105 (2016).
2. B. J. Braams and J. M. Bowman, *Int. Rev. Phys. Chem.* **28**, 577 (2009).
3. P. R. Bunker and P. Jensen, *Molecular Symmetry and Spectroscopy*. (NRC Research Press, Ottawa, 1998).
- *4. Y. Guan, H. Guo and D. R. Yarkony, *J. Chem. Theo. Comput.* **16**, 302 (2020).
- *5. Y. Guan and D. R. Yarkony, *J. Phys. Chem. Lett.* **11**, 1848 (2020).
6. P. V. Demekhin and L. S. Cederbaum, *J. Chem. Phys.* **139**, 154314 (2013).
7. T. J. Penfold, E. Gindensperger, C. Daniel and C. M. Marian, *Chem. Rev.* **118**, 6975 (2018).
- *8. Y. Wang, C. Xie, H. Guo and D. R. Yarkony, *J. Phys. Chem. A* **123**, 5231 (2019).
9. G. J. Atchity, S. S. Xantheas and K. Ruedenberg, *J. Chem. Phys.* **95**, 1862 (1991).
10. M. G. D. Nix, A. L. Devine, B. Cronin, R. N. Dixon and M. N. R. Ashfold, *J. Chem. Phys.* **125**, 133318 (2006).
- *11. C. Xie, B. Zhao, C. L. Malbon, D. R. Yarkony, D. Xie and H. Guo, *J. Phys. Chem. Lett.* **11**, 191 (2020).
12. X. Zhu, C. L. Malbon and D. R. Yarkony, *J. Chem. Phys.* **144**, 124312 (2016).
- *13. Y. Shu, J. Kryven, A. G. Sampaio de Oliveira-Filho, L. Zhang, G.-L. Song, S. L. Li, R. Meana-Pañeda, B. Fu, J. M. Bowman and D. G. Truhlar, *J. Chem. Phys.* **151**, 104311 (2019).
- *14. L. Zhang, D. G. Truhlar and S. Sun, *J. Chem. Phys.* **151**, 154306 (2019).
- *15. Y. Shu, L. Zhang, Z. Varga, K. A. Parker, S. Kanchanakungwankul, S. Sun and D. G. Truhlar, *J. Phys. Chem. Lett.* **11**, 1135 (2020).
- *16. D. G. Truhlar, P. C. Hiberty, S. Shaik, M. S. Gordon and D. Danovich, *Angew. Chem. Int. Ed.* **58**, 12332 (2019).
- *17. L. Xing, J. L. Bao, Z. Wang, X. Wang and D. G. Truhlar, *J. Am. Chem. Soc.* **140**, 17556 (2018).
- *18. J. L. Bao and D. G. Truhlar, *Phys. Chem. Chem. Phys.* **20**, 30475 (2018).
- *19. B. Long, J. L. Bao and D. G. Truhlar, *J. Am. Chem. Soc.* **141**, 611 (2019).
- *20. R. M. Zhang, D. G. Truhlar and X. Xu, *Research* **2019**, 19 (2019).
- *21. L. Xing, Z. Wang and D. G. Truhlar, *J. Am. Chem. Soc.* **141**, 18531 (2019).
- *22. L. Zhang, D. G. Truhlar and S. Sun, *Proc. Natl. Acad. Sci. U. S. A.*, 201920018 (2020).
- *23. J. Wu, L. G. Gao, W. Ren and D. G. Truhlar, *Chem. Sci.* **11**, 2511 (2020).
- *24. J. Wu, L. G. Gao, H. Ning, W. Ren and D. G. Truhlar, *Combust. Flame* **216**, 82 (2020).
- *25. J. Wu, L. G. Gao, Z. Varga, X. Xu, W. Ren and D. G. Truhlar, *Angew. Chem. Int. Ed.*, in press.
- *26. C. Xie, C. L. Malbon, H. Guo and D. R. Yarkony, *Acc. Chem. Res.* **52**, 501 (2019).
- *27. D. R. Yarkony, C. Xie, X. Zhu, Y. Wang, C. L. Malbon and H. Guo, *Comput. Theo. Chem.* **1152**, 41 (2019).
- *28. S. Han, X. Zheng, S. Ndengué, Y. Song, R. Dawes, D. Xie, J. Zhang and H. Guo, *Sci. Adv.* **5**, eaau0582 (2019).
- *29. C. Xie, C. L. Malbon, D. Xie, D. R. Yarkony and H. Guo, *J. Phys. Chem. A* **123**, 1937 (2019).

- *30. Y. Guan, H. Guo and D. R. Yarkony, *J. Chem. Phys.* **150**, 214101 (2019).
- *31. Y. Guan, D. H. Zhang, H. Guo and D. R. Yarkony, *Phys. Chem. Chem. Phys.* **21**, 14205 (2019).
- *32. J. Zuo, Q. Chen, X. Hu, H. Guo and D. Xie, *Phys. Chem. Chem. Phys.* **21**, 1408 (2019).
- *33. D.-d. Lu, C.-j. Xie, J. Li and H. Guo, *Chin. J. Chem. Phys.* **32**, 84 (2019).
- *34. D. Lu, J. Li and H. Guo, *Chem. Sci.* **10**, 7994 (2019).
- *35. F. An, S. Han, X. Hu, D. Xie and H. Guo, *Phys. Chem. Chem. Phys.* **21**, 8645 (2019).
- *36. J. Chang, L. Guo, R. Wang, J. Mou, H. Ren, J. Ma and H. Guo, *J. Phys. Chem. A* **123**, 4232 (2019).
- *37. C. Amarasinghe, H. Li, C. A. Perera, M. Besemer, A. van der Avoird, G. C. Groenenboom, C. Xie, H. Guo and A. G. Suits, *J. Phys. Chem. Lett.* **10**, 2422 (2019).
- *38. X. Hu, J. Zuo, C. Xie, R. Dawes, H. Guo and D. Xie, *Phys. Chem. Chem. Phys.* **21**, 13766 (2019).
- *39. Y. Liu, H. Song, D. Xie, J. Li and H. Guo, *J. Am. Chem. Soc.* **142**, 3331 (2020).